# Recent Progress in Emerging Hybrid Nanomaterials Towards the Energy Storage and Heat Transfer Applications: A review

[1]M.K. Muhamad Azim, [2,3]A. Arifutzzaman*, [3,4]R. Saidur, [1]M.U. Khandaker, [1]D.A. Bradley

[1]*Center for Biomedical Physics, School of Healthcare and Medical Sciences, Sunway University, 47500 Bandar Sunway, Selangor Darul Ehsan, Malaysia.*
[2]*Research Centre for Carbon Dioxide Capture and Utilisation (CCDCU), School of Engineering and Technology, Sunway University, No. 5, Jalan Universiti, Bandar Sunway, Petaling Jaya, 47500 Selangor Darul Ehsan, Malaysia.*
[3]*Research Center for Nano-Materials and Energy Technology (RCNMET), School of Science and Technology, Sunway University, Bandar Sunway, Petaling Jaya, 47500, Selangor Darul Ehsan, Malaysia*
[4]*Department of Engineering, Lancaster University, Lancaster, LA1 4YW, UK*

* For correspondence: A. Arifutzzaman: Email: arifrahat@sunway.edu.my, Contact: +60182500971 (cell).

**Abstract:** Hybrid nanomaterials, which is a combination of two or more nanoparticles have been extensively evaluated as a promising candidate for energy storage and heat transfer applications, benefitting from the rise of synergistic effects between them. The unique form of this emerging combination of nanomaterials not only offers the improved features of the integrated nanoparticles but gives us the opportunity to tailor their physicochemical properties simply by modifying their composition and morphology. Scientific findings have demonstrated that the dispersion of hybrid nanomaterials in the base fluids, known as - hybrid nanofluids gives us the alternative way to replace mono nanofluid and the conventional heat transfer fluids as it provides a much better heat transfer enhancement that is beneficial for advanced heat transfer devices. On the other hand, when hybrid nanomaterials were utilized for energy storage devices, it exhibits an outstanding electrochemical performance, providing a significant contribution to the specific capacitance which permits a new strategy to design new electrodes for advanced energy storage devices. In this article review, we summarised the recent advancements made on the emerging hybrid nanomaterials, comprising of the general overview of the emerging nanomaterials, the synthesis routes for hybrid nanomaterials and their acquired hybrid structures along with their practical applications as electrodes in electrochemical energy storage and as heat transfer fluids for advanced heat transfer devices. Finally, we have also outlined some challenging issues associated with hybrid nanomaterials that requires further attention for future research.

**Keywords:** Emerging Nanomaterials, Hybridization of Nanomaterials, Energy Storage and Heat Transfer Application.

## 1. Introduction

Over the centuries, the evolution of human society has caused energy to be utilized progressively, highlighting that consumption of energy is the key for the functioning of our ultra-modern society, the thriving of our nations and the endurance of our civilization. With the proliferation of the human race that is presently almost 7 billion and is expected to increase abruptly year-by-year, immediate need arises for the development of technologies correlated to the usage of renewable and sustainable energy

in order to power the future. The exponential increase in energy consumption, utilizing non-renewable energy such as fossil fuel for transportation, electricity generation and heating process have led to the significant increase in the global environmental pollution and at the same time gives a serious tension to the availability of fossil fuels for the coming decades due to the current excessive consumptions [1]. Consequently, progressive developments of renewable and sustainable energy associated with various energy applications including energy generation, conversion and storage of energy have been made, and to date, it has become the fastest growing area in material science and engineering. In fact, according to the International Energy Agency (IEA), the first quartile of 2020 has seen a 1.5 % increase in renewable energy demands even though there was a slight decline in the global energy market due to the COVID-19 pandemic. However, the demand for renewable energy is expected to rise over time, owing to their low operating cost and favourable access to most of the power systems [2]. It is also reported that renewable energy will have its rapid growth in the electricity generation, supplying about 30% of power demand by 2023, an increment of 6 % from 2017 [3]. Nowadays, the use of solar technology becomes prominent for their application as the energy generator, conversion and storage. It is believed that solar energy radiated by the Sun for several hours can fulfil the energy demand for the whole year [4]. However, the major drawback to solar energy technologies such as photovoltaic thermal (PV/T) and solar collectors are their inadequate performance due to the inconsistent efficiency, resulting in their operation to not be fully utilized. The use of traditional heat transfer fluids e.g. oil, water and ethylene glycol as the working fluids are restricted by poor heat transfer properties making them improvident for round-trip efficiency for the conversion of heat-to-electricity [5]. Recent studies on the usage of nanofluids, which is an engineered colloidal suspension of particles in nanometre-dimensions into base fluids as the working media in solar energy systems has shown its great potential in enhancing the operating efficiency of solar collector as it possess a remarkable thermal and optical properties [6]. It should be noted that working fluids portray a major contribution in determining the performance, cost and reliability of solar thermal systems [7]. Employing nanofluids as the working

media in solar energy technology is capable of maximising its operations by providing rapid heat transfer and concurrently acts as the absorber fluids. Apart from being utilised as a working media in solar energy technology, nanofluids are also applied to advanced heat transfer devices such as heat pipe, heat exchanger and electronic components as a cooling media. It should be mentioned that utilising a working fluid which has a high heat transfer capability is the key to the high performance and efficient systems.

With the rapid growth of energy generation from solar energy technologies, energy conversion which is the transformation of generated energy to the forms of energy storage which can be used by humans also have received considerable attention due to the expeditious growth and continuous escalation in demands for wearable and bendable smart electronic devices [8]. This is in view to the fact that the conventional graphite anodes embedded in the rechargeable Lithium-ion batteries can only convey a capacity within an ace of 370 mAh $g^{-1}$ [9], giving us the urgent hint to seek for high-performance anode materials for the next generation renewable energy devices, which able to fulfil the growing energy demands. It is clearly understood that the performance of these electronic devices are mainly governed by the properties of the nanomaterials used for its electrodes [10].

With respect to the advancement of nanotechnology in the past few years, scientists and engineers are showing their great passion and interest in learning to hybridize different kinds of nanomaterials in the effort of tailoring the physicochemical properties of the hybrid nanomaterials [11]. Such hybridization of emerging nanomaterials is reported to exhibit superior physicochemical properties which is better than any other reported single nanoparticles. It is well known that a single nanomaterial does not have all superior properties, which is required for a specific application, making them uncompetitive to be employed [12]. Hybrid nanomaterials can be defined as a combination of two or more components constituted at nanometre scale, integrating the intrinsic physical and chemical properties of the constituent materials simultaneously and is expected to yield better physicochemical properties that is useful for energy storage and heat transfer applications compared to that of individual nanomaterial,

benefitting from the rise of synergistic effects between the materials. Hybrid nanomaterials offer the flexibility to alter their properties simply by modifying their composition and morphology, providing us with a tailored material composed of superior physicochemical properties such as high thermal stability, mechanical strength, electrical conductivity, optical properties and controlled wetting features [13] [14]. For instance, the introduction of graphene (G) into aluminium oxide ($Al_2O_3$) by Selvaraj et al. [15] has created G/$Al_2O_3$ hybrid nanofluids with high surface area, permitting more heat to be conducted and thereby exhibits a superior heat transfer enhancement. It is well acknowledged that the preparation of $Al_2O_3$ mono nanofluids is quite challenging at neutral pH state as it possess a high stability of dispersion at higher pH numbers, which is not suitable for its practical application as a heat transfer fluid, considering the effect of nanofluid at alkaline pH may cause the metallic surfaces to corrode [16]. By encasing the alumina with graphene shell, the water-based hybrid nanofluids can achieve its high suspension stability at pH 7 accompanied by enhanced physicochemical properties, benefitting from the outstanding stability, thermal and electrical conductivity of graphene nanoparticle as well as its synergistic effect with alumina. In addition, the hybrid nanofluids also demonstrated only an insignificant drawback in pumping power cost since it provides a much better heat transfer enhancement compared to the stable alumina mono nanofluid dispersion. n another work, Tong et al. [17] inserted multi-walled carbon nanotubes (MWCNT) into iron oxide ($Fe_3O_4$) nanofluid in the effort of nurturing the photo-thermal energy conversion efficiency. The addition of MWCNT into $Fe_3O_4$ not only enhanced thermal conductivity but it also recorded an improved photo-thermal energy conversion efficiency, providing almost two times augmentation of efficiency compared to that of single $Fe_3O_4$ nanofluids as a result of the outstanding thermal and optical properties of MWCNT. Even though $Fe_3O_4$ has its own ability to enhance thermal properties by subjecting it to the magnetic field, it can be further tuned by the addition of MWCNT. MWCNT not only enhanced the thermal conductivity of the hybrid nanomaterials, but it also provides excellent dispersion stability in the base fluids as $Fe_3O_4$ nanoparticles can be easily bound to MWCNT nanoparticles, owing to its unique cylindrical structure.

As a result, a chainlike structure of MWCNT/$Fe_3O_4$ hybrid nanofluids can be formed under the magnetic effect, providing an efficient thermal energy transportation that is beneficial for heat transfer applications.

In the effort of improving electrochemical energy storage, Li et al [18] introduced graphene as the solution to the relatively small sized MXene (~ 200 nm). The hybrid inks between MXene ($Ti_3C_2T_x$) nanosheets and electrochemically exfoliated graphene has given rise to an alternately stacked structure, providing a profusion surface area which is lucrative for the ion's liberations. The formation of MXene layers in between the graphene nanosheets served as an active material and ideal connection to ease the ion transports and electron movements. In addition, $Ti_3C_2T_x$ MXene sheets also behaved as a conducting spacer within the graphene layers which eventually can hinder the formation of re-stacked π–π graphene nanosheets, thus enabling such hybrid combinations to exhibit excellent volumetric capacitances. Bharath et al [19] also reported good electrochemical properties between trimanganese tetraoxide ($Mn_3O_4$) and reduced graphene oxide (rGO) hybrid nanomaterials for the application of capacitive deionization (CDI). Hybridising a wire-like $Mn_3O_4$ on graphene-based nanomaterials seems to possess a fast-Faradaic reaction since the nanocomposite exhibits a broader active material that offers a much greater conductivity route for easy ion movements, providing them an ideal pseudocapacitive behaviour. The addition of rGO to the typical pseudocapacitive site of $Mn_3O_4$ can create an electrode with excellent electrical conductivity, which may provide higher energy storage capacity.

Even though hybrid nanomaterials show a significant improvement in energy storage and heat transfer applications, which may lead them to superior performance of energy conversion and storage devices, the synthesis, preparation, design and their usage into practical applications still remains as a huge challenge. In regards to the continuation of research on nanotechnology, a few published papers have recently discussed the application of hybrid nanomaterials in heat transfer fluids such as the work by Yang et al. [20] and Gupta et al. [21]. These two review papers have comprehensively discussed the

factors that govern the performance of hybrid nanofluids and also the important physical parameters that should be taken into account. However, only few emphasises has been put on how particular hybridization synthesis routes are useful or unique for their extensive applications, especially for heat transfer fluid applications in which the priorities were always given to the preparation of nanofluid consisting of one or two steps methods. It is widely acknowledged that nanomaterials used for a particular application portray a significant contribution in achieving outstanding performance and a highly efficient system. Therefore, in this paper we have focussed on how a particular synthesis route of hybrid nanomaterials are beneficial for their extensive applications. Besides that, most of the review papers associated with hybrid nanomaterials are focussing on one particular application such as only for electrochemical energy storages, heat transfer fluids and also medical applications. In view of that, in this paper, we combine and summarize the recent advancement made on hybrid nanomaterials and the importance of developing such emerging multifunctional hybrid nanomaterials for energy storage and heat transfer applications. In section two, we provide the general overview of the emerging nanomaterials comprising MXene, graphene, carbon nanotubes and metal oxides. In the next section, we have discussed the common synthesis techniques of hybrid nanomaterials along with their obtained structures, relating on how a particular synthesis route is useful for their extensive applications. The practical applications of hybrid nanomaterials in electrochemical energy storage devices and their applications as heat transfer fluids in advanced heat transfer devices will be discussed in section four. Lastly, we also highlight some issues and challenges faced by hybrid nanomaterials. This article review intends to give the general overview of the published works related to hybrid nanomaterials which consists of their major findings and the recent progress made.

## 2. The Emerging Nanomaterials

It is widely acknowledged that the advancement of technology is driven by the emergence of nanomaterials. With these kinds of emerging nanomaterials, a new and highly efficient system can be created as a result of their peculiar properties that are beneficial in improving the overall performance

of the system [22]. Nanotechnology can be defined as a sort of toolbox in which it allows the creation of nanomaterials with special and emerging properties. Employing these kinds of emerging nanomaterials will not only improve the system but it could also play an integral part in the revolution of technology. Therefore, the exploration of new nanomaterials that will lead to that goal are of paramount importance in nanotechnology. In this section, some of the emerging nanomaterials corresponding to the application in energy storage and heat transfer fluids will be discussed.

## 2.1 Carbon Nanotubes

Carbon nanotubes (CNTs) are allotrope of carbon which consists of rolled graphite sheets that are tubular in shape. CNTs comprise of two types depending on how it is rolled up: Single-walled carbon nanotubes (SWCNTs) and Multiple-walled carbon nanotubes (MWCNTs) as shown in Figure 1. CNTs have diameters that vary from <1 nm up to 70 nm and the lengths of several microns [23]. SWCNTs are composed of single layer graphene in which it requires a catalyst for synthesis and their bulk synthesis is quite complex since it needs a proper control of growth and atmospheric condition. It also suffers from poor purity as it possesses higher chances of defect during functionalization. SWCNTs also can be easily twisted due to its single layer graphene. In contrast, MWCNTs are made up of multiple layers of graphene where it does not need any catalyst for the synthesis process and their bulk synthesis is much easier compared to SWCNTs. MWCNTs also possess a high purity as it only has small chances of defect during the functionalization process. In addition, MWCNTs are difficult to be twisted due to their multiple layers of graphene [24].

CNTs comprise three different structural forms which are *armchair, zigzag and chiral*. The formations of CNTs mainly depend on the use of the chiral vector concept which results in a pair of integers *'n'* and '*m'* that correspond to the number of unit vectors along the two directions in the honeycomb crystal lattice [25]. The formation of *zigzag* structure can be achieved when $m=0$ whereas *armchair* structure arises when $n=m$. *Chiral* structure can be formed when $n>m>0$ and this kind of structure is believed to give huge contributions to the electrical, mechanical and optical properties of CNTs [26].

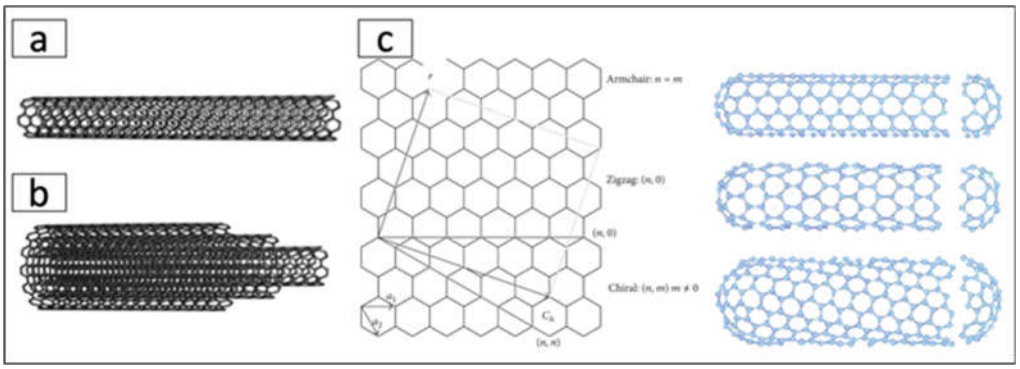


Figure 1: Representation of (a) SWCNTs, (b) MWCNTs, and (c) formation of CNTs with three different structural forms: *armchair, zigzag* and *chiral* tubes [25].

The unique structure of CNTs offers a combination of superlative mechanical, thermal and electronic properties, making them a promising candidate for energy storage, sensing and heat transfer applications. CNT's Young modulus has values greater than 1 TPa which is 5 times greater than steel [24].It also exhibits high thermal conductivity at RT ~3000 W/mK, which is expected to be higher than diamond [26]It is noteworthy that the electrical properties of CNTs can be classified as metallic or semiconducting, depending on the relationship of the axial direction and the unit vectors which describe the hexagonal lattice.

## 2.2 Graphene

The introduction of Graphene in 2004 has unlocked a new era in the field of science and technology [23]. Graphene, a carbon formation composed of a single layer of $sp^2$-bonded carbon atoms, which densely packed into a hexagonal crystal lattice is considered as a rising star and has attracted considerable attention in various fields such as heat transfer and energy storage as well as sensors, catalysts, electrodes, and in biological applications [27]. The honeycomb lattice is the building block of all carbon allotrope materials: it can be muffled to 0D fullerenes, rolled into 1D carbon nanotubes or stacked to form 3D graphite when the layers of single honeycomb graphitic lattices are subjected to a weak van der Waals force, as schematically shown in Figure 2 [28].

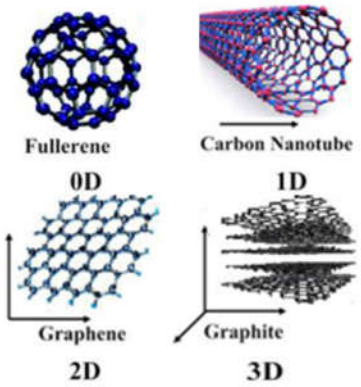


Figure 2: The building block of all carbonaceous material at different dimensions [28].

In single layer graphene, each of the covalently bonded carbon atoms is essentially $sp^2$ hybridised. The tightly packed arrangement of carbon atoms along with the $sp^2$ orbital hybridization, which is a mixture of *s,* $p_x$ and $p_y$ orbitals will give rise to the formation of σ-bond. Hence, the stable hexagonal structure of graphene is due to the existence of these three σ bonds connections. It should be mentioned that in the honeycomb structure, each carbon atom is covalently held by three distinct carbon atoms where all of them are $sp^2$ hybridized, leaving one free electron for every carbon atom. This free electron is then being held by the final $p_z$ orbital which lies on the top of the plane, forming the π bond. The hybridization of the π bond with another π bond will lead to the formation of the π-bands and π*-bands which generally contribute to the numerous graphene's outstanding physical and chemical properties, through their half-filled band that permits the free electrons to move [29], [30]. Graphene may exist in the form of nanoribbon where their energy barrier can be tuned by controlling the width of the nanoribbon. Such an energy barrier can be increased by decreasing the width of the nanoribbon [34]. This kind of property has made graphene a favourable material for electronic devices. Similar to CNT, the graphene edge can be categorized into two: *zigzag* and *armchair* which depends on the carbon chains (Figure 3). Typically, graphene with a *zigzag* edge is a metal while graphene with an armchair edge can be either metal or semiconductor, which could conduct electricity [29].

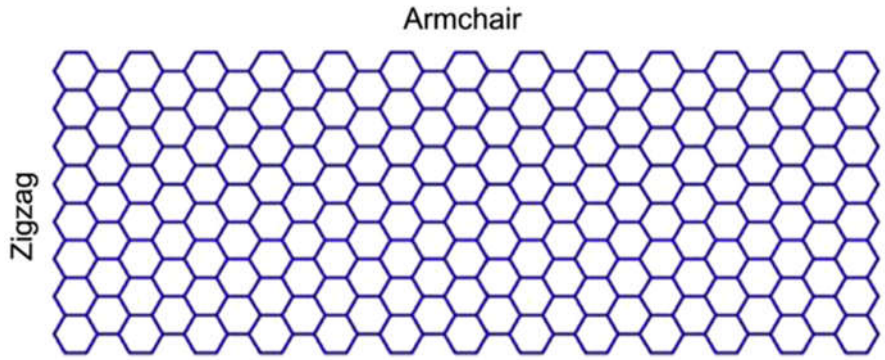


Figure 3: Graphene nanoribbon with two different edges. Reproduced from Reference [29] with permission from Elsevier.

Owing to the unique 2D structure, graphene exhibits outstanding physical and chemical properties. With a conductivity of $10^6$ S/m, graphene emerges as the most conductive material at room temperature (RT) accompanied by a sheet resistance of 31 Ω/sq, as a result of its extremely high carrier mobility of 2 x $10^5$ $cm^2$/V-s which is 140 times greater than the mobility of silicon. This is useful for ultrafast electronics and optoelectronics applications [31]. Graphene also possesses a high thermal conductivity (~ 5 x $10^3$ W/mK, 10 times better than copper at RT [32], high optical properties (97.7 %, only 2.3 % of visible light is absorbed) [33], high mechanical properties (Young's modulus of ~ 1.0 TPa and a tensile strength of ~ 130 GPa) [31] and extremely high specific surface area (theoretically, 2675 $m^2$ $g^{-1}$)[38], suggesting it as a potential candidate for energy storage and heat transfer applications. It should be noted that graphene has two main derivatives known as graphene oxide (GO) and reduced graphene oxide (rGO). GO can be achieved by oxidation of graphite, which is usually accompanied with an extensive modification of the basal plane while rGO can be produced by reducing the GO using any physical or chemical process e.g. thermal or acid treatment in the effort of reducing its oxygen content [39]. In general, GO is a chemically treated graphene which mainly consist of different functional groups e.g. hydroxyl, epoxy and carboxyl, permitting GO to be attached with other molecules. The rGO can be considered identical to that of pristine graphene. However, it has oxygen-containing groups along with some defects in which it can be controlled by manipulating the degree of oxygen reduction [40]. A schematic representation of graphene and its derivatives synthesis routes is depicted in Figure 4. A summary of various synthesis techniques from recent literature is also given in Table 1,

highlighting the experimental parameters obtained and some important findings. Further information regarding the available synthesis techniques and properties of graphene and its derivative can be found in these two recommended articles; [30] and [34].

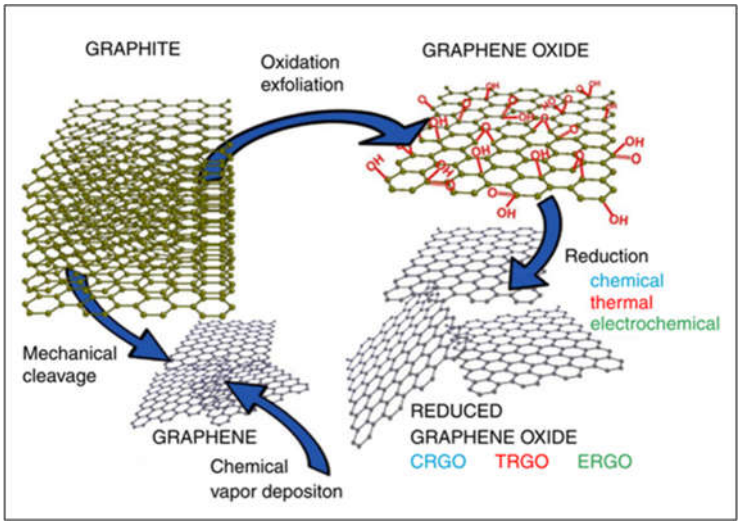


Figure 4: A schematic illustration of the possible ways to synthesis graphene and its derivatives [35].

Table 1: Summary on some available synthesis techniques of graphene.

| Synthesis Techniques | Physical Parameters/ Characteristics | Important Findings | Limitations | Reference |
|---|---|---|---|---|
| Tape-peeling | Few hundreds nm to ~1 $\mu$m, Few layers | ▪ Graphene thickness are controllable<br>▪ Can produce uniform few layers<br>▪ Low defects | Very small production scale when the number of peelings are increased | [36] |
| Chemical exfoliation via two-steps microwave irradiation | Few hundreds $\mu$m, Multilayered of thin graphitic structure | ▪ Synthesis of graphite to graphene only takes about 15 min<br>▪ Have a good electrical conductivity of ~ $2.03\times10^5$ S $m^{-1}$<br>▪ High quality with only few structural defects. | Graphene sheets obtained have a trace of stacking | [37] |
| Ball milling - ultrasonication process | Few layers | ▪ High production with low cost. | Have some structural defects as a result of the ball milling process. | [38] |
| Pyrolysis of 6H-silicon carbide | 0.7-0.8 nm, single layer | ▪ High quality graphene | Expensive starting material: 6H-SiC crystal | [39] |

| | | | | |
|---|---|---|---|---|
| | | ▪ Few defects of graphene can be obtained using 2000 °C with the flow of Ar at 15 Torr. | | |
| Plasma CVD | 7.5 $\mu$m, single layer | ▪ Hydrogen species act as etchant which activates surface bound carbon.<br>▪ High quality graphene is produced at 850 °C, over the power of 50 W.<br>▪ Increasing the plasma power will accelerates the growth rates of graphene. | Extreme increase of plasma power will lead to the growth of stacked graphene | [40] |
| Thermal CVD | Few $\mu$m, very thin layer | ▪ High quality but low in small production scale.<br>▪ Reduced the wear rate by ~ 6%. | Have small defects due to the impurity effect of Cu. | [41] |

## 2.3 MXene

Over the last few years, MXene - an emerging family of two dimensional (2D) atom thick material extracted from transition metal carbides, nitrides or carbonitrides has received prime attention since its discovery in 2011 by Naguib et al. [42]. MXene comes under the spotlight after showing remarkable electrical and electrochemical properties for various applications especially in energy storage due to its good electronic, optical and plasmonic properties, surface hydrophilicity, metallic conductivity and chemical stability, benefitting from their intrinsic 2D atomic layered structures [43][44]. Since MXene does not have the elementary 3D precursor, it must be derived by selectively etching the A layers from the precursor MAX phases with designated chemical formula of $M_{n+1}AX_n$, where M represents an early transition metal, A is IIIA or IVA group element, X stands for carbon and/ or nitrogen and n = 1-3. MAX phases seem to have multi-layered hexagonal structures in which the A layers are alternately stacked between $M_{n+1}X_n$ units [10]. Because the M-X bonds primarily consist of covalent and ionic bonds, it is much stronger than the metal bonds of M-A, giving the possibility for A layers to be separated from the MAX phase due to its relatively weak M-A layer binding force [45]. As a result of the A layer removal, MXene which could be formulated as $M_{n+1}X_nT_x$ can be achieved where $T_x$ designates as surface termination i.e. -OH, =O and -F functional groups (Figure 5) [46]. It should be noted that MXene produced in chemical etching will always introduce a surface termination of O, OH,

F or probably a concoction of all elements depending on the type of chemical environment used, rendering them hydrophilicity and capable of solution processing [47]. It is also eminent that termination exists when transition metal spontaneously reacts with water or fluoride ions. The existence of functional group in MXene will lead to the formation of semiconducting functionalized MXenes e.g. $Ti_3C_2(OH)_2$ while pristine MXenes ($Ti_3C_2$) are always metallic [48]. To date, there are about 70 MAX phases discovered but only a few MXenes have been established using etching method such as $Ti_3C_2$, $Ti_2C$, $(Ti_{0.5}, Nb_{0.5})_2C$, $(V_{0.5}, Cr_{0.5})_3C_2$, $Ti_3CN$, $Ta_4C_3$, $Nb_2C$, $V_2C$ and $Nb_4C_3$ [49]. The first kind MXene, 2D titanium carbide ($Ti_3C_2$) was fabricated by using hydrofluoric acid (HF) etching process at RT (50% HF for 2h) [42].

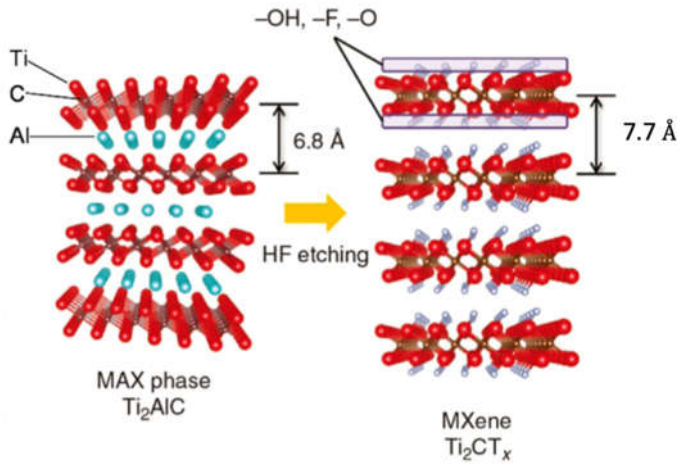


Figure 5: Schematic illustration for the formation of MXenes with surface terminations [46].

A common synthesis route of MXenes usually comprises two steps: etching and exfoliating as shown in Figure 6. The MAX bonds are quite strong to be separated by any mechanical processes. In order to exfoliate MXene, an etching process must be carried out to break the strong chemical bond between the elements of M and A in the MAX phase. Since the more chemically functionalized A atomic layers cause the M-A bonds and interatomic A-A bonds to be less strong compared to that of M-X bonds [50], the etching process can simply be done by treating MAX phase with chemical agents e.g. a solution of HF at a particular concentration with a specific amount of time without breaking M-X bonds [51]. The reaction of the HF solutions with $Ti_3AlC_2$ MAX phase will terminate the metal surface

with the functional groups (-OH and -F). The reactions involved can be summarized using the following equations:

$$Ti_3AlC_2 + 3HF = AlF_3 + 3/2\ H_2 + Ti_3C_2 \quad (1)$$

$$Ti_3C_2 + 2H_2O = Ti_3C_2(OH)_2 + H_2 \quad (2)$$

$$Ti_3C_2 + 2HF = Ti_3C_2F_2 + H_2 \quad (3)$$

MAX powders are then subjected under centrifugation followed by washing with deionized water until its pH reaches the range of 4 and 6. The solution is then filtered to obtain MXene. It should be noted that without exfoliation/delamination, MXene will consist of multi-layered structures. The layered structures are further subjected to ultrasonication to obtain a single layer of MXene, however, continuous sonication for a long time might break the MXene sheets or give an effect on the edges of the lamellar structure [51]. It is also important to note that HF is not the only etchant available to synthesis MXene. A summary on different use of etchants along with their conditions to synthesis MXenes is given in Table 2.

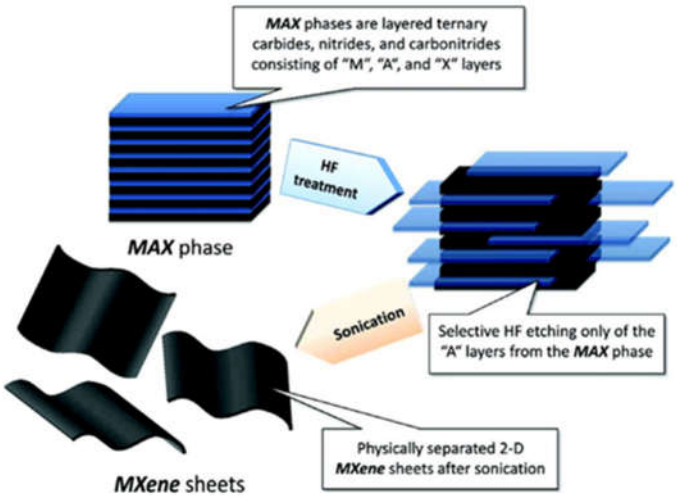


Figure 6: Schematic of the synthesis route of MXene. Reproduced from Reference [43] with permission from ACS Publications.

Table 2: Summary of different etchants used to synthesis MXene along with their conditions.

| Method | Etchants | MAX | MXene | Conditions | Reference |
|---|---|---|---|---|---|
| Non-fluorine | Ultraviolet (UV) irradiation | Ternary nanomilated Carbide ($Mo_2GaC$) | $Mo_2C$ | Magnetic stirring at 1000 rpm under UV light (100 W, distance ~8 cm), 3-5 h | [52] |
| Acid with Fluorine | Hydrofluoric acid, HF + Hydrogen peroxide, $H_2O_2$ | Titanium Silicon Carbide ($Ti_3SiC_2$ ) | $Ti_3C_2$ | 40°C, 45 h | [53] |
| Hydrothermal | Sodium Hydroxide (NaOH) | Titanium(IV) Carbide ($Ti_3AlC_2$) | $Ti_3C_2T_x$ | 270 °C with 27.5 M NaOH | [54] |
| Acid with Fluorine | Ammonium hydrogen difluoride ( $NH_4HF_2$) | $Ti_3AlC_2$ | $Ti_3C_2T_x$ | 60 °C, 8h | [55] |
| Acid with Fluorine | Hydrochloric acid, HCl + Lithium fluoride, LiF | $Ti_3AlC_2$ | $Ti_3C_2T_x$ | 1350 °C, 2 hours | [56] |
| Electrochemical | HCl | Titanium aluminum carbide lump ($Ti_2AlC$) | $Ti_2C$ | Ball milled for 24 hours at 300 rpm, 1400 °C, 4 hours, Argon gas flow | [57] |
| Molten Salt | LiF + Sodium fluoride, NaF + Potassium fluoride, KF | Titanium Aluminum Nitride ($Ti_4AlN_3$) | $Ti_4N_3T_x$ | 550 °C for 30min, Ar atmosphere | [58] |

One of the emerging properties of MXenes is their metallic conductivity. Pristine MXene usually possess a metallic behaviour due to the high electron densities near the Fermi level. This metallic behaviour can be adjusted with the formation of the additional Ti-X bonds. MXenes can possess a

narrow band-gap semiconductor behaviour by inserting the functional groups [59]. Surface functionalization that exists on the MXene surface plays a vital role in manipulating the electronic properties of MXene. Since it can change the electronic properties of MXene thus, it is important to analyse it based on their synthesis routes [60]. Surface terminations are responsible for reducing the density of states (DOS) causing the d band to lift up on top of the Fermi level, thereby, allowing the creation of a band gap. This occurs as a result of the integration of *d* orbitals of M elements with the *p* orbitals of surface functionalization [48]. It is noteworthy that F and OH terminations exhibit identical effects on MXenes electronic structures because they allow the acceptance of a single electron. In contrast, oxygen termination results in a different behaviour since it accepts two electrons at equilibrium state. Thus, the electronic structures of MXene are mainly governed by the type of M and X atoms along with their surface terminations. MXene can exist in the form of metallic, semi-metallic and semiconducting types, depending on the morphological structures and surface terminations. In general, a good connection (no gaps) between individual flakes and large flakes size will result in highly conductive MXene. It is reported that electrical conductivities of $Ti_3C_2T_x$ can be up to 9880 S $cm^{-1}$ for low defects MXene flakes while it can be 850 S $cm^{-1}$ for highly defective MXene flakes [61]. Lowering HF concentrations and etching time can produce a MXene with fewer defects. Besides that, MXene also possesses an outstanding thermal conductivity (e.g. Silicene ($Sc_2CF_2$) has 722 $Wm^{-1}$ $K^{-1}$) which is beneficial for electronic devices and for the heat transfer process. In general, thermal conductivity of MXene depends on lateral size and can be tailored by manipulating the flake length. It is also reported that MXene nanosheets dispersed in solution possess excellent electrical conductivity and outstanding optical properties, suggesting its great potential to be applied in photo-electronics, energy storage devices, sensing applications, transparent conductive coatings and photo-thermal conversions [59]. For example, the use of vacuum free solution processable electrohydrodynamic atomization (EHDA) technique reported by Ali et al. [62] resulted in a conductive MXene-based transparent films, indicating the outstanding optical transmittance of ~86.7% at a thickness of 135 nm

along with the low resistivity of 3.4 x $10^{-4}$ $\Omega$ cm. Increasing the film thickness will lead to the decrease of the optical transmittance and the increase of resistivity. The drastic decrease of electrical conductivity is due to the increase in grain boundaries, which is not favourable for electron flow. Detailed information regarding the synthesis route, properties and potential applications of MXene can be found in these two recommended literatures [48][60]. One of the major challenges in employing MXene as the electrode materials in electrochemical energy storage is that their functional groups terminations were anticipated to extremely affect their electronic, optical, mechanical, and magnetic properties. Due to the removal of the Al layer, $Ti_3C_2Ti_x$ layers seem to possess lower electrical conductivity than its precursor, $Ti_3AlC_2$. Etching Al layer will cause MXene structure to re-stack and eventually create a very dense structure, which is not favourable for ion movements due to the reduction of specific surface area resulting in inefficient performance of electrode materials [45].

## 2.4 Metal Oxides

Besides MXene, Graphene and CNTs, metal oxides nanoparticles also play a vital role in the field of materials science and engineering as a result of their excellent and unique physicochemical properties such as high surface-to-volume ratio, quantum size effect and electrodynamic interactions, which makes them differ from bulk materials [63]. Metal oxides are widely used in energy storage technologies, benefitting from their ability to generate charge carriers when energy is applied. With a wide variety of oxidation states, metal oxides are commonly employed as electrode materials for redox charge transfer [64]. It is also reported that dispersing metal oxides in the base fluids will result in heat transfer enhancements, which is beneficial for heat transfer fluids in photo-thermal conversion and also cooling process [65]. Owing to their high intrinsic surface to volume ratios, metal and metal oxides are not only able to enhance the heat transfer properties, but it also provides an improved suspensions stability which leads them to a better thermal management for high temperature energy application compared to the usage of conventional fluids, which possess low thermal conductivity [66]. In addition, metal oxides are also useful in harnessing solar energy because of its high optical properties

and ability to withstand high temperatures. However, the usage of single metal oxides dispersions remains as a huge challenge because it does not have all favourable properties which hinders them from extensive applications. It may either have better thermal conductivity or rheological properties. For instance, aluminium oxide possesses outstanding thermal stability and chemical inertness, however it suffers from poor electrical conductivity [65]. In certain cases, metal oxides could be one of the emerging nanomaterials. For instance, MXene has excellent electrical conductivity and low diffusion barrier. However, the surface termination of O, OH and/or F groups on MXene sheets will cause the specific capacity of $Ti_3C_2T_x$ to decrease. In order to overcome this drawback, MXene nanosheets must be integrated with transition metal oxides (TMOs). TMOs have been extensively evaluated as the promising lithium-ion battery (LIB) anode candidates since they have high specific capacities but poor electrical conductivity and large volume changes during lithiation and delithiation process. In this regard, Kong et al. [67] integrated MXene nanosheets with $Fe_3O_4$ and reported that a desirable electrochemical performance of anode material was obtained, providing high specific capacity and remarkable electrical conductivity due to the synergistic effect between the two materials. Examples of the common metal oxides used are spinel ($Li_4Ti_5O_{12}$) and transition metal oxides (TMOs) (e.g., Mn, Cu, Co, and Ti oxides) [64].

Overall, easy synthesis and ability to maintain high purity during the functionalization process, good resistance against twisting and its unique combination of superlative mechanical, thermal and electronic properties making the CNTs a promising candidate for energy storage, sensing and heat transfer applications. Importantly, due to the unique 2D structure and outstanding physio-chemical properties of graphene with high thermo-electrical conductivity, high opto-mechanical properties and extremely high specific surface area dominates as a potential candidate for energy storage and heat transfer applications. Mentionable that for the synthesis of CNTs and graphene with manageable chirality, predetermined size, layers or length, super-alignment still stays in enormous challenges. Additionally, the powerful coupling among the CNTs or graphene structures, production procedures,

post-treatments, properties as well as applications are yet obstacles. On the other hand, 2D MXenes attracts as another encouraging nominees in the modern energy storage implications as due to their high metallic conductivity, packing density as well as pseudocapacitive performance towards the improved areal and volumetric capacitances. However, for the efficient and highly scalable synthesis techniques of MXenes such as secure etching agent than acids are still in major bottleneck for the implementation in energy storage application. Besides a high surface-to-volume ratio, quantum size effect and electrodynamic interactions of metal oxides nanoparticles are also widely used in energy storage technologies, benefitting from their ability to generate charge carriers. However, owing to their high intrinsic surface to volume ratios and low thermal conductivity they are better in thermal management in high-temperature energy application rather in conventional fluids.

## 3. Hybridization of Nanomaterials

Hybrid nanomaterials can be synthesised using physical and chemical routes. In general, physical synthesis routes offer a much easier way to hybridize the nanomaterials without any strict requirement to go through the complex steps. In contrast, chemical synthesis routes require some chemical treatment and must be strictly controlled [45]. For the hybrid nanofluids preparation, the hybrid nanomaterials will be synthesized firstly before dispersing it into the base fluids. This section will discuss the preparation of hybrid nanomaterials for its extensive applications in electrochemical energy storage and heat transfer fluids.

### 3.1 Physical Methods

#### 3.1.1 Mechanical Mixing

Mechanical mixing involves the use of mechanical devices such as magnetic stirrer and ultra-sonicator to aid the dispersion of nanomaterials. The usage of these mechanical devices is able to prevent the prepared nanomaterials from stacking or agglomerates. Van et al. [68] prepared the ethylene glycol based nanofluid of graphene-carbon nanotubes (CNT) hybrid nanomaterials by directly mixing the

nanoparticles under ultrasonication. Before dispersing the hybrid nanomaterials into the base fluids using the ultrasonication technique, graphene and MWCNT nanoparticles were terminated with different functional groups including -OH and -COOH by treating them with the mixture of nitric acid ($HNO_3$) and sulphuric acid ($H_2SO_4$) (Figure 7a). With the surface modification and the aid of ultra-sonicator, graphene-CNT hybrid nanoparticles were dispersed homogenously without any agglomeration due to the existence of molecular bonding of COOH and OH groups (Figure 7f-g). Graphene-CNT hybrid nanofluids demonstrated an outstanding thermal conductivity improvement with 50 % enhancement relative to the base fluids at 50 °C with the particle concentration of 0.07 vol.%, owing to the combination of superior thermal conductivity of CNT and graphene along with the large surface area possessed by graphene-CNT hybrid nanomaterials (Figure 7h).

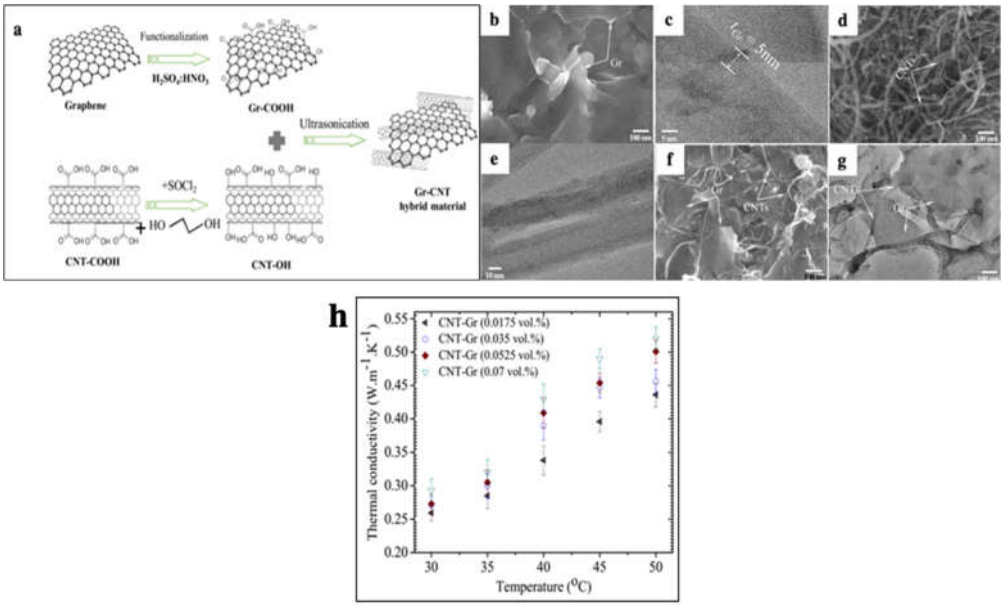


Figure 7: (a) Schematic representation of mechanical mixing procedure for synthesis of graphene-CNT hybrid nanomaterials. SEM and TEM images of (b) and (c) graphene; (d) and (e) CNTs; (f) and (g) graphene-CNT hybrid nanocomposites; and (h) thermal conductivity of graphene-CNT hybrid nanofluids at different temperatures and concentrations. Reproduced from Reference [68] with permission from Elsevier.

Zhao et al. [69] fabricated MXene and reduced graphene oxide ($Ti_3C_2T_x$/rGO) hybrid nanocomposites using the ultrasonication technique for the high performance supercapacitors. The rGO powder was first dispersed in ethanol by using the ultrasonication followed by the mixture of $Ti_3C_2T_x$ powder in the solution. The composite was then filtered from the solvent and dried at 80 °C for 12h. From the

FESEM images of $Ti_3C_2T_x$ (Figure 8a-b), it can be seen that MXene sheets possess a typical multi-layered structure, which is favourable for ion transport due to the large surface area, leading to an improved pseudo-capacitance performance. When rGO was integrated with $Ti_3C_2T_x$ layers, a further surface modification of $Ti_3C_2T_x$ structure was obtained where rGO served as conductive bridge and nanoscale collector for the movement of electrons (Figure 8c). The presence of rGO could connect the different blocks of $Ti_3C_2T_x$ which enables the improvement of the contact area and thus ease the electronic movement process to the current collector, producing an outstanding electrochemical performance of the electrode.

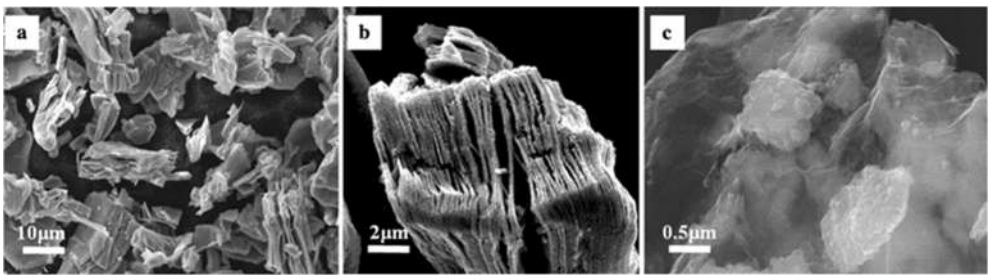


**Figure 8:** FESEM images of (a) $Ti_3C_2T_x$, (b) enlarged view of $Ti_3C_2T_x$ in (a), and (c) $Ti_3C_2T_x$/rGO nanocomposites. Reproduced from Reference [69] with permission from ACS Publications.

### 3.1.2 Self-assembly method

In order to create electrostatic self-assembly interaction, it requires two materials: a poly-electrolytes that is usually soluble in water or have strong adsorption capability, and a material that is opposite in charges to that of polyelectrolytes. When these two nanometre-size materials are combined together, polyelectrolytes tend to adsorb it as a result of the interaction between the two opposite charges, producing a stable nanocomposites material. This method is simple as it is able to produce a stable hybrid nanomaterials without any chemical bonds [70].

Jin et al. [71] synthesized the alternately stacked manganese dioxide-MXene ($MnO_2$-$Ti_3C_2$) and manganese dioxide-reduced graphene oxide ($MnO_2$-rGO) hybrid nanomaterials using the electrostatic derived self-assembly method. The electrostatic interaction between the positive charge of $Mn^{2+}$ possessed by $MnO_2$ and the negative surface charges of $Ti_3C_2$ and rGO nanosheets make them possible for the preparation of homogeneous combinations of hybrid nanomaterials that are highly stable. As

can be seen in Figure 9a, the obtained colloidal mixtures of $MnO_2$-$Ti_3C_2$ and $MnO_2$-rGO hybrid nanomaterials were synthesized using the electrostatic self-assembly of $H^+$ since $MnO_2$-$Ti_3C_2$ mixtures possess negative zeta potential while $MnO_2$-rGO possess negative surface charge. The FESEM images in Figure 9b clearly shows the presence of uniformly nano-porous structures of 2D nanosheets, indicating the homogenous mixture of $MnO_2$-$Ti_3C_2$ and $MnO_2$-rGO hybrid nanomaterials while Figure 9(c-d) shows the TEM analysis of the interrupted nano-porous stacking structure of the extremely thin 2D nanosheets along with the elemental mapping analysis. The synthesized hybrid nanomaterials of $MnO_2$-$Ti_3C_2$ exhibits a better electrochemical performance compared to that of $MnO_2$-rGO, indicating the favourable integration of MXene nanosheets with $MnO_2$ as a hybridization matrix in escalating the electrochemical performance of metal oxide as shown in Figure 9(f-i). The hybridization matrix of MXene is able to provide huge contributions to the $MnO_2$ electrode performance as it enhances the interfacial coupling, porosity and ion diffusivity due to the significant increase in surface area (active sites) for ion transport. The outstanding performance of the $MnO_2$-$Ti_3C_2$ hybrid nanomaterials can be related to their low tendency of self-stacking due to favourable combination of the two nanoparticles, hydrophilic in nature and high rigidity of $\pi$ electron-free MXene nanosheets.

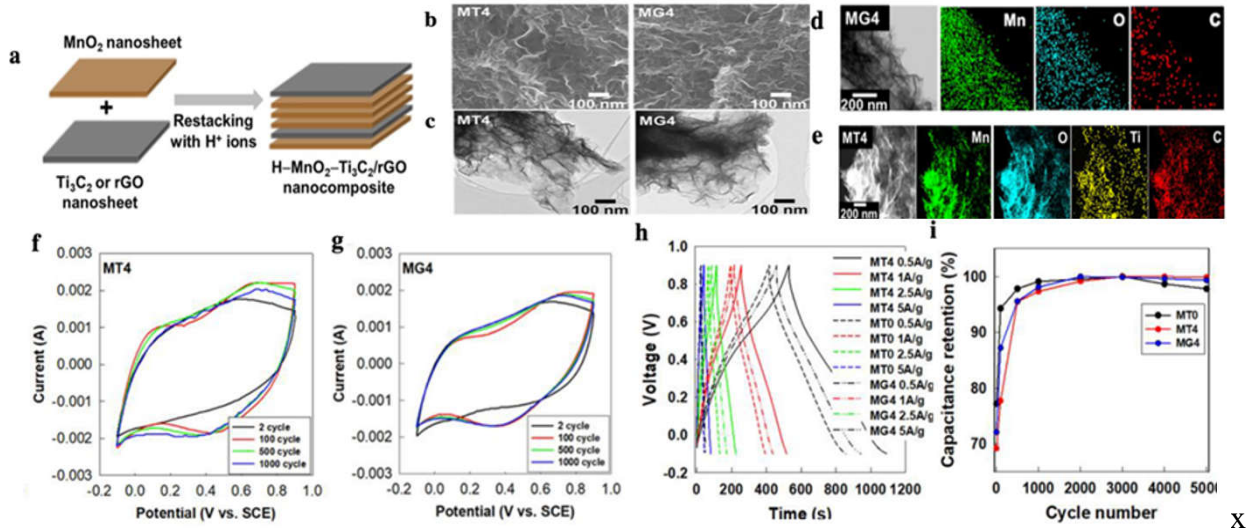


Figure 9: (a) A schematic illustration for the synthesis route of hetero-layered MT and MG hybrid nanomaterials. (b) FESEM, (c) TEM, and (d, e) TEM-elemental mapping data of the MT and MG nanocomposites. (f, g) CV curves for MT and MG nanocomposites, (h) CD curves, and (i) capacitance retention plots for the MT and MG nanocomposites. Note that MT and MG represent as $MnO_2$-$Ti_3C_2$

and $MnO_2$-rGO hybrid nanomaterials, respectively. Reproduced from Reference [71] with permission from Elsevier.

## 3.2 Chemical Methods

### 3.2.1 Hydrothermal

Hydrothermal method is one of the common synthesis routes for hybrid nanomaterials, which mainly depends on the solubility of aqueous solution under hot water and high temperature. To operate, it requires an autoclave (strong container) filled with a solution to withstand the high temperature and pressure. Typically, the precursor is put into the autoclave at a certain temperature for a particular amount of time, which is then followed by any necessary post-treatment e.g. washing and drying [51]. Recently, Wang et al. [72] fabricated fibre-like rGO/MXene hybrid nanomaterials under the low temperature of 60 °C using a facile one-step self-assembled hydrothermal method (Figure 10a). The hydrothermal treatment not only generates a reduced graphene oxide, but is also able to integrate GO with MXene nanosheets, forming a hybrid nanomaterial composed of a robust skeleton of large graphene sheets filled with MXene nanosheets between the spaces. It is reported that the surface morphologies of the obtained hybrid nanomaterials demonstrated an uneven surface along with irregular wrinkles when compared to that of pure rGO, indicating the incorporation of $Ti_3C_2T_x$ layers with rGO. With the increased mass of $Ti_3C_2T_x$, the uneven surface roughness of the hybrid nanomaterials becomes more prominent due to the large size discrepancies between the two materials (Figure 10b-d). The Energy Dispersive X-ray Spectroscopy (EDS) mapping further confirmed the presence of $Ti_3C_2T_x$ in graphene nanosheets (Figure 10e). The as prepared fiber-like hybrid nanomaterials were reported to possess an outstanding electrical conductivity of 1339 S $m^{-1}$ with large volumetric and gravimetric capacitance albeit with low particle loading of MXene, benefitting from the rise of synergistic effects between the two materials. In addition, the integration of these two nanomaterials is able to prevent MXene sheets from being oxidised when they are subjected under the high temperature. Graphene layers act as a protector to that of MXene sheets especially for the low particle loading of MXene.

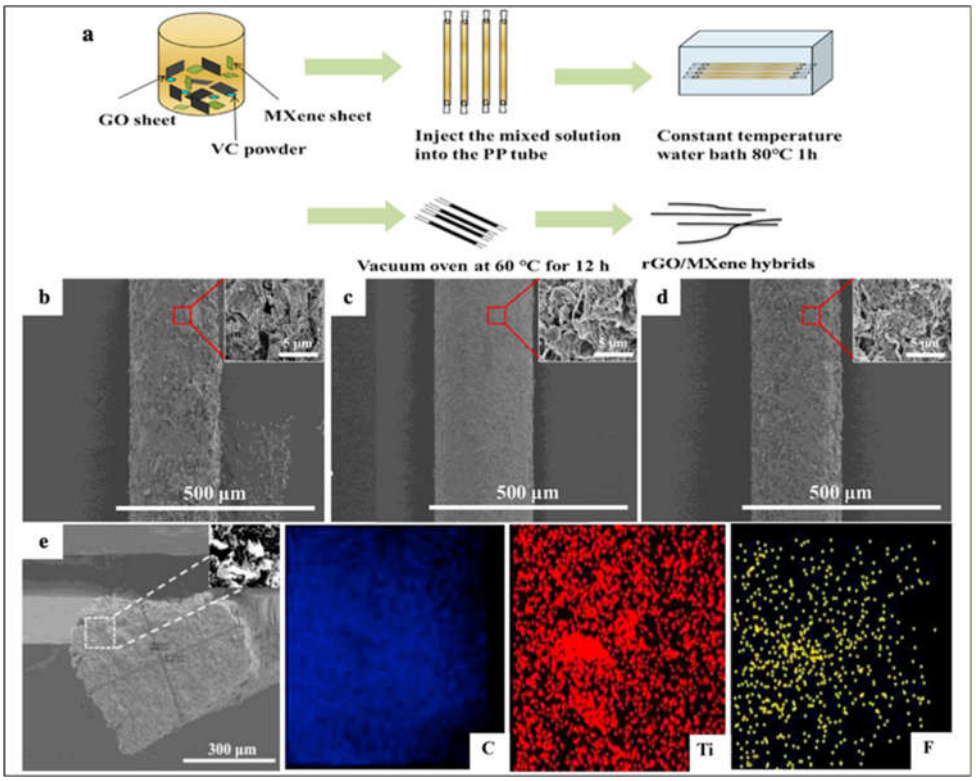


Figure 10: (a) Schematic illustration for the fabrication procedure of rGO/MXene fibre-like hybrid nanomaterials. SEM images of (b) rGO/ $Ti_3C_2T_x$ -5, (c)rGO/ $Ti_3C_2T_x$ -10 and (d)rGO/ $Ti_3C_2T_x$ -15; (e) SEM image of the cross section rGO/ $Ti_3C_2T_x$ -5 along with the EDS mapping of C, Ti and F. Reproduced from Reference [72] with permission from Elsevier.

In another work, Bharath et al. [19] employed the hydrothermal synthesis process to fabricate $Mn_3O_4$/rGO nanocomposites with hierarchical pores in the effort of improving the ion transport pathways (Figure 11a). With the use of hydrothermal treatment at the temperature of 180 °C for 12 h, $Mn_3O_4$ nuclei were generated from the intermediate phases of manganite (MnOOH) while graphene oxide (GO) was transformed into rGO, leading to the homogeneously immobilization of $Mn_3O_4$ on the surface of rGO nanosheets due to the presence of negatively charged oxygen moieties on the rGO. It should be noted that the oxygen moieties on the rGO plays a significant role in providing the anchoring sites for easy attachment of manganese nuclei. A well crystalline and uniform sized of $Mn_3O_4$ nanowires formed on the rGO nanosheets can be clearly observed on Figure 11(f-g). The unique structure of this wire-like $Mn_3O_4$/rGO is able to provide large active sites for the ion transport, allowing the favourable contact between $Mn_3O_4$/rGO electrodes and electrolytes for energy storage applications.

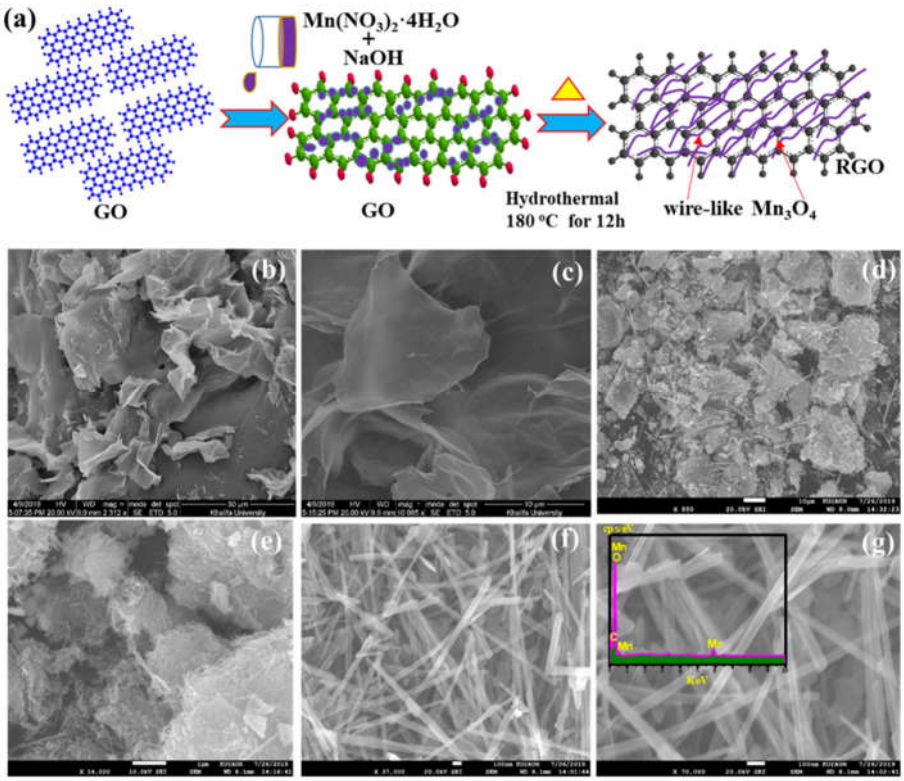


Figure 11: (a) A schematic illustration for the synthesis route of wire-like $Mn_3O_4$/rGO hybrid nanomaterials, (b and c) FESEM images of GO, (d-f) FESEM images of $Mn_3O_4$/rGO hybrid nanomaterials and (g) EDS of $Mn_3O_4$/rGO hybrid nanomaterials. Reproduced from Reference [19] with permission from Elsevier.

### 3.2.2 Solvothermal Method

In addition to the hydrothermal method, the solvothermal method is also one of the simple and feasible methods to synthesis hybrid nanomaterials. Like the hydrothermal method, the solvothermal method also requires an autoclave to operate. Through the solvothermal synthesis route, the size, shape distribution and nanostructure products can be tuned simply by changing the reaction temperature, reaction time, surfactant used and also the nanomaterials' precursor.

Wu et al. [9] used the solvothermal method to synthesis tin sulfide-graphene nanosheets ($SnS_2$-GNS) hybrid nanocomposite. By employing a solvothermal method, the uniform layer of $SnS_2$ can be grown on graphene nanosheets through covalent bonds, creating $SnS_2$ nanoparticles integrated with graphene nanosheets as shown in Figure 12. Hybridising graphene nanosheets with $SnS_2$ was able to prevent the graphene sheets from being cross linked and re-stacking. Like $SnS_2$, a stand-alone $SnS_2$ nanoparticles

will lead to the formation of large pieces of structure, which tends to be self-assembled into a flower-like shape, creating a very dense structure which is unsuitable for ion transports. By using this synthesis route, $SnS_2$-GNS hybrid nanocomposites were able to deliver a superior lithium storage performance which was much greater than any other Sn-based materials reported. This outstanding lithium performance was achieved owing to the existence of synergistic effect between the two nanomaterials. It was also revealed that carbon materials can be easily integrated with Sn-based nanomaterials using this process in addition to the ball milling and hydrothermal method.

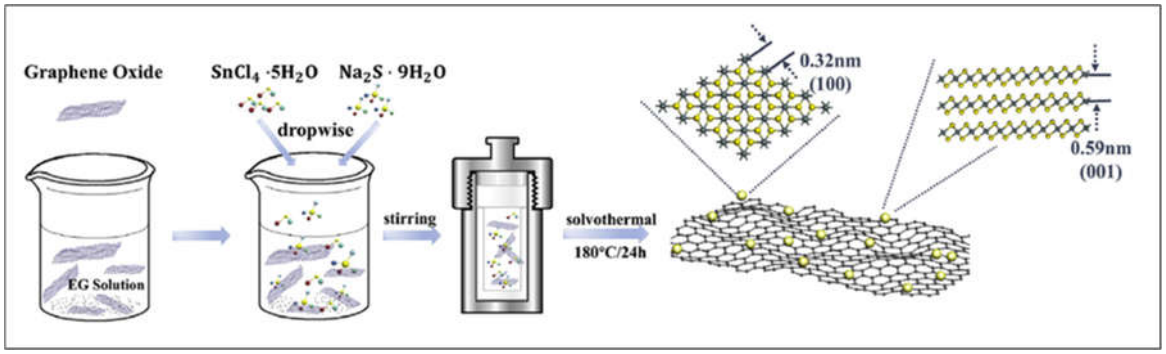


Figure 12: Schematic representation for the solvothermal method used to synthesis $SnS_2$@GNS hybrid nanocomposite. Reproduced from Reference [9] with permission from Elsevier.

### 3.2.3 *In Situ* Growth Method

Besides the hydrothermal method, the synthesis route *via in situ* method also shows a promising way in obtaining hybrid nanomaterials for energy storage and heat transfer applications. *In situ* growth refers to a synthesis process that is conducted in the same place of reaction mixtures without isolating or altering the original condition. It should be noted that *in situ* method is beneficial for allowing a uniform particle growth on the surface of the substrate because it is able to prevent the introduction of impurities and the synthesis processes are usually conducted under the mild conditions [73].

Kong et al. [67] synthesized iron oxide-MXene sheets ($Fe_3O_4$-$Ti_3C_2$) hybrid nanomaterials using *in situ* method by growing the $Fe_3O_4$ nanoparticles on the multi-layered $Ti_3C_2$ in the effort of enhancing the electrochemical performance of the anode electrodes (Figure 13a). With the MXene substrate, $Fe_3O_4$ is reported to be growth homogeneously with a uniform distribution of nanoparticles that are

bound with a strong chemical combination. It should be noted that without the MXene substrate, $Fe_3O_4$ tends to clump and agglomerate. As shown in Figure 13(c-e), the increase of $Fe_3O_4$ content will cause the particle size to increase due to the addition of $Fe^{2+}$. The variation of $Fe_3O_4$ nanoparticles content can be seen clearly from the TEM images of $Fe_3O_4$@$Ti_3C_2$ nanocomposites as depicted in Figure 13(f-h). The nanocomposites recorded a superior electrochemical performance as a result of the excellent capacity of the magnetite and a favourable electrical conductivity of $Ti_3C_2$ which make them suitable for Li-ion storage. In addition, the rate capacities of nanocomposites were also significant when tested at high currents. When compared with previous researches using the same material and content of nanocomposites, it is reported that the *in situ* formed of $Fe_3O_4$@$Ti_3C_2$ nanocomposites provide a much higher capacity than that of physically mixed $Fe_3O_4$@$Ti_3C_2$ nanocomposites.

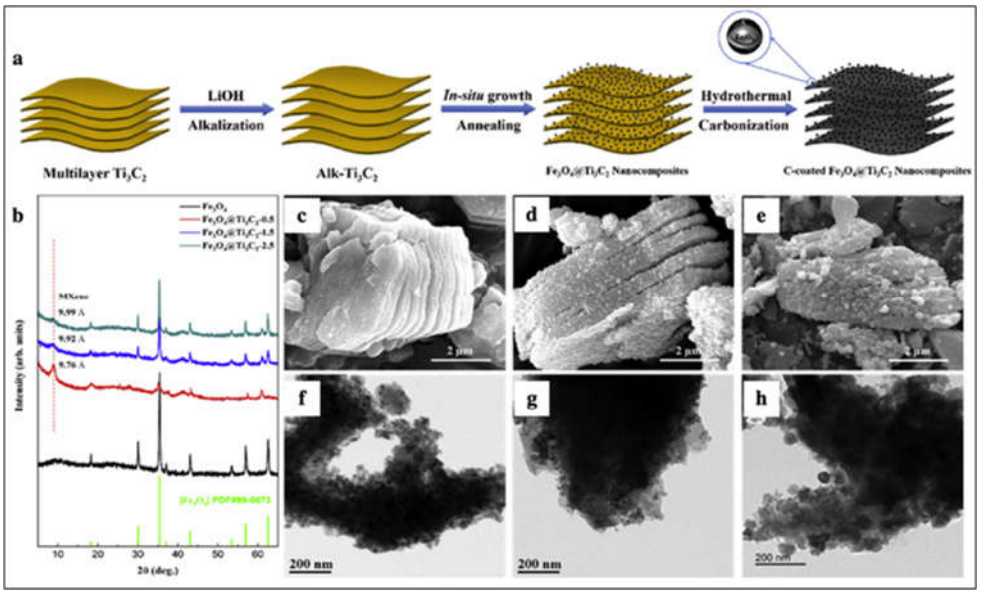


Figure 13: (a) A schematic illustration for the fabrication of $Fe_3O_4$@$Ti_3C_2$ hybrid nanomaterials, (b) XRD patterns of $Fe_3O_4$@$Ti_3C_2$ nanocomposites and pure $Fe_3O_4$, (c-e) SEM images of $Fe_3O_4$@$Ti_3C_2$-0.5, $Fe_3O_4$@$Ti_3C_2$-1.5, and $Fe_3O_4$@$Ti_3C_2$-2.5, and (f-h) TEM images of $Fe_3O_4$@$Ti_3C_2$-0.5, $Fe_3O_4$@$Ti_3C_2$-1.5, and $Fe_3O_4$@$Ti_3C_2$-2.5. Note that the value of 0.5, 1.5 and 2.5 represent the addition of $FeCl_2 \cdot 4H_2O$ in unit mmol. Reproduced from Reference [67] with permission from Elsevier.

Sundar et al. [74] also prepared nano diamond-nickel (ND-Ni) nanocomposites for its application as hybrid nanofluids using *in situ* growth and chemical co-precipitation method in order to enhance the performance of hybrid nanomaterials as a heat transfer fluid. With the aid of acid treatment on the

surface of ND, the Ni nanoparticles can be grown on the ND surface due to the existence of carboxyl (COOH) layers. It is reported that the homogenous dispersion of ND-Ni nanocomposites in the base fluids has led to the thermal conductivity and viscosity enhancements of 29.39% and 23.24%, respectively with the particle concentration of 0.3 wt% at 60 °C compared with the base fluid of distilled water.

In another work, Li et al. [75] synthesized CNTs@$Ti_3C_2T_x$ nanocomposites for the high performance of supercapacitor electrodes where CNTs were *in situ* grown on $Ti_3C_2T_x$@PDA layers via simple pyrolysis method, utilising urea as the source of carbon (Figure 14). The thin layer of polydopamine (PDA) coated on the surface of $Ti_3C_2T_x$ acts as a protective cover which contributes to high structural stability of $Ti_3C_2T_x$. As a result, $Co^{2+}$ was introduced on the surface of $Ti_3C_2T_x$ due to the exchange between positively charged Co ions and phenolic hydroxyl in PDA. The pyrolysis process at 900 °C for 1 hr in an Ar atmosphere causes $Co^{2+}$ to be oxidised and reduced to Co nanoparticles which acts as a catalyst to grow the CNTs. With Co catalyst, urea will be fully converted into carbon nitride gases and it will grow as CNTs via *in situ* method. The growth of CNTs on $Ti_3C_2T_x$ leads to the enlargement of interlayer space of $Ti_3C_2T_x$ which provides a favourable channel for electrolyte transport.

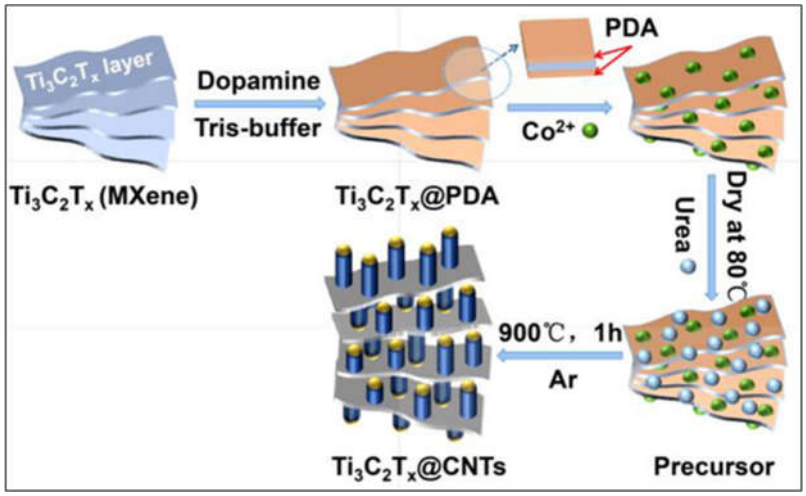


Figure 14: A schematic illustration for in situ growth synthesis of CNTs@$Ti_3C_2T_x$ nanocomposites. Reproduced from Reference [75] with permission from Elsevier.

### 3.2.4 Heat Treatment Method

Thermal reduction method is another route to prepare the hybrid nanomaterials. It is simpler, user-friendly and more economic path compared to the other techniques. This method is also one of the favourable methods to achieve high purity of nanoparticles e.g. graphene, Zinc oxide (ZnO) and etc. [76][77]. It is also reported that thermal reduction method using microwave irradiation is more effective where the reaction time can be reduced significantly.

Shen et al. [78] prepared spinel lithium titanate-MXene ($Li_4Ti_5O_{12}/Ti_3C_2T_x$) hybrid nanomaterials by treating the mixture of LiOH/ $Ti_3C_2T_x$ with the high temperature calcination of 800 °C for 5 hours under the Ar atmosphere (Figure 15a). Calcination refers to a thermal process used to synthesis materials before shaping or dispersing it in which its temperature and environment must be strictly controlled. It is intended to produce a stable form of a material so that decomposition, shrinkage or other reactions do not occur when it is heated again. The use of high temperature calcination is able to reduce lithium hydroxide (LiOH) to $Li_4Ti_5O_{12}$. However, it should be noted that the amount of LiOH gives a significant contribution in the formation of $Li_4Ti_5O_{12}/Ti_3C_2T_x$ nanocomposites. Excessive content of LiOH will give rise to the creation of $LiTiO_2$ which may cause the conductive path of $Ti_3C_2T_x$ layer to break, leading to the degradation of the sample's performance as shown in Figure 15b. Figure 15(c-h) clearly shows progressive damage of the layer structure with additional amount of LiOH. The optimized T-LTO-B (hybrid nanomaterials which corresponds to the addition of 0.5 g LiOH) demonstrated a remarkable electrochemical performance with an improved rate capability, benefitting from the effective $Li^+$ diffusion path, superior conductivity and high structural stability of nanocomposites. The enhancement of electrochemical properties may be associated with the enlargement of electrode active materials that is beneficial for electrolyte contact, contributed by the combination of 0D/2D nanocomposite and also due to the relatively high conductivity of $Ti_3C_2T_x$ nanolayer.

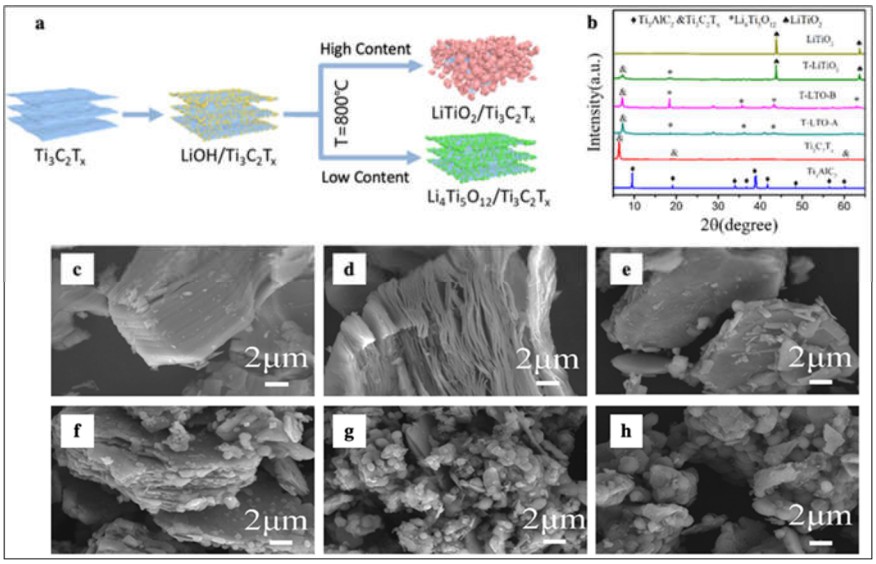


Figure 15: (a) Schematic diagram of the fabrication of $Li_4Ti_5O_{12}/Ti_3C_2T_x$ hybrid nanocomposites, (b) XRD patterns of the samples. FESEM images of: (c) $Ti_3AlC_2$, (d)$Ti_3C_2T_x$, (e) T-LTO-A, (f) T-LTO-B, (g) T- $LiTiO_2$, and (h) $LiTiO_2$. Note that T-LTO-A, T-LTO-B, T- $LiTiO_2$, and $LiTiO_2$ corresponding to the addition of 0.25 g, 0.5 g, 1.0 g and1.5 g LiOH, respectively. Reproduced from Reference [78] with permission from Elsevier.

Furthermore, Tu et al. [79] used a microwave-assisted reduction strategy to prepare multi-layered reduced graphene oxide sheets with TiN nanoparticles hybrid nanocomposite (TiN/rGO) under $N_2$ atmosphere at 1200 °C from the precursors of $TiO_2$/GO. In general, the formation of TiN using gas/solid phase reaction under conventional heating methods cannot be easily achieved due to the very strong N≡N covalent bonding [80]. However, microwave irradiation was able to synthesis TiN/rGO easily along with the good crystallinity and dispersion due to its lower initial reaction temperature and uniform accelerated temperature distribution during the heating process [88]. The hybrid nanocomposites were reported to be favourable for sulphur host material because it allows free movement of lithium ions and electrons. In addition, the uniform distribution of TiN nanoparticles that were bonded on the graphene surface served as an adsorbent that was able to trap lithium polysulfides (LiPSs) due to the superior chemical interaction.

At the end of this section, it can be said that hybridization of nanomaterials has been conducted with the aid of various physical and chemical synthesis routes. Mentionable, physical synthesis routes are

pretend to be much easier than the chemical synthesis routes in terms of strict requirement and complex steps. Among the physical approaches, mechanical mixing process involves the use of mechanical devices to disperse the nanomaterials uniformly and preventing them from stacking or agglomerations. Besides, self-assembly method is a simple route without any chemical bonds implemented to create electrostatic self-assembly interaction between the two materials which able to produce a stable nanocomposites material. Also, hydrothermal and solvothermal synthesis routes been employed for the hybridization of nanomaterials. In these techniques an autoclave is used filled with a solution to withstand the high temperature and pressure. However, solvothermal synthesis route, the size, shape distribution and nanostructure products can be tuned simply by changing the reaction time and temperature, surfactant used as well as the precursor of the nanomaterials. On the other hand, *in-situ* growth method has also showed a promising way in obtaining hybrid nanomaterials for energy storage and heat transfer applications. It is conducted in the same place of reaction mixtures without isolating or altering the original condition, which is beneficial for allowing a uniform particle growth on the substrate surface as well as offers the prevention of impurities formation. Lastly heat treatment method is also discussed as one of the simpler and economic paths to prepare the high purity hybrid nanomaterials. It uses microwave irradiation for more effectivity with a significant reduction of reaction time.

## 4. Application of Hybrid Nanomaterials

### 4.1 Hybrid Nanomaterials in Energy Storage Application

#### 4.1.1 Electrochemical Energy Storage

Energy storage devices are a built-in apparatus which can be used to store a certain amount of energy and transmitting it when necessary. In addressing the current energy crisis to counter global warming, the development of energy storage technologies in the field of renewable energy becomes stringently important. To date, major problems for most electrode materials include poor volume expansion,

inadequate interlayer spacing, incapable of solution processing and low conductivity due to surface oxidation or defects, which hinders their extensive applications in electrochemical energy storage and conversion [81][82]. The use of suitable active materials, e.g. hybrid nanomaterials capable of encountering all of these major problems is an indispensable factor to the high performance, cost-effective and environmentally friendly energy storage devices. Hybrid nanomaterials are expected to offer a large specific surface area that is beneficial for providing a greater extent of active sites for enhancing the energy storage capacity [83].

#### 4.1.1.1 Supercapacitors

The development of supercapacitors plays a significant role in meeting the tremendous growth in energy demands. Supercapacitor is known as an electrical energy storage device that is able to store electricity by creating electrical double layers at the interface of electrodes [48]. It is different from the ordinary capacitor due to its exceptionally high capacitance. The energy storage mechanisms in supercapacitors arise as a result of the electrostatic interaction between the polarized surface of the porous carbon electrode and the electrolyte which forms the electric double layer, rendering a fast response time to charge and discharge the devices [84] [85]. In addition, supercapacitors also offer a greater recharge cycle lifespan, enabling them to be facilitated in hybrid vehicles and backup power stations. Despite having a higher power density compared to batteries, the commercialization of supercapacitors remains a big challenge due to their low energy density, which is influenced by its electrodes capacitance and the working voltage of the cell [86].Thus, in the attempt to escalate the energy density of the supercapacitor, the enlargement of the electrode's capacitance or the working voltage of the devices becomes obligatory. Recently, enormous effort has been made to improve the capacitance of the electrodes since it will affect the availability of surface area for the creation of the electrically charged double layer. In general, 3D carbon often provides complex ion diffusions compared to 2D nanosheets which usually expose their active sites directly to the electrolyte. 2D nanosheets are expected to provide a larger specific surface area, effective ion diffusion path and good

electron conductivity, which will contribute to high electrochemical performance [45]. It is well known that a large surface area will be able to accommodate more electrolyte ions, which in turn increase the double layer capacitance. This will give rise to a higher capacity of charge storage, hence, increasing the capacitance value [83][87]. Figure 16 shows the structure design of different types of two dimensional nanomaterials which will lead to the optimal performance of flexible supercapacitors.

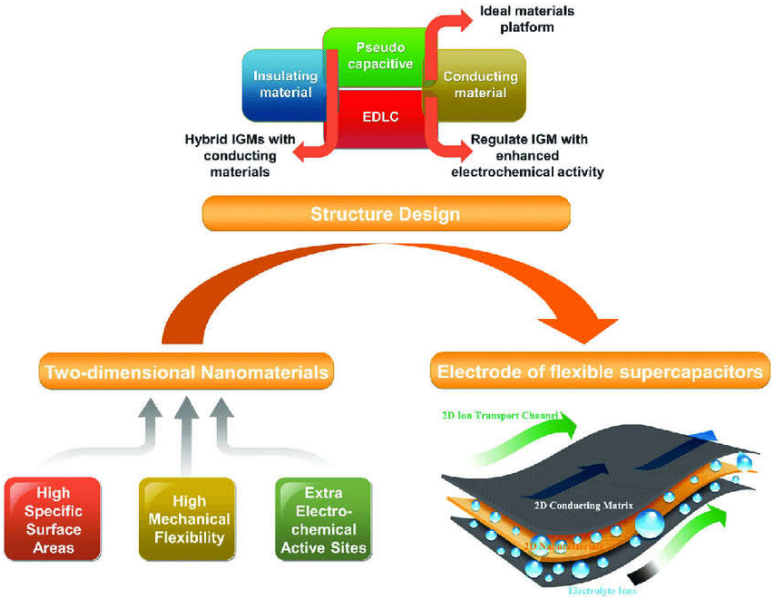


Figure 16: Schematic illustration from 2D nanomaterials to the electrodes of flexible supercapacitors. Reproduced from Reference [88] with permission from The Royal Society of Chemistry.

Recently, Hwang et al. [89] demonstrated that moderate specific surface area of graphene and single walled carbon nanohorn composites (SWCNH) with high bulk density can contribute to high electrochemical performance. They reported that the volumetric capacitance-voltage (CV) curve of the spray-dried reduced graphene oxide and single walled carbon nanohorn composites being treated with nitric acid, $HNO_3$ (rS-GO/NHO) displayed a common double-layer capacitive behaviour with rectangular CV curve, demonstrating its lower resistivity compared to the commercial activated carbon (AC) which displayed an elliptical CV curve of a much higher resistance (Figure 17a). The introduction of SWCNHs is to prevent the graphene nanosheets from being self-restacked during the reduction process. Even though SWCNHs offer a relatively low specific surface area around 400 $m^2$ $g^{-1}$, this surface area can be further enlarged by treating it with a simple chemical treatment known as

the "hole opening process". The highly nano-porous structure of rS-GO/NHO exhibits a superior volumetric capacitance of 80 F $cm^{-3}$ whereas the commercial AC only exhibit 57F $cm^{-3}$ when measured at 1 mA $cm^{-2}$ even though its specific surface area is larger than rS-GO/NHO with the values of 1928 and 786 $m^2$ $g^{-1}$, respectively (Figure 17b). This magnificent result is associated with the high bulk density appearing in the rS-GO/NHO nanocomposites, indicating the excellent electrical conductivity possessed by the favourable combination of GO/SWCNH. Note that the measured bulk density for the rS-GO/NHO and commercial AC are 1.23 and 0.65 g $cm^{-3}$, respectively. The Nyquist plot of charge transfer resistances $R_{ct}$ in Figure 17c also showed that rS-GO/NHO had the lowest charge transfer resistance in the high frequency range, benefitting from the integration of a highly conductive graphene and SWCNHs. On the other hand, the charge and discharge cycling test at 10 mA $cm^{-2}$ showed that the rS-GO/NHO electrode possesses 91% retention after 10,000 cycles, while AC electrodes showed only 88% (Figure 17d).

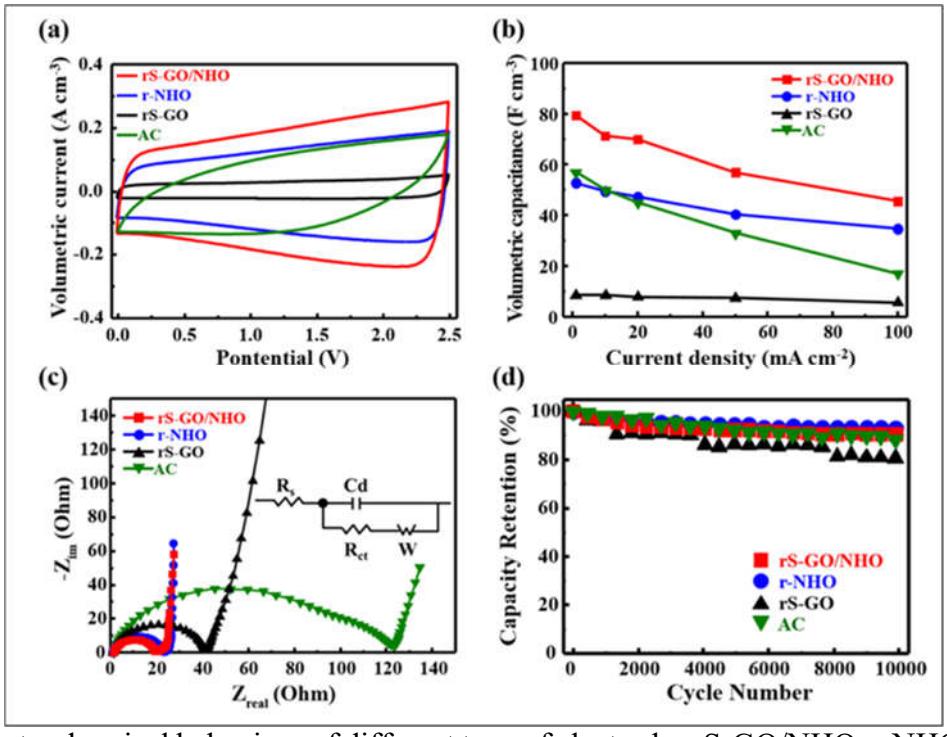


Figure 17: Electrochemical behaviour of different type of electrodes rS-GO/NHO, r-NHO, rS-GO, and commercial AC: (a) Volumetric CV curves measured at 10 mV·$s^{-1}$, (b) volumetric capacitance as a function of current density, (c) Nyquist plots, and (d) charge-discharge cycle performance at 10 mA·$cm^{-2}$. Reproduced from Reference [89] with permission from Elsevier.

Wang et al. [72] prepared fiber-like reduced graphene oxide (rGO)/MXene. With the optimal weight percentage of MXene in fiber-like hybrid, rGO/M-5 (5%wt of MXene) manifests as the highest gravimetric specific capacitance with lengthen discharge time compared to rGO/M-10, rGO-M-15 and rGO fiber. It also showed a CV curve of rectangular shape and able to remain rectangular and symmetrical triangular shapes even though at high current densities, demonstrating its superior capacitive behaviour (Figure 18a-d). Apart from that, rGO/M-5 is able to exhibit a considerably high capacitance value of 345.2 F $cm^{-3}$ at 0.1 A $g^{-1}$. The outstanding electrochemical properties is due to the synergistic effects that exist when the appropriate amount of MXene disperses homogeneously with the graphene layer. This synergistic effect causes graphene oxide to steer the fiber formation and the homogenous dispersion of MXene contributes to the electrical conductivity and volumetric electrochemical performance. It should be noted that the optimized weight of fiber-like hybrids will cause the MXene thin layers to integrate favourably with graphene fibers, preventing the graphene sheets from being restacked. This will expand the active sites of electrodes to the electrolyte, hence, shortening the ion-diffusion pathway compared to the usage of single rGO (Figure 18e). Besides that, the highly conductive MXene sheets embedded in graphene may contribute to a long-term conductivity and vigorous network, enabling the rapid transfer of electrons within the electrodes.

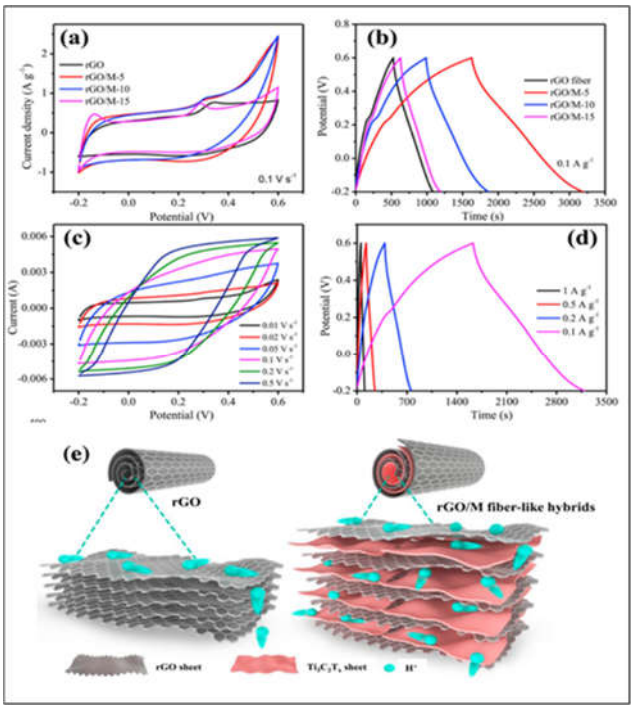


Figure 18: (a) CV curves measured at 10 mV $s^{-1}$and (b)galvanostatic charge-discharge curves at 0.1 A $g^{-1}$ for several samples; (c) CV curves at various scan rates and (d) galvanostatic charge-discharge curves at various current densities for rGO/M-5 and (e) Schematic diagram of $H^+$ ions flow during electrochemical reaction. Reproduced from Reference [72] with permission from Elsevier.

In another work, Zheng et al. [90] demonstrated that a suitable introduction of CNT decorated with nickel selenide ($NiSe_2$) may enhanced the specific capacitance because the optimal value of CNT can increase the conductivity of nanocomposites and contribute to microwave heating, as well as the reduction of $NiSe_2$ aggregation. When 20 mg CNT was employed, the nanocomposite recorded the highest specific capacitance value of 980.5 F $g^{-1}$ at 1 A $g^{-1}$ and the structure exhibited an outstanding long-term cycle stability of 82% even after 9000 cycles, showing its stable and reversible characteristics. It is also reported that the excessive addition of selenium powder will lower the specific capacitance due to unreacted selenium powder. Therefore, the mass ratio of the optimum reaction condition for $NiSe_2$@CNT nanocomposite were 20:40:20 of CNT:$Ni(NO_3)_2{\cdot}6H_2O$:Se. The introduction of nickel-selenide (Ni-Se) into CNT led to a high specific capacitance and outstanding electrochemical performance [91] due to the incorporation of the two nanomaterials.

Jin et al. [71] also compared the electrochemical performance of $MnO_2$-$Ti_3C_2$ (MT) and $MnO_2$-rGO (MG) electrodes with different weight percentages of $Ti_3C_2$ and rGO, respectively. The resulting

materials were denoted as MT/G-2, MT/G-4 and MT/G-6 for the 2, 4, and 6wt% of $Ti_3C_2$ and rGO, respectively. Among all MT hybrid nanomaterials, MT4 exhibited a much larger specific capacitance of 306 F $g^{-1}$ at 5000th cycle with an outstanding stability compared to other MT nanohybrids. Similarly, MG4 also demonstrated a larger specific capacitance of 261 F $g^{-1}$ at the same cycle compared to other MG nanohybrids. When comparing the performance of MT and MG, it is clearly observed that the hybridization of $MnO_2$ with MXene nanosheets can improve the electrochemical performance of the electrode due to the fact that the interaction of hydrophilic species ($MnO_2$) with hydrophilic species ($Ti_3C_2$) is much favourable compared to the interaction between hydrophilic and hydrophobic species, rendering a much stronger interfacial chemical interaction between $MnO_2$-$Ti_3C_2$ compared to $MnO_2$-rGO. Besides that, $MnO_2$-$Ti_3C_2$ electrode exhibits a much bigger surface area for easy ion transports compared to that of $MnO_2$-rGO, highlighting that the hybridization of $MnO_2$ with $Ti_3C_2$ nanosheets able to prevent MXene nanosheets from self-stacking, leading to a high charge storage capacity. Table 3 summarized recent studies made to date on the hybridization of nanomaterials for supercapacitors application.

Table 3: Summary of previous researches on supercapacitors application using hybrid nanomaterials.

| Electrode | Electrolyte | Maximum gravimetric capacitance (F $g^{-1}$) | Maximum volumetric capacitance (F $cm^{-3}$) | High current density cycle retention (%/ cycle-index) | Reference |
|---|---|---|---|---|---|
| Trimanganese tetraoxide-Reduced graphene oxide ($Mn_3O_4$/rGO) | 1.0 M sodium chloride (NaCl) | 437 | -- | 100/10 | [19] |
| Reduced graphene oxide-MXene (rGO/$Ti_3C_2T_x$) | 1.0 M sulphuric acid ($H_2SO_4$) | 195 | 345.2 | 124.8/7500 | [72] |
| Nickel selenide-Carbon nanotube ($NiSe_2$/CNT) | 6.0 M Potassium hydroxide (KOH) | 980.5 | -- | 82/9000 | [90] |

| | | | | | |
|---|---|---|---|---|---|
| Reduced graphene oxide-Single walled carbon nanohorn composites with nitric acid (rS-GO/NHO) | 1.0 M tetrafluoroborate ($TEABF_4$) | -- | 80 | 91/10000 | [89] |
| | 1.0 M $H_2SO_4$ | -- | 87 | 94/3000 | [89] |
| Manganese dioxide- Titanium carbide ($MnO_2/Ti_3C_2$) | 0.2 M sodium sulfate ($Na_2SO_4$) | 306 | -- | 98/5000 | [71] |
| Manganese dioxide- Reduced graphene oxide ($MnO_2$/rGO) | 0.2 M $Na_2SO_4$ | 261 | -- | 85/5000 | [71] |
| Manganese dioxide- MXene ($MnO_2$/ $Ti_3C_2T_x$) | Polyvinyl alcohol (PVA)/$H_2SO_4$ | 130.5 | -- | 90/1000 | [92] |
| MXene-Carbon nanotubes ($Ti_3C_2T_x$/CNTs) | 6.0 M KOH | 109.6 | -- | 78.1/10000 | [75] |
| Exfoliated Graphene/MXene | PVA /Phosphoric acid ($H_3PO_4$) | -- | 216 | 82/2500 | [18] |

#### 4.1.1.2 Lithium-ion Batteries

Lithium ion battery (LIB) is a rechargeable battery which usually depends on the liberation of $Li^+$ from the accommodating electrodes through the electrochemical redox reactions for the charging and discharging process. Throughout the charging and discharging processes, $Li^+$ will move back and forth between the positive (e.g. Lithium cobalt oxide, $LiCoO_2$) and negative electrodes, producing ion intercalation/ de-intercalation processes [48] (see Figure 19). LIB appeared as the most common power source in small portable electronic devices, electric vehicles, and hybrid electric vehicles due to their high energy density, low rate of self-discharge, and long cycling stability [93]. However, the limitations on the theoretical capacity of 372 mAh $g^{-1}$ and the poor rate performance of the conventional graphite anode in LIB have restricted their extensive applications [94]. Therefore, the development of energy storage devices consisting of high power and high energy density becomes essential in order to satisfy the growing energy demands.

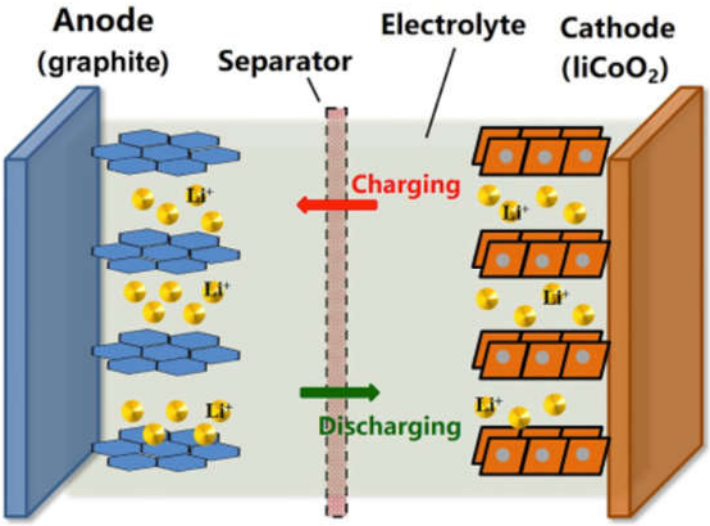


Figure 19: Schematic diagram of the lithium intercalation and deintercalation reaction mechanism in a rechargeable lithium-ion battery containing solid electrodes and a liquid electrolyte. Reproduced from Reference [95].

Generally, these energy storage advancements will depend on the innovation made for the system i.e. developing an electrode made of emerging nanomaterials that is capable of being charged and discharged at all current rates [96]. In recent years, tremendous effort has been made to develop an electrode made by emerging hybrid nanomaterials as the tailored nanomaterials are able to offer a better electrochemical performance. It is well noted that the diffusion of Li-ion is mainly influenced by the ion transport path and the active sites available at the electrode's surface. Therefore, the use of nanocomposite electrodes will not only pioneer the reaction mechanisms but is also expected to boost the electrochemical performances by producing a much higher energy storage capacity, superior charge-discharge ability and good long-term cycle stability, benefitting from the short ion diffusion path and large effective contact area between the active materials and electrolyte [96]. To examine this, Wu et al. [9] synthesised a nanocomposite of tin-sulfide ($SnS_2$) nanoparticle and graphene nanosheets (GNS) through a facile solvothermal process. The unique structure of $SnS_2$@GNS delivered a superior lithium storage performance of 1250.8 mA h $g^{-1}$ at 0.1 A $g^{-1}$ even after cycling 150 times (Figure 20a, b, d). Besides that, $SnS_2$@GNS also exhibited a much higher capacitance value

compared to single particle $SnS_2$ and rGO (Figure 20c, e). The highest coulombic efficiency of 98.53% obtained by the nanocomposite may be due to the formation of C-S bond between $SnS_2$ and GNS nanomaterials, rendering a good structural stability of the anode materials. A further test on cycle capacities of $SnS_2$@GNS at high current density of 0.5 A $g^{-1}$ confirmed that the nanocomposite achieved ~798.6 mAh $g^{-1}$ after 100 cycles without any drastic decline in capacity (Figure 20f). It is well observed that the engineered nano crystallization of $SnS_2$ and compounding it with the carbon-based materials can uplift their cycling performance and improve fast charge/ discharge process. This could be due to the large active sites available and superior adsorption of $Li^+$ contributed by the extremely thin graphene nanosheets. It is noteworthy that the addition of graphene yields large active sites for the electron and ions transportation. The unique combination of $SnS_2$@GNS also led to a remarkable impact in improving the electrochemical properties where the ultra-small particles of $SnS_2$ provided a shorter ion diffusion path whereas graphene was able to enhance the electrical conductivity of the hybrid structure

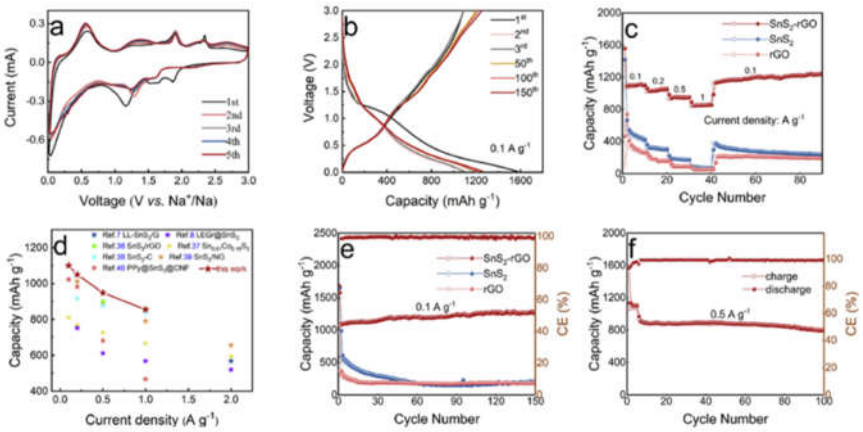


Figure 20: a) CV curves of $SnS_2$@GNS measured at 0.1 mV $s^{-1}$. b) Charge/discharge process of $SnS_2$@GNS at different number of cycles, measured at 0.1 A $g^{-1}$. c) Rate performance of $SnS_2$@GNS, $SnS_2$, and GNS. d) The comparison of rate performance behaviour of $SnS_2$@GNS with other reported $SnS_2$-based materials. e) Cycling performance of $SnS_2$@GNS, $SnS_2$, and GNS measured at 0.1 A $g^{-1}$. f) Cycle performance of $SnS_2$@GNS when measured at high current density. Reproduced from Reference [9] with permission from Elsevier.

Fang et al. [97] studied the electrochemical performance of titanium dioxide and reduced graphene oxide ($TiO_2$/rGO) nanocomposite as an anode for LIBs. As shown in Figure 21a, the nanocomposite

demonstrates a large storage capacity due to the improved conductivity and capacitive behaviour, leaving pure $Ti_2C$-$TiO_2$ nanoparticles with much lower electrochemical performance. The enhanced electrochemical performance is due to the addition of rGO, suggesting that rGO nanosheets are well integrated with $TiO_2$ nanoparticles. The introduction of GO not only gave rise to smaller $Ti_2C$ nanosheet formation but also prevented the $TiO_2$ from re-stacking. It is also reported that the increased capacity is not fully contributed by rGO only, but the enhancement of the rate ability properties of $TiO_2$ after being hybridised. The charge-discharge profiles of $TiO_2$/rGO which mainly consists of three parts: high-voltage slope, plateau, and low-voltage slope confirmed the existence of fast Li-ion storage on the $TiO_2$ surface (Figure 21b-c). A near-rectangle shape of the CV curve also confirmed that $TiO_2$/rGO possess a much larger capacity compared to $TiO_2$, demonstrating the addition of rGO contributes to high capacitive behaviour by enhancing the conductivity of the nanocomposite (Figure 21d). In addition, $TiO_2$/rGO nanocomposite showed a remarkable cycling performance with ~ 86% capacity retention after 1000 cycles, showing the outstanding structural stability of $TiO_2$ and the addition of rGO was able to prevent volume change during ion intercalations (Figure 21e).

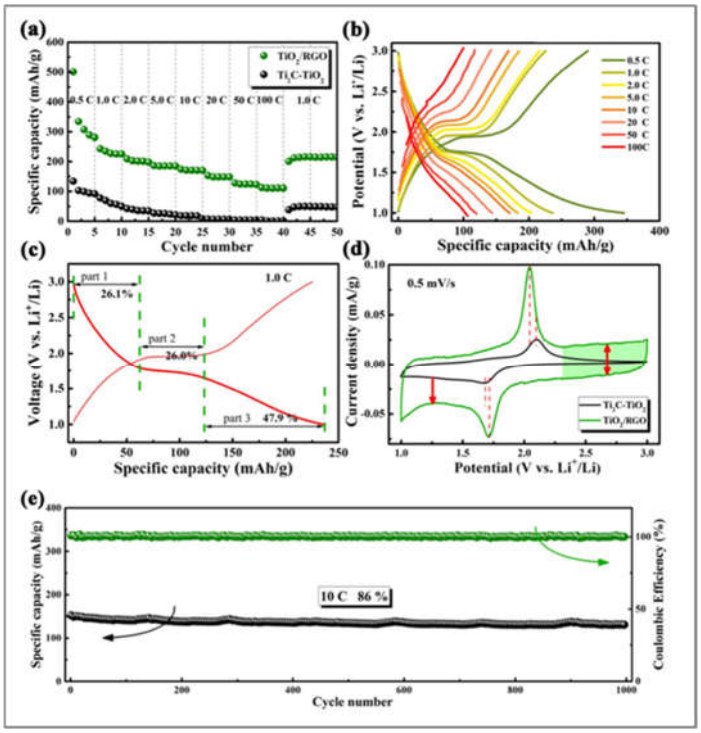


Figure 21: Electrochemical properties of $TiO_2$/rGO anode for LIBs. (a) The cycle rate performance of $TiO_2$/rGO and $TiO_2$. Charge-discharge curves of $TiO_2$/rGO at (b) different rates, and (c) 1C rate. (d)

CV curves of $TiO_2$/rGO and $TiO_2$ measured at 0.5 mV/s. (e) Cycling performance of $TiO_2$/rGO at 10 C. Note that C represents current density (1C = 168 mA $g^{-1}$). Reproduced from Reference [97] with permission from The Royal Society of Chemistry.

The use of conductive graphene with modified mesoporous anatase (M-$TiO_2$-GS) nanocomposite for flexible LIBs by Luo et al. [98] showed the outstanding $Li^+$ properties with high specific capacity of 205 mAh $g^{-1}$ at 0.5 C with 0° bending condition. To demonstrate the feasibility of the as-formed electrode, the authors bend it at 2 different angles of 90° (flat) and 180° (bent) to show its flexible properties and good electrochemical performance for flexible cells. At flat condition, the M-$TiO_2$-GS anode exhibited a reversible capacity of 200 mAh $g^{-1}$ at 0.5C and a stable cycle performance with 91.3% capacity retention over 100 cycles at 1 C. Interestingly, in a bending condition of 180°, M-$TiO_2$-GS still demonstrated a revisable capacity up to 191 mAh $g^{-1}$ at 0.5C with a better capacity retention of ~ 93.5% over 100 cycles at 1C. The good electrochemical performance was achieved because the dispersive M-$TiO_2$ was sandwiched layer-by-layer with graphene sheets, offering an effective ion transport pathway. A summary of recent researches on LIBs application using hybrid nanomaterials is given in Table 4.

Table 4: Summary of previous researches for LIBs application using hybrid nanomaterials. Note that 1C = 170 mA $g^{-1}$ and $LiPF_6$ represents as lithium hexafluorophosphate.

| Electrode | Electrolyte | Capacitance (mAh $g^{-1}$) | High current density cycle retention (%/ cycle-index) | Ref |
|---|---|---|---|---|
| $SnS_2$@GNS | 1.0 M $LiPF_6$ | 1250.8 at 0.1 A $g^{-1}$ | 98.53/150 | [9] |
| $TiO_2$-rGO | 1.0 M $LiPF_6$ | 130.6 at 10 C | 86/1000 | [97] |
| M-$TiO_2$-GS | 1.0 M $LiPF_6$ | 94 at 5 C | 70.5/3500 | [98] |
| $Li_4Ti_5O_{12}$/$Ti_3C_2T_x$ | 1.0 M $LiPF_6$ | 236 at 50 mA $g^{-1}$ | -- | [78] |
| $Fe_3O_4$@$Ti_3C_2$ | 1.0 M $LiPF_6$ | 342.9 at 1 C | 77.1/100 | [67] |
| C-coated $Fe_3O_4$@$Ti_3C_2$ | 1.0 M $LiPF_6$ | 382.9 at 1 C | 88.1/100 | [67] |

### 4.1.2 Thermal Energy Storage

Thermal energy storage (TES) has been extensively evaluated as an important technology in bringing the gap between energy demand and energy supply. TES systems are capable of storing thermal energy

supplied to it, conveying a complete storage cycle of charging, storing and discharging which enables the stored energy to be used at a later time. It should be mentioned that the storage of thermal energy can be in form of sensible heat and latent heat in which sensible heat storage stored thermal energy only by increasing the storage medium temperature, utilising rocks or water as the storage medium, whereas latent heat storage system stored energy using phase change materials (PCMs) [99]. Among these two forms of energy storage, latent heat energy storage utilising PCMs are widely used to store thermal energy owing to its massive amount of latent heat during phase change, high energy storage density and only small temperature variation due to isothermal nature of the working process which not only minimise the mismatch between energy demand and supply, but at the same time provides an environmental-friendly technologies (see Figure 22).

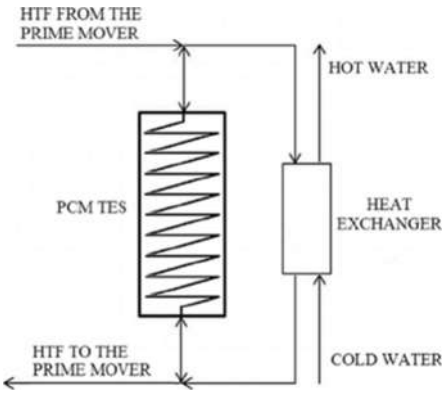


Figure 22: Schematic representation of the latent heat thermal energy storage configuration system. Note that HTF represents as heat transfer fluids. Reproduced from Reference [100] with permission from Elsevier.

With all the mentioned features, latent heat thermal energy storage using PCM emerged as one of the most effective way in storing thermal energy and it has been proved to be a desirable TES in a wide of applications such as solar energy storage, industrial waste heat recovery, intelligent air-condition buildings, electric appliance and thermo-regulated textiles [101]. Even though PCM has desirable characteristics in storing the thermal energy, it has a major drawback associated with the leaking problem during the solid-liquid phase transition which in turns increases the thermal resistance, hence, limiting its practical application. Therefore, improving the stability of PCM and also its thermal conductivity properties are the key to the highly efficient thermal energy storage system. In the past

few years, nanomaterials such as graphite foams, carbon nanotubes, graphene nanomaterials boron nitride and metal materials have been extensively studied as the supporting material for PCM, providing a desirable thermal conductivity enhancement due to the rapid heat transfer possessed by PCM and nanoparticles [102]. However, it should be noted that although these PCMs can avoid leaking or possess a remarkable higher thermal conductivity compared to that of pure PCM materials, the thermal energy storage density of composite PCMs is reduced seriously due to a portion of their working substance is replaced by supporting materials which does not undergoes phase change within their operating temperature range . Therefore, the exploration of new way in improving the stability, thermal conductivity and maintaining the energy storage density should be one of paramount importance.

In order to examine this, Qi et al. [103] evaluated the performance of latent heat thermal energy storage system utilising graphene oxide and graphene nanoplatelets with polyethylene glycol (GO/GNP/PEG) nanocomposite PCM. The authors reported that the incorporation of hybrid GO and GNP with PCM emerged as one of the effective supporting materials and conductive materials for PCM, providing a desirable thermal conductivity enhancement of 490% (1.72 W/mK) relative to that of pure PEG (0.29 W/mK), and surpassing PEG/GNP nanocomposite (1.61 W/mK) at the optimised particle loading of 2:4 for GO and GNP. The effect of addition of GO/GNP as the supporting materials to that of PEG also did not exert a negative effect towards thermal energy storage density, in which it still have 98.2% energy storage density compared to pure PEG, demonstrating its promising potential as hybrid fillers for latent heat thermal energy storage applications.

In the effort of improving the thermal conductivity of the PCM used for thermal energy storage (TES), Zhou et al. [104] prepared the rGO/GNP-paraffin microencapsulated phase change materials (MePCMs) by encapsulating paraffin with reduced graphene oxide (GO) and also graphene nanoplatelets (GNP) through self-assembly method, causing the hybrid shell to arise as a result of the $\pi - \pi$ interaction between rGO and GNP. With the optimised mass ratio (7:3 for rGO:GNP), the as

prepared MePCMs demonstrated an excellent thermal conductivity enhancement, increasing from 0.67 W/mK for PCM with only rGO shell to 0.90 W/mK (Figure 23a). The authors reported that the usage of nano-dimension sheets of rGO and GNP ease the encapsulation process especially for the extremely low content of PCM, optimising the paraffin loading and hence capable of maximising the energy storage capacity.

In another work, Sharma et al. [105] studied the performance of latent heat storage systems by utilising paraffin wax as PCM and hybrid zinc-cobalt-iron oxide nanofluid. The authors reported that by using the mixture of hybrid nanofluid, the efficiency of the thermal energy storage system is increased due to the optimisation of the charging time of PCM. The authors reported that the charging and discharging time of TES were reduced up to 25% and 20%, respectively, indicating the improved TES performance due to the addition of hybrid nanoparticles. Figure 23b depicts the difference between the charging time of PCM with and without the addition of nanofluids. As shown in Figure 23b, in order

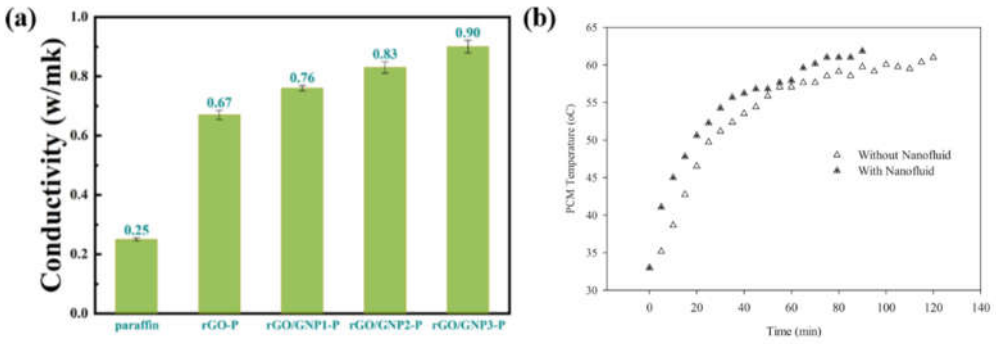


to reach a stable temperature approximately at 62 °C, PCM with nanofluid only need around 90 minutes charging time whereas PCM without nanofluid requires about 120 minutes.

Figure 23: (a) Thermal conductivity of paraffin and MePCMs at different mass ratio, and (b) Charging time of PCM with and without the addition of nanofluid. Reproduced from Reference [104] and [105] with permission from Elsevier.

Song et al. [101] evaluated the performance of thermal energy storage using halloysite-Ag/polyethylene glycol PCM (HNT-Ag/PEG). It has been reported that the usage of hybrid nanomaterials with PCM able to simultaneously provide a high latent heat storage and enhanced thermal conductivity. The optimised nanocomposite PCM (3.3 wt.%) demonstrated an outstanding

phase change temperature of 33.6 °C at a relatively high thermal energy storage density of 71.3 J/g and also a significantly enhanced thermal conductivity of 0.9 W/mK, providing almost 2.8 times augmentation of thermal conductivity enhancement compared to that of 0.2926 W/mK for a stand-alone PEG. The authors reported that the significant improvement in thermal conductivity is associated with the successful construction of numerous conductive pathways and homogenous dispersion of a continuous 3D HNT framework decorated with the highly thermal conductivity of Ag nanoparticles. Furthermore, Liu et al. [106] investigated the performance of microencapsulated PCM based on graphene oxide (GO) and carbon nanotube (CNT) hybrid filler. The optimised integration of 1D CNT and also 2D graphene sheets at 3:1 in creating a 3D nanostructure has led to a remarkable thermal conductivity enhancement of 195% with 0.6 wt.% of hybrid filler loading, an improvement of 2.95 times compared to single particle MePCM/CNT due to the synergistic effect between CNT and GO. The evaluation of thermal storage properties revealed that the encapsulation of MePCM/GO-CNT gives a higher average latent heat of 162.9 J/g compared to 158.8 J/g for a single particle MePCM/CNT, demonstrating good dispersion of MePCM/GO-CNT, thus providing more energy storage capacity.

### 4.2 Hybrid Nanomaterials in Heat Transfer Application

The advancement of nanotechnology in creating hybrid nanomaterials has influenced the creation of a new kind of nanofluid e.g. hybrid nanofluids for its extensive applications as heat transfer fluids. In general, the dispersion of hybrid nanomaterials in the base fluid are called hybrid nanofluids and it is a rapidly growing field in material science and engineering [80]. Due to the enhancement of physicochemical properties possessed by the constituent materials as a result of their synergistic effect, hybrid nanofluids received its prime attention from the various researchers around the world to evaluate its thermal performance for advance heat transfer applications. A brief summary of published work dealing with hybrid nanofluids is given in Table 5. It should be mentioned that most of the literature is focusing on the thermo-physical properties of hybrid nanofluids specifically for cooling

process ability and heat transfer applications. In the next section, we discussed the potential application of hybrid nanofluids.

In accordance with the findings, increasing the temperature and particle concentration will lead to thermal conductivity enhancement [107][108][109]. The use of high working temperature and nanoparticles concentration will give rise to intense Brownian motion due to the interaction of nanoparticles in the base fluid. Increasing the particle loading means increasing the number of suspended nanoparticles, causing the closer gap between particle-to-particle distances. This will lead to rapid increase in surface-area-to-volume ratio and collision between nanoparticles. This triggered the frequency of lattice vibration to increase, which in turn enhanced the thermal conductivity. This mechanism is known as the percolation effect [110]. With the enhanced thermal conductivity of hybrid nanofluids, it indicates the potential of such emerging combinations of nanofluids in replacing the conventional coolants in advanced heat transfer devices.

It should be noted that stability also plays a significant role in hybrid nanofluids as they are the key in preserving the thermophysical properties of the fluid. Therefore, enhancing and maintaining the nanofluids stability will lead to the outstanding performance of heat transfer fluids. It is widely acknowledged that one of the major challenges faced by nanofluids is their poor suspension stability as a result of the interaction between the particles themselves and also between the nanoparticles and the base fluid itself. This phenomenon can be related to the two opposing forces: 1)Van der Waals attractive forces that are arises on the particles surface, causing the particles to be attracted towards each other, forming clusters or agglomerations which cause them to be separated from the base fluid and become sedimented due to gravitational force, and 2) electrical double layer repulsive force that tends to separate the particles from each other via electrostatic repulsion. In this regard, a good suspension stability can be obtained if and only the electrical double layer repulsive force surpasses the Van der Waals attractive forces [111].

Table 5: Summary of previous works done for hybrid nanofluids, highlighting the important findings obtained for that particular studies. Note that DI, DW and EG represent deionised water, distilled water and ethylene glycol, respectively.

| Hybrid NM | BF | Method | Concentration | Findings | | | Ref |
|---|---|---|---|---|---|---|---|
| | | | | Stability | TC Enhancement (%) | Viscosity | |
| Multi-walled carbon nanotube-Iron oxide (MWCNT-$Fe_3O_4$) | Water-EG (80:20) | Two steps | 0.01 wt.% | Stable with no agglomeration observed for 1 month. | 8 (20 °C) | -- | [17] |
| Graphene oxide-Aluminium oxide GO-$Al_2O_3$ | DI | Two steps | 0.3 vol.% | Stable without any agglomeration up to 15 days. | 45 (25 °C) | All the prepared nanofluids possessed Newtonian behaviour in the temperature range of 20-70 °C. | [15] |
| Functionalized carbon nanofiber-reduced graphene oxide (F-CNF/rGO) | DW | Two steps | 0.04 vol.% | F-CNF/rGO hybrid nanofluids demonstrated Zeta potential value of -45 mV on the 1st day and -33.4 mV on the 180th day with no sign of visible sedimentation. | 24.6 (55 °C) | F-CNF/rGO hybrid nanofluid has the least viscosity enhancement (6.3%) compared to CNF, F-CNF and rGO nanofluids (15.2%, 12.5% and 7.2%, respectively). | [112] |
| Graphene nanoplatelets-Titanium dioxide (GnPs-$TiO_2$) | DW-EG | Two steps | 0.1 wt.% | Stable up to 40 days due to the addition of hexadecyl-trimethylammonium bromide (CTAB) as surfactant. | 21.59 (60 °C) | The viscosity enhancement for hybrid nanofluids is lower compared to that of mono nanofluids. | [110] |
| Silicon carbide-Copper Oxide with Carbon (SiC–CuO/C) | EG | Two steps | 3.13 wt.% | All samples have a good stability of dispersion even after 30 days. | 8.8 (25 °C) | The highest viscosity enhancement of 205% was observed for 3.13 wt.% | [107] |
| Single-walled carbon nanotubes-Magnesium oxide (SWCNTs-MgO) | EG | Two steps | 0.55 wt.% | -- | 35 (50 °C) | -- | [108] |
| Aluminium Oxide- | Water | Two steps | 0.2 vol.% | Stability test showed that hybrid nanofluid | 14 (65 °C) | Both mono and hybrid nanofluids exhibited Newtonian behaviour as | [113] |

| | | | | | | | |
|---|---|---|---|---|---|---|---|
| Iron ($Al_2O_3$-Fe) | | | | possessed high stability at pH 12 with Zeta potential of -45 mV at all concentrations | | there is a linear relationship between the shear stress and shear rate. | |
| Magnesium oxide-Titanium dioxide (MgO-$TiO_2$) | DW | Two steps | 0.5 vol.% | All the prepared hybrid nanofluids are reported to have a good stability with Zeta potential ranging from ± 25 mV to ± 45 mV. | 21.8 (60 °C) | At all concentrations and temperature, hybrid nanofluids possessed Newtonian behaviour. The highest viscosity enhancement of 28.7% is achieved by 80 wt% MgO-20 wt% $TiO_2$ at 60 °C. | [114] |
| Nano diamond-Nickel (ND-Ni) | DW | Two steps | 0.3 wt.% | -- | 29.39 (60 °C) | Viscosity enhancement of 25.53% is achieved at 60 °C. | [74] |
| Multi-walled carbon nanotubes-Silicon carbide (MWCNTs-SiC) | Water-EG | Two steps | 0.75 vol.% | -- | 28.86 (50 °C) | -- | [109] |
| Aluminium oxide-Multi-walled carbon nanotube ($Al_2O_3$-MWCNT) | Oil | Two steps | 1.5 vol.% | Highly stable suspension is achieved even after 7 days with Zeta potential ranging from 50 – 60 mV. | 45 (50 °C) | At all concentrations, maximum enhancement of viscosity is recorded at the temperature of 40 °C, where the dynamic viscosity for 1.5 vol.% increased by 81% relative to the base fluid. | [115] |
| Titanium oxide-Copper oxide/Carbon ($TiO_2$-CuO/C) | EG | Two steps | 2.0 vol.% | Hybrid nanofluid were found to be stable only at pH 10 with Zeta potential ranging from 36 to 42 mV at different volume concentrations. | 5.6 (60 °C) | Hybrid nanofluid shows Newtonian behaviour at the temperature range of 25 – 60 °C. Highest viscosity increment of 70% is recorded at 60 °C. | [116] |
| Iron Oxide-Copper Oxide ($Al_2O_3$-CuO) | Water-EG (80:20) | Two steps | 0.2 vol.% | -- | 45 (60 °C) | -- | [117] |
| Copper-Zinc (Cu-Zn) | Vegetable oil | Two steps | 0.5 vol.% | All the prepared nanofluids were reported to be stable up to 72 h. | 53 (30 °C) | Hybrid nanofluids possessed Newtonian behaviour and exhibited less amount of deformation or shear thinning with application of shear to it. | [118] |

| | | | | | | | |
|---|---|---|---|---|---|---|---|
| Tungsten trioxide - Silver ($WO_3$-Ag) | Transformer oil | Two steps | 4.0 wt.% | Good stability of dispersion with Zeta potential ranging from 46 mV to 55 mV at different concentrations. | 41 (100 °C) | -- | [119] |
| Iron Oxide-Aluminium OXide ($Fe_2O_3$-$Al_2O_3$) | 10W40 Engine oil | Two steps | 4.0 wt.% | -- | 33 (65 °C) | -- | [120] |
| Graphene-Silicon Oxide (G-$SiO_2$) | Mineral oil | Two steps | 0.04 wt.% | Highest suspension stability is at pH 11 with no agglomeration or sedimentation even after two weeks. | 80 (100 °C) | 29.7% highest viscosity enhancement was observed with 0.04 wt%. | [121] |

### 4.2.1 Solar Energy

Solar energy has been extensively evaluated as the ultimate solution to the energy crisis, and it is also the key to a clean energy future. The use of solar energy technologies will give us opportunities to reduce environmental pollution, enhance sustainability, prevent rapid climate change and minimise the consumption of fossil fuels [122]. As mentioned earlier, the major drawback for solar energy technologies is its low efficiency in collecting and converting solar radiation into electricity. Enormous effort has been made to improve the efficiency of the solar energy collectors and photovoltaic-thermal (PV/T) and one of the novel approaches is to use the novelty working fluids e.g. hybrid nanofluids which have high capability of heat transfer and outstanding optical properties. It should be noted that the type of working fluids used is the prime factor to achieve highly efficient solar energy harnessing systems. Utilising hybrid nanofluids as working fluids for solar energy technology enables us to boost the overall performance of the system as it offers an improved heat transfer coefficients as a result of its outstanding thermal conductivity behaviour, the ability to lower the absorber temperature by transferring heat quickly and the potential to absorb solar radiation, which are not being carried out by PV solar cell, benefitting from its superior optical properties [123]. In solar technology various types

of hybrid nanofluids have been utilized as the working media. A brief summary of the previous researches carried out utilising various hybrid nanofluids in solar energy systems is presented in Table 6. It should be mentioned that the performance of hybrid nanofluids in solar energy is greatly influenced by the thermal properties and optical parameters such as absorption coefficient, solar weighted absorption, transmittivity, scattering and etc. which can be altered by modifying the concentration of nanoparticles, particle size and type of base fluids [124].

**Table 6:** Summary of application of hybrid nanofluids in solar energy systems. Note that DI, DW and EG represent deionised water, distilled water and ethylene glycol, respectively. DASC and PV/T represent direct absorption solar collector and photovoltaic thermal solar panel, respectively.

| Hybrid Nanoparticles | Working Fluids | Solar System | Findings | Ref |
|---|---|---|---|---|
| Multi-walled carbon nanotubes-Iron oxide (MWCNT/ $Fe_3O_4$) | EG and DW (20:80) | DASC | The efficiency of photo-thermal energy conversion is 22% for the MWCNT/$Fe_3O_4$ hybrid nanofluid which was ~11% for the $Fe_3O_4$ nanofluid. | [17] |
| Multi-walled carbon nanotubes-Silicon dioxide with Silver (MWCNT-$SiO_2$/Ag) | DW | DASC | Photo-thermal conversion efficiency enhanced by 97.6% at 35 °C and 42.7% at 70 °C for 0.1wt.%. | [125] |
| Aluminium oxide-Cobalt tetraoxide ($Al_2O_3$/$Co_3O_4$) | DI | DASC | The hybrid nanofluid has the ability to absorb more than 80% of the radiation at 20 mm penetration depth | [65] |
| Copper oxide-Zinc Oxide (CuO/ZnO) | DW | Not mentioned | Photo-thermal conversion efficiency improved by 97.35% at 30 °C and 34.70% at 70 °C | [126] |
| Gold-Silver (Au-Ag) | DW | DASC | The photo-thermal conversion efficiency improved by 30.97%. | [127] |
| Zinc Oxide _ Gold (ZnO-Au) | Silicone oil | DASC | The hybrid nanofluid yielded 58% photo-thermal conversion efficiency at 1.0 mg $mL^{-1.}$ | [128] |
| Aluminium Oxide-Titanium dioxide ($Al_2O_3$- $TiO_2$) | DW | Flat Plate | Photo-thermal efficiency is enhanced by 26%. | [129] |
| Iron-Nickel with Carbon (FeNi/C) | Ethylene glycol | DASC | Photo-thermal conversion efficiency enhanced by 47.3%. Addition of external magnetic field improved the efficiency to 58.1%. | [130] |
| Aluminium Oxide- Zinc Oxide ($Al_2O_3$-ZnO) | DW | PV/T | Thermal, electrical and overall energy efficiency enhanced by 4.054%, 0.038% and 4.092%. | [131] |

| | | | | |
|---|---|---|---|---|
| Phase change material with Silicon carbide (PCM-SiC) | DW | PV/T | 9.92%, 12.32% and 13.70% enhancement in electrical efficiency for water, PCM/water and PCM+SiC/water. | [132] |
| Silver - Silicon dioxide (Ag-$SiO_2$) | DW | PV/T | The overall efficiency of hybrid nanofluids enhanced by 33.2% for 0.025 wt.%. | [133] |

#### 4.2.1.1 Solar Collectors

Solar collector is commonly used for photothermal conversion. It is a device capable of absorbing solar radiation from the Sun and transports the absorbed heat to the working fluid. It converts the solar energy to thermal energy. Among the many types of solar collectors, the direct absorption solar collector (DASC) is the most efficient in exploiting the solar energy due to its ability to absorb solar radiation with minimum heat loss [134], however, flat plate solar collector (FPSC) emerges as the most cost effective solar collector but it suffers from the low efficiency due to the poor working fluids. Figure 24 shows the schematic diagram of DASC and FPSC. DASC does not need any absorber plate. The incident light rays will strike the fluid directly and will be absorbed. Since there is only a minimum convective loss, the effectiveness of this solar collector is much higher compared to FPSC. It also offers less thermal resistance compared to FPSC. In contrast, FPSC requires an absorber plate to extract the solar radiation. The absorber plate is enclosed in an insulated metal. The presence of air gap between the plate help to contain the heat, preventing them from escaping into the atmosphere. As the absorber plate becomes hotter, it will transport the heat to the fluid within the collector, but there is also heat loss to the surrounding. The temperature rise in this type of collector is of the order of 0-50 °C. The construction of FPSC is quite simple and it is easy to maintain since it has low operating cost. In general, finding a novel working fluid that can absorb solar energy effectively and reduce heat loss is one of the key successes in developing high performance solar energy technology. It is well known that thermal and optical properties are main factors in governing the heat transfer efficiency. The optical properties of the working fluids are usually evaluated with respect to its extinction coefficient,

light absorptivity, transmittivity, scattering coefficient and solar weighted absorption. The efficiency of solar energy collectors can be calculated using the following equation [124][17]:

$$\eta = \frac{mc_p(T_f - T_i)}{AG\Delta t} \quad (4)$$

Where, m and $c_p$ denote as the mass and specific heat of the nanofluid, respectively, $T_i$ represents the initial temperature of the nanofluid, $T_f$ reflects the final temperature, A represents the area of exposure, G designates the heat flux of the Sun, and Δt is the time exposed to solar radiation.

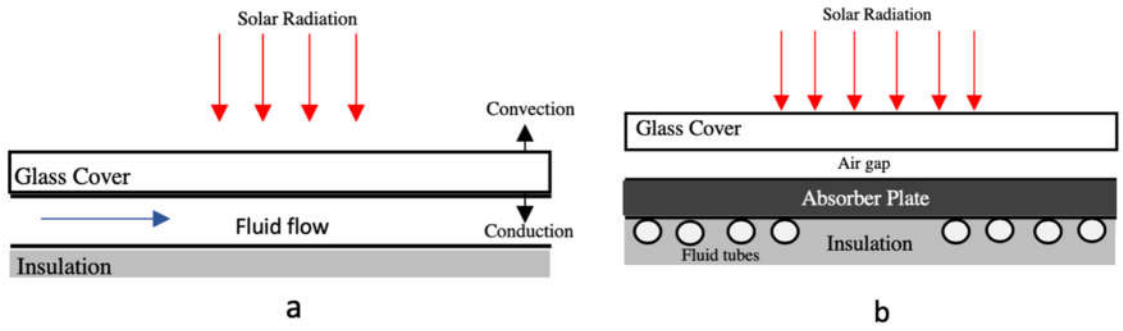


Figure 24: Schematic illustration of: (a) direct absorption solar collector (DASC) and (b) flat-plate solar collector (FPSC). Redrawn from Reference [134].

The dispersion of hybrid nanomaterials such as MWCNT/$Fe_3O_4$, MWCNT-$SiO_2$/Ag, CuO/ZnO, $Al_2O_3$-ZnO, $Al_2O_3$-$TiO_2$ in the different base fluids, acting as working media in the solar collector have been rapidly investigated and most of them have been reported to possess better photo-thermal conversion efficiency compared to that of single particle nanofluid due to their synergistic effect in enhancing thermal conductivity and optical absorption, resulting in a highly efficient solar energy system [125][131][129][126].

Tong et al. [17] compared the performance of mono and hybrid nanofluids of $Fe_3O_4$ and MWCNT/ $Fe_3O_4$, respectively in direct absorption solar collectors. In this study, the authors used a mixture of EG and water (weight ratio 20:80) as the base fluid. The highest thermal conductivity of 0.562 W/m °C was obtained from the optimized mixing ratio of 4:1 for MWCNT/ $Fe_3O_4$ hybrid nanofluid compared to only 0.541 W/m °C for $Fe_3O_4$ nanofluid. The significant proportion of MWCNT in such emerging combinations of nanomaterials gives the dominant effect to thermal conductivity

enhancement. With the high light absorbance properties of the MWCNT, the light transmittance for MWCNT/$Fe_3O_4$ is almost zero at 0.01wt.% whereas $Fe_3O_4$ nanofluid required a higher concentration (0.2wt%) to achieve the same result. The hybrid nanofluids of MWCNT/$Fe_3O_4$ were reported to have a greater performance of solar energy absorption compared to that of $Fe_3O_4$ mono nanofluids as it has the ability to absorb nearly all solar radiation at all concentrations. In view of that, the MWCNT/$Fe_3O_4$ hybrid nanofluids achieved a considerably high efficiency of photo-thermal energy conversion in comparison to that of $Fe_3O_4$ nanofluid at 0.01wt.% with the efficiency decreased from ~ 61 to 22 % for hybrid nanofluids and ~ 33 to 11 % for $Fe_3O_4$ nanofluid, over a period of 6000s.

The study of the impact of using MWCNT-$SiO_2$/Ag hybrid nanofluids suspended in the base fluid of deionized water for solar thermal conversion by Zeng et al. [125] revealed that solar weighted absorption fraction of the nanofluid mixture was impressively high compared to the mono nanofluids of MWCNT and the hybrid nanofluids of $SiO_2$/Ag as the introduction of MWCNT into $SiO_2$/Ag leads to greater ability of light absorption. The superior performance of hybrid nanofluids could be due to the fact that MWCNT has an impressive ability to absorb solar energy at all solar irradiance wavelengths and also a remarkably high thermal conduction. Moreover, the prepared MWCNT-$SiO_2$/Ag hybrid nanofluids also possessed a good dispersion stability with Zeta potential more than 30 mV compared to that of mono nanofluids of MWCNT and the hybrid nanofluids of $SiO_2$/Ag which recorded a value that is less than 30 mV. At the penetration distance of 1 cm, the binary nanomaterial suspension of 0.005 vol% gives a solar weighted absorption fraction of 74.5%, compared to 73.2% and 69.1% for the MWCNT and SiO2/Ag nanoparticle suspensions.

Bhalla et al. [65] explored the photo-thermal energy conversion performance of the blended $Al_2O_3$/$Co_3O_4$ hybrid nanofluids suspended in the base fluid of deionized water. They reported that the homogenized suspension of $Al_2O_3$/$Co_3O_4$ in base fluids has a broadband solar spectrum in the visible region, showing huge quantities of solar radiation can be absorbed by the working fluid. The calculation of solar-weighted absorptivity further confirmed that the homogenous blended hybrid

nanofluid can absorb more than ~80% of the solar radiation at the penetration depth of ~20 mm compared to that of pure base fluid of deionized water which only capable of absorbing only 20% of the solar radiation.

The evaluation of optical absorption and photo-thermal energy conversion efficiency of binary CuO/ZnO nanofluids performed by Fang et al. [126] revealed that the utilisation of hybrid nanofluids gave a significant contribution to the overall performance of solar energy collectors. They reported that the suspension of ZnO with CuO in the base fluid of water has led to the high performance of optical absorption specifically in the visible light region. CuO/ZnO hybrid nanofluids also recorded higher thermal conductivity compared to single particle CuO nanofluids. The authors also reported that the optimized introduction of Cuo in CuO/ZnO nanocomposite (0.7:0.3) exhibits the highest photothermal efficiency with ~97.35% compared to only ~95.90% by the pure CuO nanofluids at 30 °C. The optical absorption performance was found to be decreased with the high content of ZnO. This implies that a suitable combination of hybrid nanoparticles will boost the photo-thermal conversion efficiency.

#### 4.2.1.2 Photovoltaic Thermal

Photovoltaic Thermal (PV/T) is known as a hybrid solar collector that is able to convert solar radiation into thermal and electrical energy. PV/T is a combination of photovoltaic solar cell which transforms sunlight into electrical energy and a solar thermal collector which transfers the unconsumed heat or waste from PV module to a heat transfer fluid. The ability of PV/T to produce thermal and electrical energy simultaneously has led PV/T to emerge as a highly efficient solar energy harvesting system, benefitting from its fully utilized solar spectrum compared to the solar photovoltaic (PV) or solar thermal alone [135]. The current commercial solar panels suffer from a relatively low efficiency which is only about 20% efficient while almost 80% of the absorbed solar energy is not being utilised after conversion. These unconsumed energies have caused PV to overheat, resulting in an inefficient increase of its operating temperature. The merging of PV/T is able to reduce the operating temperature

as all unconsumed heat will be transferred to the working fluids [136]. Figure 25 depicts the schematic illustration of PV/T. Based on our findings, there is very limited work on the employment of hybrid nanofluids as the working media for PV/T. Most of them are focussed on mono nanofluid. In fact, the most recent investigation regarding PV/T made by Abdelrazik et al. [137] and Aslfattahi et al. [49] are focussing on MXene based mono nanofluids.

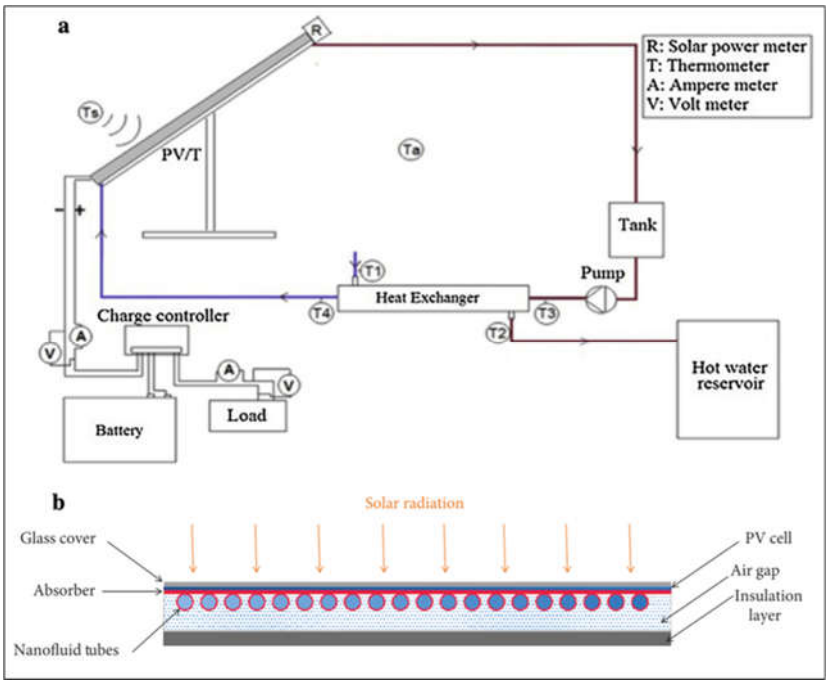


Figure 25: Schematic illustration of: (a) Solar energy conversion system of PV/T [132], and (b) PV/T system with nanofluid as the working fluid [131]. Figure 25(a) reproduced from Reference [132] with permission from Elsevier.

Recently, Han et al. [138] investigated the performance of PV/T utilising Ag/$CoSO_4$-propylene glycol (PG) hybrid nanofluids as the optical filter. The authors reported that the efficiencies of the PV/T systems were enhanced by more than 5 times compared to the stand-alone PV cell when Ag/$CoSO_4$-PG nanofluids were employed. When compared with different base fluid, the overall efficiency of PV/T system with Ag/CoSO4-PG hybrid nanofluids (total efficiency 79.82%) filter increased by 9% compared to that of PV/T system with Ag/CoSO4-water hybrid nanofluids (total efficiency 70.80%) filter, demonstrating the huge role of PG in enhancing the efficiency of PV/T.

Al-Waeli et al. [132] analysed the effect of utilising SiC-PCM/water nanofluids towards the electrical efficiency of PV/T. The authors prepared four systems consisting of conventional PV, water coolant, PCM and PCM+SiC/water hybrid nanofluids for the comparison purposes. It is reported that the addition of nanoparticles into PCM has greatly increased its performance, attributed by the promising heat transfer enhancement of nanoparticles. The electrical efficiency of PV is only ~7.11% when there is not any conventional heat transfer fluid for the cooling process. The electrical efficiency of PV/T has increased when the working fluids were employed with the values of ~9.92, ~12.32 and ~ 13.70 % for water, PCM/water and PCM+SiC/water hybrid nanofluids, respectively, indicating that utilizing PCM/water and PCM+SiC/water hybrid nanofluids in the PV/T system improved the thermal and electrical energy efficiency, which in turn increased the overall PV/T efficiencies. It is also reported that [+SiC/water hybrid nanofluids recorded the lowest maximum operating temperature with only 39.52 °C compared to 68.3, 45.22 and 42.22 °C for PV/T without working fluid, water and PCM/water, respectively. Figure 26 shows the schematic illustration for the experimental setup.

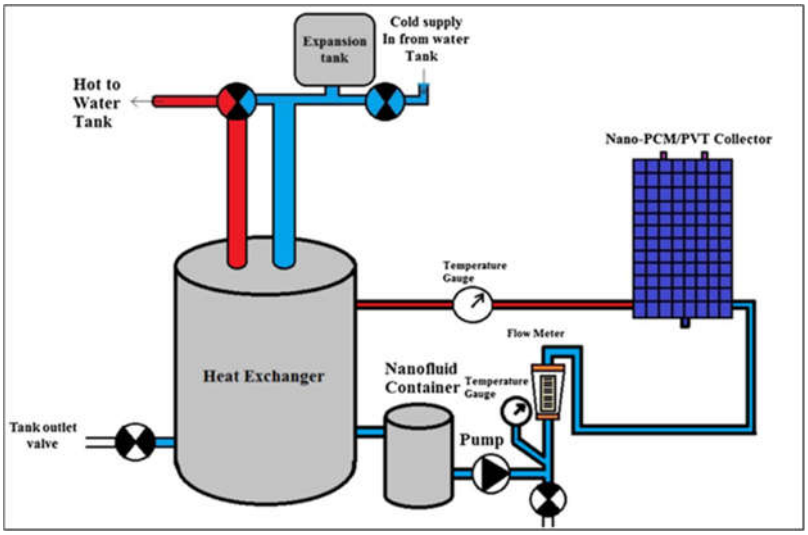


Figure 26: Schematic representation of experimental setup. Reproduced from Reference [132] with permission from Elsevier.

In another work, Crisostomo et al. [133] evaluated the performance of core-shell Ag-$SiO_2$ hybrid nanofluids as the working fluid for optimum performance of PV/T by varying the particle concentration. It has been reported that thermal output rises with the increase of particle loading, however, electrical output decreases. The highest particle loading of Ag-$SiO_2$ hybrid nanofluids

contributed about 33.2% enhancement in the overall efficiency compared to only ~ 12.4% for the stand-alone system. The improved efficiency is due to the usage of hybrid nanofluids which possessed an outstanding optical property, leading to the optimum operating system.

### 4.2.2 Electronic Cooling

The development of the integration and compaction chip which is small in size, high performance and an improved computational speed to meet customer demands has led to new challenges in thermal management [139] [15]. The excessive amount of heat generated from these electronic devices will lead to sudden thermal breakdown, which may affect their performances, reducing its reliability and lifetime expectancy [140]. Therefore, providing the system with convenient temperature and rapid cooling procedure becomes mandatory for their optimal operation. Even though there is an enormous effort that has been made to reduce the operating temperature of the electronic devices such as using phase change materials (PCM) materials, thermoelectric cooling, design of heat sink, usage of heat pump and the insertion of fins, its performances is still unable to fulfil the requirement of electronic cooling for advanced heat generating electronic devices. In addition, the use of the conventional coolant has shown to possess poor performances to the electronic devices caused by their low heat transfer capability. To date, the poor removal of increased heat transfer flux and the inconsistency of power dissipation remains as big challenges in electronic cooling [141]. In fact, Agostini et al. has reported that semiconductor industries faced difficulties in maintaining the electronic devices at 85 °C while operating at high heat flux of 300 W/cm$^2$ [142]. Recent progress in research demonstrated that hybrid nanofluids provide better electronic cooling performance compared to conventional fluid and also single nanofluid due to enhanced thermal conductivity [112]. It enabled electronic devices to operate at their best operating modes without being compromised.

Recently, Bahiraei et al. [143] evaluated the effectiveness of using the hybrid nanofluids composed of graphene nanoplatelets encased in silver nanoparticles (GNPs-Ag) in three blocks of liquid for Central Processing Unit (CPU) cooling. In this study, a novel distributor liquid block was introduced along

with the two conventional liquid blocks. The authors reported that the new distributor heat sink exhibits a superior efficiency based on its thermal performance and irreversibility. It is also reported that applying hybrid nanofluids provides better cooling performances compared to pure water, leading to more uniform distribution of temperatures. Figure 27 shows the temperature patterns of three liquid blocks measured at different Reynolds numbers using two different fluids. As can be seen in Figure 27b, hybrid nanofluids are able to significantly reduce the temperature contour of the liquid blocks especially at Re=500 and 750, indicating its high performance in providing rapid heat transfer process. This implies that the temperature of the wall and the uniformity of temperature distribution were improved with the increasing Reynolds number.

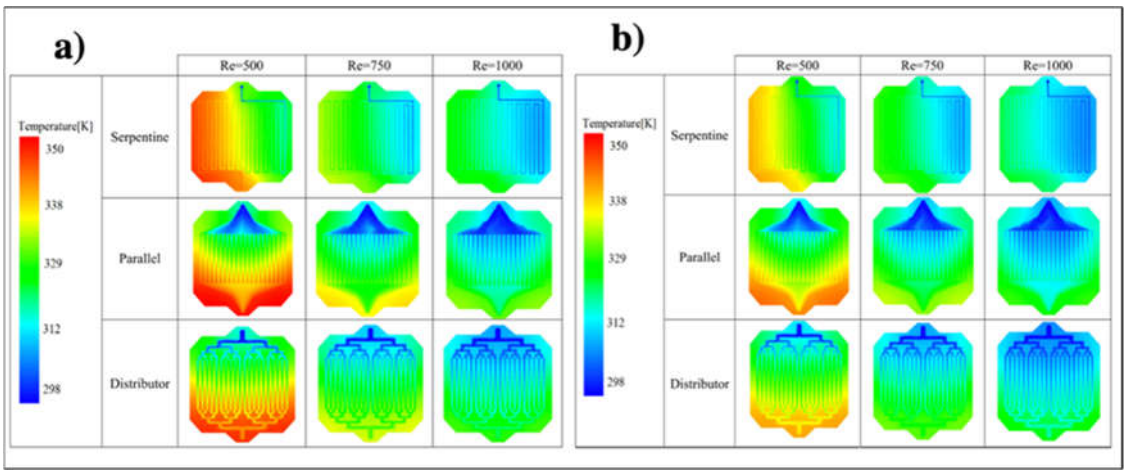


Figure 27: Temperature contours of three different liquid blocks, measured at different Reynolds numbers in: (a) pure water and (b) hybrid nanofluids. Reproduced from Reference [143] with permission from Elsevier.

It should be noted that the heat transfer coefficient is mainly governed by the Reynolds number, the volume fraction of nanofluids, temperature, thermal properties of the base fluid and the purity of nanoparticles [140]. Hybrid nanofluids seem to have the potential of removing heat at a faster rate than the rate of heat production. Having an outstanding performance of electronic components equipped with rapid cooling fluids enables the impediment of the component from any potential thermal breakdown [144]. To examine this, Barewar et al. [144] conducted an experiment to evaluate the thermal conductivity of ethylene glycol-based silver and zinc oxide (Ag/ZnO) hybrid nanofluids. Enhancement of 15.66% was observed at 0.2 vol.% after the introduction of Ag/ZnO hybrid

nanomaterials to the ethylene glycol base fluid at 25 °C. At 55 °C, the hybrid nanofluids recorded its highest thermal conductivity enhancement of 20.53 %. They reported that thermal conductivity enhancement was caused by a uniformly coated Ag on ZnO nanoparticles, making ZnO nanoparticles hydrophilic in nature, which led to the homogenous mixture of hybrid nanofluids. The physical observation on the stability of dispersion indicated that the hybrid nanofluids demonstrated a good suspension stability with no sign of agglomerations even after 15 days and Zeta potential measurement further confirmed the suspension stability in which all nanofluids at different volume concentrations possessed Zeta potential value ranging from 36 to 51 mV.

Moreover, Okonkwo et al [113] studied the thermal conductivity of water based aluminium oxide and iron ($Al_2O_3$-Fe) hybrid nanofluids by varying the nanoparticle concentrations (0.05-0.2%). A 14% thermal conductivity enhancement is obtained at 0.2% volume concentration. However, at a lower concentration, the $Al_2O_3$-Fe hybrid nanofluid did not display any significant improvement in thermal conductivity, reflecting that there are no synergistic effects between two nanoparticles at that concentration. Increasing the ratio of Fe in nanocomposite may lead to a much better thermal conductivity as Fe possesses a higher value of thermal conductivity compared to alumina [152].

### 4.2.3 Heat Pipe

Heat pipe is known as a passive device that can be served as a medium for heat transfer, which can be employed to transfer heat from the heat source (high temperature environment or evaporator) to the heat sink (low temperature environment or condenser) over a relatively long distance via heat vaporization of working media. The main structure comprises an evaporator, adiabatic and condenser as shown in Figure 28. Heat pipe acts as an evacuated tube which is able to minimise the loss of heat to the surrounding. In order to operate efficiently, it requires a working fluid that has high heat transfer capability to absorb latent heat of evaporation at evaporator and transfer it as a latent heat of condensation at condenser [145]. In general, a lower vapour temperature along the length of the heat pipe demonstrates the capability of the heat pipe to work at higher heat loads. It should be mentioned

that the important parameter of the heat pipe are the thermal resistance ($R_{HP}$) and the effective thermal conductivity ($k_{eff}$) which can be defined using the equation below [146]:

$$R_{HP} = \frac{T_{E,wall} - T_{C,wall}}{Q} \quad (5)$$

$$k_{eff} = \frac{A_c}{R_{HP}} \quad (6)$$

where Q, $T_E$, $T_C$ and $A_C$ are heat input, evaporator and condenser wall temperatures and the total cross-sectional area of the heat pipe, respectively.

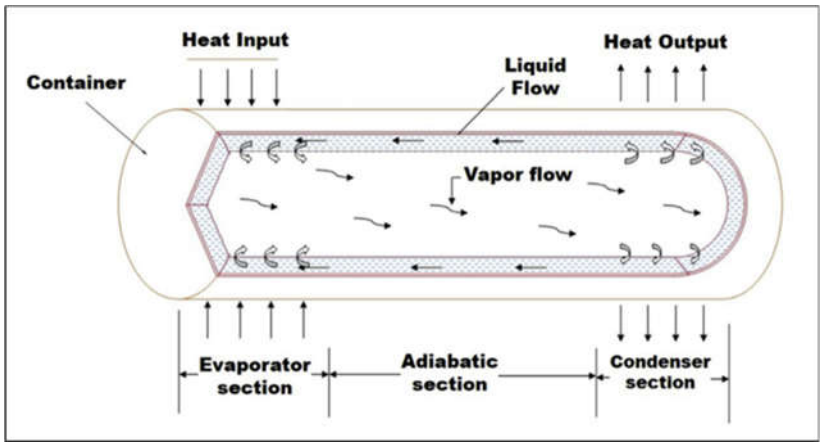


Figure 28: Schematic diagram of heat pipe. Reproduced from Reference [145] with permission from Elsevier.

Swapnil et al. [147] investigated the performance of circular heat pipes by dispersing the hybrid nanomaterials of aluminium oxide and boron nitride ($Al_2O_3$-BN) in the base fluid of DW. They studied the effect of concentration, impact of heat inclination and heat input of thermal resistance towards the circular heat pipe. Based on their studies, the increase of particle concentration and inclination angle may reduce the thermal resistance of circular heat pipes. At 2 vol.%, the thermal resistance of the circular heat pipe decreased by 39.92 % relative to the base fluid of distilled water.

Ramachandran et al. [148] studied the effect of using hybrid nanofluids as a working fluid in screen mesh cylindrical heat pipes by varying the working fluids from DI water, $Al_2O_3$/DI water nanofluid, ($Al_2O_3$ 50%-CuO 50%)/ DI water hybrid nanofluids and ($Al_2O_3$ 25%-CuO 75%)/DI water hybrid nanofluids. They reported that the unique structure of hybrid nanofluids able to boost the heat pipe

operating range up to 250 W. Also, significant thermal conductivity enhancement can be observed when hybrid nanofluids were employed with 41.47% for $Al_2O_3$-CuO/DI water (1:1) and 79.35% for $Al_2O_3$-CuO/DI water (1:3), depending on the effect of particle mixing ratio compared to the $Al_2O_3$/DI water (38.34%) and the base fluid of DI water.

In a similar study, Ramachandran et al. [146] investigated the thermal performances of cylindrical screen mesh heat pipe by varying the different proportion of $Al_2O_3$-CuO/DI water (25-75, 50-50 and 75-25 %) hybrid nanofluids. They reported that the optimized hybrid nanofluids of $Al_2O_3$ 25%-CuO 75% recorded as the highest reduction in thermal resistance with 44.25 % compared to base fluid when operating at high heat load of 250 W. The superior reduction in thermal resistance could be due to the maximum deposit of nanoparticles, forming a nano-porous layer in the screen wick. It should be mentioned that thermal resistance represents the temperature difference between evaporator and condenser wall, indicating the ability of a heat pipe to take higher heat loads. This implies that the higher the reduction in thermal resistance, the effective thermal conductivity should be increased as presented in equation (6). It should be noted that the use of effective working fluids e.g. hybrid nanofluids will increase the lifespan of the equipment, provide better cooling rate and lead to efficient operation of the systems.

#### 4.2.4 Heat Exchanger

The influence of hybrid nanofluids that possess high heat transfer performances have made it possible to be used as a working fluid in heat exchanger. Heat exchangers have always been important in many industries to prevent overheating of the equipment. The use of the conventional coolant is not enough to fulfil the industrial cooling requirements, resulting in the industries to encounter deterioration of the equipment and production losses. Heat exchanger is a device that is able to transfer heat from one medium to another. The media is separated by a solid wall, so it will prevent the fluids from having any physical contact towards each other [149]. The operation of heat exchangers is always accompanied by two types of losses: losses related to the heat transfer across a finite temperature

difference and/or loss due to pressure drop causing the friction in a heat exchanger. For a heat exchanger to operate efficiently, it should be designed to have a large heat transfer area or to be equipped with materials that have the least thermal resistances and use effective working fluids with high heat transfer capabilities. With the impressive growth of technology, the compact and innovative design of heat exchangers becomes essential especially in the automotive industry, leaving the first approach is not favourable because the enlargement of heat transfer area will result in a bigger size of system, leading to a greater frictional loss and higher pressure drop as well as high pumping cost requirements [150][151]. The two losses can be quantified by evaluating the total entropy generated from the heat exchanger. An ideal heat exchanger should have a minimum total entropy generation which can be obtained by enhancing the thermal conductivity and Nusselt number [150]. In view of that, several studies have been coordinated to evaluate the heat transfer capability of hybrid nanofluids in heat exchangers. Table 7 summarised several recent researches regarding the heat transfer performance of hybrid nanofluids for heat exchangers.

Table 7: Summary of several researches regarding the heat transfer performance in heat exchangers. Note that Re, DW and DI represent Reynolds number, distilled water and deionised water.

| Hybrid NM | Base Fluid | Concentration | Flow Regime | Findings | Ref |
|---|---|---|---|---|---|
| Graphene-Aluminium oxide ($G/Al_2O_3$) | DW | 0.1 vol. % | Re: 200 - 1000 (Laminar) | • Total entropy generation decreased from 0.0361 W/K to 0.0184 W/K at the maximum applied heat flux of 25000W/$m^2$.<br>• Enhancement of 88.62% in convective heat transfer coefficient. | [150] |
| Aluminium oxide- Copper ($Al_2O_3/Cu$) | DW | 0.05-2.00 wt.% | Re: 800 – 2400 (Laminar, turbulent) | • Addition of hybrid nanoparticles give huge enhancement in the heat transfer coefficient and Nusselt number (40% enhancement) due to the improved thermal conductivity.<br>• Pressure drop increases with increase in Reynold numbers.<br>• The heat transfer rate enhances with increase in Reynolds number. Heat transfer rate increased by 78% when the Reynold number increase from 844.4 to 2321.54. | [149] |
| Iron oxide - Carbon nanotube ($Fe_2O_3$/CNT) | DW | 0.1-0.2 wt.% | Re: 1698-6070 (Laminar, transient, turbulent) | • Heat transfer coefficient enhanced with the increase of Reynolds number and temperature.<br>• Rate of heat transfer coefficient enhancement decreases with the increase of voltage from 80-150 V. | [152] |
| Aluminium oxide- Multi-walled carbon nanotubes ($Al_2O_3$/MWCNT) | DI | 0.01 wt.% | Re: 150-350 (Laminar) | • Heat transfer coefficient increases with the addition of nanoparticles. A maximum of 15.2% enhancement has been recorded.<br>• Pumping power increases negligibly with the addition of nanoparticles in base fluid. | [153] |

| | | | | | |
|---|---|---|---|---|---|
| Aluminium nitride - Aluminium oxide (AlN/ $Al_2O_3$) | DI | 1-4 vol.% | Re: 5000-17000 (Turbulent) | • Pressure drop increased as Reynold numbers and volume concentrations increased.<br>• The optimized vol. concentration (3%) recorded a 50% enhancement in Nusselt number when hybrid nanofluids flow through the flat tube.<br>• Heat transfer enhancement increased from 28-50% for 1-3.00 vol.%. | [154] |
| Copper-Aluminium oxide (Cu/ $Al_2O_3$) | DI | 1-2 wt.% | Re:100-1000 | • Friction factors decrease with the increase of Reynolds numbers.<br>• The addition of hybrid nanoparticles has led to a significant impact in Nusselt number, in which 22% enhancement was recorded for 2.0 wt.%. | [146] |

Ahammed et al. [150] analysed the entropy production of water based aluminium oxide and graphene ($Al_2O_3$-Gr) hybrid nanofluids in multiport mini-channel heat exchanger by comparing it with single particle of $Al_2O_3$/water nanofluid and Graphene/water nanofluid. They reported that total entropy production for Graphene/water nanofluid is minimum with average reductions in thermal entropy generation of ~ 32.37, ~21.62 and ~ 8.16 % for Graphene, $Al_2O_3$-Graphene and $Al_2O_3$ nanofluids respectively. The graphene/water nanofluid also recorded a superior enhancement of ~88.62 % in the convective heat transfer coefficient compared to 63.13% and 31.89% for $Al_2O_3$-Gr and $Al_2O_3$ nanofluids, respectively. The poor performance of hybrid nanofluids could be due to the lower synergistic effect between the two materials. Figure 29 shows the schematic illustration for the experimental setup.

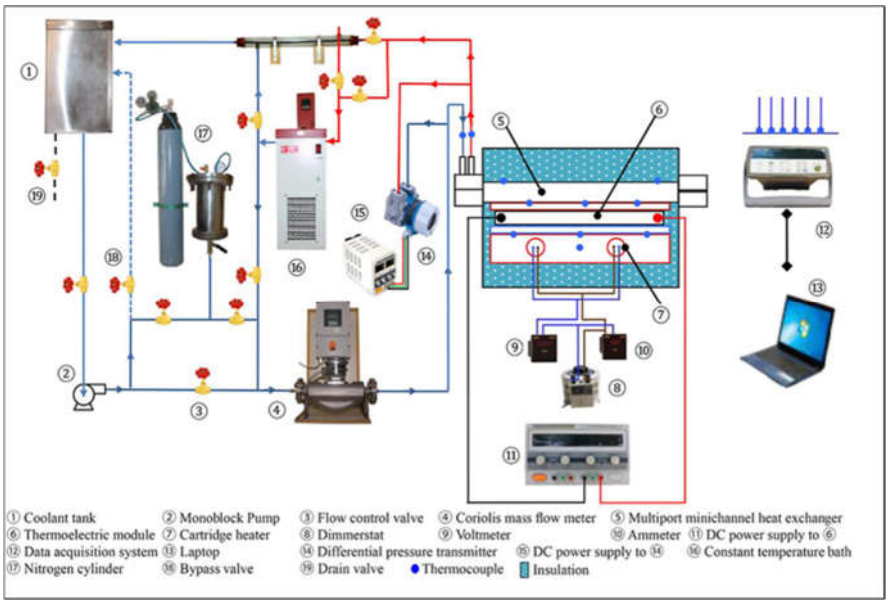


Figure 29: Schematic of the experimental setup. Reproduced from Reference [150] with permission from Elsevier.

Anitha et al. [149] studied the impact of using water based aluminium oxide with copper ($Al_2O_3$-Cu) hybrid nanofluids on the performance of shell and tube heat exchanger (STHE). Utilisation of hybrid nanofluids in STHE has led to the significant enhancement in heat transfer coefficient and Nusselt number, which in turn provides an improved performance of heat exchanger. Hybrid nanofluids demonstrated the highest effectiveness when used as coolant compared to single particle nanofluids and the base fluids. At Re of ~ 844.4, the percentage of heat transfer coefficient enhancement for hybrid nanofluids are 139 and 25 % compared to that of water and Cu/water nanofluids, respectively. The authors also reported that the heat transfer performance of hybrid nanofluids improved with the increase of nanoparticles volume concentration. Allahyar at el. [155] compared the thermal performance of $Al_2O_3$-Ag/water hybrid nanofluids and mono nanofluid of $Al_2O_3$/water in a coiled heat exchanger. The authors reported when the hybrid nanofluids is employed, a maximum enhancement of Nusselt number (~31.58 %) can be achieved with Reynolds number of ~ 4687, which is higher than the $Al_2O_3$ mono nanofluids (~28.42%) at the same operating condition, indicating the outstanding performance of hybrid nanofluids in escalating the thermal performance of heat exchangers.

Aghabozorg et al. [152] evaluated the thermal performance of water based Iron oxide with carbon nanotubes ($Fe_2O_3$-CNT) hybrid nanofluids inside a horizontal STHE which subjected to laminar, transient and turbulent flow with three different heat fluxes. This study illustrated that the heat transfer coefficients enhanced with the increases of voltage, nanoparticle loading and Reynolds number. The convective heat transfer coefficient enhancement may be due to the turbulence in the boundary layer of heat particles and the magnetic particles.

In addition, Bhattad et al. [153] explored the effect of using different particle mixing ratios of aluminium oxide with multi-walled carbon nanotubes $Al_2O_3$-MWCNT hybrid nanofluids towards the cooling performance of the plate heat exchanger. In this study, the authors dispersed the hybrid nanoparticles into the base fluid of DI water. When comparing with single particle $Al_2O_3$ nanofluids,

the application of hybrid nanofluids causes the heat transfer coefficients to increase due to the difference of thermo-physical properties of the two materials and as a result of favourable integration of nanoparticles suspended into the base fluid. It is also observed that the heat transfer coefficients increase as the volume ratio of MWCNT nanoparticles increases owing to the superior thermal conductivity possessed by MWCNT and also due to the fact that $Al_2O_3$ suffers from low thermal conductivity. In response to that, the authors reported that MWCNT (0:5) mono nanofluid showed a better heat transfer enhancement for the cooling process of plate heat exchangers. In general, hybrid nanofluids are able to improve the cooling performance of the heat exchangers. However, the combination of nanomaterials for dispersion into base fluids plays a significant role in enhancing the overall efficiency of the heat exchangers.

## 5. Conclusions

Hybrid nanomaterials are the new type of nanomaterials which were created as a result of the advancement in nanotechnology. The research associated with this kind of material has been on a continuous upsurge, owing to their unique features and the flexibility to tailor their physicochemical properties simply by controlling the mixture composition and morphology. The unique structural form of hybrid nanomaterials which possess improved physicochemical properties have led them to become an intriguing material for electrochemical energy storages and heat transfer applications. In particular, the rise of synergistic effect and the interactions between the single nanoparticle components within the integrated nanoparticles gives the significant contributions to the outstanding physicochemical properties it has. Employing hybrid nanomaterials in the electrochemical energy storage devices shows an improved capacitance, energy density, power density, and system lifetime, contributing to the outstanding electrochemical performances. In general, hybridisation of 2D materials such as MXene and graphene with other nanomaterials is able to prevent the 2D nanosheets from self-stacking. This will avoid the formation of a very dense structure, which is not suitable for their applications. On the other hand, utilisation of hybrid nanomaterials in creating hybrid nanofluids also demonstrated that

such emerging combinations of nanoparticles is able to acquire a remarkable thermal conductivity enhancement, surpassing mono nanofluids and even the conventional base fluids. In general, hybridisation of nanomaterials not only enhances the thermal conductivity but it also offers high dispersion stability. It is well noted that thermal conductivity improvement comes with the increase of temperature and high particle loading. Since hybrid nanomaterials are still considered as new and under the developing phase, extensive research must be carried out in order to bring them to a commercial scale or to be employed in real life applications. Therefore, the synthesis routes, characterization and the practical applications of hybrid nanomaterials must be understood rigorously. It should be noted that the current progress made on hybrid nanomaterials is very limited especially on the theoretical models in evaluating the performance of hybrid nanomaterials. This will create a gap between experimental works performed by various researchers even though the same hybrid nanomaterials were used. In this review paper, we have focused on recent trends and advances made on hybrid nanomaterials in the field of electrochemical energy storage and heat transfer applications. We also comprehensively summarized numerous synthesis routes adapted by various researchers to produce hybrid nanomaterials and their findings on hybrid structures were well discussed. Although there are a lot of synthesis routes currently available to fabricate hybrid nanomaterials, an efficient and highly scalable synthesis technique still needs to be considered in order to produce high quality hybrid nanomaterials at a low cost.

## 6. Current Challenges and New Opportunities

Hybrid nanomaterials seem to provide a significant contribution in improving the overall performances of advanced heat transfer devices and also able to provide an outstanding performance of electrodes for energy storage devices. However, hybrid nanomaterials are facing some challenges that may hinder it from the extensive applications. Below, we highlighted several challenges faced by hybrid nanomaterials and provide new opportunities that may be useful for future research:

- Firstly, the use of different synthesis routes with different parameters by different researchers have eventually led to uncertain results due to lack of agreement with the results achieved. This will therefore create a gap between the results obtained from one research to another even though the same materials were being used. Therefore, there exists an urgent need to develop a theoretical model to predict the behaviour of the nanocomposites, which can serve as a reference or guidance for the experimental work.
- The fabrication cost for hybrid nanomaterials is usually high. For the hybrid nanomaterials to be implemented commercially, it requires a low-cost fabrication technique with high-quality products for large-scale production. To date, there is only a little emphasis made for low-cost fabrication techniques, however, there are some literatures that have introduced facile methods for the synthesis of hybrid nanomaterials such as using one-step hydrothermal strategy, *in situ* solvent method and solvothermal method. Therefore, the key for a wide application of hybrid nanomaterials is to find the alternative fabrication method, however, there is still a need for exploration on the kinds of emerging hybrid nanomaterials that are useful for particular purposes.
- Next, it is important to merge and integrate suitable nanomaterials together as the right combination of hybrid nanomaterials will give rise to the synergistic effect. It is understood that an unfavorable combination of nanomaterials will lead to the poor thermal performance, resulting in the low efficiency of the systems. However, there is no proper guidance available for the suitable combination of nanomaterials, highlighting that hybrid nanomaterials are the new kinds of nanomaterial and their performance and suitability evaluation are in the phase of development.
- Furthermore, there is no optimum mixing ratio of nanoparticles for the high performance of hybrid nanomaterials developed, causing the implementation of this emerging hybrid nanomaterials as a big challenge. However, since hybrid nanomaterials give us the flexibility

to tailor their physicochemical properties, it is important to study and analyze the optimum mixing ratio of nanoparticles in nanocomposites on a case-by-case basis.

- In addition, even though employing hybrid nanomaterials as heat transfer fluids gives a significant improvement to the overall efficiency of the devices due to the improved heat transfer capability, the stability of the dispersion still remains a huge challenge. The difficulty of hybrid nanofluids to sustain the suspension for a long time will affect its performance. It is well understood that stability is one of the important factors in hybrid nanofluids and it is the key to the high thermal performance which enhances the heat transfer capability. Therefore, it is important to evaluate the stability performance of hybrid nanofluids and explore any new possibility to improve the suspension stability.
- Viscosity also has been one of the major issues related to hybrid nanofluids. It has always been reported that thermal conductivity enhancement increases with the increase of particle concentration. This will lead to high viscosity. As we know, high viscosity will create high surface tension which may cause high penalties in pressure drops and requires a high pumping power ,which results in high operating costs. Hence, it is important to assess viscosity measurement and their effect towards the system operation. This could be done using simulation models and analysis.

## 7. ACKNOWLEDGEMENTS

"Authors would like to acknowledge the financial support provided by the Sunway University, Malaysia internal Grant scheme through the project No. # GRTIN-RSF-SHMS-CBP-03-2020".

## 8. REFERENCES

[1] A. Borode, N. Ahmed, and P. Olubambi, "A review of solar collectors using carbon-based nanofluids," *J. Clean. Prod.*, vol. 241, p. 118311, 2019, doi: 10.1016/j.jclepro.2019.118311.

[2] IEA, "Global Energy Review 2020," *Iea*, 2020, [Online]. Available: https://www.iea.org/reports/global-energy-review-2020.

[3] International Energy Agency (IEA), "Market Report Series Renewables 2O18 Analysis and Forecast to 2023," *Int. Energy Agency*, p. 211, 2018, [Online]. Available: https://www.iea.org/reports/renewables-2018.

[4] P. Raj and S. Subudhi, “A review of studies using nanofluids in flat-plate and direct absorption solar collectors,” *Renew. Sustain. Energy Rev.*, vol. 84, no. August 2017, pp. 54–74, 2018, doi: 10.1016/j.rser.2017.10.012.

[5] C. Yu *et al.*, “High Temperature Energy Storage (HiTES) with Pebble Heater Technology and Gas Turbine,” *Intech*, p. 13, 2012, doi: 10.1016/j.colsurfa.2011.12.014.

[6] Y. Kameya and K. Hanamura, “Enhancement of solar radiation absorption using nanoparticle suspension,” *Sol. Energy*, vol. 85, no. 2, pp. 299–307, 2011, doi: 10.1016/j.solener.2010.11.021.

[7] A. Lenert, E. Wang, and Y. Nam, “Heat Transfer Fluids,” *Annu. Rev. Heat Transf. ,* vol. 15, no. January, pp. 93–129, 2012, doi: 10.1615/AnnualRevHeatTransfer.2012004122.

[8] H. Wang, X. Liang, J. Wang, S. Jiao, and D. Xue, “Multifunctional inorganic nanomaterials for energy applications,” *Nanoscale*, vol. 12, no. 1, pp. 14–42, 2020, doi: 10.1039/c9nr07008g.

[9] Y. Q. Wu *et al.*, “SnS2 nanoparticle-integrated graphene nanosheets as high-performance and cycle-stable anodes for lithium and sodium storage,” *J. Alloys Compd.*, vol. 822, p. 153686, 2020, doi: 10.1016/j.jallcom.2020.153686.

[10] X. Zhan, C. Si, J. Zhou, and Z. Sun, “MXene and MXene-based composites: Synthesis, properties and environment-related applications,” *Nanoscale Horizons*, vol. 5, no. 2, pp. 235–258, 2020, doi: 10.1039/c9nh00571d.

[11] Z. Zhou, J. Gong, Y. Guo, and L. Mu, “Multifunctional Hybrid Nanomaterials for Energy Storage,” *J. Nanomater.*, vol. 2019, pp. 1–3, 2019, doi: 10.1155/2019/3013594.

[12] D. Kumar and V. A. Amirtham, “A review on preparation , characterization , properties and applications of nano fl uids,” vol. 60, pp. 21–40, 2016.

[13] D. Meroni and S. Ardizzone, “Preparation and application of hybrid nanomaterials,” *Nanomaterials*, vol. 8, no. 11, pp. 2–5, 2018, doi: 10.3390/nano8110891.

[14] R. Hayami *et al.*, “Preparation and properties of organic-inorganic hybrid materials using titanium phosphonate cluster,” *Polym. J.*, vol. 49, no. 9, pp. 665–669, 2017, doi: 10.1038/pj.2017.34.

[15] V. Selvaraj and H. Krishnan, “Synthesis of graphene encased alumina and its application as nanofluid for cooling of heat-generating electronic devices,” *Powder Technol.*, vol. 363, pp. 665–675, 2020, doi: 10.1016/j.powtec.2020.01.050.

[16] M. F. Zawrah, R. M. Khattab, L. G. Girgis, H. El Daidamony, and R. E. Abdel Aziz, “ Stability and electrical conductivity of water-base Al 2 O 3 nanofluids for different applications ,” *HBRC J.*, vol. 12, no. 3, pp. 227–234, 2016, doi: 10.1016/j.hbrcj.2014.12.001.

[17] Y. Tong, T. Boldoo, J. Ham, and H. Cho, “Improvement of photo-thermal energy conversion performance of MWCNT/Fe3O4 hybrid nanofluid compared to Fe3O4 nanofluid,” *Energy*, vol. 196, p. 117086, 2020, doi: 10.1016/j.energy.2020.117086.

[18] H. Li, Y. Hou, F. Wang, M. R. Lohe, X. Zhuang, and L. Niu, “Flexible All-Solid-State Supercapacitors with High Volumetric Capacitances Boosted by Solution Processable MXene and Electrochemically Exfoliated Graphene,” pp. 2–7, 2016, doi: 10.1002/aenm.201601847.

[19] G. Bharath *et al.*, “Synthesis of hierarchical Mn3O4 nanowires on reduced graphene oxide nanoarchitecture as effective pseudocapacitive electrodes for capacitive desalination application,” *Electrochim. Acta*, vol. 337, p. 135668, 2020, doi: 10.1016/j.electacta.2020.135668.

[20] L. Yang, W. Ji, M. Mao, and J. nan Huang, “An updated review on the properties, fabrication and application of hybrid-nanofluids along with their environmental effects,” *J. Clean. Prod.*, vol. 257, p. 120408, 2020, doi: 10.1016/j.jclepro.2020.120408.

[21] M. Gupta, V. Singh, S. Kumar, S. Kumar, N. Dilbaghi, and Z. Said, “Up to date review on the synthesis and thermophysical properties of hybrid nanofluids,” *J. Clean. Prod.*, vol. 190, pp. 169–192, 2018, doi: 10.1016/j.jclepro.2018.04.146.

[22] P. Thangadurai, S. Joicy, R. Beura, J. Santhosh Kumar, and K. Chitrarasu, *Emerging Nanomaterials in Energy and Environmental Science: An Overview*. 2019.
[23] S. K. Tiwari, V. Kumar, A. Huczko, R. Oraon, A. De Adhikari, and G. C. Nayak, "Magical Allotropes of Carbon: Prospects and Applications," *Crit. Rev. Solid State Mater. Sci.*, vol. 41, no. 4, pp. 257–317, 2016, doi: 10.1080/10408436.2015.1127206.
[24] J. Pitroda, "A Critical Review on Carbon Nanotubes," *Int. J. Constr. Res. Civ. Eng.*, vol. 2, no. 5, pp. 36–42, 2016, doi: 10.20431/2454-8693.0205007.
[25] N. Saifuddin, A. Z. Raziah, and A. R. Junizah, "Carbon nanotubes: A review on structure and their interaction with proteins," *J. Chem.*, vol. 2013, 2013, doi: 10.1155/2013/676815.
[26] T. Han, A. Nag, S. Chandra Mukhopadhyay, and Y. Xu, "Carbon nanotubes and its gas-sensing applications: A review," *Sensors Actuators, A Phys.*, vol. 291, pp. 107–143, 2019, doi: 10.1016/j.sna.2019.03.053.
[27] H. P. Cong, J. F. Chen, and S. H. Yu, "Graphene-based macroscopic assemblies and architectures: An emerging material system," *Chem. Soc. Rev.*, vol. 43, no. 21, pp. 7295–7325, 2014, doi: 10.1039/c4cs00181h.
[28] Q. Zheng and J.-K. Kim, *Graphene for Transparent Conductors*. 2015.
[29] Z. Zhen and H. Zhu, *Structure and Properties of Graphene*. Elsevier Inc., 2018.
[30] S. K. Tiwari, S. Sahoo, N. Wang, and A. Huczko, "Graphene research and their outputs: Status and prospect," *J. Sci. Adv. Mater. Devices*, vol. 5, no. 1, pp. 10–29, 2020, doi: 10.1016/j.jsamd.2020.01.006.
[31] K. S. Kim *et al.*, "Large-scale pattern growth of graphene films for stretchable transparent electrodes," *Nature*, vol. 457, no. 7230, pp. 706–710, 2009, doi: 10.1038/nature07719.
[32] X. Li and L. Zhi, "Graphene hybridization for energy storage applications," *Chem. Soc. Rev.*, vol. 47, no. 9, pp. 3189–3216, 2018, doi: 10.1039/c7cs00871f.
[33] R. R. Nair *et al.*, "Fine structure constant defines visual transparency of graphene," *Science (80-. ).*, vol. 320, no. 5881, p. 1308, 2008, doi: 10.1126/science.1156965.
[34] M. Tahriri *et al.*, "Graphene and its derivatives: Opportunities and challenges in dentistry," *Mater. Sci. Eng. C*, vol. 102, no. April, pp. 171–185, 2019, doi: 10.1016/j.msec.2019.04.051.
[35] S. J. Rowley-Neale, E. P. Randviir, A. S. Abo Dena, and C. E. Banks, "An overview of recent applications of reduced graphene oxide as a basis of electroanalytical sensing platforms," *Appl. Mater. Today*, vol. 10, pp. 218–226, 2018, doi: 10.1016/j.apmt.2017.11.010.
[36] J. Yang *et al.*, "Studies on directly grown few layer graphene processed using tape-peeling method," *Carbon N. Y.*, vol. 158, no. xxxx, pp. 749–755, 2020, doi: 10.1016/j.carbon.2019.11.049.
[37] W. Wu *et al.*, "Fast chemical exfoliation of graphite to few-layer graphene with high quality and large size via a two-step microwave-assisted process," *Chem. Eng. J.*, vol. 381, no. August 2019, 2020, doi: 10.1016/j.cej.2019.122592.
[38] S. Thamer, B. H. Al-Tamimi, and S. B. H. Farid, "Preparation of graphene nano-sheets from graphite flakes via milling-ultrasonication promoted process," *Mater. Today Proc.*, vol. 20, no. xxxx, pp. 579–582, 2020, doi: 10.1016/j.matpr.2019.09.192.
[39] H. Zhang, F. Ding, H. Li, F. Qu, H. Meng, and H. Gu, "Controlled synthesis of monolayer graphene with a high quality by pyrolysis of silicon carbide," *Mater. Lett.*, vol. 244, pp. 171–174, 2019, doi: 10.1016/j.matlet.2019.02.038.
[40] H. K. Hong *et al.*, "Synthesis of high-quality monolayer graphene by low-power plasma," *Curr. Appl. Phys.*, vol. 19, no. 1, pp. 44–49, 2019, doi: 10.1016/j.cap.2018.11.003.
[41] D. Dai *et al.*, "Thermal CVD growth of graphene on copper particles targeting tungsten-copper composites with superior wear and arc ablation resistance properties," *Diam. Relat. Mater.*, vol. 104, no. December 2019, p. 107765, 2020, doi: 10.1016/j.diamond.2020.107765.
[42] M. Naguib *et al.*, "Two-dimensional nanocrystals produced by exfoliation of Ti 3AlC 2," *Adv. Mater.*, vol. 23, no. 37, pp. 4248–4253, 2011, doi: 10.1002/adma.201102306.

[43] M. Naguib *et al.*, "Two-dimensional transition metal carbides," *ACS Nano*, vol. 6, no. 2, pp. 1322–1331, 2012, doi: 10.1021/nn204153h.
[44] Q. Yang *et al.*, "MXene/graphene hybrid fibers for high performance flexible supercapacitors," *J. Mater. Chem. A*, vol. 5, no. 42, pp. 22113–22119, 2017, doi: 10.1039/c7ta07999k.
[45] Y. Liu, J. Yu, D. Guo, Z. Li, and Y. Su, "Ti3C2Tx MXene/graphene nanocomposites: Synthesis and application in electrochemical energy storage," *J. Alloys Compd.*, vol. 815, p. 152403, 2020, doi: 10.1016/j.jallcom.2019.152403.
[46] X. Wang *et al.*, "Pseudocapacitance of MXene nanosheets for high-power sodium-ion hybrid capacitors," *Nat. Commun.*, vol. 6, pp. 1–6, 2015, doi: 10.1038/ncomms7544.
[47] K. Hantanasirisakul and Y. Gogotsi, "Electronic and Optical Properties of 2D Transition Metal Carbides and Nitrides (MXenes)," *Adv. Mater.*, vol. 30, no. 52, pp. 1–30, 2018, doi: 10.1002/adma.201804779.
[48] J. Pang *et al.*, "Applications of 2D MXenes in energy conversion and storage systems," *Chem. Soc. Rev.*, vol. 48, no. 1, pp. 72–133, 2019, doi: 10.1039/c8cs00324f.
[49] N. Aslfattahi, L. Samylingam, A. S. Abdelrazik, A. Arifutzzaman, and R. Saidur, "MXene based new class of silicone oil nanofluids for the performance improvement of concentrated photovoltaic thermal collector," *Sol. Energy Mater. Sol. Cells*, vol. 211, no. April, p. 110526, 2020, doi: 10.1016/j.solmat.2020.110526.
[50] N. R. Hemanth and B. Kandasubramanian, "Recent advances in 2D MXenes for enhanced cation intercalation in energy harvesting Applications: A review," *Chem. Eng. J.*, p. 123678, 2019, doi: 10.1016/j.cej.2019.123678.
[51] S. Venkateshalu and A. N. Grace, "MXenes—A new class of 2D layered materials: Synthesis, properties, applications as supercapacitor electrode and beyond," *Appl. Mater. Today*, vol. 18, p. 100509, 2020, doi: 10.1016/j.apmt.2019.100509.
[52] J. Mei, G. A. Ayoko, C. Hu, J. M. Bell, and Z. Sun, "Two-dimensional fluorine-free mesoporous Mo2C MXene via UV-induced selective etching of Mo2Ga2C for energy storage," *Sustain. Mater. Technol.*, vol. 25, p. e00156, 2020, doi: 10.1016/j.susmat.2020.e00156.
[53] M. Alhabeb *et al.*, "Selective Etching of Silicon from Ti3SiC2 (MAX) To Obtain 2D Titanium Carbide (MXene)," *Angew. Chemie - Int. Ed.*, vol. 57, no. 19, pp. 5444–5448, 2018, doi: 10.1002/anie.201802232.
[54] T. Li *et al.*, "Fluorine-Free Synthesis of High-Purity Ti3C2Tx (T=OH, O) via Alkali Treatment," *Angew. Chemie - Int. Ed.*, vol. 57, no. 21, pp. 6115–6119, 2018, doi: 10.1002/anie.201800887.
[55] A. Feng *et al.*, "Fabrication and thermal stability of NH4HF2-etched Ti3C2 MXene," *Ceram. Int.*, vol. 43, no. 8, pp. 6322–6328, 2017, doi: 10.1016/j.ceramint.2017.02.039.
[56] T. Zhang *et al.*, "Synthesis of two-dimensional Ti3C2TxMXene using HCl+LiF etchant: Enhanced exfoliation and delamination," *J. Alloys Compd.*, vol. 695, pp. 818–826, 2017, doi: 10.1016/j.jallcom.2016.10.127.
[57] W. Sun *et al.*, "Electrochemical etching of Ti2AlC to Ti2CT:X (MXene) in low-concentration hydrochloric acid solution," *J. Mater. Chem. A*, vol. 5, no. 41, pp. 21663–21668, 2017, doi: 10.1039/c7ta05574a.
[58] P. Urbankowski *et al.*, "Synthesis of two-dimensional titanium nitride Ti4N3 (MXene)," *Nanoscale*, vol. 8, no. 22, pp. 11385–11391, 2016, doi: 10.1039/c6nr02253g.
[59] C. (John) Zhang *et al.*, "Two-Dimensional Transition Metal Carbides and Nitrides (MXenes): Synthesis, Properties, and Electrochemical Energy Storage Applications," *Energy Environ. Mater.*, pp. 1–27, 2019, doi: 10.1002/eem2.12058.
[60] R. M. Ronchi, J. T. Arantes, and S. F. Santos, "Synthesis, structure, properties and applications of MXenes: Current status and perspectives," *Ceram. Int.*, vol. 45, no. 15, pp.

18167–18188, 2019, doi: 10.1016/j.ceramint.2019.06.114.
[61] L. Verger, V. Natu, M. Carey, and M. W. Barsoum, “MXenes: An Introduction of Their Synthesis, Select Properties, and Applications,” *Trends Chem.*, vol. 1, no. 7, pp. 656–669, 2019, doi: 10.1016/j.trechm.2019.04.006.
[62] A. Ali, A. Belaidi, S. Ali, M. I. Helal, and K. A. Mahmoud, “Transparent and conductive Ti3C2Tx (MXene) thin film fabrication by electrohydrodynamic atomization technique,” *J. Mater. Sci. Mater. Electron.*, vol. 27, no. 5, pp. 5440–5445, 2016, doi: 10.1007/s10854-016-4447-z.
[63] Y. L. and M. Ballauff, *Hybrid Nanomaterials*. United States: Wiley, 2011.
[64] Y. Wu and T. van Ree, *Introduction: Energy technologies and their role in our life*. Elsevier Inc., 2018.
[65] V. Bhalla, V. Khullar, and H. Tyagi, “Experimental investigation of photo-thermal analysis of blended nanoparticles (Al2O3/Co3O4) for direct absorption solar thermal collector,” *Renew. Energy*, vol. 123, no. February, pp. 616–626, 2018, doi: 10.1016/j.renene.2018.01.042.
[66] I. Chopkar, S. Sudarshan, P. K. Das, and I. Manna, “Effect of particle size on thermal conductivity of nanofluid,” *Metall. Mater. Trans. A Phys. Metall. Mater. Sci.*, vol. 39, no. 7, pp. 1535–1542, 2008, doi: 10.1007/s11661-007-9444-7.
[67] F. Kong *et al.*, “Further surface modification by carbon coating for in-situ growth of Fe3O4 nanoparticles on MXene Ti3C2 multilayers for advanced Li-ion storage,” *Electrochim. Acta*, vol. 289, pp. 228–237, 2018, doi: 10.1016/j.electacta.2018.09.007.
[68] P. Van Trinh, N. N. Anh, N. T. Hong, P. N. Hong, P. N. Minh, and B. H. Thang, “Experimental study on the thermal conductivity of ethylene glycol-based nanofluid containing Gr-CNT hybrid material,” *J. Mol. Liq.*, vol. 269, pp. 344–353, 2018, doi: 10.1016/j.molliq.2018.08.071.
[69] C. Zhao, Q. Wang, H. Zhang, S. Passerini, and X. Qian, “Two-Dimensional Titanium Carbide/RGO Composite for High-Performance Supercapacitors,” *ACS Appl. Mater. Interfaces*, vol. 8, no. 24, pp. 15661–15667, 2016, doi: 10.1021/acsami.6b04767.
[70] J.-F. Berret *et al.*, “Electrostatic Self-assembly : A New Route Towards Nanostructures,” p. 5, 2005, [Online]. Available: http://arxiv.org/abs/cond-mat/0501083.
[71] X. Jin *et al.*, “Superior role of MXene nanosheet as hybridization matrix over graphene in enhancing interfacial electronic coupling and functionalities of metal oxide,” *Nano Energy*, vol. 53, pp. 841–848, 2018, doi: 10.1016/j.nanoen.2018.09.055.
[72] Z. Wang *et al.*, “Facile fabrication of flexible rGO/MXene hybrid fiber-like electrode with high volumetric capacitance,” *J. Power Sources*, vol. 448, no. August, p. 227398, 2020, doi: 10.1016/j.jpowsour.2019.227398.
[73] X. W. Liu, F. Y. Wang, F. Zhen, and J. R. Huang, “In situ growth of Au nanoparticles on the surfaces of Cu2O nanocubes for chemical sensors with enhanced performance,” *RSC Adv.*, vol. 2, no. 20, pp. 7647–7651, 2012, doi: 10.1039/c2ra20789c.
[74] L. S. Sundar, M. K. Singh, and A. C. M. Sousa, “Turbulent heat transfer and friction factor of nanodiamond-nickel hybrid nanofluids flow in a tube: An experimental study,” *Int. J. Heat Mass Transf.*, vol. 117, pp. 223–234, 2018, doi: 10.1016/j.ijheatmasstransfer.2017.09.109.
[75] X. Li, J. Zhu, L. Wang, W. Wu, and Y. Fang, “In–situ growth of carbon nanotubes on two–dimensional titanium carbide for enhanced electrochemical prformance,” *Electrochim. Acta*, vol. 258, pp. 291–301, 2017, doi: 10.1016/j.electacta.2017.11.004.
[76] A. M. Pourrahimi, D. Liu, V. Ström, M. S. Hedenqvist, R. T. Olsson, and U. W. Gedde, “Heat treatment of ZnO nanoparticles: new methods to achieve high-purity nanoparticles for high-voltage applications,” *J. Mater. Chem. A*, vol. 3, no. 33, pp. 17190–17200, 2015, doi: 10.1039/c5ta03120f.
[77] I. Sengupta, S. Chakraborty, M. Talukdar, S. K. Pal, and S. Chakraborty, “Thermal reduction of graphene oxide: How temperature influences purity,” *J. Mater. Res.*, vol. 33, no. 23, pp.

4113–4122, 2018, doi: 10.1557/jmr.2018.338.
[78] C. Shen *et al.*, “Novel Li4Ti5O12/Ti3C2Tx nanocomposite as a high rate anode material for lithium ion batteries,” *J. Alloys Compd.*, vol. 735, pp. 530–535, 2018, doi: 10.1016/j.jallcom.2017.11.164.
[79] J. Tu *et al.*, “Facile synthesis of TiN nanocrystals/graphene hybrid to chemically suppress the shuttle effect for lithium-sulfur batteries,” *J. Alloys Compd.*, vol. 822, p. 153751, 2020, doi: 10.1016/j.jallcom.2020.153751.
[80] H. Shi *et al.*, “Synthesis of TiN nanostructures by Mg-assisted nitriding TiO2 in N2 for lithium ion storage,” *Chem. Eng. J.*, vol. 336, no. August 2017, pp. 12–19, 2018, doi: 10.1016/j.cej.2017.11.036.
[81] N. K. Chaudhari, H. Jin, B. Kim, D. San Baek, S. H. Joo, and K. Lee, “MXene: An emerging two-dimensional material for future energy conversion and storage applications,” *J. Mater. Chem. A*, vol. 5, no. 47, pp. 24564–24579, 2017, doi: 10.1039/c7ta09094c.
[82] M. Boota *et al.*, “Interaction of Polar and Nonpolar Polyfluorenes with Layers of Two-Dimensional Titanium Carbide (MXene): Intercalation and Pseudocapacitance,” *Chem. Mater.*, vol. 29, no. 7, pp. 2731–2738, 2017, doi: 10.1021/acs.chemmater.6b03933.
[83] M. Sethi, H. Bantawal, U. S. Shenoy, and D. K. Bhat, “Eco-friendly synthesis of porous graphene and its utilization as high performance supercapacitor electrode material,” *J. Alloys Compd.*, vol. 799, pp. 256–266, 2019, doi: 10.1016/j.jallcom.2019.05.302.
[84] A. Yu, V. Chabot, and J. Zhang, *Electrochemical Supercapacitors For Energy Storage and Delivery*. 2013.
[85] I. Piñeiro-Prado, D. Salinas-Torres, R. Ruiz-Rosas, E. Morallón, and D. Cazorla-Amorós, “Design of activated carbon/activated carbon asymmetric capacitors,” *Front. Mater.*, vol. 3, no. March, pp. 1–12, 2016, doi: 10.3389/fmats.2016.00016.
[86] M. Inagaki, F. Kang, M. Toyoda, and H. Konno, “Carbon Materials for Electrochemical Capacitors,” *Adv. Mater. Sci. Eng. Carbon*, vol. 2, pp. 237–265, 2014, doi: 10.1016/b978-0-12-407789-8.00011-9.
[87] M. Sevilla, R. Mokaya, and A. B. Fuertes, “Ultrahigh surface area polypyrrole-based carbons with superior performance for hydrogen storage,” *Energy Environ. Sci.*, vol. 4, no. 8, pp. 2930–2936, 2011, doi: 10.1039/c1ee01608c.
[88] X. Peng, L. Peng, C. Wu, and Y. Xie, “Two dimensional nanomaterials for flexible supercapacitors,” *Chem. Soc. Rev.*, vol. 43, no. 10, pp. 3303–3323, 2014, doi: 10.1039/c3cs60407a.
[89] H. Hwang, C. H. Kim, J. H. Wee, J. H. Han, and C. M. Yang, “High-density graphene/single-walled carbon nanohorn composite supercapacitor electrode with high volumetric capacitance,” *Appl. Surf. Sci.*, vol. 489, no. May, pp. 708–716, 2019, doi: 10.1016/j.apsusc.2019.05.332.
[90] Y. Zheng, Y. Tian, S. Sarwar, J. Luo, and X. Zhang, “Carbon nanotubes decorated NiSe2 nanosheets for high-performance supercapacitors,” *J. Power Sources*, vol. 452, no. August 2019, p. 227793, 2020, doi: 10.1016/j.jpowsour.2020.227793.
[91] A. Chang, C. Zhang, Y. Yu, Y. Yu, and B. Zhang, “Plasma-Assisted Synthesis of NiSe 2 Ultrathin Porous Nanosheets with Selenium Vacancies for Supercapacitor,” *ACS Appl. Mater. Interfaces*, vol. 10, no. 49, pp. 41861–41865, 2018, doi: 10.1021/acsami.8b16072.
[92] H. Jiang *et al.*, “A novel MnO2/Ti3C2Tx MXene nanocomposite as high performance electrode materials for flexible supercapacitors,” *Electrochim. Acta*, vol. 290, pp. 695–703, 2018, doi: 10.1016/j.electacta.2018.08.096.
[93] J. B. Goodenough and K. S. Park, “The Li-ion rechargeable battery: A perspective,” *J. Am. Chem. Soc.*, vol. 135, no. 4, pp. 1167–1176, 2013, doi: 10.1021/ja3091438.
[94] H. Yang *et al.*, “Hierarchical porous mnco2o4 yolk-shell microspheres from mofs as secondary nanomaterials for high power lithium ion batteries,” *Dalt. Trans.*, vol. 48, no. 25,

pp. 9205–9213, 2019, doi: 10.1039/c9dt00613c.
[95] H. Xu, Z. Sun, and J. Chen, *Graphene-based anode materials for lithium-ion batteries*. INC, 2020.
[96] C. Jiang, E. Hosono, and H. Zhou, "Nanomaterials for lithium ion batteries," *Nano Today*, vol. 1, no. 4, pp. 28–33, 2006, doi: 10.1016/S1748-0132(06)70114-1.
[97] Y. Fang *et al.*, "MXene-derived TiO2/reduced graphene oxide composite with an enhanced capacitive capacity for Li-ion and K-ion batteries," *J. Mater. Chem. A*, vol. 7, no. 10, pp. 5363–5372, 2019, doi: 10.1039/c8ta12069b.
[98] H. Luo *et al.*, "Highly conductive graphene-modified TiO2 hierarchical film electrode for flexible Li-ion battery anode," *Electrochim. Acta*, vol. 313, pp. 10–19, 2019, doi: 10.1016/j.electacta.2019.05.018.
[99] I. Dincer and Y. Bicer, *System integration for multigeneration*. 2020.
[100] L. Mongibello, M. Capezzuto, and G. Graditi, "Technical and cost analyses of two different heat storage systems for residential micro-CHP plants," *Appl. Therm. Eng.*, vol. 71, no. 2, pp. 636–642, 2014, doi: 10.1016/j.applthermaleng.2013.10.026.
[101] S. Song *et al.*, "Polyethylene glycol/halloysite@Ag nanocomposite PCM for thermal energy storage: Simultaneously high latent heat and enhanced thermal conductivity," *Sol. Energy Mater. Sol. Cells*, vol. 193, no. December 2018, pp. 237–245, 2019, doi: 10.1016/j.solmat.2019.01.023.
[102] D. S. Ezhumalai, G. Sriharan, and S. Harikrishnan, "Improved Thermal Energy Storage Behavior of CuO/Palmitic acid Composite as Phase Change Material," *Mater. Today Proc.*, vol. 5, no. 6, pp. 14618–14627, 2018, doi: 10.1016/j.matpr.2018.03.053.
[103] G. Q. Qi *et al.*, "Enhanced comprehensive performance of polyethylene glycol based phase change material with hybrid graphene nanomaterials for thermal energy storage," *Carbon N. Y.*, vol. 88, pp. 196–205, 2015, doi: 10.1016/j.carbon.2015.03.009.
[104] Y. Zhou, C. Li, H. Wu, and S. Guo, "Construction of hybrid graphene oxide/graphene nanoplates shell in paraffin microencapsulated phase change materials to improve thermal conductivity for thermal energy storage," *Colloids Surfaces A Physicochem. Eng. Asp.*, vol. 597, no. February, p. 124780, 2020, doi: 10.1016/j.colsurfa.2020.124780.
[105] H. K. Sharma, S. K. Verma, P. K. Singh, S. Kumar, M. Kant Paswan, and P. Singhal, "Performance analysis of paraffin wax as PCM by using hybrid zinc-cobalt-iron oxide nano-fluid on latent heat energy storage system," *Mater. Today Proc.*, vol. 26, no. xxxx, pp. 1461–1464, 2020, doi: 10.1016/j.matpr.2020.02.300.
[106] Z. Liu, Z. Chen, and F. Yu, "Enhanced thermal conductivity of microencapsulated phase change materials based on graphene oxide and carbon nanotube hybrid filler," *Sol. Energy Mater. Sol. Cells*, vol. 192, no. December 2018, pp. 72–80, 2019, doi: 10.1016/j.solmat.2018.12.014.
[107] S. Akilu, A. T. Baheta, S. Chowdhury, E. Padmanabhan, and K. V. Sharma, "Thermophysical profile of SiC–CuO/C nanocomposite in base liquid ethylene glycol," *Powder Technol.*, vol. 354, pp. 540–551, 2019, doi: 10.1016/j.powtec.2019.04.061.
[108] M. H. Esfe, S. Esfandeh, M. K. Amiri, and M. Afrand, "A novel applicable experimental study on the thermal behavior of SWCNTs(60%)-MgO(40%)/EG hybrid nanofluid by focusing on the thermal conductivity," *Powder Technol.*, vol. 342, pp. 998–1007, 2019, doi: 10.1016/j.powtec.2018.10.008.
[109] A. Kakavandi and M. Akbari, "Experimental investigation of thermal conductivity of nanofluids containing of hybrid nanoparticles suspended in binary base fluids and propose a new correlation," *Int. J. Heat Mass Transf.*, vol. 124, pp. 742–751, 2018, doi: 10.1016/j.ijheatmasstransfer.2018.03.103.
[110] H. W. Xian, N. A. C. Sidik, and R. Saidur, "Impact of different surfactants and ultrasonication time on the stability and thermophysical properties of hybrid nanofluids," *Int. Commun. Heat*

*Mass Transf.*, vol. 110, 2020, doi: 10.1016/j.icheatmasstransfer.2019.104389.
[111] A. Alshare, W. Al-Kouz, and W. Khan, "Cu-Al2O3 water hybrid nanofluid transport in a periodic structure," *Processes*, vol. 8, no. 3, 2020, doi: 10.3390/pr8030285.
[112] Z. Said, M. A. Abdelkareem, H. Rezk, A. M. Nassef, and H. Z. Atwany, *Stability, thermophysical and electrical properties of synthesized carbon nanofiber and reduced-graphene oxide-based nanofluids and their hybrid along with fuzzy modeling approach*, vol. 364. Elsevier B.V, 2020.
[113] E. C. Okonkwo, I. Wole-Osho, D. Kavaz, and M. Abid, "Comparison of experimental and theoretical methods of obtaining the thermal properties of alumina/iron mono and hybrid nanofluids," *J. Mol. Liq.*, vol. 292, p. 111377, 2019, doi: 10.1016/j.molliq.2019.111377.
[114] S. M. Mousavi, F. Esmaeilzadeh, and X. P. Wang, "A detailed investigation on the thermo-physical and rheological behavior of MgO/TiO 2 aqueous dual hybrid nanofluid," *J. Mol. Liq.*, vol. 282, pp. 323–339, 2019, doi: 10.1016/j.molliq.2019.02.100.
[115] A. Asadi, M. Asadi, A. Rezaniakolaei, L. A. Rosendahl, M. Afrand, and S. Wongwises, "Heat transfer efficiency of Al2O3-MWCNT/thermal oil hybrid nanofluid as a cooling fluid in thermal and energy management applications: An experimental and theoretical investigation," *Int. J. Heat Mass Transf.*, vol. 117, pp. 474–486, 2018, doi: 10.1016/j.ijheatmasstransfer.2017.10.036.
[116] S. Akilu, A. T. Baheta, and K. V. Sharma, "Experimental measurements of thermal conductivity and viscosity of ethylene glycol-based hybrid nanofluid with TiO2-CuO/C inclusions," *J. Mol. Liq.*, vol. 246, pp. 396–405, 2017, doi: 10.1016/j.molliq.2017.09.017.
[117] S. Kannaiyan, C. Boobalan, A. Umasankaran, A. Ravirajan, S. Sathyan, and T. Thomas, "Comparison of experimental and calculated thermophysical properties of alumina/cupric oxide hybrid nanofluids," *J. Mol. Liq.*, vol. 244, pp. 469–477, 2017, doi: 10.1016/j.molliq.2017.09.035.
[118] M. S. Kumar, V. Vasu, and A. V. Gopal, "Thermal conductivity and rheological studies for Cu–Zn hybrid nanofluids with various basefluids," *J. Taiwan Inst. Chem. Eng.*, vol. 66, pp. 321–327, 2016, doi: 10.1016/j.jtice.2016.05.033.
[119] S. Aberoumand and A. Jafarimoghaddam, "Tungsten (III) oxide (WO3) – Silver/transformer oil hybrid nanofluid: Preparation, stability, thermal conductivity and dielectric strength," *Alexandria Eng. J.*, vol. 57, no. 1, pp. 169–174, 2018, doi: 10.1016/j.aej.2016.11.003.
[120] M. Tahmasebi Sulgani and A. Karimipour, "Improve the thermal conductivity of 10w40-engine oil at various temperature by addition of Al 2 O 3 /Fe 2 O 3 nanoparticles," *J. Mol. Liq.*, vol. 283, pp. 660–666, 2019, doi: 10.1016/j.molliq.2019.03.140.
[121] S. H. Qing, W. Rashmi, M. Khalid, T. C. S. M. Gupta, M. Nabipoor, and M. T. Hajibeigy, "Thermal conductivity and electrical properties of Hybrid SiO2-graphene naphthenic mineral oil nanofluid as potential transformer oil," *Mater. Res. Express*, vol. 4, no. 1, 2017, doi: 10.1088/2053-1591/aa550e.
[122] M. Karami, "Experimental investigation of first and second laws in a direct absorption solar collector using hybrid Fe 3 O 4 /SiO 2 nanofluid," *J. Therm. Anal. Calorim.*, vol. 136, no. 2, pp. 661–671, 2019, doi: 10.1007/s10973-018-7624-x.
[123] A. Ahmed, H. Baig, S. Sundaram, and T. K. Mallick, "Use of Nanofluids in Solar PV/Thermal Systems," *Int. J. Photoenergy*, vol. 2019, pp. 1–17, 2019, doi: 10.1155/2019/8039129.
[124] T. R. Shah and H. M. Ali, "Applications of hybrid nanofluids in solar energy, practical limitations and challenges: A critical review," *Sol. Energy*, vol. 183, no. February, pp. 173–203, 2019, doi: 10.1016/j.solener.2019.03.012.
[125] J. Zeng and Y. Xuan, "Enhanced solar thermal conversion and thermal conduction of MWCNT-SiO2/Ag binary nanofluids," *Appl. Energy*, vol. 212, no. December 2017, pp. 809–819, 2018, doi: 10.1016/j.apenergy.2017.12.083.
[126] J. Fang and Y. Xuan, "Investigation of optical absorption and photothermal conversion

characteristics of binary CuO/ZnO nanofluids," *RSC Adv.*, vol. 7, no. 88, pp. 56023–56033, 2017, doi: 10.1039/c7ra12022b.
[127] M. Chen, Y. He, J. Huang, and J. Zhu, "Synthesis and solar photo-thermal conversion of Au, Ag, and Au-Ag blended plasmonic nanoparticles," *Energy Convers. Manag.*, vol. 127, pp. 293–300, 2016, doi: 10.1016/j.enconman.2016.09.015.
[128] X. Wang, Y. He, M. Chen, and Y. Hu, "ZnO-Au composite hierarchical particles dispersed oil-based nanofluids for direct absorption solar collectors," *Sol. Energy Mater. Sol. Cells*, vol. 179, no. August 2017, pp. 185–193, 2018, doi: 10.1016/j.solmat.2017.11.012.
[129] E. Farajzadeh, S. Movahed, and R. Hosseini, "Experimental and numerical investigations on the effect of Al2O3/TiO2-H2O nanofluids on thermal efficiency of the flat plate solar collector," *Renew. Energy*, vol. 118, pp. 122–130, 2018, doi: 10.1016/j.renene.2017.10.102.
[130] D. Wang *et al.*, "Enhanced photothermal conversion properties of magnetic nanofluids through rotating magnetic field for direct absorption solar collector," *J. Colloid Interface Sci.*, vol. 557, pp. 266–275, 2019, doi: 10.1016/j.jcis.2019.09.022.
[131] A. Younis, M. Onsa, Y. Alhorr, and E. Elsarrag, "The Influence of Al2O3- ZnO-H2O Nanofluid on the Thermodynamic Performance of Photovoltaic- Thermal Hybrid Solar Collector System," *Innov. Energy Res.*, vol. 07, no. 01, pp. 1–8, 2018, doi: 10.4172/2576-1463.1000187.
[132] A. H. A. Al-Waeli *et al.*, "Evaluation of the nanofluid and nano-PCM based photovoltaic thermal (PVT) system: An experimental study," *Energy Convers. Manag.*, vol. 151, no. September, pp. 693–708, 2017, doi: 10.1016/j.enconman.2017.09.032.
[133] F. Crisostomo, N. Hjerrild, S. Mesgari, Q. Li, and R. A. Taylor, "A hybrid PV/T collector using spectrally selective absorbing nanofluids," *Appl. Energy*, vol. 193, pp. 1–14, 2017, doi: 10.1016/j.apenergy.2017.02.028.
[134] R. Nasrin, S. Parvin, and M. A. Alim, "Heat transfer and collector efficiency through a direct absorption solar collector with radiative heat flux effect," *Numer. Heat Transf. Part A Appl.*, vol. 68, no. 8, pp. 887–907, 2015, doi: 10.1080/10407782.2015.1023122.
[135] M. Du, G. H. Tang, and T. M. Wang, "Exergy analysis of a hybrid PV/T system based on plasmonic nanofluids and silica aerogel glazing," *Sol. Energy*, vol. 183, no. November 2018, pp. 501–511, 2019, doi: 10.1016/j.solener.2019.03.057.
[136] M. Hissouf, M. Feddaoui, M. Najim, and A. Charef, "Numerical study of a covered Photovoltaic-Thermal Collector (PVT) enhancement using nanofluids," *Sol. Energy*, vol. 199, no. August 2019, pp. 115–127, 2020, doi: 10.1016/j.solener.2020.01.083.
[137] A. S. Abdelrazik, K. H. Tan, N. Aslfattahi, A. Arifutzzaman, R. Saidur, and F. A. Al-Sulaiman, "Optical, stability and energy performance of water-based MXene nanofluids in hybrid PV/thermal solar systems," *Sol. Energy*, vol. 204, no. December 2019, pp. 32–47, 2020, doi: 10.1016/j.solener.2020.04.063.
[138] X. Han, X. Chen, Y. Sun, and J. Qu, "Performance improvement of a PV/T system utilizing Ag/CoSO4-propylene glycol nanofluid optical filter," *Energy*, vol. 192, p. 116611, 2020, doi: 10.1016/j.energy.2019.116611.
[139] S. S. Khaleduzzaman *et al.*, "Energy and exergy analysis of alumina-water nanofluid for an electronic liquid cooling system," *Int. Commun. Heat Mass Transf.*, vol. 57, pp. 118–127, 2014, doi: 10.1016/j.icheatmasstransfer.2014.07.015.
[140] R. Saidur, K. Y. Leong, and H. A. Mohammed, "A review on applications and challenges of nanofluids," *Renew. Sustain. Energy Rev.*, vol. 15, no. 3, pp. 1646–1668, 2011, doi: 10.1016/j.rser.2010.11.035.
[141] S. M. Sohel Murshed and C. A. Nieto de Castro, "A critical review of traditional and emerging techniques and fluids for electronics cooling," *Renew. Sustain. Energy Rev.*, vol. 78, no. February, pp. 821–833, 2017, doi: 10.1016/j.rser.2017.04.112.
[142] B. Agostini, M. Fabbri, J. E. Park, L. Wojtan, J. R. Thome, and B. Michel, "State of the art of

high heat flux cooling technologies," *Heat Transf. Eng.*, vol. 28, no. 4, pp. 258–281, 2007, doi: 10.1080/01457630601117799.
[143] M. Bahiraei and S. Heshmatian, "Efficacy of a novel liquid block working with a nanofluid containing graphene nanoplatelets decorated with silver nanoparticles compared with conventional CPU coolers," *Appl. Therm. Eng.*, vol. 127, pp. 1233–1245, 2017, doi: 10.1016/j.applthermaleng.2017.08.136.
[144] S. D. Barewar, S. Tawri, and S. S. Chougule, "Experimental investigation of thermal conductivity and its ANN modeling for glycol-based Ag/ZnO hybrid nanofluids with low concentration," *J. Therm. Anal. Calorim.*, vol. 139, no. 3, pp. 1779–1790, 2020, doi: 10.1007/s10973-019-08618-6.
[145] R. K. Bumataria, N. K. Chavda, and H. Panchal, "Current research aspects in mono and hybrid nanofluid based heat pipe technologies," *Heliyon*, vol. 5, no. 5, p. e01627, 2019, doi: 10.1016/j.heliyon.2019.e01627.
[146] R. Ramachandran, K. Ganesan, M. R. Rajkumar, L. G. Asirvatham, and S. Wongwises, "Comparative study of the effect of hybrid nanoparticle on the thermal performance of cylindrical screen mesh heat pipe," *Int. Commun. Heat Mass Transf.*, vol. 76, pp. 294–300, 2016, doi: 10.1016/j.icheatmasstransfer.2016.05.030.
[147] K. Swapnil, P. Dhananjay, Z. Gaurav, R. Anand, and D. P. Kamble, "Heat Transfer Enhancement of Circular Heat Pipe with Al2O3 BN / Water Hybrid Nanofluid," vol. 4, no. 4, pp. 138–143, 2016.
[148] R. N. Ramachandran, K. Ganesan, and L. G. Asirvatham, "The role of hybrid nanofluids in improving the thermal characteristics of screen mesh cylindrical heat pipes," *Therm. Sci.*, vol. 20, no. 6, pp. 2027–2035, 2016, doi: 10.2298/TSCI150710006R.
[149] S. Anitha, T. Thomas, V. Parthiban, and M. Pichumani, "What dominates heat transfer performance of hybrid nanofluid in single pass shell and tube heat exchanger?," *Adv. Powder Technol.*, vol. 30, no. 12, pp. 3107–3117, 2019, doi: 10.1016/j.apt.2019.09.018.
[150] N. Ahammed, L. G. Asirvatham, and S. Wongwises, "Entropy generation analysis of graphene–alumina hybrid nanofluid in multiport minichannel heat exchanger coupled with thermoelectric cooler," *Int. J. Heat Mass Transf.*, vol. 103, pp. 1084–1097, 2016, doi: 10.1016/j.ijheatmasstransfer.2016.07.070.
[151] M. H. Ahmadi, M. Ghazvini, M. Sadeghzadeh, M. Alhuyi Nazari, and M. Ghalandari, "Utilization of hybrid nanofluids in solar energy applications: A review," *Nano-Structures and Nano-Objects*, vol. 20, p. 100386, 2019, doi: 10.1016/j.nanoso.2019.100386.
[152] M. H. Aghabozorg, A. Rashidi, and S. Mohammadi, "Experimental investigation of heat transfer enhancement of Fe2O3-CNT/water magnetic nanofluids under laminar, transient and turbulent flow inside a horizontal shell and tube heat exchanger," *Exp. Therm. Fluid Sci.*, vol. 72, pp. 182–189, 2016, doi: 10.1016/j.expthermflusci.2015.11.011.
[153] A. Bhattad, J. Sarkar, and P. Ghosh, "Experimentation on effect of particle ratio on hydrothermal performance of plate heat exchanger using hybrid nanofluid," *Appl. Therm. Eng.*, vol. 162, no. April, p. 114309, 2019, doi: 10.1016/j.applthermaleng.2019.114309.
[154] S. A. Kaska, R. A. Khalefa, and A. M. Hussein, "Hybrid nanofluid to enhance heat transfer under turbulent flow in a flat tube," *Case Stud. Therm. Eng.*, vol. 13, no. March, p. 100398, 2019, doi: 10.1016/j.csite.2019.100398.
[155] H. R. Allahyar, F. Hormozi, and B. ZareNezhad, "Experimental investigation on the thermal performance of a coiled heat exchanger using a new hybrid nanofluid," *Exp. Therm. Fluid Sci.*, vol. 76, pp. 324–329, 2016, doi: 10.1016/j.expthermflusci.2016.03.027.

# Recent Progress in Emerging Hybrid Nanomaterials Towards the Energy Storage and Heat Transfer Applications: A review

[1]M.K. Muhamad Azim, [2,3]A. Arifutzzaman*, [3,4]R. Saidur, [1]M.U. Khandaker, [1]D.A. Bradley

[1]*Center for Biomedical Physics, School of Healthcare and Medical Sciences, Sunway University, 47500 Bandar Sunway, Selangor Darul Ehsan, Malaysia.*
[2]*Research Centre for Carbon Dioxide Capture and Utilisation (CCDCU), School of Engineering and Technology, Sunway University, No. 5, Jalan Universiti, Bandar Sunway, Petaling Jaya, 47500 Selangor Darul Ehsan, Malaysia.*
[3]*Research Center for Nano-Materials and Energy Technology (RCNMET), School of Science and Technology, Sunway University, Bandar Sunway, Petaling Jaya, 47500, Selangor Darul Ehsan, Malaysia*
[4]*Department of Engineering, Lancaster University, Lancaster, LA1 4YW, UK*

* For correspondence: A. Arifutzzaman: Email: arifrahat@sunway.edu.my, Contact: +60182500971 (cell).

**Abstract:** Hybrid nanomaterials, which is a combination of two or more nanoparticles have been extensively evaluated as a promising candidate for energy storage and heat transfer applications, benefitting from the rise of synergistic effects between them. The unique form of this emerging combination of nanomaterials not only offers the improved features of the integrated nanoparticles but gives us the opportunity to tailor their physicochemical properties simply by modifying their composition and morphology. Scientific findings have demonstrated that the dispersion of hybrid nanomaterials in the base fluids, known as - hybrid nanofluids gives us the alternative way to replace mono nanofluid and the conventional heat transfer fluids as it provides a much better heat transfer enhancement that is beneficial for advanced heat transfer devices. On the other hand, when hybrid nanomaterials were utilized for energy storage devices, it exhibits an outstanding electrochemical performance, providing a significant contribution to the specific capacitance which permits a new strategy to design new electrodes for advanced energy storage devices. In this article review, we summarised the recent advancements made on the emerging hybrid nanomaterials, comprising of the general overview of the emerging nanomaterials, the synthesis routes for hybrid nanomaterials and their acquired hybrid structures along with their practical applications as electrodes in electrochemical energy storage and as heat transfer fluids for advanced heat transfer devices. Finally, we have also outlined some challenging issues associated with hybrid nanomaterials that requires further attention for future research.

**Keywords:** Emerging Nanomaterials, Hybridization of Nanomaterials, Energy Storage and Heat Transfer Application.

## 1. Introduction

Over the centuries, the evolution of human society has caused energy to be utilized progressively, highlighting that consumption of energy is the key for the functioning of our ultra-modern society, the thriving of our nations and the endurance of our civilization. With the proliferation of the human race that is presently almost 7 billion and is expected to increase abruptly year-by-year, immediate need arises for the development of technologies correlated to the usage of renewable and sustainable energy

in order to power the future. The exponential increase in energy consumption, utilizing non-renewable energy such as fossil fuel for transportation, electricity generation and heating process have led to the significant increase in the global environmental pollution and at the same time gives a serious tension to the availability of fossil fuels for the coming decades due to the current excessive consumptions [1]. Consequently, progressive developments of renewable and sustainable energy associated with various energy applications including energy generation, conversion and storage of energy have been made, and to date, it has become the fastest growing area in material science and engineering. In fact, according to the International Energy Agency (IEA), the first quartile of 2020 has seen a 1.5 % increase in renewable energy demands even though there was a slight decline in the global energy market due to the COVID-19 pandemic. However, the demand for renewable energy is expected to rise over time, owing to their low operating cost and favourable access to most of the power systems [2]. It is also reported that renewable energy will have its rapid growth in the electricity generation, supplying about 30% of power demand by 2023, an increment of 6 % from 2017 [3]. Nowadays, the use of solar technology becomes prominent for their application as the energy generator, conversion and storage. It is believed that solar energy radiated by the Sun for several hours can fulfil the energy demand for the whole year [4]. However, the major drawback to solar energy technologies such as photovoltaic thermal (PV/T) and solar collectors are their inadequate performance due to the inconsistent efficiency, resulting in their operation to not be fully utilized. The use of traditional heat transfer fluids e.g. oil, water and ethylene glycol as the working fluids are restricted by poor heat transfer properties making them improvident for round-trip efficiency for the conversion of heat-to-electricity [5]. Recent studies on the usage of nanofluids, which is an engineered colloidal suspension of particles in nanometre-dimensions into base fluids as the working media in solar energy systems has shown its great potential in enhancing the operating efficiency of solar collector as it possess a remarkable thermal and optical properties [6]. It should be noted that working fluids portray a major contribution in determining the performance, cost and reliability of solar thermal systems [7]. Employing nanofluids as the working

media in solar energy technology is capable of maximising its operations by providing rapid heat transfer and concurrently acts as the absorber fluids. Apart from being utilised as a working media in solar energy technology, nanofluids are also applied to advanced heat transfer devices such as heat pipe, heat exchanger and electronic components as a cooling media. It should be mentioned that utilising a working fluid which has a high heat transfer capability is the key to the high performance and efficient systems.

With the rapid growth of energy generation from solar energy technologies, energy conversion which is the transformation of generated energy to the forms of energy storage which can be used by humans also have received considerable attention due to the expeditious growth and continuous escalation in demands for wearable and bendable smart electronic devices [8]. This is in view to the fact that the conventional graphite anodes embedded in the rechargeable Lithium-ion batteries can only convey a capacity within an ace of 370 mAh $g^{-1}$ [9], giving us the urgent hint to seek for high-performance anode materials for the next generation renewable energy devices, which able to fulfil the growing energy demands. It is clearly understood that the performance of these electronic devices are mainly governed by the properties of the nanomaterials used for its electrodes [10].

With respect to the advancement of nanotechnology in the past few years, scientists and engineers are showing their great passion and interest in learning to hybridize different kinds of nanomaterials in the effort of tailoring the physicochemical properties of the hybrid nanomaterials [11]. Such hybridization of emerging nanomaterials is reported to exhibit superior physicochemical properties which is better than any other reported single nanoparticles. It is well known that a single nanomaterial does not have all superior properties, which is required for a specific application, making them uncompetitive to be employed [12]. Hybrid nanomaterials can be defined as a combination of two or more components constituted at nanometre scale, integrating the intrinsic physical and chemical properties of the constituent materials simultaneously and is expected to yield better physicochemical properties that is useful for energy storage and heat transfer applications compared to that of individual nanomaterial,

benefitting from the rise of synergistic effects between the materials. Hybrid nanomaterials offer the flexibility to alter their properties simply by modifying their composition and morphology, providing us with a tailored material composed of superior physicochemical properties such as high thermal stability, mechanical strength, electrical conductivity, optical properties and controlled wetting features [13] [14]. For instance, the introduction of graphene (G) into aluminium oxide ($Al_2O_3$) by Selvaraj et al. [15] has created G/$Al_2O_3$ hybrid nanofluids with high surface area, permitting more heat to be conducted and thereby exhibits a superior heat transfer enhancement. It is well acknowledged that the preparation of $Al_2O_3$ mono nanofluids is quite challenging at neutral pH state as it possess a high stability of dispersion at higher pH numbers, which is not suitable for its practical application as a heat transfer fluid, considering the effect of nanofluid at alkaline pH may cause the metallic surfaces to corrode [16]. By encasing the alumina with graphene shell, the water-based hybrid nanofluids can achieve its high suspension stability at pH 7 accompanied by enhanced physicochemical properties, benefitting from the outstanding stability, thermal and electrical conductivity of graphene nanoparticle as well as its synergistic effect with alumina. In addition, the hybrid nanofluids also demonstrated only an insignificant drawback in pumping power cost since it provides a much better heat transfer enhancement compared to the stable alumina mono nanofluid dispersion. n another work, Tong et al. [17] inserted multi-walled carbon nanotubes (MWCNT) into iron oxide ($Fe_3O_4$) nanofluid in the effort of nurturing the photo-thermal energy conversion efficiency. The addition of MWCNT into $Fe_3O_4$ not only enhanced thermal conductivity but it also recorded an improved photo-thermal energy conversion efficiency, providing almost two times augmentation of efficiency compared to that of single $Fe_3O_4$ nanofluids as a result of the outstanding thermal and optical properties of MWCNT. Even though $Fe_3O_4$ has its own ability to enhance thermal properties by subjecting it to the magnetic field, it can be further tuned by the addition of MWCNT. MWCNT not only enhanced the thermal conductivity of the hybrid nanomaterials, but it also provides excellent dispersion stability in the base fluids as $Fe_3O_4$ nanoparticles can be easily bound to MWCNT nanoparticles, owing to its unique cylindrical structure.

As a result, a chainlike structure of MWCNT/$Fe_3O_4$ hybrid nanofluids can be formed under the magnetic effect, providing an efficient thermal energy transportation that is beneficial for heat transfer applications.

In the effort of improving electrochemical energy storage, Li et al [18] introduced graphene as the solution to the relatively small sized MXene (~ 200 nm). The hybrid inks between MXene ($Ti_3C_2T_x$) nanosheets and electrochemically exfoliated graphene has given rise to an alternately stacked structure, providing a profusion surface area which is lucrative for the ion's liberations. The formation of MXene layers in between the graphene nanosheets served as an active material and ideal connection to ease the ion transports and electron movements. In addition, $Ti_3C_2T_x$ MXene sheets also behaved as a conducting spacer within the graphene layers which eventually can hinder the formation of re-stacked π–π graphene nanosheets, thus enabling such hybrid combinations to exhibit excellent volumetric capacitances. Bharath et al [19] also reported good electrochemical properties between trimanganese tetraoxide ($Mn_3O_4$) and reduced graphene oxide (rGO) hybrid nanomaterials for the application of capacitive deionization (CDI). Hybridising a wire-like $Mn_3O_4$ on graphene-based nanomaterials seems to possess a fast-Faradaic reaction since the nanocomposite exhibits a broader active material that offers a much greater conductivity route for easy ion movements, providing them an ideal pseudocapacitive behaviour. The addition of rGO to the typical pseudocapacitive site of $Mn_3O_4$ can create an electrode with excellent electrical conductivity, which may provide higher energy storage capacity.

Even though hybrid nanomaterials show a significant improvement in energy storage and heat transfer applications, which may lead them to superior performance of energy conversion and storage devices, the synthesis, preparation, design and their usage into practical applications still remains as a huge challenge. In regards to the continuation of research on nanotechnology, a few published papers have recently discussed the application of hybrid nanomaterials in heat transfer fluids such as the work by Yang et al. [20] and Gupta et al. [21]. These two review papers have comprehensively discussed the

factors that govern the performance of hybrid nanofluids and also the important physical parameters that should be taken into account. However, only few emphasises has been put on how particular hybridization synthesis routes are useful or unique for their extensive applications, especially for heat transfer fluid applications in which the priorities were always given to the preparation of nanofluid consisting of one or two steps methods. It is widely acknowledged that nanomaterials used for a particular application portray a significant contribution in achieving outstanding performance and a highly efficient system. Therefore, in this paper we have focussed on how a particular synthesis route of hybrid nanomaterials are beneficial for their extensive applications. Besides that, most of the review papers associated with hybrid nanomaterials are focussing on one particular application such as only for electrochemical energy storages, heat transfer fluids and also medical applications. In view of that, in this paper, we combine and summarize the recent advancement made on hybrid nanomaterials and the importance of developing such emerging multifunctional hybrid nanomaterials for energy storage and heat transfer applications. In section two, we provide the general overview of the emerging nanomaterials comprising MXene, graphene, carbon nanotubes and metal oxides. In the next section, we have discussed the common synthesis techniques of hybrid nanomaterials along with their obtained structures, relating on how a particular synthesis route is useful for their extensive applications. The practical applications of hybrid nanomaterials in electrochemical energy storage devices and their applications as heat transfer fluids in advanced heat transfer devices will be discussed in section four. Lastly, we also highlight some issues and challenges faced by hybrid nanomaterials. This article review intends to give the general overview of the published works related to hybrid nanomaterials which consists of their major findings and the recent progress made.

## 2. The Emerging Nanomaterials

It is widely acknowledged that the advancement of technology is driven by the emergence of nanomaterials. With these kinds of emerging nanomaterials, a new and highly efficient system can be created as a result of their peculiar properties that are beneficial in improving the overall performance

of the system [22]. Nanotechnology can be defined as a sort of toolbox in which it allows the creation of nanomaterials with special and emerging properties. Employing these kinds of emerging nanomaterials will not only improve the system but it could also play an integral part in the revolution of technology. Therefore, the exploration of new nanomaterials that will lead to that goal are of paramount importance in nanotechnology. In this section, some of the emerging nanomaterials corresponding to the application in energy storage and heat transfer fluids will be discussed.

## 2.1 Carbon Nanotubes

Carbon nanotubes (CNTs) are allotrope of carbon which consists of rolled graphite sheets that are tubular in shape. CNTs comprise of two types depending on how it is rolled up: Single-walled carbon nanotubes (SWCNTs) and Multiple-walled carbon nanotubes (MWCNTs) as shown in Figure 1. CNTs have diameters that vary from <1 nm up to 70 nm and the lengths of several microns [23]. SWCNTs are composed of single layer graphene in which it requires a catalyst for synthesis and their bulk synthesis is quite complex since it needs a proper control of growth and atmospheric condition. It also suffers from poor purity as it possesses higher chances of defect during functionalization. SWCNTs also can be easily twisted due to its single layer graphene. In contrast, MWCNTs are made up of multiple layers of graphene where it does not need any catalyst for the synthesis process and their bulk synthesis is much easier compared to SWCNTs. MWCNTs also possess a high purity as it only has small chances of defect during the functionalization process. In addition, MWCNTs are difficult to be twisted due to their multiple layers of graphene [24].

CNTs comprise three different structural forms which are *armchair, zigzag and chiral*. The formations of CNTs mainly depend on the use of the chiral vector concept which results in a pair of integers *'n'* and '*m'* that correspond to the number of unit vectors along the two directions in the honeycomb crystal lattice [25]. The formation of *zigzag* structure can be achieved when $m=0$ whereas *armchair* structure arises when $n=m$. *Chiral* structure can be formed when $n>m>0$ and this kind of structure is believed to give huge contributions to the electrical, mechanical and optical properties of CNTs [26].

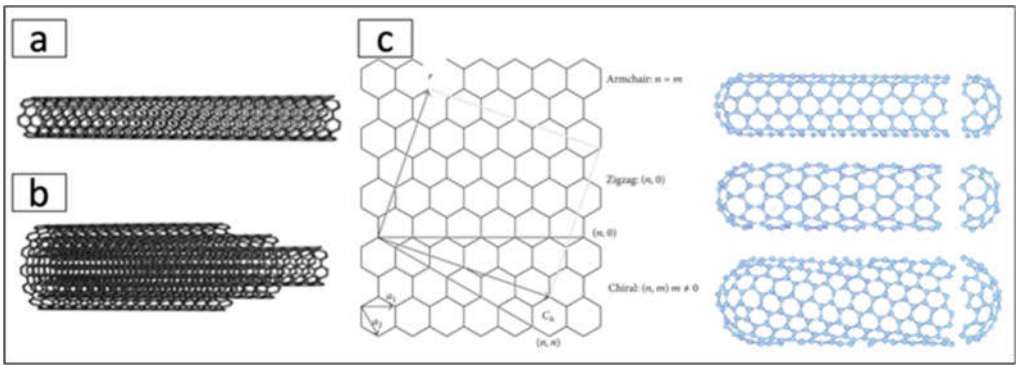

Figure 1: Representation of (a) SWCNTs, (b) MWCNTs, and (c) formation of CNTs with three different structural forms: *armchair, zigzag* and *chiral* tubes [25].

The unique structure of CNTs offers a combination of superlative mechanical, thermal and electronic properties, making them a promising candidate for energy storage, sensing and heat transfer applications. CNT's Young modulus has values greater than 1 TPa which is 5 times greater than steel [24].It also exhibits high thermal conductivity at RT ~3000 W/mK, which is expected to be higher than diamond [26]It is noteworthy that the electrical properties of CNTs can be classified as metallic or semiconducting, depending on the relationship of the axial direction and the unit vectors which describe the hexagonal lattice.

## 2.2 Graphene

The introduction of Graphene in 2004 has unlocked a new era in the field of science and technology [23]. Graphene, a carbon formation composed of a single layer of $sp^2$-bonded carbon atoms, which densely packed into a hexagonal crystal lattice is considered as a rising star and has attracted considerable attention in various fields such as heat transfer and energy storage as well as sensors, catalysts, electrodes, and in biological applications [27]. The honeycomb lattice is the building block of all carbon allotrope materials: it can be muffled to 0D fullerenes, rolled into 1D carbon nanotubes or stacked to form 3D graphite when the layers of single honeycomb graphitic lattices are subjected to a weak van der Waals force, as schematically shown in Figure 2 [28].

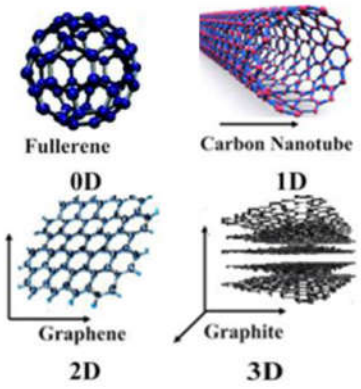


Figure 2: The building block of all carbonaceous material at different dimensions [28].

In single layer graphene, each of the covalently bonded carbon atoms is essentially $sp^2$ hybridised. The tightly packed arrangement of carbon atoms along with the $sp^2$ orbital hybridization, which is a mixture of *s,* $p_x$ and $p_y$ orbitals will give rise to the formation of σ-bond. Hence, the stable hexagonal structure of graphene is due to the existence of these three σ bonds connections. It should be mentioned that in the honeycomb structure, each carbon atom is covalently held by three distinct carbon atoms where all of them are $sp^2$ hybridized, leaving one free electron for every carbon atom. This free electron is then being held by the final $p_z$ orbital which lies on the top of the plane, forming the π bond. The hybridization of the π bond with another π bond will lead to the formation of the π-bands and π*-bands which generally contribute to the numerous graphene's outstanding physical and chemical properties, through their half-filled band that permits the free electrons to move [29], [30]. Graphene may exist in the form of nanoribbon where their energy barrier can be tuned by controlling the width of the nanoribbon. Such an energy barrier can be increased by decreasing the width of the nanoribbon [34]. This kind of property has made graphene a favourable material for electronic devices. Similar to CNT, the graphene edge can be categorized into two: *zigzag* and *armchair* which depends on the carbon chains (Figure 3). Typically, graphene with a *zigzag* edge is a metal while graphene with an armchair edge can be either metal or semiconductor, which could conduct electricity [29].

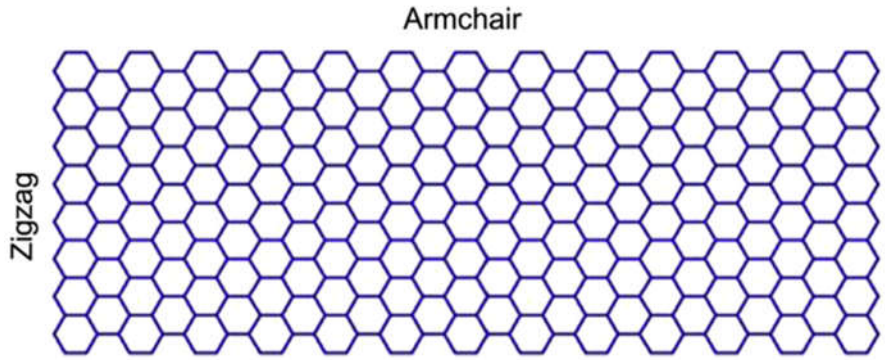


Figure 3: Graphene nanoribbon with two different edges. Reproduced from Reference [29] with permission from Elsevier.

Owing to the unique 2D structure, graphene exhibits outstanding physical and chemical properties. With a conductivity of $10^6$ S/m, graphene emerges as the most conductive material at room temperature (RT) accompanied by a sheet resistance of 31 Ω/sq, as a result of its extremely high carrier mobility of 2 x $10^5$ $cm^2$/V-s which is 140 times greater than the mobility of silicon. This is useful for ultrafast electronics and optoelectronics applications [31]. Graphene also possesses a high thermal conductivity (~ 5 x $10^3$ W/mK, 10 times better than copper at RT [32], high optical properties (97.7 %, only 2.3 % of visible light is absorbed) [33], high mechanical properties (Young's modulus of ~ 1.0 TPa and a tensile strength of ~ 130 GPa) [31] and extremely high specific surface area (theoretically, 2675 $m^2$ $g^{-1}$)[38], suggesting it as a potential candidate for energy storage and heat transfer applications. It should be noted that graphene has two main derivatives known as graphene oxide (GO) and reduced graphene oxide (rGO). GO can be achieved by oxidation of graphite, which is usually accompanied with an extensive modification of the basal plane while rGO can be produced by reducing the GO using any physical or chemical process e.g. thermal or acid treatment in the effort of reducing its oxygen content [39]. In general, GO is a chemically treated graphene which mainly consist of different functional groups e.g. hydroxyl, epoxy and carboxyl, permitting GO to be attached with other molecules. The rGO can be considered identical to that of pristine graphene. However, it has oxygen-containing groups along with some defects in which it can be controlled by manipulating the degree of oxygen reduction [40]. A schematic representation of graphene and its derivatives synthesis routes is depicted in Figure 4. A summary of various synthesis techniques from recent literature is also given in Table 1,

highlighting the experimental parameters obtained and some important findings. Further information regarding the available synthesis techniques and properties of graphene and its derivative can be found in these two recommended articles; [30] and [34].

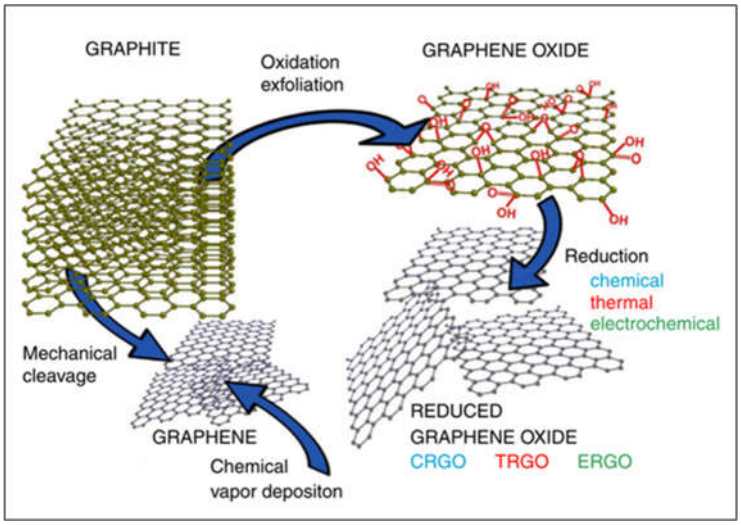


Figure 4: A schematic illustration of the possible ways to synthesis graphene and its derivatives [35].

Table 1: Summary on some available synthesis techniques of graphene.

| **Synthesis Techniques** | **Physical Parameters/ Characteristics** | **Important Findings** | **Limitations** | **Reference** |
|---|---|---|---|---|
| Tape-peeling | Few hundreds nm to ~1 $\mu$m, Few layers | ▪ Graphene thickness are controllable<br>▪ Can produce uniform few layers<br>▪ Low defects | Very small production scale when the number of peelings are increased | [36] |
| Chemical exfoliation via two-steps microwave irradiation | Few hundreds $\mu$m, Multilayered of thin graphitic structure | ▪ Synthesis of graphite to graphene only takes about 15 min<br>▪ Have a good electrical conductivity of ~ $2.03\times10^5$ S $m^{-1}$<br>▪ High quality with only few structural defects. | Graphene sheets obtained have a trace of stacking | [37] |
| Ball milling - ultrasonication process | Few layers | ▪ High production with low cost. | Have some structural defects as a result of the ball milling process. | [38] |
| Pyrolysis of 6H-silicon carbide | 0.7-0.8 nm, single layer | ▪ High quality graphene | Expensive starting material: 6H-SiC crystal | [39] |

| | | | | |
|---|---|---|---|---|
| | | ▪ Few defects of graphene can be obtained using 2000 °C with the flow of Ar at 15 Torr. | | |
| Plasma CVD | 7.5 $\mu$m, single layer | ▪ Hydrogen species act as etchant which activates surface bound carbon.<br>▪ High quality graphene is produced at 850 °C, over the power of 50 W.<br>▪ Increasing the plasma power will accelerates the growth rates of graphene. | Extreme increase of plasma power will lead to the growth of stacked graphene | [40] |
| Thermal CVD | Few $\mu$m, very thin layer | ▪ High quality but low in small production scale.<br>▪ Reduced the wear rate by ~ 6%. | Have small defects due to the impurity effect of Cu. | [41] |

### 2.3 MXene

Over the last few years, MXene - an emerging family of two dimensional (2D) atom thick material extracted from transition metal carbides, nitrides or carbonitrides has received prime attention since its discovery in 2011 by Naguib et al. [42]. MXene comes under the spotlight after showing remarkable electrical and electrochemical properties for various applications especially in energy storage due to its good electronic, optical and plasmonic properties, surface hydrophilicity, metallic conductivity and chemical stability, benefitting from their intrinsic 2D atomic layered structures [43][44]. Since MXene does not have the elementary 3D precursor, it must be derived by selectively etching the A layers from the precursor MAX phases with designated chemical formula of $M_{n+1}AX_n$, where M represents an early transition metal, A is IIIA or IVA group element, X stands for carbon and/ or nitrogen and n = 1-3. MAX phases seem to have multi-layered hexagonal structures in which the A layers are alternately stacked between $M_{n+1}X_n$ units [10]. Because the M-X bonds primarily consist of covalent and ionic bonds, it is much stronger than the metal bonds of M-A, giving the possibility for A layers to be separated from the MAX phase due to its relatively weak M-A layer binding force [45]. As a result of the A layer removal, MXene which could be formulated as $M_{n+1}X_nT_x$ can be achieved where $T_x$ designates as surface termination i.e. -OH, =O and -F functional groups (Figure 5) [46]. It should be noted that MXene produced in chemical etching will always introduce a surface termination of O, OH,

F or probably a concoction of all elements depending on the type of chemical environment used, rendering them hydrophilicity and capable of solution processing [47]. It is also eminent that termination exists when transition metal spontaneously reacts with water or fluoride ions. The existence of functional group in MXene will lead to the formation of semiconducting functionalized MXenes e.g. $Ti_3C_2(OH)_2$ while pristine MXenes ($Ti_3C_2$) are always metallic [48]. To date, there are about 70 MAX phases discovered but only a few MXenes have been established using etching method such as $Ti_3C_2$, $Ti_2C$, $(Ti_{0.5}, Nb_{0.5})_2C$, $(V_{0.5}, Cr_{0.5})_3C_2$, $Ti_3CN$, $Ta_4C_3$, $Nb_2C$, $V_2C$ and $Nb_4C_3$ [49]. The first kind MXene, 2D titanium carbide ($Ti_3C_2$) was fabricated by using hydrofluoric acid (HF) etching process at RT (50% HF for 2h) [42].

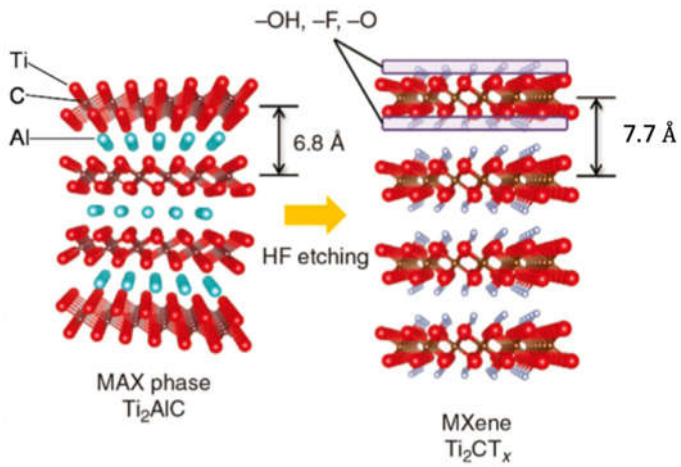


Figure 5: Schematic illustration for the formation of MXenes with surface terminations [46].

A common synthesis route of MXenes usually comprises two steps: etching and exfoliating as shown in Figure 6. The MAX bonds are quite strong to be separated by any mechanical processes. In order to exfoliate MXene, an etching process must be carried out to break the strong chemical bond between the elements of M and A in the MAX phase. Since the more chemically functionalized A atomic layers cause the M-A bonds and interatomic A-A bonds to be less strong compared to that of M-X bonds [50], the etching process can simply be done by treating MAX phase with chemical agents e.g. a solution of HF at a particular concentration with a specific amount of time without breaking M-X bonds [51]. The reaction of the HF solutions with $Ti_3AlC_2$ MAX phase will terminate the metal surface

with the functional groups (-OH and -F). The reactions involved can be summarized using the following equations:

$$Ti_3AlC_2 + 3HF = AlF_3 + 3/2\ H_2 + Ti_3C_2 \quad (1)$$

$$Ti_3C_2 + 2H_2O = Ti_3C_2(OH)_2 + H_2 \quad (2)$$

$$Ti_3C_2 + 2HF = Ti_3C_2F_2 + H_2 \quad (3)$$

MAX powders are then subjected under centrifugation followed by washing with deionized water until its pH reaches the range of 4 and 6. The solution is then filtered to obtain MXene. It should be noted that without exfoliation/delamination, MXene will consist of multi-layered structures. The layered structures are further subjected to ultrasonication to obtain a single layer of MXene, however, continuous sonication for a long time might break the MXene sheets or give an effect on the edges of the lamellar structure [51]. It is also important to note that HF is not the only etchant available to synthesis MXene. A summary on different use of etchants along with their conditions to synthesis MXenes is given in Table 2.

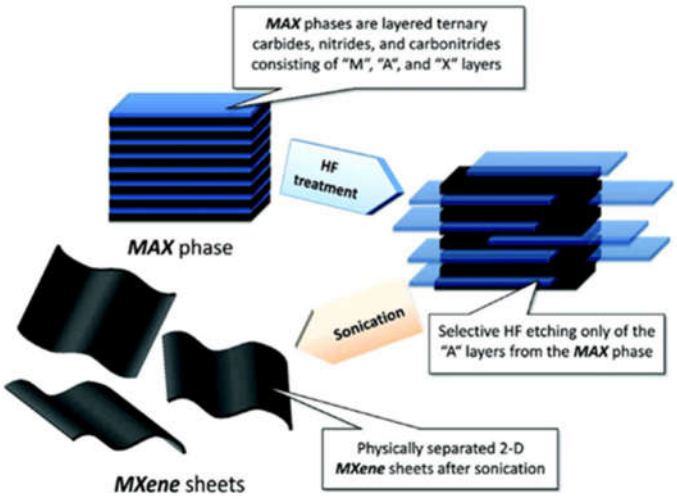


Figure 6: Schematic of the synthesis route of MXene. Reproduced from Reference [43] with permission from ACS Publications.

Table 2: Summary of different etchants used to synthesis MXene along with their conditions.

| Method | Etchants | MAX | MXene | Conditions | Reference |
|---|---|---|---|---|---|
| Non-fluorine | Ultraviolet (UV) irradiation | Ternary nanomilated Carbide ($Mo_2GaC$) | $Mo_2C$ | Magnetic stirring at 1000 rpm under UV light (100 W, distance ~8 cm), 3-5 h | [52] |
| Acid with Fluorine | Hydrofluoric acid, HF + Hydrogen peroxide, $H_2O_2$ | Titanium Silicon Carbide ($Ti_3SiC_2$ ) | $Ti_3C_2$ | 40°C, 45 h | [53] |
| Hydrothermal | Sodium Hydroxide (NaOH) | Titanium(IV) Carbide ($Ti_3AlC_2$) | $Ti_3C_2T_x$ | 270 °C with 27.5 M NaOH | [54] |
| Acid with Fluorine | Ammonium hydrogen difluoride ( $NH_4HF_2$) | $Ti_3AlC_2$ | $Ti_3C_2T_x$ | 60 °C, 8h | [55] |
| Acid with Fluorine | Hydrochloric acid, HCl + Lithium fluoride, LiF | $Ti_3AlC_2$ | $Ti_3C_2T_x$ | 1350 °C, 2 hours | [56] |
| Electrochemical | HCl | Titanium aluminum carbide lump ($Ti_2AlC$) | $Ti_2C$ | Ball milled for 24 hours at 300 rpm, 1400 °C, 4 hours, Argon gas flow | [57] |
| Molten Salt | LiF + Sodium fluoride, NaF + Potassium fluoride, KF | Titanium Aluminum Nitride ($Ti_4AlN_3$) | $Ti_4N_3T_x$ | 550 °C for 30min, Ar atmosphere | [58] |

One of the emerging properties of MXenes is their metallic conductivity. Pristine MXene usually possess a metallic behaviour due to the high electron densities near the Fermi level. This metallic behaviour can be adjusted with the formation of the additional Ti-X bonds. MXenes can possess a

narrow band-gap semiconductor behaviour by inserting the functional groups [59]. Surface functionalization that exists on the MXene surface plays a vital role in manipulating the electronic properties of MXene. Since it can change the electronic properties of MXene thus, it is important to analyse it based on their synthesis routes [60]. Surface terminations are responsible for reducing the density of states (DOS) causing the d band to lift up on top of the Fermi level, thereby, allowing the creation of a band gap. This occurs as a result of the integration of *d* orbitals of M elements with the *p* orbitals of surface functionalization [48]. It is noteworthy that F and OH terminations exhibit identical effects on MXenes electronic structures because they allow the acceptance of a single electron. In contrast, oxygen termination results in a different behaviour since it accepts two electrons at equilibrium state. Thus, the electronic structures of MXene are mainly governed by the type of M and X atoms along with their surface terminations. MXene can exist in the form of metallic, semi-metallic and semiconducting types, depending on the morphological structures and surface terminations. In general, a good connection (no gaps) between individual flakes and large flakes size will result in highly conductive MXene. It is reported that electrical conductivities of $Ti_3C_2T_x$ can be up to 9880 S $cm^{-1}$ for low defects MXene flakes while it can be 850 S $cm^{-1}$ for highly defective MXene flakes [61]. Lowering HF concentrations and etching time can produce a MXene with fewer defects. Besides that, MXene also possesses an outstanding thermal conductivity (e.g. Silicene ($Sc_2CF_2$) has 722 $Wm^{-1}$ $K^{-1}$) which is beneficial for electronic devices and for the heat transfer process. In general, thermal conductivity of MXene depends on lateral size and can be tailored by manipulating the flake length. It is also reported that MXene nanosheets dispersed in solution possess excellent electrical conductivity and outstanding optical properties, suggesting its great potential to be applied in photo-electronics, energy storage devices, sensing applications, transparent conductive coatings and photo-thermal conversions [59]. For example, the use of vacuum free solution processable electrohydrodynamic atomization (EHDA) technique reported by Ali et al. [62] resulted in a conductive MXene-based transparent films, indicating the outstanding optical transmittance of ~86.7% at a thickness of 135 nm

along with the low resistivity of 3.4 x $10^{-4}$ $\Omega$ cm. Increasing the film thickness will lead to the decrease of the optical transmittance and the increase of resistivity. The drastic decrease of electrical conductivity is due to the increase in grain boundaries, which is not favourable for electron flow. Detailed information regarding the synthesis route, properties and potential applications of MXene can be found in these two recommended literatures [48][60]. One of the major challenges in employing MXene as the electrode materials in electrochemical energy storage is that their functional groups terminations were anticipated to extremely affect their electronic, optical, mechanical, and magnetic properties. Due to the removal of the Al layer, $Ti_3C_2Ti_x$ layers seem to possess lower electrical conductivity than its precursor, $Ti_3AlC_2$. Etching Al layer will cause MXene structure to re-stack and eventually create a very dense structure, which is not favourable for ion movements due to the reduction of specific surface area resulting in inefficient performance of electrode materials [45].

### 2.4 Metal Oxides

Besides MXene, Graphene and CNTs, metal oxides nanoparticles also play a vital role in the field of materials science and engineering as a result of their excellent and unique physicochemical properties such as high surface-to-volume ratio, quantum size effect and electrodynamic interactions, which makes them differ from bulk materials [63]. Metal oxides are widely used in energy storage technologies, benefitting from their ability to generate charge carriers when energy is applied. With a wide variety of oxidation states, metal oxides are commonly employed as electrode materials for redox charge transfer [64]. It is also reported that dispersing metal oxides in the base fluids will result in heat transfer enhancements, which is beneficial for heat transfer fluids in photo-thermal conversion and also cooling process [65]. Owing to their high intrinsic surface to volume ratios, metal and metal oxides are not only able to enhance the heat transfer properties, but it also provides an improved suspensions stability which leads them to a better thermal management for high temperature energy application compared to the usage of conventional fluids, which possess low thermal conductivity [66]. In addition, metal oxides are also useful in harnessing solar energy because of its high optical properties

and ability to withstand high temperatures. However, the usage of single metal oxides dispersions remains as a huge challenge because it does not have all favourable properties which hinders them from extensive applications. It may either have better thermal conductivity or rheological properties. For instance, aluminium oxide possesses outstanding thermal stability and chemical inertness, however it suffers from poor electrical conductivity [65]. In certain cases, metal oxides could be one of the emerging nanomaterials. For instance, MXene has excellent electrical conductivity and low diffusion barrier. However, the surface termination of O, OH and/or F groups on MXene sheets will cause the specific capacity of $Ti_3C_2T_x$ to decrease. In order to overcome this drawback, MXene nanosheets must be integrated with transition metal oxides (TMOs). TMOs have been extensively evaluated as the promising lithium-ion battery (LIB) anode candidates since they have high specific capacities but poor electrical conductivity and large volume changes during lithiation and delithiation process. In this regard, Kong et al. [67] integrated MXene nanosheets with $Fe_3O_4$ and reported that a desirable electrochemical performance of anode material was obtained, providing high specific capacity and remarkable electrical conductivity due to the synergistic effect between the two materials. Examples of the common metal oxides used are spinel ($Li_4Ti_5O_{12}$) and transition metal oxides (TMOs) (e.g., Mn, Cu, Co, and Ti oxides) [64].

Overall, easy synthesis and ability to maintain high purity during the functionalization process, good resistance against twisting and its unique combination of superlative mechanical, thermal and electronic properties making the CNTs a promising candidate for energy storage, sensing and heat transfer applications. Importantly, due to the unique 2D structure and outstanding physio-chemical properties of graphene with high thermo-electrical conductivity, high opto-mechanical properties and extremely high specific surface area dominates as a potential candidate for energy storage and heat transfer applications. Mentionable that for the synthesis of CNTs and graphene with manageable chirality, predetermined size, layers or length, super-alignment still stays in enormous challenges. Additionally, the powerful coupling among the CNTs or graphene structures, production procedures,

post-treatments, properties as well as applications are yet obstacles. On the other hand, 2D MXenes attracts as another encouraging nominees in the modern energy storage implications as due to their high metallic conductivity, packing density as well as pseudocapacitive performance towards the improved areal and volumetric capacitances. However, for the efficient and highly scalable synthesis techniques of MXenes such as secure etching agent than acids are still in major bottleneck for the implementation in energy storage application. Besides a high surface-to-volume ratio, quantum size effect and electrodynamic interactions of metal oxides nanoparticles are also widely used in energy storage technologies, benefitting from their ability to generate charge carriers. However, owing to their high intrinsic surface to volume ratios and low thermal conductivity they are better in thermal management in high-temperature energy application rather in conventional fluids.

## 3. Hybridization of Nanomaterials

Hybrid nanomaterials can be synthesised using physical and chemical routes. In general, physical synthesis routes offer a much easier way to hybridize the nanomaterials without any strict requirement to go through the complex steps. In contrast, chemical synthesis routes require some chemical treatment and must be strictly controlled [45]. For the hybrid nanofluids preparation, the hybrid nanomaterials will be synthesized firstly before dispersing it into the base fluids. This section will discuss the preparation of hybrid nanomaterials for its extensive applications in electrochemical energy storage and heat transfer fluids.

### 3.1 Physical Methods

#### 3.1.1 Mechanical Mixing

Mechanical mixing involves the use of mechanical devices such as magnetic stirrer and ultra-sonicator to aid the dispersion of nanomaterials. The usage of these mechanical devices is able to prevent the prepared nanomaterials from stacking or agglomerates. Van et al. [68] prepared the ethylene glycol based nanofluid of graphene-carbon nanotubes (CNT) hybrid nanomaterials by directly mixing the

nanoparticles under ultrasonication. Before dispersing the hybrid nanomaterials into the base fluids using the ultrasonication technique, graphene and MWCNT nanoparticles were terminated with different functional groups including -OH and -COOH by treating them with the mixture of nitric acid ($HNO_3$) and sulphuric acid ($H_2SO_4$) (Figure 7a). With the surface modification and the aid of ultra-sonicator, graphene-CNT hybrid nanoparticles were dispersed homogenously without any agglomeration due to the existence of molecular bonding of COOH and OH groups (Figure 7f-g). Graphene-CNT hybrid nanofluids demonstrated an outstanding thermal conductivity improvement with 50 % enhancement relative to the base fluids at 50 °C with the particle concentration of 0.07 vol.%, owing to the combination of superior thermal conductivity of CNT and graphene along with the large surface area possessed by graphene-CNT hybrid nanomaterials (Figure 7h).

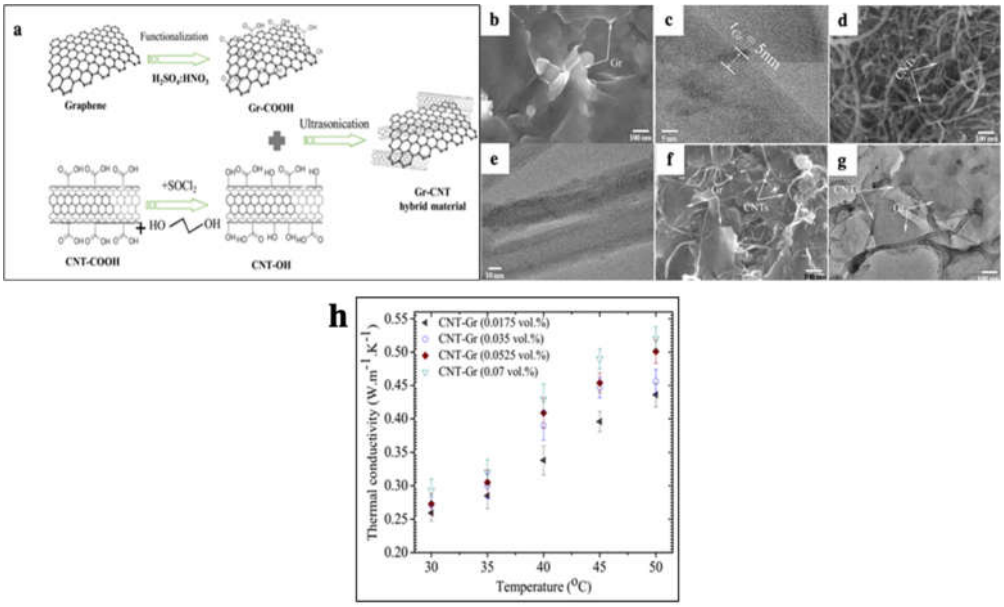


Figure 7: (a) Schematic representation of mechanical mixing procedure for synthesis of graphene-CNT hybrid nanomaterials. SEM and TEM images of (b) and (c) graphene; (d) and (e) CNTs; (f) and (g) graphene-CNT hybrid nanocomposites; and (h) thermal conductivity of graphene-CNT hybrid nanofluids at different temperatures and concentrations. Reproduced from Reference [68] with permission from Elsevier.

Zhao et al. [69] fabricated MXene and reduced graphene oxide ($Ti_3C_2T_x$/rGO) hybrid nanocomposites using the ultrasonication technique for the high performance supercapacitors. The rGO powder was first dispersed in ethanol by using the ultrasonication followed by the mixture of $Ti_3C_2T_x$ powder in the solution. The composite was then filtered from the solvent and dried at 80 °C for 12h. From the

FESEM images of $Ti_3C_2T_x$ (Figure 8a-b), it can be seen that MXene sheets possess a typical multi-layered structure, which is favourable for ion transport due to the large surface area, leading to an improved pseudo-capacitance performance. When rGO was integrated with $Ti_3C_2T_x$ layers, a further surface modification of $Ti_3C_2T_x$ structure was obtained where rGO served as conductive bridge and nanoscale collector for the movement of electrons (Figure 8c). The presence of rGO could connect the different blocks of $Ti_3C_2T_x$ which enables the improvement of the contact area and thus ease the electronic movement process to the current collector, producing an outstanding electrochemical performance of the electrode.

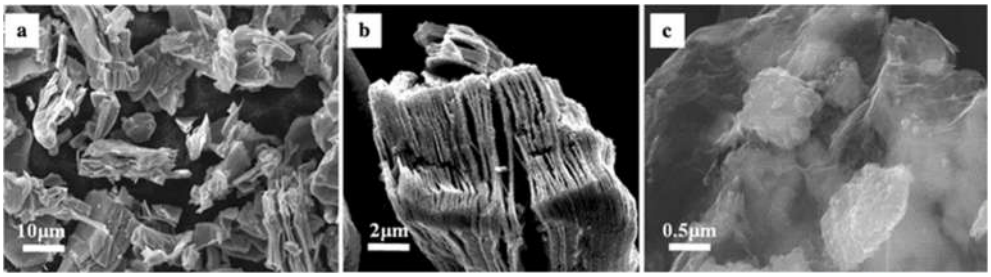


**Figure 8:** FESEM images of (a) $Ti_3C_2T_x$, (b) enlarged view of $Ti_3C_2T_x$ in (a), and (c) $Ti_3C_2T_x$/rGO nanocomposites. Reproduced from Reference [69] with permission from ACS Publications.

### 3.1.2 Self-assembly method

In order to create electrostatic self-assembly interaction, it requires two materials: a poly-electrolytes that is usually soluble in water or have strong adsorption capability, and a material that is opposite in charges to that of polyelectrolytes. When these two nanometre-size materials are combined together, polyelectrolytes tend to adsorb it as a result of the interaction between the two opposite charges, producing a stable nanocomposites material. This method is simple as it is able to produce a stable hybrid nanomaterials without any chemical bonds [70].

Jin et al. [71] synthesized the alternately stacked manganese dioxide-MXene ($MnO_2$-$Ti_3C_2$) and manganese dioxide-reduced graphene oxide ($MnO_2$-rGO) hybrid nanomaterials using the electrostatic derived self-assembly method. The electrostatic interaction between the positive charge of $Mn^{2+}$ possessed by $MnO_2$ and the negative surface charges of $Ti_3C_2$ and rGO nanosheets make them possible for the preparation of homogeneous combinations of hybrid nanomaterials that are highly stable. As

can be seen in Figure 9a, the obtained colloidal mixtures of $MnO_2$-$Ti_3C_2$ and $MnO_2$-rGO hybrid nanomaterials were synthesized using the electrostatic self-assembly of $H^+$ since $MnO_2$-$Ti_3C_2$ mixtures possess negative zeta potential while $MnO_2$-rGO possess negative surface charge. The FESEM images in Figure 9b clearly shows the presence of uniformly nano-porous structures of 2D nanosheets, indicating the homogenous mixture of $MnO_2$-$Ti_3C_2$ and $MnO_2$-rGO hybrid nanomaterials while Figure 9(c-d) shows the TEM analysis of the interrupted nano-porous stacking structure of the extremely thin 2D nanosheets along with the elemental mapping analysis. The synthesized hybrid nanomaterials of $MnO_2$-$Ti_3C_2$ exhibits a better electrochemical performance compared to that of $MnO_2$-rGO, indicating the favourable integration of MXene nanosheets with $MnO_2$ as a hybridization matrix in escalating the electrochemical performance of metal oxide as shown in Figure 9(f-i). The hybridization matrix of MXene is able to provide huge contributions to the $MnO_2$ electrode performance as it enhances the interfacial coupling, porosity and ion diffusivity due to the significant increase in surface area (active sites) for ion transport. The outstanding performance of the $MnO_2$-$Ti_3C_2$ hybrid nanomaterials can be related to their low tendency of self-stacking due to favourable combination of the two nanoparticles, hydrophilic in nature and high rigidity of $\pi$ electron-free MXene nanosheets.

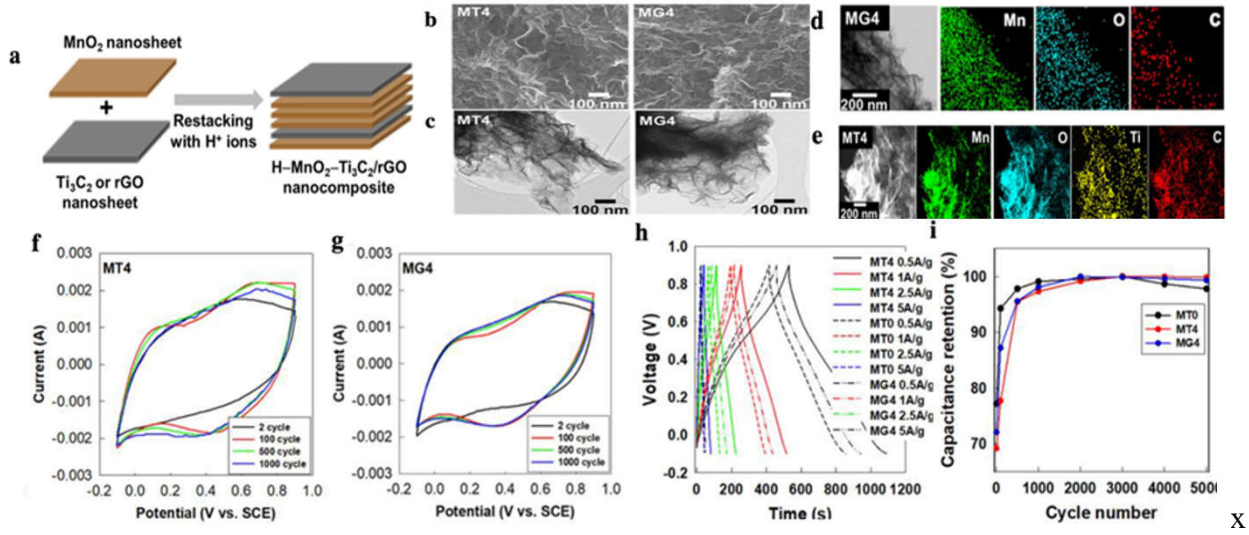


Figure 9: (a) A schematic illustration for the synthesis route of hetero-layered MT and MG hybrid nanomaterials. (b) FESEM, (c) TEM, and (d, e) TEM-elemental mapping data of the MT and MG nanocomposites. (f, g) CV curves for MT and MG nanocomposites, (h) CD curves, and (i) capacitance retention plots for the MT and MG nanocomposites. Note that MT and MG represent as $MnO_2$-$Ti_3C_2$

and $MnO_2$-rGO hybrid nanomaterials, respectively. Reproduced from Reference [71] with permission from Elsevier.

## 3.2 Chemical Methods

### 3.2.1 Hydrothermal

Hydrothermal method is one of the common synthesis routes for hybrid nanomaterials, which mainly depends on the solubility of aqueous solution under hot water and high temperature. To operate, it requires an autoclave (strong container) filled with a solution to withstand the high temperature and pressure. Typically, the precursor is put into the autoclave at a certain temperature for a particular amount of time, which is then followed by any necessary post-treatment e.g. washing and drying [51]. Recently, Wang et al. [72] fabricated fibre-like rGO/MXene hybrid nanomaterials under the low temperature of 60 °C using a facile one-step self-assembled hydrothermal method (Figure 10a). The hydrothermal treatment not only generates a reduced graphene oxide, but is also able to integrate GO with MXene nanosheets, forming a hybrid nanomaterial composed of a robust skeleton of large graphene sheets filled with MXene nanosheets between the spaces. It is reported that the surface morphologies of the obtained hybrid nanomaterials demonstrated an uneven surface along with irregular wrinkles when compared to that of pure rGO, indicating the incorporation of $Ti_3C_2T_x$ layers with rGO. With the increased mass of $Ti_3C_2T_x$, the uneven surface roughness of the hybrid nanomaterials becomes more prominent due to the large size discrepancies between the two materials (Figure 10b-d). The Energy Dispersive X-ray Spectroscopy (EDS) mapping further confirmed the presence of $Ti_3C_2T_x$ in graphene nanosheets (Figure 10e). The as prepared fiber-like hybrid nanomaterials were reported to possess an outstanding electrical conductivity of 1339 S $m^{-1}$ with large volumetric and gravimetric capacitance albeit with low particle loading of MXene, benefitting from the rise of synergistic effects between the two materials. In addition, the integration of these two nanomaterials is able to prevent MXene sheets from being oxidised when they are subjected under the high temperature. Graphene layers act as a protector to that of MXene sheets especially for the low particle loading of MXene.

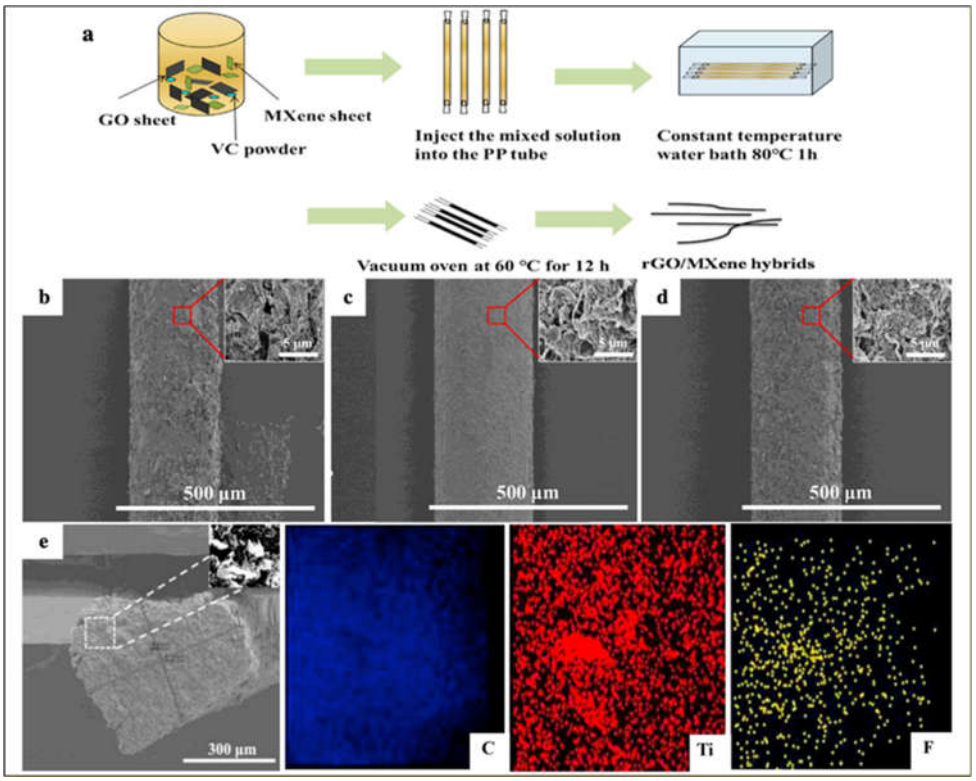


Figure 10: (a) Schematic illustration for the fabrication procedure of rGO/MXene fibre-like hybrid nanomaterials. SEM images of (b) rGO/ $Ti_3C_2T_x$ -5, (c)rGO/ $Ti_3C_2T_x$ -10 and (d)rGO/ $Ti_3C_2T_x$ -15; (e) SEM image of the cross section rGO/ $Ti_3C_2T_x$ -5 along with the EDS mapping of C, Ti and F. Reproduced from Reference [72] with permission from Elsevier.

In another work, Bharath et al. [19] employed the hydrothermal synthesis process to fabricate $Mn_3O_4$/rGO nanocomposites with hierarchical pores in the effort of improving the ion transport pathways (Figure 11a). With the use of hydrothermal treatment at the temperature of 180 °C for 12 h, $Mn_3O_4$ nuclei were generated from the intermediate phases of manganite (MnOOH) while graphene oxide (GO) was transformed into rGO, leading to the homogeneously immobilization of $Mn_3O_4$ on the surface of rGO nanosheets due to the presence of negatively charged oxygen moieties on the rGO. It should be noted that the oxygen moieties on the rGO plays a significant role in providing the anchoring sites for easy attachment of manganese nuclei. A well crystalline and uniform sized of $Mn_3O_4$ nanowires formed on the rGO nanosheets can be clearly observed on Figure 11(f-g). The unique structure of this wire-like $Mn_3O_4$/rGO is able to provide large active sites for the ion transport, allowing the favourable contact between $Mn_3O_4$/rGO electrodes and electrolytes for energy storage applications.

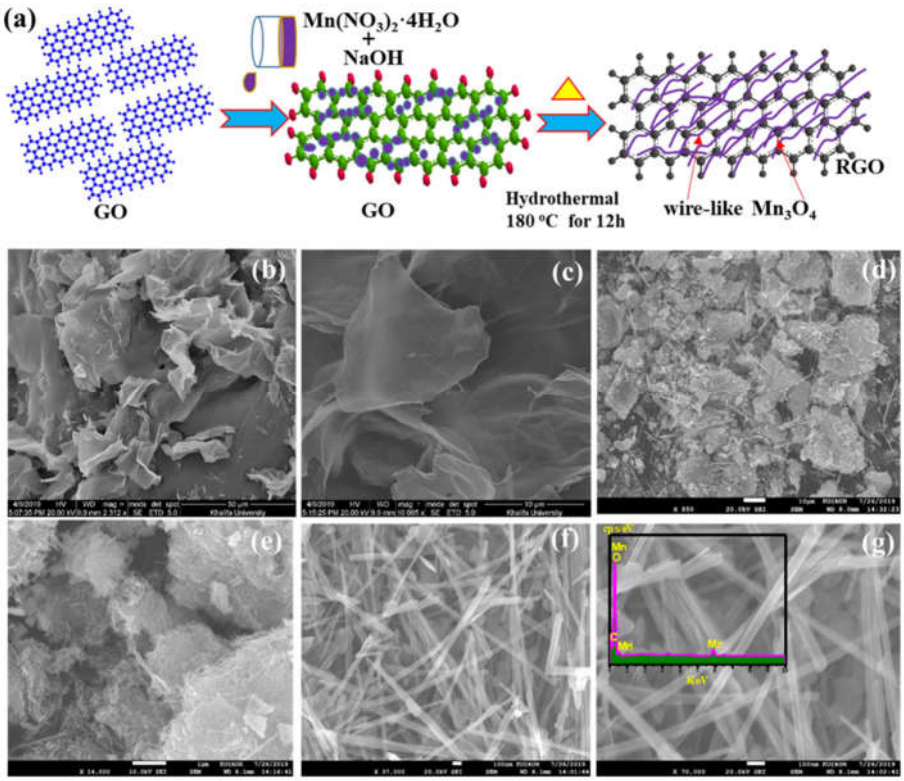


Figure 11: (a) A schematic illustration for the synthesis route of wire-like $Mn_3O_4$/rGO hybrid nanomaterials, (b and c) FESEM images of GO, (d-f) FESEM images of $Mn_3O_4$/rGO hybrid nanomaterials and (g) EDS of $Mn_3O_4$/rGO hybrid nanomaterials. Reproduced from Reference [19] with permission from Elsevier.

### 3.2.2 Solvothermal Method

In addition to the hydrothermal method, the solvothermal method is also one of the simple and feasible methods to synthesis hybrid nanomaterials. Like the hydrothermal method, the solvothermal method also requires an autoclave to operate. Through the solvothermal synthesis route, the size, shape distribution and nanostructure products can be tuned simply by changing the reaction temperature, reaction time, surfactant used and also the nanomaterials' precursor.

Wu et al. [9] used the solvothermal method to synthesis tin sulfide-graphene nanosheets ($SnS_2$-GNS) hybrid nanocomposite. By employing a solvothermal method, the uniform layer of $SnS_2$ can be grown on graphene nanosheets through covalent bonds, creating $SnS_2$ nanoparticles integrated with graphene nanosheets as shown in Figure 12. Hybridising graphene nanosheets with $SnS_2$ was able to prevent the graphene sheets from being cross linked and re-stacking. Like $SnS_2$, a stand-alone $SnS_2$ nanoparticles

will lead to the formation of large pieces of structure, which tends to be self-assembled into a flower-like shape, creating a very dense structure which is unsuitable for ion transports. By using this synthesis route, $SnS_2$-GNS hybrid nanocomposites were able to deliver a superior lithium storage performance which was much greater than any other Sn-based materials reported. This outstanding lithium performance was achieved owing to the existence of synergistic effect between the two nanomaterials. It was also revealed that carbon materials can be easily integrated with Sn-based nanomaterials using this process in addition to the ball milling and hydrothermal method.

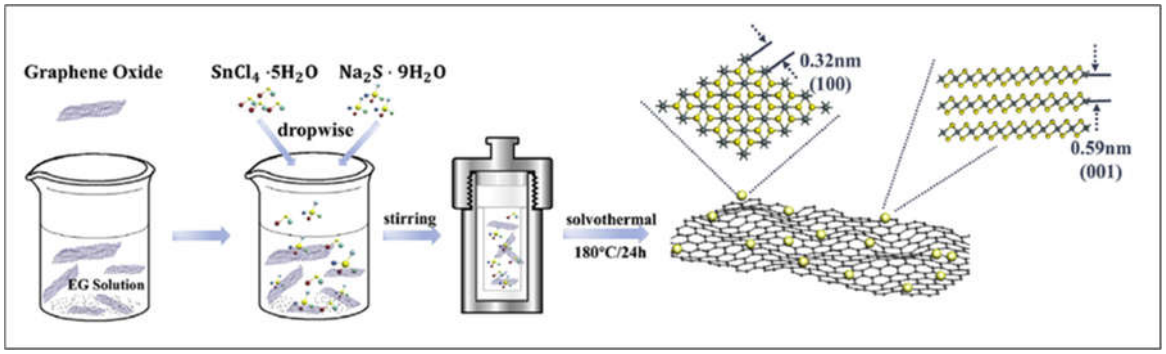


Figure 12: Schematic representation for the solvothermal method used to synthesis $SnS_2$@GNS hybrid nanocomposite. Reproduced from Reference [9] with permission from Elsevier.

### 3.2.3 *In Situ* Growth Method

Besides the hydrothermal method, the synthesis route *via in situ* method also shows a promising way in obtaining hybrid nanomaterials for energy storage and heat transfer applications. *In situ* growth refers to a synthesis process that is conducted in the same place of reaction mixtures without isolating or altering the original condition. It should be noted that *in situ* method is beneficial for allowing a uniform particle growth on the surface of the substrate because it is able to prevent the introduction of impurities and the synthesis processes are usually conducted under the mild conditions [73].

Kong et al. [67] synthesized iron oxide-MXene sheets ($Fe_3O_4$-$Ti_3C_2$) hybrid nanomaterials using *in situ* method by growing the $Fe_3O_4$ nanoparticles on the multi-layered $Ti_3C_2$ in the effort of enhancing the electrochemical performance of the anode electrodes (Figure 13a). With the MXene substrate, $Fe_3O_4$ is reported to be growth homogeneously with a uniform distribution of nanoparticles that are

bound with a strong chemical combination. It should be noted that without the MXene substrate, $Fe_3O_4$ tends to clump and agglomerate. As shown in Figure 13(c-e), the increase of $Fe_3O_4$ content will cause the particle size to increase due to the addition of $Fe^{2+}$. The variation of $Fe_3O_4$ nanoparticles content can be seen clearly from the TEM images of $Fe_3O_4$@$Ti_3C_2$ nanocomposites as depicted in Figure 13(f-h). The nanocomposites recorded a superior electrochemical performance as a result of the excellent capacity of the magnetite and a favourable electrical conductivity of $Ti_3C_2$ which make them suitable for Li-ion storage. In addition, the rate capacities of nanocomposites were also significant when tested at high currents. When compared with previous researches using the same material and content of nanocomposites, it is reported that the *in situ* formed of $Fe_3O_4$@$Ti_3C_2$ nanocomposites provide a much higher capacity than that of physically mixed $Fe_3O_4$@$Ti_3C_2$ nanocomposites.

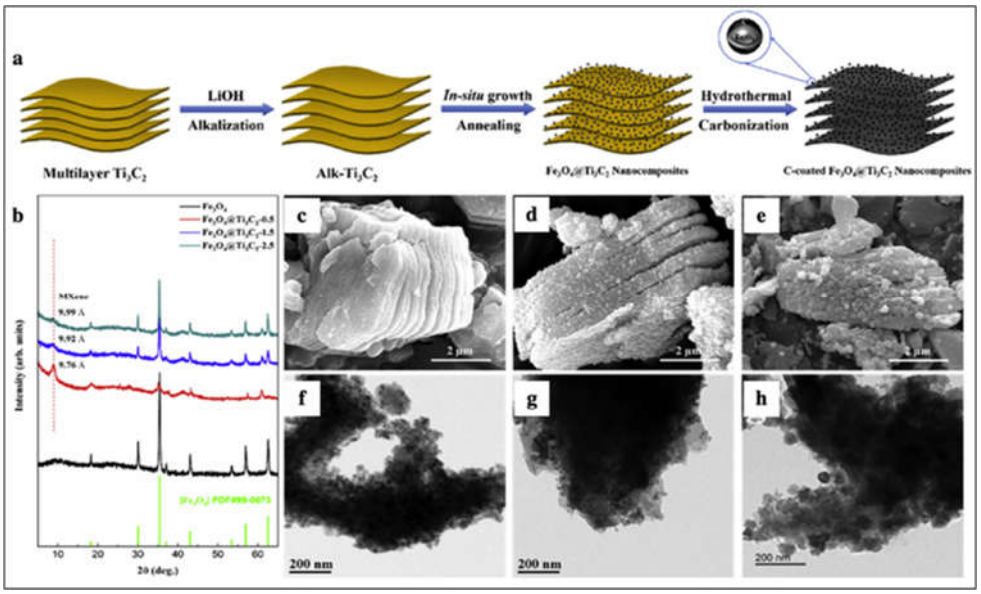


Figure 13: (a) A schematic illustration for the fabrication of $Fe_3O_4$@$Ti_3C_2$ hybrid nanomaterials, (b) XRD patterns of $Fe_3O_4$@$Ti_3C_2$ nanocomposites and pure $Fe_3O_4$, (c-e) SEM images of $Fe_3O_4$@$Ti_3C_2$-0.5, $Fe_3O_4$@$Ti_3C_2$-1.5, and $Fe_3O_4$@$Ti_3C_2$-2.5, and (f-h) TEM images of $Fe_3O_4$@$Ti_3C_2$-0.5, $Fe_3O_4$@$Ti_3C_2$-1.5, and $Fe_3O_4$@$Ti_3C_2$-2.5. Note that the value of 0.5, 1.5 and 2.5 represent the addition of $FeCl_2 \cdot 4H_2O$ in unit mmol. Reproduced from Reference [67] with permission from Elsevier.

Sundar et al. [74] also prepared nano diamond-nickel (ND-Ni) nanocomposites for its application as hybrid nanofluids using *in situ* growth and chemical co-precipitation method in order to enhance the performance of hybrid nanomaterials as a heat transfer fluid. With the aid of acid treatment on the

surface of ND, the Ni nanoparticles can be grown on the ND surface due to the existence of carboxyl (COOH) layers. It is reported that the homogenous dispersion of ND-Ni nanocomposites in the base fluids has led to the thermal conductivity and viscosity enhancements of 29.39% and 23.24%, respectively with the particle concentration of 0.3 wt% at 60 °C compared with the base fluid of distilled water.

In another work, Li et al. [75] synthesized CNTs@$Ti_3C_2T_x$ nanocomposites for the high performance of supercapacitor electrodes where CNTs were *in situ* grown on $Ti_3C_2T_x$@PDA layers via simple pyrolysis method, utilising urea as the source of carbon (Figure 14). The thin layer of polydopamine (PDA) coated on the surface of $Ti_3C_2T_x$ acts as a protective cover which contributes to high structural stability of $Ti_3C_2T_x$. As a result, $Co^{2+}$ was introduced on the surface of $Ti_3C_2T_x$ due to the exchange between positively charged Co ions and phenolic hydroxyl in PDA. The pyrolysis process at 900 °C for 1 hr in an Ar atmosphere causes $Co^{2+}$ to be oxidised and reduced to Co nanoparticles which acts as a catalyst to grow the CNTs. With Co catalyst, urea will be fully converted into carbon nitride gases and it will grow as CNTs via *in situ* method. The growth of CNTs on $Ti_3C_2T_x$ leads to the enlargement of interlayer space of $Ti_3C_2T_x$ which provides a favourable channel for electrolyte transport.

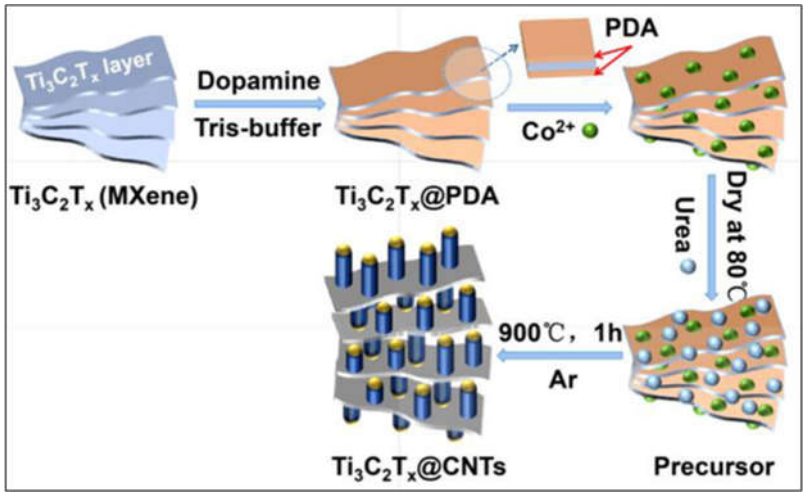


Figure 14: A schematic illustration for in situ growth synthesis of CNTs@$Ti_3C_2T_x$ nanocomposites. Reproduced from Reference [75] with permission from Elsevier.

### 3.2.4 Heat Treatment Method

Thermal reduction method is another route to prepare the hybrid nanomaterials. It is simpler, user-friendly and more economic path compared to the other techniques. This method is also one of the favourable methods to achieve high purity of nanoparticles e.g. graphene, Zinc oxide (ZnO) and etc. [76][77]. It is also reported that thermal reduction method using microwave irradiation is more effective where the reaction time can be reduced significantly.

Shen et al. [78] prepared spinel lithium titanate-MXene ($Li_4Ti_5O_{12}/Ti_3C_2T_x$) hybrid nanomaterials by treating the mixture of LiOH/ $Ti_3C_2T_x$ with the high temperature calcination of 800 °C for 5 hours under the Ar atmosphere (Figure 15a). Calcination refers to a thermal process used to synthesis materials before shaping or dispersing it in which its temperature and environment must be strictly controlled. It is intended to produce a stable form of a material so that decomposition, shrinkage or other reactions do not occur when it is heated again. The use of high temperature calcination is able to reduce lithium hydroxide (LiOH) to $Li_4Ti_5O_{12}$. However, it should be noted that the amount of LiOH gives a significant contribution in the formation of $Li_4Ti_5O_{12}/Ti_3C_2T_x$ nanocomposites. Excessive content of LiOH will give rise to the creation of $LiTiO_2$ which may cause the conductive path of $Ti_3C_2T_x$ layer to break, leading to the degradation of the sample's performance as shown in Figure 15b. Figure 15(c-h) clearly shows progressive damage of the layer structure with additional amount of LiOH. The optimized T-LTO-B (hybrid nanomaterials which corresponds to the addition of 0.5 g LiOH) demonstrated a remarkable electrochemical performance with an improved rate capability, benefitting from the effective $Li^+$ diffusion path, superior conductivity and high structural stability of nanocomposites. The enhancement of electrochemical properties may be associated with the enlargement of electrode active materials that is beneficial for electrolyte contact, contributed by the combination of 0D/2D nanocomposite and also due to the relatively high conductivity of $Ti_3C_2T_x$ nanolayer.

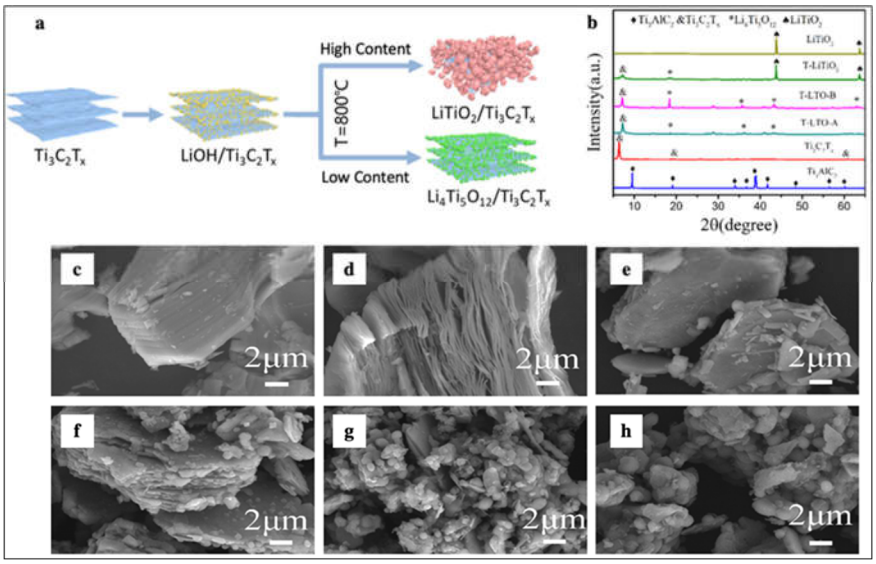


Figure 15: (a) Schematic diagram of the fabrication of $Li_4Ti_5O_{12}/Ti_3C_2T_x$ hybrid nanocomposites, (b) XRD patterns of the samples. FESEM images of: (c) $Ti_3AlC_2$, (d)$Ti_3C_2T_x$, (e) T-LTO-A, (f) T-LTO-B, (g) T- $LiTiO_2$, and (h) $LiTiO_2$. Note that T-LTO-A, T-LTO-B, T- $LiTiO_2$, and $LiTiO_2$ corresponding to the addition of 0.25 g, 0.5 g, 1.0 g and1.5 g LiOH, respectively. Reproduced from Reference [78] with permission from Elsevier.

Furthermore, Tu et al. [79] used a microwave-assisted reduction strategy to prepare multi-layered reduced graphene oxide sheets with TiN nanoparticles hybrid nanocomposite (TiN/rGO) under $N_2$ atmosphere at 1200 °C from the precursors of $TiO_2$/GO. In general, the formation of TiN using gas/solid phase reaction under conventional heating methods cannot be easily achieved due to the very strong N≡N covalent bonding [80]. However, microwave irradiation was able to synthesis TiN/rGO easily along with the good crystallinity and dispersion due to its lower initial reaction temperature and uniform accelerated temperature distribution during the heating process [88]. The hybrid nanocomposites were reported to be favourable for sulphur host material because it allows free movement of lithium ions and electrons. In addition, the uniform distribution of TiN nanoparticles that were bonded on the graphene surface served as an adsorbent that was able to trap lithium polysulfides (LiPSs) due to the superior chemical interaction.

At the end of this section, it can be said that hybridization of nanomaterials has been conducted with the aid of various physical and chemical synthesis routes. Mentionable, physical synthesis routes are

pretend to be much easier than the chemical synthesis routes in terms of strict requirement and complex steps. Among the physical approaches, mechanical mixing process involves the use of mechanical devices to disperse the nanomaterials uniformly and preventing them from stacking or agglomerations. Besides, self-assembly method is a simple route without any chemical bonds implemented to create electrostatic self-assembly interaction between the two materials which able to produce a stable nanocomposites material. Also, hydrothermal and solvothermal synthesis routes been employed for the hybridization of nanomaterials. In these techniques an autoclave is used filled with a solution to withstand the high temperature and pressure. However, solvothermal synthesis route, the size, shape distribution and nanostructure products can be tuned simply by changing the reaction time and temperature, surfactant used as well as the precursor of the nanomaterials. On the other hand, *in-situ* growth method has also showed a promising way in obtaining hybrid nanomaterials for energy storage and heat transfer applications. It is conducted in the same place of reaction mixtures without isolating or altering the original condition, which is beneficial for allowing a uniform particle growth on the substrate surface as well as offers the prevention of impurities formation. Lastly heat treatment method is also discussed as one of the simpler and economic paths to prepare the high purity hybrid nanomaterials. It uses microwave irradiation for more effectivity with a significant reduction of reaction time.

## 4. Application of Hybrid Nanomaterials

### 4.1 Hybrid Nanomaterials in Energy Storage Application

#### 4.1.1 Electrochemical Energy Storage

Energy storage devices are a built-in apparatus which can be used to store a certain amount of energy and transmitting it when necessary. In addressing the current energy crisis to counter global warming, the development of energy storage technologies in the field of renewable energy becomes stringently important. To date, major problems for most electrode materials include poor volume expansion,

inadequate interlayer spacing, incapable of solution processing and low conductivity due to surface oxidation or defects, which hinders their extensive applications in electrochemical energy storage and conversion [81][82]. The use of suitable active materials, e.g. hybrid nanomaterials capable of encountering all of these major problems is an indispensable factor to the high performance, cost-effective and environmentally friendly energy storage devices. Hybrid nanomaterials are expected to offer a large specific surface area that is beneficial for providing a greater extent of active sites for enhancing the energy storage capacity [83].

#### 4.1.1.1 Supercapacitors

The development of supercapacitors plays a significant role in meeting the tremendous growth in energy demands. Supercapacitor is known as an electrical energy storage device that is able to store electricity by creating electrical double layers at the interface of electrodes [48]. It is different from the ordinary capacitor due to its exceptionally high capacitance. The energy storage mechanisms in supercapacitors arise as a result of the electrostatic interaction between the polarized surface of the porous carbon electrode and the electrolyte which forms the electric double layer, rendering a fast response time to charge and discharge the devices [84] [85]. In addition, supercapacitors also offer a greater recharge cycle lifespan, enabling them to be facilitated in hybrid vehicles and backup power stations. Despite having a higher power density compared to batteries, the commercialization of supercapacitors remains a big challenge due to their low energy density, which is influenced by its electrodes capacitance and the working voltage of the cell [86].Thus, in the attempt to escalate the energy density of the supercapacitor, the enlargement of the electrode's capacitance or the working voltage of the devices becomes obligatory. Recently, enormous effort has been made to improve the capacitance of the electrodes since it will affect the availability of surface area for the creation of the electrically charged double layer. In general, 3D carbon often provides complex ion diffusions compared to 2D nanosheets which usually expose their active sites directly to the electrolyte. 2D nanosheets are expected to provide a larger specific surface area, effective ion diffusion path and good

electron conductivity, which will contribute to high electrochemical performance [45]. It is well known that a large surface area will be able to accommodate more electrolyte ions, which in turn increase the double layer capacitance. This will give rise to a higher capacity of charge storage, hence, increasing the capacitance value [83][87]. Figure 16 shows the structure design of different types of two dimensional nanomaterials which will lead to the optimal performance of flexible supercapacitors.

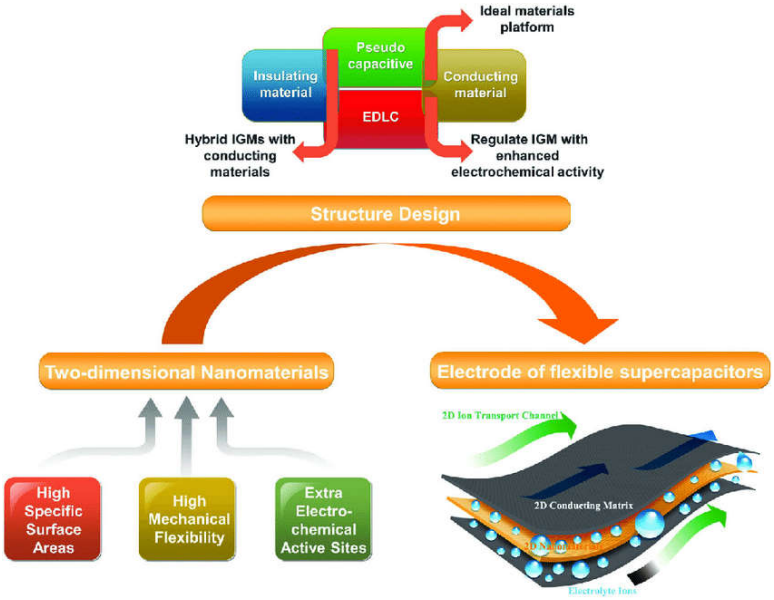


Figure 16: Schematic illustration from 2D nanomaterials to the electrodes of flexible supercapacitors. Reproduced from Reference [88] with permission from The Royal Society of Chemistry.

Recently, Hwang et al. [89] demonstrated that moderate specific surface area of graphene and single walled carbon nanohorn composites (SWCNH) with high bulk density can contribute to high electrochemical performance. They reported that the volumetric capacitance-voltage (CV) curve of the spray-dried reduced graphene oxide and single walled carbon nanohorn composites being treated with nitric acid, $HNO_3$ (rS-GO/NHO) displayed a common double-layer capacitive behaviour with rectangular CV curve, demonstrating its lower resistivity compared to the commercial activated carbon (AC) which displayed an elliptical CV curve of a much higher resistance (Figure 17a). The introduction of SWCNHs is to prevent the graphene nanosheets from being self-restacked during the reduction process. Even though SWCNHs offer a relatively low specific surface area around 400 $m^2$ $g^{-1}$, this surface area can be further enlarged by treating it with a simple chemical treatment known as

the “hole opening process”. The highly nano-porous structure of rS-GO/NHO exhibits a superior volumetric capacitance of 80 F $cm^{-3}$ whereas the commercial AC only exhibit 57F $cm^{-3}$ when measured at 1 mA $cm^{-2}$ even though its specific surface area is larger than rS-GO/NHO with the values of 1928 and 786 $m^2$ $g^{-1}$, respectively (Figure 17b). This magnificent result is associated with the high bulk density appearing in the rS-GO/NHO nanocomposites, indicating the excellent electrical conductivity possessed by the favourable combination of GO/SWCNH. Note that the measured bulk density for the rS-GO/NHO and commercial AC are 1.23 and 0.65 g $cm^{-3}$, respectively. The Nyquist plot of charge transfer resistances $R_{ct}$ in Figure 17c also showed that rS-GO/NHO had the lowest charge transfer resistance in the high frequency range, benefitting from the integration of a highly conductive graphene and SWCNHs. On the other hand, the charge and discharge cycling test at 10 mA $cm^{-2}$ showed that the rS-GO/NHO electrode possesses 91% retention after 10,000 cycles, while AC electrodes showed only 88% (Figure 17d).

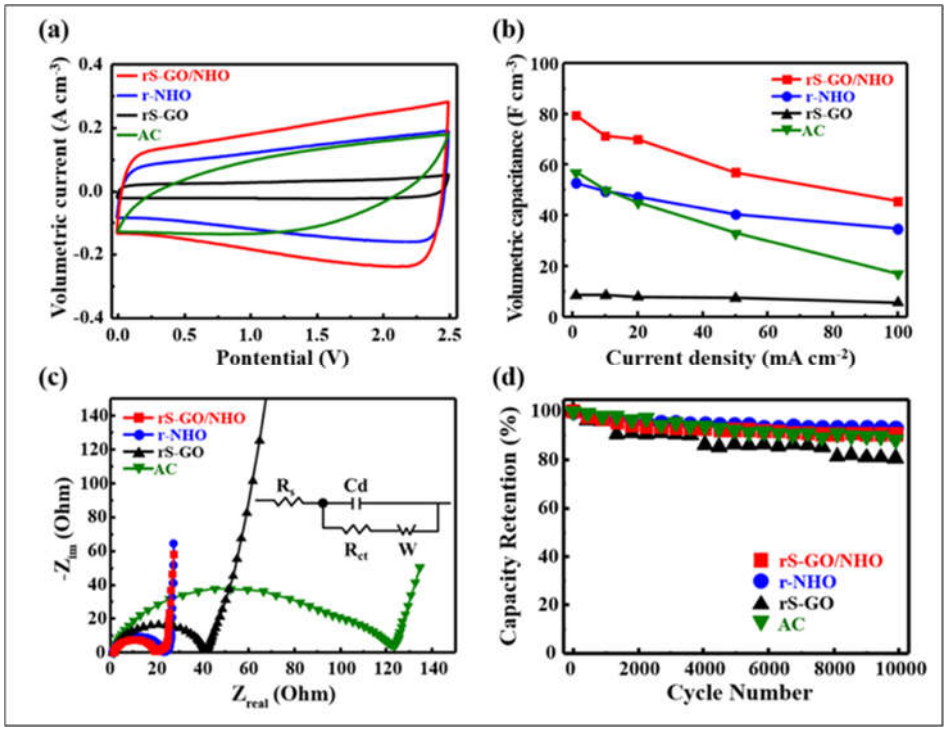


Figure 17: Electrochemical behaviour of different type of electrodes rS-GO/NHO, r-NHO, rS-GO, and commercial AC: (a) Volumetric CV curves measured at 10 mV·$s^{-1}$, (b) volumetric capacitance as a function of current density, (c) Nyquist plots, and (d) charge-discharge cycle performance at 10 mA·$cm^{-2}$. Reproduced from Reference [89] with permission from Elsevier.

Wang et al. [72] prepared fiber-like reduced graphene oxide (rGO)/MXene. With the optimal weight percentage of MXene in fiber-like hybrid, rGO/M-5 (5%wt of MXene) manifests as the highest gravimetric specific capacitance with lengthen discharge time compared to rGO/M-10, rGO-M-15 and rGO fiber. It also showed a CV curve of rectangular shape and able to remain rectangular and symmetrical triangular shapes even though at high current densities, demonstrating its superior capacitive behaviour (Figure 18a-d). Apart from that, rGO/M-5 is able to exhibit a considerably high capacitance value of 345.2 F $cm^{-3}$ at 0.1 A $g^{-1}$. The outstanding electrochemical properties is due to the synergistic effects that exist when the appropriate amount of MXene disperses homogeneously with the graphene layer. This synergistic effect causes graphene oxide to steer the fiber formation and the homogenous dispersion of MXene contributes to the electrical conductivity and volumetric electrochemical performance. It should be noted that the optimized weight of fiber-like hybrids will cause the MXene thin layers to integrate favourably with graphene fibers, preventing the graphene sheets from being restacked. This will expand the active sites of electrodes to the electrolyte, hence, shortening the ion-diffusion pathway compared to the usage of single rGO (Figure 18e). Besides that, the highly conductive MXene sheets embedded in graphene may contribute to a long-term conductivity and vigorous network, enabling the rapid transfer of electrons within the electrodes.

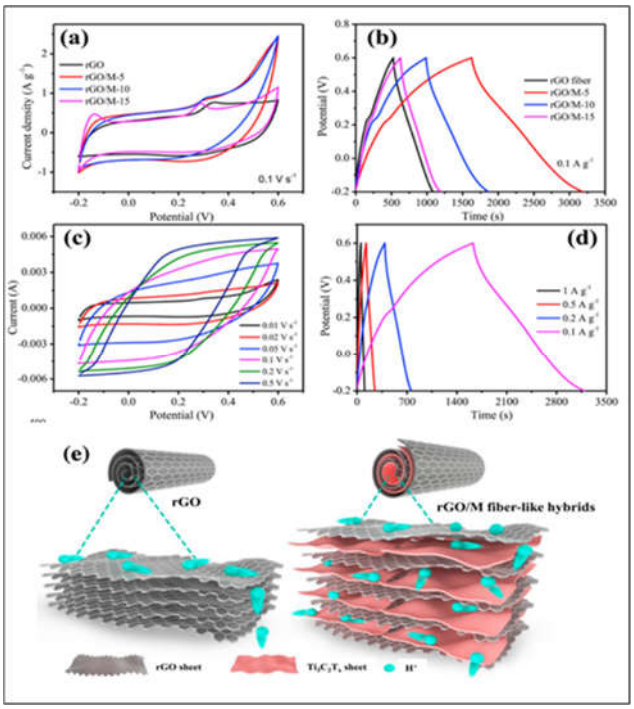


Figure 18: (a) CV curves measured at 10 mV $s^{-1}$and (b)galvanostatic charge-discharge curves at 0.1 A $g^{-1}$ for several samples; (c) CV curves at various scan rates and (d) galvanostatic charge-discharge curves at various current densities for rGO/M-5 and (e) Schematic diagram of $H^+$ ions flow during electrochemical reaction. Reproduced from Reference [72] with permission from Elsevier.

In another work, Zheng et al. [90] demonstrated that a suitable introduction of CNT decorated with nickel selenide ($NiSe_2$ ) may enhanced the specific capacitance because the optimal value of CNT can increase the conductivity of nanocomposites and contribute to microwave heating, as well as the reduction of $NiSe_2$ aggregation. When 20 mg CNT was employed, the nanocomposite recorded the highest specific capacitance value of 980.5 F $g^{-1}$ at 1 A $g^{-1}$ and the structure exhibited an outstanding long-term cycle stability of 82% even after 9000 cycles, showing its stable and reversible characteristics. It is also reported that the excessive addition of selenium powder will lower the specific capacitance due to unreacted selenium powder. Therefore, the mass ratio of the optimum reaction condition for $NiSe_2$@CNT nanocomposite were 20:40:20 of CNT:$Ni(NO_3)_2{\cdot}6H_2O$:Se. The introduction of nickel-selenide (Ni-Se) into CNT led to a high specific capacitance and outstanding electrochemical performance [91] due to the incorporation of the two nanomaterials.

Jin et al. [71] also compared the electrochemical performance of $MnO_2$-$Ti_3C_2$ (MT) and $MnO_2$-rGO (MG) electrodes with different weight percentages of $Ti_3C_2$ and rGO, respectively. The resulting

materials were denoted as MT/G-2, MT/G-4 and MT/G-6 for the 2, 4, and 6wt% of $Ti_3C_2$ and rGO, respectively. Among all MT hybrid nanomaterials, MT4 exhibited a much larger specific capacitance of 306 F $g^{-1}$ at 5000th cycle with an outstanding stability compared to other MT nanohybrids. Similarly, MG4 also demonstrated a larger specific capacitance of 261 F $g^{-1}$ at the same cycle compared to other MG nanohybrids. When comparing the performance of MT and MG, it is clearly observed that the hybridization of $MnO_2$ with MXene nanosheets can improve the electrochemical performance of the electrode due to the fact that the interaction of hydrophilic species ($MnO_2$) with hydrophilic species ($Ti_3C_2$) is much favourable compared to the interaction between hydrophilic and hydrophobic species, rendering a much stronger interfacial chemical interaction between $MnO_2$-$Ti_3C_2$ compared to $MnO_2$-rGO. Besides that, $MnO_2$-$Ti_3C_2$ electrode exhibits a much bigger surface area for easy ion transports compared to that of $MnO_2$-rGO, highlighting that the hybridization of $MnO_2$ with $Ti_3C_2$ nanosheets able to prevent MXene nanosheets from self-stacking, leading to a high charge storage capacity. Table 3 summarized recent studies made to date on the hybridization of nanomaterials for supercapacitors application.

Table 3: Summary of previous researches on supercapacitors application using hybrid nanomaterials.

| **Electrode** | **Electrolyte** | **Maximum gravimetric capacitance (F $g^{-1}$)** | **Maximum volumetric capacitance (F $cm^{-3}$)** | **High current density cycle retention (%/ cycle-index)** | **Reference** |
|---|---|---|---|---|---|
| Trimanganese tetraoxide-Reduced graphene oxide ($Mn_3O_4$/rGO) | 1.0 M sodium chloride (NaCl) | 437 | -- | 100/10 | [19] |
| Reduced graphene oxide-MXene (rGO/$Ti_3C_2T_x$) | 1.0 M sulphuric acid ($H_2SO_4$) | 195 | 345.2 | 124.8/7500 | [72] |
| Nickel selenide-Carbon nanotube ($NiSe_2$/CNT) | 6.0 M Potassium hydroxide (KOH) | 980.5 | -- | 82/9000 | [90] |

| | | | | | |
|---|---|---|---|---|---|
| Reduced graphene oxide-Single walled carbon nanohorn composites with nitric acid (rS-GO/NHO) | 1.0 M tetrafluoroborate ($TEABF_4$) | -- | 80 | 91/10000 | [89] |
| | 1.0 M $H_2SO_4$ | -- | 87 | 94/3000 | [89] |
| Manganese dioxide- Titanium carbide ($MnO_2/Ti_3C_2$) | 0.2 M sodium sulfate ($Na_2SO_4$) | 306 | -- | 98/5000 | [71] |
| Manganese dioxide- Reduced graphene oxide ($MnO_2$/rGO) | 0.2 M $Na_2SO_4$ | 261 | -- | 85/5000 | [71] |
| Manganese dioxide- MXene ($MnO_2$/ $Ti_3C_2T_x$) | Polyvinyl alcohol (PVA)/$H_2SO_4$ | 130.5 | -- | 90/1000 | [92] |
| MXene-Carbon nanotubes ($Ti_3C_2T_x$/CNTs) | 6.0 M KOH | 109.6 | -- | 78.1/10000 | [75] |
| Exfoliated Graphene/MXene | PVA /Phosphoric acid ($H_3PO_4$) | -- | 216 | 82/2500 | [18] |

#### 4.1.1.2 Lithium-ion Batteries

Lithium ion battery (LIB) is a rechargeable battery which usually depends on the liberation of $Li^+$ from the accommodating electrodes through the electrochemical redox reactions for the charging and discharging process. Throughout the charging and discharging processes, $Li^+$ will move back and forth between the positive (e.g. Lithium cobalt oxide, $LiCoO_2$) and negative electrodes, producing ion intercalation/ de-intercalation processes [48] (see Figure 19). LIB appeared as the most common power source in small portable electronic devices, electric vehicles, and hybrid electric vehicles due to their high energy density, low rate of self-discharge, and long cycling stability [93]. However, the limitations on the theoretical capacity of 372 mAh $g^{-1}$ and the poor rate performance of the conventional graphite anode in LIB have restricted their extensive applications [94]. Therefore, the development of energy storage devices consisting of high power and high energy density becomes essential in order to satisfy the growing energy demands.

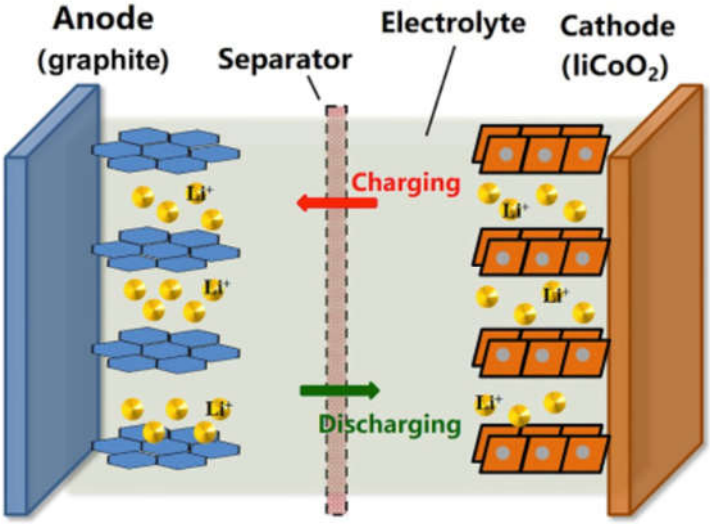


Figure 19: Schematic diagram of the lithium intercalation and deintercalation reaction mechanism in a rechargeable lithium-ion battery containing solid electrodes and a liquid electrolyte. Reproduced from Reference [95].

Generally, these energy storage advancements will depend on the innovation made for the system i.e. developing an electrode made of emerging nanomaterials that is capable of being charged and discharged at all current rates [96]. In recent years, tremendous effort has been made to develop an electrode made by emerging hybrid nanomaterials as the tailored nanomaterials are able to offer a better electrochemical performance. It is well noted that the diffusion of Li-ion is mainly influenced by the ion transport path and the active sites available at the electrode's surface. Therefore, the use of nanocomposite electrodes will not only pioneer the reaction mechanisms but is also expected to boost the electrochemical performances by producing a much higher energy storage capacity, superior charge-discharge ability and good long-term cycle stability, benefitting from the short ion diffusion path and large effective contact area between the active materials and electrolyte [96]. To examine this, Wu et al. [9] synthesised a nanocomposite of tin-sulfide ($SnS_2$) nanoparticle and graphene nanosheets (GNS) through a facile solvothermal process. The unique structure of $SnS_2$@GNS delivered a superior lithium storage performance of 1250.8 mA h $g^{-1}$ at 0.1 A $g^{-1}$ even after cycling 150 times (Figure 20a, b, d). Besides that, $SnS_2$@GNS also exhibited a much higher capacitance value

compared to single particle $SnS_2$ and rGO (Figure 20c, e). The highest coulombic efficiency of 98.53% obtained by the nanocomposite may be due to the formation of C-S bond between $SnS_2$ and GNS nanomaterials, rendering a good structural stability of the anode materials. A further test on cycle capacities of $SnS_2$@GNS at high current density of 0.5 A $g^{-1}$ confirmed that the nanocomposite achieved ~798.6 mAh $g^{-1}$ after 100 cycles without any drastic decline in capacity (Figure 20f). It is well observed that the engineered nano crystallization of $SnS_2$ and compounding it with the carbon-based materials can uplift their cycling performance and improve fast charge/ discharge process. This could be due to the large active sites available and superior adsorption of $Li^+$ contributed by the extremely thin graphene nanosheets. It is noteworthy that the addition of graphene yields large active sites for the electron and ions transportation. The unique combination of $SnS_2$@GNS also led to a remarkable impact in improving the electrochemical properties where the ultra-small particles of $SnS_2$ provided a shorter ion diffusion path whereas graphene was able to enhance the electrical conductivity of the hybrid structure

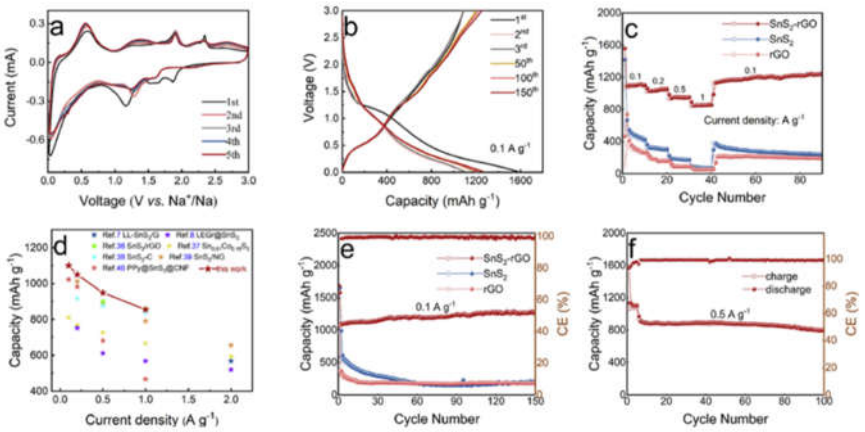


Figure 20: a) CV curves of $SnS_2$@GNS measured at 0.1 mV $s^{-1}$. b) Charge/discharge process of $SnS_2$@GNS at different number of cycles, measured at 0.1 A $g^{-1}$. c) Rate performance of $SnS_2$@GNS, $SnS_2$, and GNS. d) The comparison of rate performance behaviour of $SnS_2$@GNS with other reported $SnS_2$-based materials. e) Cycling performance of $SnS_2$@GNS, $SnS_2$, and GNS measured at 0.1 A $g^{-1}$. f) Cycle performance of $SnS_2$@GNS when measured at high current density. Reproduced from Reference [9] with permission from Elsevier.

Fang et al. [97] studied the electrochemical performance of titanium dioxide and reduced graphene oxide ($TiO_2$/rGO) nanocomposite as an anode for LIBs. As shown in Figure 21a, the nanocomposite

demonstrates a large storage capacity due to the improved conductivity and capacitive behaviour, leaving pure $Ti_2C$-$TiO_2$ nanoparticles with much lower electrochemical performance. The enhanced electrochemical performance is due to the addition of rGO, suggesting that rGO nanosheets are well integrated with $TiO_2$ nanoparticles. The introduction of GO not only gave rise to smaller $Ti_2C$ nanosheet formation but also prevented the $TiO_2$ from re-stacking. It is also reported that the increased capacity is not fully contributed by rGO only, but the enhancement of the rate ability properties of $TiO_2$ after being hybridised. The charge-discharge profiles of $TiO_2$/rGO which mainly consists of three parts: high-voltage slope, plateau, and low-voltage slope confirmed the existence of fast Li-ion storage on the $TiO_2$ surface (Figure 21b-c). A near-rectangle shape of the CV curve also confirmed that $TiO_2$/rGO possess a much larger capacity compared to $TiO_2$, demonstrating the addition of rGO contributes to high capacitive behaviour by enhancing the conductivity of the nanocomposite (Figure 21d). In addition, $TiO_2$/rGO nanocomposite showed a remarkable cycling performance with ~ 86% capacity retention after 1000 cycles, showing the outstanding structural stability of $TiO_2$ and the addition of rGO was able to prevent volume change during ion intercalations (Figure 21e).

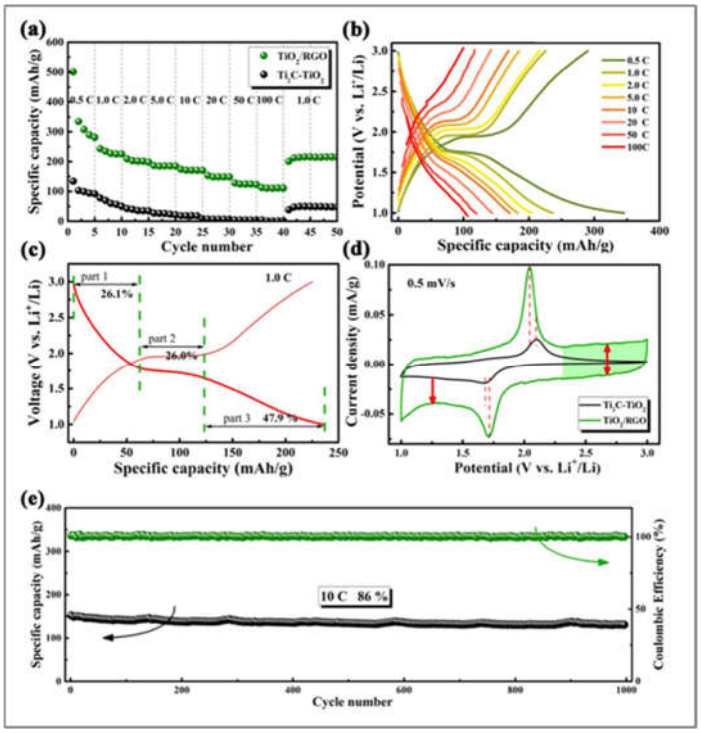


Figure 21: Electrochemical properties of $TiO_2$/rGO anode for LIBs. (a) The cycle rate performance of $TiO_2$/rGO and $TiO_2$. Charge-discharge curves of $TiO_2$/rGO at (b) different rates, and (c) 1C rate. (d)

CV curves of $TiO_2$/rGO and $TiO_2$ measured at 0.5 mV/s. (e) Cycling performance of $TiO_2$/rGO at 10 C. Note that C represents current density (1C = 168 mA $g^{-1}$). Reproduced from Reference [97] with permission from The Royal Society of Chemistry.

The use of conductive graphene with modified mesoporous anatase (M-$TiO_2$-GS) nanocomposite for flexible LIBs by Luo et al. [98] showed the outstanding $Li^+$ properties with high specific capacity of 205 mAh $g^{-1}$ at 0.5 C with 0° bending condition. To demonstrate the feasibility of the as-formed electrode, the authors bend it at 2 different angles of 90° (flat) and 180° (bent) to show its flexible properties and good electrochemical performance for flexible cells. At flat condition, the M-$TiO_2$-GS anode exhibited a reversible capacity of 200 mAh $g^{-1}$ at 0.5C and a stable cycle performance with 91.3% capacity retention over 100 cycles at 1 C. Interestingly, in a bending condition of 180°, M-$TiO_2$-GS still demonstrated a revisable capacity up to 191 mAh $g^{-1}$ at 0.5C with a better capacity retention of ~ 93.5% over 100 cycles at 1C. The good electrochemical performance was achieved because the dispersive M-$TiO_2$ was sandwiched layer-by-layer with graphene sheets, offering an effective ion transport pathway. A summary of recent researches on LIBs application using hybrid nanomaterials is given in Table 4.

Table 4: Summary of previous researches for LIBs application using hybrid nanomaterials. Note that 1C = 170 mA $g^{-1}$ and $LiPF_6$ represents as lithium hexafluorophosphate.

| **Electrode** | **Electrolyte** | **Capacitance (mAh $g^{-1}$)** | **High current density cycle retention (%/ cycle-index)** | **Ref** |
|---|---|---|---|---|
| $SnS_2$@GNS | 1.0 M $LiPF_6$ | 1250.8 at 0.1 A $g^{-1}$ | 98.53/150 | [9] |
| $TiO_2$-rGO | 1.0 M $LiPF_6$ | 130.6 at 10 C | 86/1000 | [97] |
| M-$TiO_2$-GS | 1.0 M $LiPF_6$ | 94 at 5 C | 70.5/3500 | [98] |
| $Li_4Ti_5O_{12}$/$Ti_3C_2T_x$ | 1.0 M $LiPF_6$ | 236 at 50 mA $g^{-1}$ | -- | [78] |
| $Fe_3O_4$@$Ti_3C_2$ | 1.0 M $LiPF_6$ | 342.9 at 1 C | 77.1/100 | [67] |
| C-coated $Fe_3O_4$@$Ti_3C_2$ | 1.0 M $LiPF_6$ | 382.9 at 1 C | 88.1/100 | [67] |

### 4.1.2 Thermal Energy Storage

Thermal energy storage (TES) has been extensively evaluated as an important technology in bringing the gap between energy demand and energy supply. TES systems are capable of storing thermal energy

supplied to it, conveying a complete storage cycle of charging, storing and discharging which enables the stored energy to be used at a later time. It should be mentioned that the storage of thermal energy can be in form of sensible heat and latent heat in which sensible heat storage stored thermal energy only by increasing the storage medium temperature, utilising rocks or water as the storage medium, whereas latent heat storage system stored energy using phase change materials (PCMs) [99]. Among these two forms of energy storage, latent heat energy storage utilising PCMs are widely used to store thermal energy owing to its massive amount of latent heat during phase change, high energy storage density and only small temperature variation due to isothermal nature of the working process which not only minimise the mismatch between energy demand and supply, but at the same time provides an environmental-friendly technologies (see Figure 22).

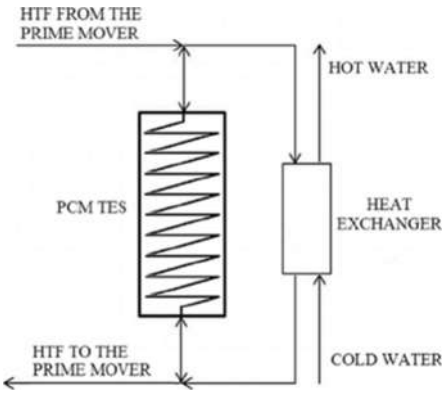


Figure 22: Schematic representation of the latent heat thermal energy storage configuration system. Note that HTF represents as heat transfer fluids. Reproduced from Reference [100] with permission from Elsevier.

With all the mentioned features, latent heat thermal energy storage using PCM emerged as one of the most effective way in storing thermal energy and it has been proved to be a desirable TES in a wide of applications such as solar energy storage, industrial waste heat recovery, intelligent air-condition buildings, electric appliance and thermo-regulated textiles [101]. Even though PCM has desirable characteristics in storing the thermal energy, it has a major drawback associated with the leaking problem during the solid-liquid phase transition which in turns increases the thermal resistance, hence, limiting its practical application. Therefore, improving the stability of PCM and also its thermal conductivity properties are the key to the highly efficient thermal energy storage system. In the past

few years, nanomaterials such as graphite foams, carbon nanotubes, graphene nanomaterials boron nitride and metal materials have been extensively studied as the supporting material for PCM, providing a desirable thermal conductivity enhancement due to the rapid heat transfer possessed by PCM and nanoparticles [102]. However, it should be noted that although these PCMs can avoid leaking or possess a remarkable higher thermal conductivity compared to that of pure PCM materials, the thermal energy storage density of composite PCMs is reduced seriously due to a portion of their working substance is replaced by supporting materials which does not undergoes phase change within their operating temperature range . Therefore, the exploration of new way in improving the stability, thermal conductivity and maintaining the energy storage density should be one of paramount importance.

In order to examine this, Qi et al. [103] evaluated the performance of latent heat thermal energy storage system utilising graphene oxide and graphene nanoplatelets with polyethylene glycol (GO/GNP/PEG) nanocomposite PCM. The authors reported that the incorporation of hybrid GO and GNP with PCM emerged as one of the effective supporting materials and conductive materials for PCM, providing a desirable thermal conductivity enhancement of 490% (1.72 W/mK) relative to that of pure PEG (0.29 W/mK), and surpassing PEG/GNP nanocomposite (1.61 W/mK) at the optimised particle loading of 2:4 for GO and GNP. The effect of addition of GO/GNP as the supporting materials to that of PEG also did not exert a negative effect towards thermal energy storage density, in which it still have 98.2% energy storage density compared to pure PEG, demonstrating its promising potential as hybrid fillers for latent heat thermal energy storage applications.

In the effort of improving the thermal conductivity of the PCM used for thermal energy storage (TES), Zhou et al. [104] prepared the rGO/GNP-paraffin microencapsulated phase change materials (MePCMs) by encapsulating paraffin with reduced graphene oxide (GO) and also graphene nanoplatelets (GNP) through self-assembly method, causing the hybrid shell to arise as a result of the $\pi - \pi$ interaction between rGO and GNP. With the optimised mass ratio (7:3 for rGO:GNP), the as

prepared MePCMs demonstrated an excellent thermal conductivity enhancement, increasing from 0.67 W/mK for PCM with only rGO shell to 0.90 W/mK (Figure 23a). The authors reported that the usage of nano-dimension sheets of rGO and GNP ease the encapsulation process especially for the extremely low content of PCM, optimising the paraffin loading and hence capable of maximising the energy storage capacity.

In another work, Sharma et al. [105] studied the performance of latent heat storage systems by utilising paraffin wax as PCM and hybrid zinc-cobalt-iron oxide nanofluid. The authors reported that by using the mixture of hybrid nanofluid, the efficiency of the thermal energy storage system is increased due to the optimisation of the charging time of PCM. The authors reported that the charging and discharging time of TES were reduced up to 25% and 20%, respectively, indicating the improved TES performance due to the addition of hybrid nanoparticles. Figure 23b depicts the difference between the charging time of PCM with and without the addition of nanofluids. As shown in Figure 23b, in order

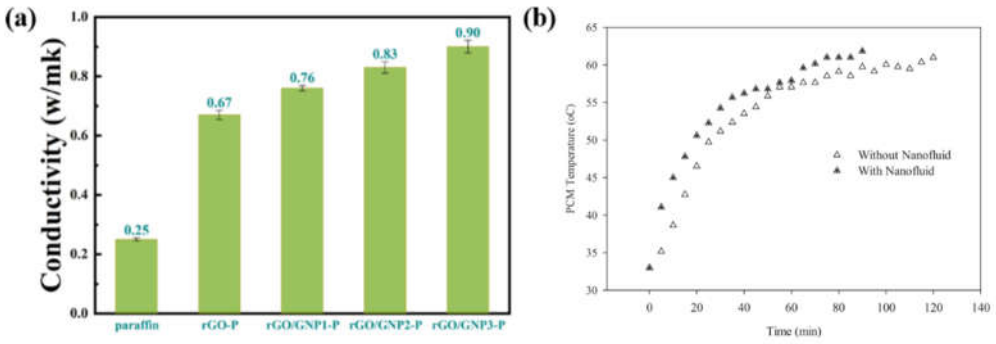


to reach a stable temperature approximately at 62 °C, PCM with nanofluid only need around 90 minutes charging time whereas PCM without nanofluid requires about 120 minutes.

Figure 23: (a) Thermal conductivity of paraffin and MePCMs at different mass ratio, and (b) Charging time of PCM with and without the addition of nanofluid. Reproduced from Reference [104] and [105] with permission from Elsevier.

Song et al. [101] evaluated the performance of thermal energy storage using halloysite-Ag/polyethylene glycol PCM (HNT-Ag/PEG). It has been reported that the usage of hybrid nanomaterials with PCM able to simultaneously provide a high latent heat storage and enhanced thermal conductivity. The optimised nanocomposite PCM (3.3 wt.%) demonstrated an outstanding

phase change temperature of 33.6 °C at a relatively high thermal energy storage density of 71.3 J/g and also a significantly enhanced thermal conductivity of 0.9 W/mK, providing almost 2.8 times augmentation of thermal conductivity enhancement compared to that of 0.2926 W/mK for a stand-alone PEG. The authors reported that the significant improvement in thermal conductivity is associated with the successful construction of numerous conductive pathways and homogenous dispersion of a continuous 3D HNT framework decorated with the highly thermal conductivity of Ag nanoparticles. Furthermore, Liu et al. [106] investigated the performance of microencapsulated PCM based on graphene oxide (GO) and carbon nanotube (CNT) hybrid filler. The optimised integration of 1D CNT and also 2D graphene sheets at 3:1 in creating a 3D nanostructure has led to a remarkable thermal conductivity enhancement of 195% with 0.6 wt.% of hybrid filler loading, an improvement of 2.95 times compared to single particle MePCM/CNT due to the synergistic effect between CNT and GO. The evaluation of thermal storage properties revealed that the encapsulation of MePCM/GO-CNT gives a higher average latent heat of 162.9 J/g compared to 158.8 J/g for a single particle MePCM/CNT, demonstrating good dispersion of MePCM/GO-CNT, thus providing more energy storage capacity.

### 4.2 Hybrid Nanomaterials in Heat Transfer Application

The advancement of nanotechnology in creating hybrid nanomaterials has influenced the creation of a new kind of nanofluid e.g. hybrid nanofluids for its extensive applications as heat transfer fluids. In general, the dispersion of hybrid nanomaterials in the base fluid are called hybrid nanofluids and it is a rapidly growing field in material science and engineering [80]. Due to the enhancement of physicochemical properties possessed by the constituent materials as a result of their synergistic effect, hybrid nanofluids received its prime attention from the various researchers around the world to evaluate its thermal performance for advance heat transfer applications. A brief summary of published work dealing with hybrid nanofluids is given in Table 5. It should be mentioned that most of the literature is focusing on the thermo-physical properties of hybrid nanofluids specifically for cooling

process ability and heat transfer applications. In the next section, we discussed the potential application of hybrid nanofluids.

In accordance with the findings, increasing the temperature and particle concentration will lead to thermal conductivity enhancement [107][108][109]. The use of high working temperature and nanoparticles concentration will give rise to intense Brownian motion due to the interaction of nanoparticles in the base fluid. Increasing the particle loading means increasing the number of suspended nanoparticles, causing the closer gap between particle-to-particle distances. This will lead to rapid increase in surface-area-to-volume ratio and collision between nanoparticles. This triggered the frequency of lattice vibration to increase, which in turn enhanced the thermal conductivity. This mechanism is known as the percolation effect [110]. With the enhanced thermal conductivity of hybrid nanofluids, it indicates the potential of such emerging combinations of nanofluids in replacing the conventional coolants in advanced heat transfer devices.

It should be noted that stability also plays a significant role in hybrid nanofluids as they are the key in preserving the thermophysical properties of the fluid. Therefore, enhancing and maintaining the nanofluids stability will lead to the outstanding performance of heat transfer fluids. It is widely acknowledged that one of the major challenges faced by nanofluids is their poor suspension stability as a result of the interaction between the particles themselves and also between the nanoparticles and the base fluid itself. This phenomenon can be related to the two opposing forces: 1)Van der Waals attractive forces that are arises on the particles surface, causing the particles to be attracted towards each other, forming clusters or agglomerations which cause them to be separated from the base fluid and become sedimented due to gravitational force, and 2) electrical double layer repulsive force that tends to separate the particles from each other via electrostatic repulsion. In this regard, a good suspension stability can be obtained if and only the electrical double layer repulsive force surpasses the Van der Waals attractive forces [111].

Table 5: Summary of previous works done for hybrid nanofluids, highlighting the important findings obtained for that particular studies. Note that DI, DW and EG represent deionised water, distilled water and ethylene glycol, respectively.

| Hybrid NM | BF | Method | Concentration | Findings | | | Ref |
|---|---|---|---|---|---|---|---|
| | | | | Stability | TC Enhancement (%) | Viscosity | |
| Multi-walled carbon nanotube-Iron oxide (MWCNT-$Fe_3O_4$) | Water-EG (80:20) | Two steps | 0.01 wt.% | Stable with no agglomeration observed for 1 month. | 8 (20 °C) | -- | [17] |
| Graphene oxide-Aluminium oxide GO-$Al_2O_3$ | DI | Two steps | 0.3 vol.% | Stable without any agglomeration up to 15 days. | 45 (25 °C) | All the prepared nanofluids possessed Newtonian behaviour in the temperature range of 20-70 °C. | [15] |
| Functionalized carbon nanofiber-reduced graphene oxide (F-CNF/rGO) | DW | Two steps | 0.04 vol.% | F-CNF/rGO hybrid nanofluids demonstrated Zeta potential value of -45 mV on the 1st day and -33.4 mV on the 180th day with no sign of visible sedimentation. | 24.6 (55 °C) | F-CNF/rGO hybrid nanofluid has the least viscosity enhancement (6.3%) compared to CNF, F-CNF and rGO nanofluids (15.2%, 12.5% and 7.2%, respectively). | [112] |
| Graphene nanoplatelets-Titanium dioxide (GnPs-$TiO_2$) | DW-EG | Two steps | 0.1 wt.% | Stable up to 40 days due to the addition of hexadecyl-trimethylammonium bromide (CTAB) as surfactant. | 21.59 (60 °C) | The viscosity enhancement for hybrid nanofluids is lower compared to that of mono nanofluids. | [110] |
| Silicon carbide-Copper Oxide with Carbon (SiC–CuO/C) | EG | Two steps | 3.13 wt.% | All samples have a good stability of dispersion even after 30 days. | 8.8 (25 °C) | The highest viscosity enhancement of 205% was observed for 3.13 wt.% | [107] |
| Single-walled carbon nanotubes-Magnesium oxide (SWCNTs-MgO) | EG | Two steps | 0.55 wt.% | -- | 35 (50 °C) | -- | [108] |
| Aluminium Oxide- | Water | Two steps | 0.2 vol.% | Stability test showed that hybrid nanofluid | 14 (65 °C) | Both mono and hybrid nanofluids exhibited Newtonian behaviour as | [113] |

| | | | | | | | |
|---|---|---|---|---|---|---|---|
| Iron ($Al_2O_3$-Fe) | | | | possessed high stability at pH 12 with Zeta potential of -45 mV at all concentrations | | there is a linear relationship between the shear stress and shear rate. | |
| Magnesium oxide-Titanium dioxide (MgO-$TiO_2$) | DW | Two steps | 0.5 vol.% | All the prepared hybrid nanofluids are reported to have a good stability with Zeta potential ranging from ± 25 mV to ± 45 mV. | 21.8 (60 °C) | At all concentrations and temperature, hybrid nanofluids possessed Newtonian behaviour. The highest viscosity enhancement of 28.7% is achieved by 80 wt% MgO-20 wt% $TiO_2$ at 60 ℃. | [114] |
| Nano diamond-Nickel (ND-Ni) | DW | Two steps | 0.3 wt.% | -- | 29.39 (60 °C) | Viscosity enhancement of 25.53% is achieved at 60 ℃. | [74] |
| Multi-walled carbon nanotubes-Silicon carbide (MWCNTs-SiC) | Water-EG | Two steps | 0.75 vol.% | -- | 28.86 (50 ℃) | -- | [109] |
| Aluminium oxide-Multi-walled carbon nanotube ($Al_2O_3$-MWCNT) | Oil | Two steps | 1.5 vol.% | Highly stable suspension is achieved even after 7 days with Zeta potential ranging from 50 – 60 mV. | 45 (50 ℃) | At all concentrations, maximum enhancement of viscosity is recorded at the temperature of 40 ℃, where the dynamic viscosity for 1.5 vol.% increased by 81% relative to the base fluid. | [115] |
| Titanium oxide-Copper oxide/Carbon ($TiO_2$-CuO/C) | EG | Two steps | 2.0 vol.% | Hybrid nanofluid were found to be stable only at pH 10 with Zeta potential ranging from 36 to 42 mV at different volume concentrations. | 5.6 (60 °C) | Hybrid nanofluid shows Newtonian behaviour at the temperature range of 25 – 60 ℃. Highest viscosity increment of 70% is recorded at 60 ℃. | [116] |
| Iron Oxide-Copper Oxide ($Al_2O_3$-CuO) | Water-EG (80:20) | Two steps | 0.2 vol.% | -- | 45 (60 °C) | -- | [117] |
| Copper-Zinc (Cu-Zn) | Vegetable oil | Two steps | 0.5 vol.% | All the prepared nanofluids were reported to be stable up to 72 h. | 53 (30 °C) | Hybrid nanofluids possessed Newtonian behaviour and exhibited less amount of deformation or shear thinning with application of shear to it. | [118] |

| | | | | | | | |
|---|---|---|---|---|---|---|---|
| Tungsten trioxide - Silver ($WO_3$-Ag) | Transformer oil | Two steps | 4.0 wt.% | Good stability of dispersion with Zeta potential ranging from 46 mV to 55 mV at different concentrations. | 41 (100 °C) | -- | [119] |
| Iron Oxide-Aluminium OXide ($Fe_2O_3$-$Al_2O_3$) | 10W40 Engine oil | Two steps | 4.0 wt.% | -- | 33 (65 °C) | -- | [120] |
| Graphene-Silicon Oxide (G-$SiO_2$) | Mineral oil | Two steps | 0.04 wt.% | Highest suspension stability is at pH 11 with no agglomeration or sedimentation even after two weeks. | 80 (100 °C) | 29.7% highest viscosity enhancement was observed with 0.04 wt%. | [121] |

### 4.2.1 Solar Energy

Solar energy has been extensively evaluated as the ultimate solution to the energy crisis, and it is also the key to a clean energy future. The use of solar energy technologies will give us opportunities to reduce environmental pollution, enhance sustainability, prevent rapid climate change and minimise the consumption of fossil fuels [122]. As mentioned earlier, the major drawback for solar energy technologies is its low efficiency in collecting and converting solar radiation into electricity. Enormous effort has been made to improve the efficiency of the solar energy collectors and photovoltaic-thermal (PV/T) and one of the novel approaches is to use the novelty working fluids e.g. hybrid nanofluids which have high capability of heat transfer and outstanding optical properties. It should be noted that the type of working fluids used is the prime factor to achieve highly efficient solar energy harnessing systems. Utilising hybrid nanofluids as working fluids for solar energy technology enables us to boost the overall performance of the system as it offers an improved heat transfer coefficients as a result of its outstanding thermal conductivity behaviour, the ability to lower the absorber temperature by transferring heat quickly and the potential to absorb solar radiation, which are not being carried out by PV solar cell, benefitting from its superior optical properties [123]. In solar technology various types

of hybrid nanofluids have been utilized as the working media. A brief summary of the previous researches carried out utilising various hybrid nanofluids in solar energy systems is presented in Table 6. It should be mentioned that the performance of hybrid nanofluids in solar energy is greatly influenced by the thermal properties and optical parameters such as absorption coefficient, solar weighted absorption, transmittivity, scattering and etc. which can be altered by modifying the concentration of nanoparticles, particle size and type of base fluids [124].

**Table 6:** Summary of application of hybrid nanofluids in solar energy systems. Note that DI, DW and EG represent deionised water, distilled water and ethylene glycol, respectively. DASC and PV/T represent direct absorption solar collector and photovoltaic thermal solar panel, respectively.

| Hybrid Nanoparticles | Working Fluids | Solar System | Findings | Ref |
|---|---|---|---|---|
| Multi-walled carbon nanotubes-Iron oxide (MWCNT/ $Fe_3O_4$) | EG and DW (20:80) | DASC | The efficiency of photo-thermal energy conversion is 22% for the MWCNT/$Fe_3O_4$ hybrid nanofluid which was ~11% for the $Fe_3O_4$ nanofluid. | [17] |
| Multi-walled carbon nanotubes-Silicon dioxide with Silver (MWCNT-$SiO_2$/Ag) | DW | DASC | Photo-thermal conversion efficiency enhanced by 97.6% at 35 °C and 42.7% at 70 °C for 0.1wt.%. | [125] |
| Aluminium oxide-Cobalt tetraoxide ($Al_2O_3$/$Co_3O_4$) | DI | DASC | The hybrid nanofluid has the ability to absorb more than 80% of the radiation at 20 mm penetration depth | [65] |
| Copper oxide-Zinc Oxide (CuO/ZnO) | DW | Not mentioned | Photo-thermal conversion efficiency improved by 97.35% at 30 °C and 34.70% at 70 °C | [126] |
| Gold-Silver (Au-Ag) | DW | DASC | The photo-thermal conversion efficiency improved by 30.97%. | [127] |
| Zinc Oxide _ Gold (ZnO-Au) | Silicone oil | DASC | The hybrid nanofluid yielded 58% photo-thermal conversion efficiency at 1.0 mg $mL^{-1.}$ | [128] |
| Aluminium Oxide-Titanium dioxide ($Al_2O_3$- $TiO_2$) | DW | Flat Plate | Photo-thermal efficiency is enhanced by 26%. | [129] |
| Iron-Nickel with Carbon (FeNi/C) | Ethylene glycol | DASC | Photo-thermal conversion efficiency enhanced by 47.3%. Addition of external magnetic field improved the efficiency to 58.1%. | [130] |
| Aluminium Oxide- Zinc Oxide ($Al_2O_3$-ZnO) | DW | PV/T | Thermal, electrical and overall energy efficiency enhanced by 4.054%, 0.038% and 4.092%. | [131] |

| | | | | |
|---|---|---|---|---|
| Phase change material with Silicon carbide (PCM-SiC) | DW | PV/T | 9.92%, 12.32% and 13.70% enhancement in electrical efficiency for water, PCM/water and PCM+SiC/water. | [132] |
| Silver - Silicon dioxide (Ag-$SiO_2$) | DW | PV/T | The overall efficiency of hybrid nanofluids enhanced by 33.2% for 0.025 wt.%. | [133] |

#### 4.2.1.1 Solar Collectors

Solar collector is commonly used for photothermal conversion. It is a device capable of absorbing solar radiation from the Sun and transports the absorbed heat to the working fluid. It converts the solar energy to thermal energy. Among the many types of solar collectors, the direct absorption solar collector (DASC) is the most efficient in exploiting the solar energy due to its ability to absorb solar radiation with minimum heat loss [134], however, flat plate solar collector (FPSC) emerges as the most cost effective solar collector but it suffers from the low efficiency due to the poor working fluids. Figure 24 shows the schematic diagram of DASC and FPSC. DASC does not need any absorber plate. The incident light rays will strike the fluid directly and will be absorbed. Since there is only a minimum convective loss, the effectiveness of this solar collector is much higher compared to FPSC. It also offers less thermal resistance compared to FPSC. In contrast, FPSC requires an absorber plate to extract the solar radiation. The absorber plate is enclosed in an insulated metal. The presence of air gap between the plate help to contain the heat, preventing them from escaping into the atmosphere. As the absorber plate becomes hotter, it will transport the heat to the fluid within the collector, but there is also heat loss to the surrounding. The temperature rise in this type of collector is of the order of 0-50 °C. The construction of FPSC is quite simple and it is easy to maintain since it has low operating cost. In general, finding a novel working fluid that can absorb solar energy effectively and reduce heat loss is one of the key successes in developing high performance solar energy technology. It is well known that thermal and optical properties are main factors in governing the heat transfer efficiency. The optical properties of the working fluids are usually evaluated with respect to its extinction coefficient,

light absorptivity, transmittivity, scattering coefficient and solar weighted absorption. The efficiency of solar energy collectors can be calculated using the following equation [124][17]:

$$\eta = \frac{mc_p(T_f - T_i)}{AG\Delta t} \qquad (4)$$

Where, m and $c_p$ denote as the mass and specific heat of the nanofluid, respectively, $T_i$ represents the initial temperature of the nanofluid, $T_f$ reflects the final temperature, A represents the area of exposure, G designates the heat flux of the Sun, and Δt is the time exposed to solar radiation.

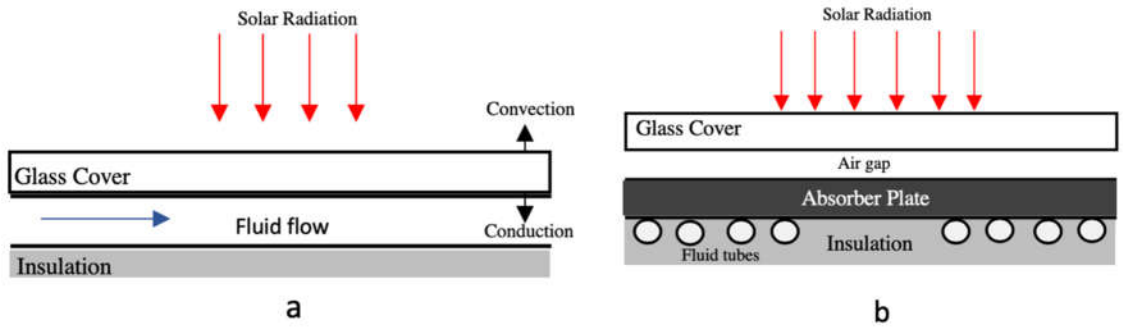


Figure 24: Schematic illustration of: (a) direct absorption solar collector (DASC) and (b) flat-plate solar collector (FPSC). Redrawn from Reference [134].

The dispersion of hybrid nanomaterials such as MWCNT/$Fe_3O_4$, MWCNT-$SiO_2$/Ag, CuO/ZnO, $Al_2O_3$-ZnO, $Al_2O_3$-$TiO_2$ in the different base fluids, acting as working media in the solar collector have been rapidly investigated and most of them have been reported to possess better photo-thermal conversion efficiency compared to that of single particle nanofluid due to their synergistic effect in enhancing thermal conductivity and optical absorption, resulting in a highly efficient solar energy system [125][131][129][126].

Tong et al. [17] compared the performance of mono and hybrid nanofluids of $Fe_3O_4$ and MWCNT/ $Fe_3O_4$, respectively in direct absorption solar collectors. In this study, the authors used a mixture of EG and water (weight ratio 20:80) as the base fluid. The highest thermal conductivity of 0.562 W/m °C was obtained from the optimized mixing ratio of 4:1 for MWCNT/ $Fe_3O_4$ hybrid nanofluid compared to only 0.541 W/m °C for $Fe_3O_4$ nanofluid. The significant proportion of MWCNT in such emerging combinations of nanomaterials gives the dominant effect to thermal conductivity

enhancement. With the high light absorbance properties of the MWCNT, the light transmittance for MWCNT/$Fe_3O_4$ is almost zero at 0.01wt.% whereas $Fe_3O_4$ nanofluid required a higher concentration (0.2wt%) to achieve the same result. The hybrid nanofluids of MWCNT/$Fe_3O_4$ were reported to have a greater performance of solar energy absorption compared to that of $Fe_3O_4$ mono nanofluids as it has the ability to absorb nearly all solar radiation at all concentrations. In view of that, the MWCNT/$Fe_3O_4$ hybrid nanofluids achieved a considerably high efficiency of photo-thermal energy conversion in comparison to that of $Fe_3O_4$ nanofluid at 0.01wt.% with the efficiency decreased from ~ 61 to 22 % for hybrid nanofluids and ~ 33 to 11 % for $Fe_3O_4$ nanofluid, over a period of 6000s.

The study of the impact of using MWCNT-$SiO_2$/Ag hybrid nanofluids suspended in the base fluid of deionized water for solar thermal conversion by Zeng et al. [125] revealed that solar weighted absorption fraction of the nanofluid mixture was impressively high compared to the mono nanofluids of MWCNT and the hybrid nanofluids of $SiO_2$/Ag as the introduction of MWCNT into $SiO_2$/Ag leads to greater ability of light absorption. The superior performance of hybrid nanofluids could be due to the fact that MWCNT has an impressive ability to absorb solar energy at all solar irradiance wavelengths and also a remarkably high thermal conduction. Moreover, the prepared MWCNT-$SiO_2$/Ag hybrid nanofluids also possessed a good dispersion stability with Zeta potential more than 30 mV compared to that of mono nanofluids of MWCNT and the hybrid nanofluids of $SiO_2$/Ag which recorded a value that is less than 30 mV. At the penetration distance of 1 cm, the binary nanomaterial suspension of 0.005 vol% gives a solar weighted absorption fraction of 74.5%, compared to 73.2% and 69.1% for the MWCNT and SiO2/Ag nanoparticle suspensions.

Bhalla et al. [65] explored the photo-thermal energy conversion performance of the blended $Al_2O_3$/$Co_3O_4$ hybrid nanofluids suspended in the base fluid of deionized water. They reported that the homogenized suspension of $Al_2O_3$/$Co_3O_4$ in base fluids has a broadband solar spectrum in the visible region, showing huge quantities of solar radiation can be absorbed by the working fluid. The calculation of solar-weighted absorptivity further confirmed that the homogenous blended hybrid

nanofluid can absorb more than ~80% of the solar radiation at the penetration depth of ~20 mm compared to that of pure base fluid of deionized water which only capable of absorbing only 20% of the solar radiation.

The evaluation of optical absorption and photo-thermal energy conversion efficiency of binary CuO/ZnO nanofluids performed by Fang et al. [126] revealed that the utilisation of hybrid nanofluids gave a significant contribution to the overall performance of solar energy collectors. They reported that the suspension of ZnO with CuO in the base fluid of water has led to the high performance of optical absorption specifically in the visible light region. CuO/ZnO hybrid nanofluids also recorded higher thermal conductivity compared to single particle CuO nanofluids. The authors also reported that the optimized introduction of Cuo in CuO/ZnO nanocomposite (0.7:0.3) exhibits the highest photothermal efficiency with ~97.35% compared to only ~95.90% by the pure CuO nanofluids at 30 °C. The optical absorption performance was found to be decreased with the high content of ZnO. This implies that a suitable combination of hybrid nanoparticles will boost the photo-thermal conversion efficiency.

#### 4.2.1.2 Photovoltaic Thermal

Photovoltaic Thermal (PV/T) is known as a hybrid solar collector that is able to convert solar radiation into thermal and electrical energy. PV/T is a combination of photovoltaic solar cell which transforms sunlight into electrical energy and a solar thermal collector which transfers the unconsumed heat or waste from PV module to a heat transfer fluid. The ability of PV/T to produce thermal and electrical energy simultaneously has led PV/T to emerge as a highly efficient solar energy harvesting system, benefitting from its fully utilized solar spectrum compared to the solar photovoltaic (PV) or solar thermal alone [135]. The current commercial solar panels suffer from a relatively low efficiency which is only about 20% efficient while almost 80% of the absorbed solar energy is not being utilised after conversion. These unconsumed energies have caused PV to overheat, resulting in an inefficient increase of its operating temperature. The merging of PV/T is able to reduce the operating temperature

as all unconsumed heat will be transferred to the working fluids [136]. Figure 25 depicts the schematic illustration of PV/T. Based on our findings, there is very limited work on the employment of hybrid nanofluids as the working media for PV/T. Most of them are focussed on mono nanofluid. In fact, the most recent investigation regarding PV/T made by Abdelrazik et al. [137] and Aslfattahi et al. [49] are focussing on MXene based mono nanofluids.

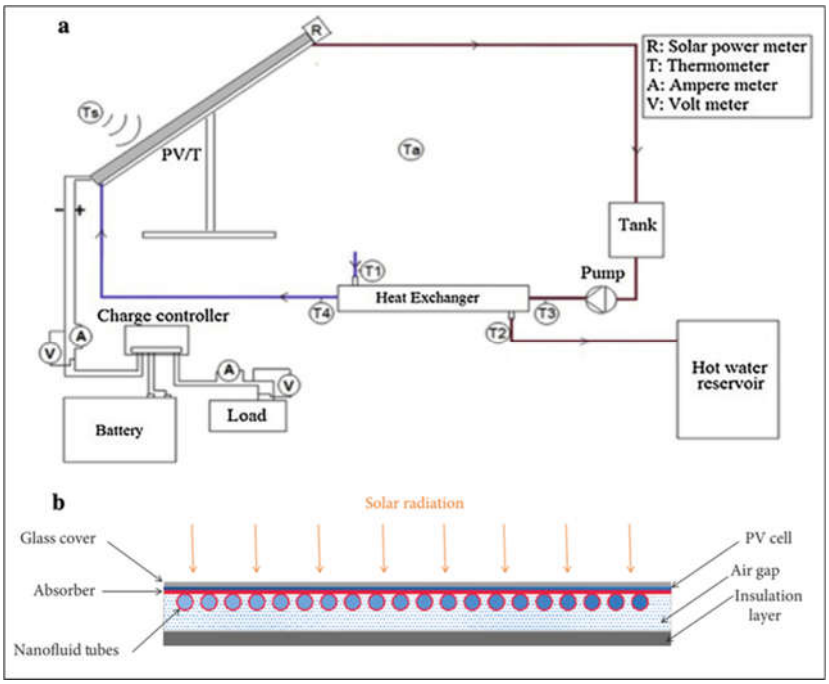


Figure 25: Schematic illustration of: (a) Solar energy conversion system of PV/T [132], and (b) PV/T system with nanofluid as the working fluid [131]. Figure 25(a) reproduced from Reference [132] with permission from Elsevier.

Recently, Han et al. [138] investigated the performance of PV/T utilising Ag/$CoSO_4$-propylene glycol (PG) hybrid nanofluids as the optical filter. The authors reported that the efficiencies of the PV/T systems were enhanced by more than 5 times compared to the stand-alone PV cell when Ag/$CoSO_4$-PG nanofluids were employed. When compared with different base fluid, the overall efficiency of PV/T system with Ag/CoSO4-PG hybrid nanofluids (total efficiency 79.82%) filter increased by 9% compared to that of PV/T system with Ag/CoSO4-water hybrid nanofluids (total efficiency 70.80%) filter, demonstrating the huge role of PG in enhancing the efficiency of PV/T.

Al-Waeli et al. [132] analysed the effect of utilising SiC-PCM/water nanofluids towards the electrical efficiency of PV/T. The authors prepared four systems consisting of conventional PV, water coolant, PCM and PCM+SiC/water hybrid nanofluids for the comparison purposes. It is reported that the addition of nanoparticles into PCM has greatly increased its performance, attributed by the promising heat transfer enhancement of nanoparticles. The electrical efficiency of PV is only ~7.11% when there is not any conventional heat transfer fluid for the cooling process. The electrical efficiency of PV/T has increased when the working fluids were employed with the values of ~9.92, ~12.32 and ~ 13.70 % for water, PCM/water and PCM+SiC/water hybrid nanofluids, respectively, indicating that utilizing PCM/water and PCM+SiC/water hybrid nanofluids in the PV/T system improved the thermal and electrical energy efficiency, which in turn increased the overall PV/T efficiencies. It is also reported that [+SiC/water hybrid nanofluids recorded the lowest maximum operating temperature with only 39.52 °C compared to 68.3, 45.22 and 42.22 °C for PV/T without working fluid, water and PCM/water, respectively. Figure 26 shows the schematic illustration for the experimental setup.

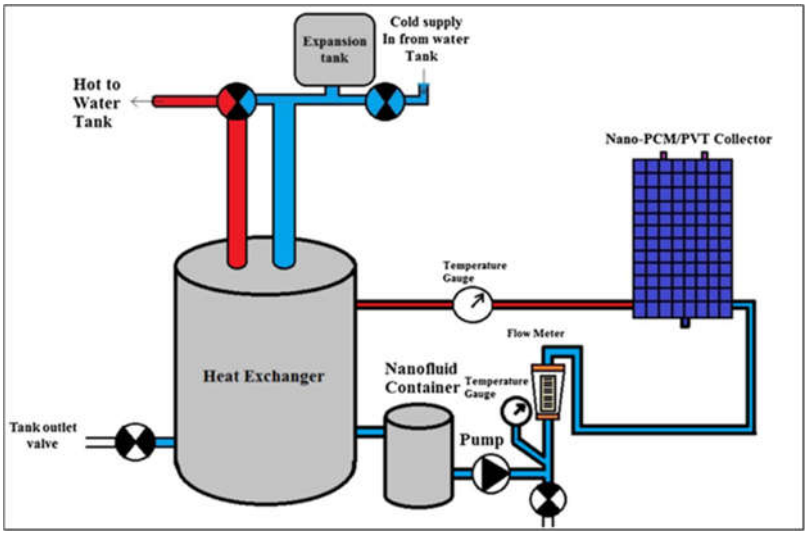


Figure 26: Schematic representation of experimental setup. Reproduced from Reference [132] with permission from Elsevier.

In another work, Crisostomo et al. [133] evaluated the performance of core-shell Ag-$SiO_2$ hybrid nanofluids as the working fluid for optimum performance of PV/T by varying the particle concentration. It has been reported that thermal output rises with the increase of particle loading, however, electrical output decreases. The highest particle loading of Ag-$SiO_2$ hybrid nanofluids

contributed about 33.2% enhancement in the overall efficiency compared to only ~ 12.4% for the stand-alone system. The improved efficiency is due to the usage of hybrid nanofluids which possessed an outstanding optical property, leading to the optimum operating system.

### 4.2.2 Electronic Cooling

The development of the integration and compaction chip which is small in size, high performance and an improved computational speed to meet customer demands has led to new challenges in thermal management [139] [15]. The excessive amount of heat generated from these electronic devices will lead to sudden thermal breakdown, which may affect their performances, reducing its reliability and lifetime expectancy [140]. Therefore, providing the system with convenient temperature and rapid cooling procedure becomes mandatory for their optimal operation. Even though there is an enormous effort that has been made to reduce the operating temperature of the electronic devices such as using phase change materials (PCM) materials, thermoelectric cooling, design of heat sink, usage of heat pump and the insertion of fins, its performances is still unable to fulfil the requirement of electronic cooling for advanced heat generating electronic devices. In addition, the use of the conventional coolant has shown to possess poor performances to the electronic devices caused by their low heat transfer capability. To date, the poor removal of increased heat transfer flux and the inconsistency of power dissipation remains as big challenges in electronic cooling [141]. In fact, Agostini et al. has reported that semiconductor industries faced difficulties in maintaining the electronic devices at 85 °C while operating at high heat flux of 300 W/cm$^2$ [142]. Recent progress in research demonstrated that hybrid nanofluids provide better electronic cooling performance compared to conventional fluid and also single nanofluid due to enhanced thermal conductivity [112]. It enabled electronic devices to operate at their best operating modes without being compromised.

Recently, Bahiraei et al. [143] evaluated the effectiveness of using the hybrid nanofluids composed of graphene nanoplatelets encased in silver nanoparticles (GNPs-Ag) in three blocks of liquid for Central Processing Unit (CPU) cooling. In this study, a novel distributor liquid block was introduced along

with the two conventional liquid blocks. The authors reported that the new distributor heat sink exhibits a superior efficiency based on its thermal performance and irreversibility. It is also reported that applying hybrid nanofluids provides better cooling performances compared to pure water, leading to more uniform distribution of temperatures. Figure 27 shows the temperature patterns of three liquid blocks measured at different Reynolds numbers using two different fluids. As can be seen in Figure 27b, hybrid nanofluids are able to significantly reduce the temperature contour of the liquid blocks especially at Re=500 and 750, indicating its high performance in providing rapid heat transfer process. This implies that the temperature of the wall and the uniformity of temperature distribution were improved with the increasing Reynolds number.

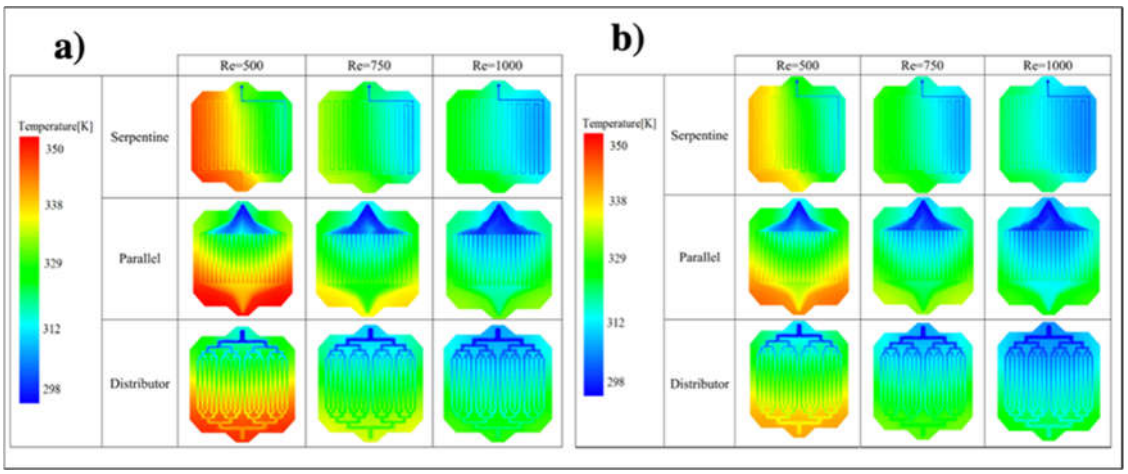


Figure 27: Temperature contours of three different liquid blocks, measured at different Reynolds numbers in: (a) pure water and (b) hybrid nanofluids. Reproduced from Reference [143] with permission from Elsevier.

It should be noted that the heat transfer coefficient is mainly governed by the Reynolds number, the volume fraction of nanofluids, temperature, thermal properties of the base fluid and the purity of nanoparticles [140]. Hybrid nanofluids seem to have the potential of removing heat at a faster rate than the rate of heat production. Having an outstanding performance of electronic components equipped with rapid cooling fluids enables the impediment of the component from any potential thermal breakdown [144]. To examine this, Barewar et al. [144] conducted an experiment to evaluate the thermal conductivity of ethylene glycol-based silver and zinc oxide (Ag/ZnO) hybrid nanofluids. Enhancement of 15.66% was observed at 0.2 vol.% after the introduction of Ag/ZnO hybrid

nanomaterials to the ethylene glycol base fluid at 25 °C. At 55 °C, the hybrid nanofluids recorded its highest thermal conductivity enhancement of 20.53 %. They reported that thermal conductivity enhancement was caused by a uniformly coated Ag on ZnO nanoparticles, making ZnO nanoparticles hydrophilic in nature, which led to the homogenous mixture of hybrid nanofluids. The physical observation on the stability of dispersion indicated that the hybrid nanofluids demonstrated a good suspension stability with no sign of agglomerations even after 15 days and Zeta potential measurement further confirmed the suspension stability in which all nanofluids at different volume concentrations possessed Zeta potential value ranging from 36 to 51 mV.

Moreover, Okonkwo et al [113] studied the thermal conductivity of water based aluminium oxide and iron ($Al_2O_3$-Fe) hybrid nanofluids by varying the nanoparticle concentrations (0.05-0.2%). A 14% thermal conductivity enhancement is obtained at 0.2% volume concentration. However, at a lower concentration, the $Al_2O_3$-Fe hybrid nanofluid did not display any significant improvement in thermal conductivity, reflecting that there are no synergistic effects between two nanoparticles at that concentration. Increasing the ratio of Fe in nanocomposite may lead to a much better thermal conductivity as Fe possesses a higher value of thermal conductivity compared to alumina [152].

### 4.2.3 Heat Pipe

Heat pipe is known as a passive device that can be served as a medium for heat transfer, which can be employed to transfer heat from the heat source (high temperature environment or evaporator) to the heat sink (low temperature environment or condenser) over a relatively long distance via heat vaporization of working media. The main structure comprises an evaporator, adiabatic and condenser as shown in Figure 28. Heat pipe acts as an evacuated tube which is able to minimise the loss of heat to the surrounding. In order to operate efficiently, it requires a working fluid that has high heat transfer capability to absorb latent heat of evaporation at evaporator and transfer it as a latent heat of condensation at condenser [145]. In general, a lower vapour temperature along the length of the heat pipe demonstrates the capability of the heat pipe to work at higher heat loads. It should be mentioned

that the important parameter of the heat pipe are the thermal resistance ($R_{HP}$) and the effective thermal conductivity ($k_{eff}$) which can be defined using the equation below [146]:

$$R_{HP} = \frac{T_{E,wall} - T_{C,wall}}{Q} \qquad (5)$$

$$k_{eff} = \frac{A_c}{R_{HP}} \qquad (6)$$

where Q, $T_E$, $T_C$ and $A_C$ are heat input, evaporator and condenser wall temperatures and the total cross-sectional area of the heat pipe, respectively.

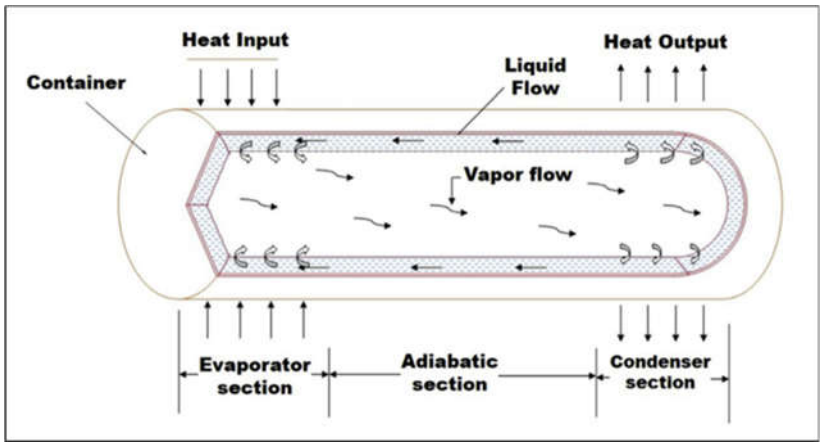


Figure 28: Schematic diagram of heat pipe. Reproduced from Reference [145] with permission from Elsevier.

Swapnil et al. [147] investigated the performance of circular heat pipes by dispersing the hybrid nanomaterials of aluminium oxide and boron nitride ($Al_2O_3$-BN) in the base fluid of DW. They studied the effect of concentration, impact of heat inclination and heat input of thermal resistance towards the circular heat pipe. Based on their studies, the increase of particle concentration and inclination angle may reduce the thermal resistance of circular heat pipes. At 2 vol.%, the thermal resistance of the circular heat pipe decreased by 39.92 % relative to the base fluid of distilled water.

Ramachandran et al. [148] studied the effect of using hybrid nanofluids as a working fluid in screen mesh cylindrical heat pipes by varying the working fluids from DI water, $Al_2O_3$/DI water nanofluid, ($Al_2O_3$ 50%-CuO 50%)/ DI water hybrid nanofluids and ($Al_2O_3$ 25%-CuO 75%)/DI water hybrid nanofluids. They reported that the unique structure of hybrid nanofluids able to boost the heat pipe

operating range up to 250 W. Also, significant thermal conductivity enhancement can be observed when hybrid nanofluids were employed with 41.47% for $Al_2O_3$-CuO/DI water (1:1) and 79.35% for $Al_2O_3$-CuO/DI water (1:3), depending on the effect of particle mixing ratio compared to the $Al_2O_3$/DI water (38.34%) and the base fluid of DI water.

In a similar study, Ramachandran et al. [146] investigated the thermal performances of cylindrical screen mesh heat pipe by varying the different proportion of $Al_2O_3$-CuO/DI water (25-75, 50-50 and 75-25 %) hybrid nanofluids. They reported that the optimized hybrid nanofluids of $Al_2O_3$ 25%-CuO 75% recorded as the highest reduction in thermal resistance with 44.25 % compared to base fluid when operating at high heat load of 250 W. The superior reduction in thermal resistance could be due to the maximum deposit of nanoparticles, forming a nano-porous layer in the screen wick. It should be mentioned that thermal resistance represents the temperature difference between evaporator and condenser wall, indicating the ability of a heat pipe to take higher heat loads. This implies that the higher the reduction in thermal resistance, the effective thermal conductivity should be increased as presented in equation (6). It should be noted that the use of effective working fluids e.g. hybrid nanofluids will increase the lifespan of the equipment, provide better cooling rate and lead to efficient operation of the systems.

### 4.2.4 Heat Exchanger

The influence of hybrid nanofluids that possess high heat transfer performances have made it possible to be used as a working fluid in heat exchanger. Heat exchangers have always been important in many industries to prevent overheating of the equipment. The use of the conventional coolant is not enough to fulfil the industrial cooling requirements, resulting in the industries to encounter deterioration of the equipment and production losses. Heat exchanger is a device that is able to transfer heat from one medium to another. The media is separated by a solid wall, so it will prevent the fluids from having any physical contact towards each other [149]. The operation of heat exchangers is always accompanied by two types of losses: losses related to the heat transfer across a finite temperature

difference and/or loss due to pressure drop causing the friction in a heat exchanger. For a heat exchanger to operate efficiently, it should be designed to have a large heat transfer area or to be equipped with materials that have the least thermal resistances and use effective working fluids with high heat transfer capabilities. With the impressive growth of technology, the compact and innovative design of heat exchangers becomes essential especially in the automotive industry, leaving the first approach is not favourable because the enlargement of heat transfer area will result in a bigger size of system, leading to a greater frictional loss and higher pressure drop as well as high pumping cost requirements [150][151]. The two losses can be quantified by evaluating the total entropy generated from the heat exchanger. An ideal heat exchanger should have a minimum total entropy generation which can be obtained by enhancing the thermal conductivity and Nusselt number [150]. In view of that, several studies have been coordinated to evaluate the heat transfer capability of hybrid nanofluids in heat exchangers. Table 7 summarised several recent researches regarding the heat transfer performance of hybrid nanofluids for heat exchangers.

Table 7: Summary of several researches regarding the heat transfer performance in heat exchangers. Note that Re, DW and DI represent Reynolds number, distilled water and deionised water.

| Hybrid NM | Base Fluid | Concentration | Flow Regime | Findings | Ref |
|---|---|---|---|---|---|
| Graphene-Aluminium oxide ($G/Al_2O_3$) | DW | 0.1 vol. % | Re: 200 - 1000 (Laminar) | ● Total entropy generation decreased from 0.0361 W/K to 0.0184 W/K at the maximum applied heat flux of 25000W/$m^2$.<br>● Enhancement of 88.62% in convective heat transfer coefficient. | [150] |
| Aluminium oxide- Copper ($Al_2O_3$/Cu) | DW | 0.05-2.00 wt.% | Re: 800 – 2400 (Laminar, turbulent) | ● Addition of hybrid nanoparticles give huge enhancement in the heat transfer coefficient and Nusselt number (40% enhancement) due to the improved thermal conductivity.<br>● Pressure drop increases with increase in Reynold numbers.<br>● The heat transfer rate enhances with increase in Reynolds number. Heat transfer rate increased by 78% when the Reynold number increase from 844.4 to 2321.54. | [149] |
| Iron oxide - Carbon nanotube ($Fe_2O_3$/CNT) | DW | 0.1-0.2 wt.% | Re: 1698-6070 (Laminar, transient, turbulent) | ● Heat transfer coefficient enhanced with the increase of Reynolds number and temperature.<br>● Rate of heat transfer coefficient enhancement decreases with the increase of voltage from 80-150 V. | [152] |
| Aluminium oxide- Multi-walled carbon nanotubes ($Al_2O_3$/MWCNT) | DI | 0.01 wt.% | Re: 150-350 (Laminar) | ● Heat transfer coefficient increases with the addition of nanoparticles. A maximum of 15.2% enhancement has been recorded.<br>● Pumping power increases negligibly with the addition of nanoparticles in base fluid. | [153] |

| | | | | | |
|---|---|---|---|---|---|
| Aluminium nitride - Aluminium oxide (AlN/ $Al_2O_3$) | DI | 1-4 vol.% | Re: 5000-17000 (Turbulent) | • Pressure drop increased as Reynold numbers and volume concentrations increased.<br>• The optimized vol. concentration (3%) recorded a 50% enhancement in Nusselt number when hybrid nanofluids flow through the flat tube.<br>• Heat transfer enhancement increased from 28-50% for 1-3.00 vol.%. | [154] |
| Copper-Aluminium oxide (Cu/ $Al_2O_3$) | DI | 1-2 wt.% | Re:100-1000 | • Friction factors decrease with the increase of Reynolds numbers.<br>• The addition of hybrid nanoparticles has led to a significant impact in Nusselt number, in which 22% enhancement was recorded for 2.0 wt.%. | [146] |

Ahammed et al. [150] analysed the entropy production of water based aluminium oxide and graphene ($Al_2O_3$-Gr) hybrid nanofluids in multiport mini-channel heat exchanger by comparing it with single particle of $Al_2O_3$/water nanofluid and Graphene/water nanofluid. They reported that total entropy production for Graphene/water nanofluid is minimum with average reductions in thermal entropy generation of ~ 32.37, ~21.62 and ~ 8.16 % for Graphene, $Al_2O_3$-Graphene and $Al_2O_3$ nanofluids respectively. The graphene/water nanofluid also recorded a superior enhancement of ~88.62 % in the convective heat transfer coefficient compared to 63.13% and 31.89% for $Al_2O_3$-Gr and $Al_2O_3$ nanofluids, respectively. The poor performance of hybrid nanofluids could be due to the lower synergistic effect between the two materials. Figure 29 shows the schematic illustration for the experimental setup.

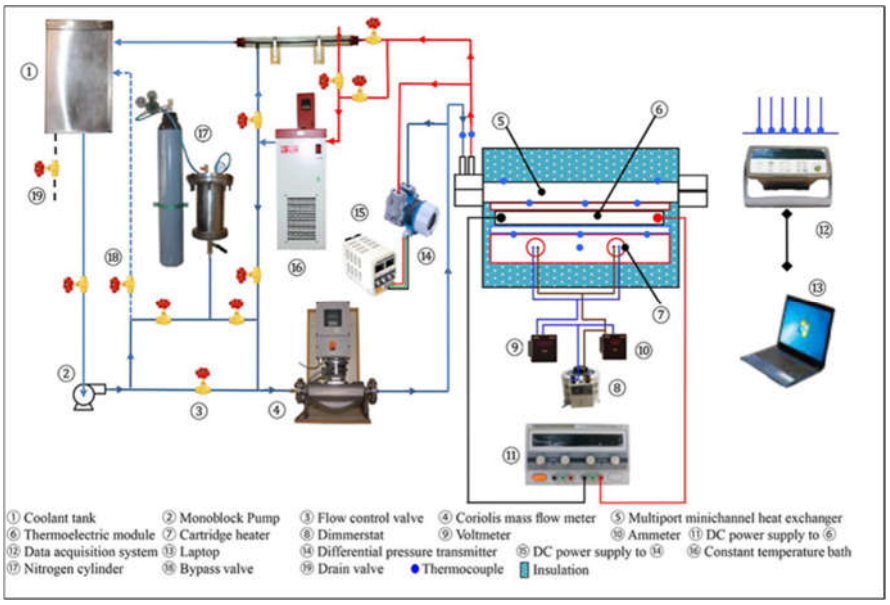


Figure 29: Schematic of the experimental setup. Reproduced from Reference [150] with permission from Elsevier.

Anitha et al. [149] studied the impact of using water based aluminium oxide with copper ($Al_2O_3$-Cu) hybrid nanofluids on the performance of shell and tube heat exchanger (STHE). Utilisation of hybrid nanofluids in STHE has led to the significant enhancement in heat transfer coefficient and Nusselt number, which in turn provides an improved performance of heat exchanger. Hybrid nanofluids demonstrated the highest effectiveness when used as coolant compared to single particle nanofluids and the base fluids. At Re of ~ 844.4, the percentage of heat transfer coefficient enhancement for hybrid nanofluids are 139 and 25 % compared to that of water and Cu/water nanofluids, respectively. The authors also reported that the heat transfer performance of hybrid nanofluids improved with the increase of nanoparticles volume concentration. Allahyar at el. [155] compared the thermal performance of $Al_2O_3$-Ag/water hybrid nanofluids and mono nanofluid of $Al_2O_3$/water in a coiled heat exchanger. The authors reported when the hybrid nanofluids is employed, a maximum enhancement of Nusselt number (~31.58 %) can be achieved with Reynolds number of ~ 4687, which is higher than the $Al_2O_3$ mono nanofluids (~28.42%) at the same operating condition, indicating the outstanding performance of hybrid nanofluids in escalating the thermal performance of heat exchangers.

Aghabozorg et al. [152] evaluated the thermal performance of water based Iron oxide with carbon nanotubes ($Fe_2O_3$-CNT) hybrid nanofluids inside a horizontal STHE which subjected to laminar, transient and turbulent flow with three different heat fluxes. This study illustrated that the heat transfer coefficients enhanced with the increases of voltage, nanoparticle loading and Reynolds number. The convective heat transfer coefficient enhancement may be due to the turbulence in the boundary layer of heat particles and the magnetic particles.

In addition, Bhattad et al. [153] explored the effect of using different particle mixing ratios of aluminium oxide with multi-walled carbon nanotubes $Al_2O_3$-MWCNT hybrid nanofluids towards the cooling performance of the plate heat exchanger. In this study, the authors dispersed the hybrid nanoparticles into the base fluid of DI water. When comparing with single particle $Al_2O_3$ nanofluids,

the application of hybrid nanofluids causes the heat transfer coefficients to increase due to the difference of thermo-physical properties of the two materials and as a result of favourable integration of nanoparticles suspended into the base fluid. It is also observed that the heat transfer coefficients increase as the volume ratio of MWCNT nanoparticles increases owing to the superior thermal conductivity possessed by MWCNT and also due to the fact that $Al_2O_3$ suffers from low thermal conductivity. In response to that, the authors reported that MWCNT (0:5) mono nanofluid showed a better heat transfer enhancement for the cooling process of plate heat exchangers. In general, hybrid nanofluids are able to improve the cooling performance of the heat exchangers. However, the combination of nanomaterials for dispersion into base fluids plays a significant role in enhancing the overall efficiency of the heat exchangers.

## 5. Conclusions

Hybrid nanomaterials are the new type of nanomaterials which were created as a result of the advancement in nanotechnology. The research associated with this kind of material has been on a continuous upsurge, owing to their unique features and the flexibility to tailor their physicochemical properties simply by controlling the mixture composition and morphology. The unique structural form of hybrid nanomaterials which possess improved physicochemical properties have led them to become an intriguing material for electrochemical energy storages and heat transfer applications. In particular, the rise of synergistic effect and the interactions between the single nanoparticle components within the integrated nanoparticles gives the significant contributions to the outstanding physicochemical properties it has. Employing hybrid nanomaterials in the electrochemical energy storage devices shows an improved capacitance, energy density, power density, and system lifetime, contributing to the outstanding electrochemical performances. In general, hybridisation of 2D materials such as MXene and graphene with other nanomaterials is able to prevent the 2D nanosheets from self-stacking. This will avoid the formation of a very dense structure, which is not suitable for their applications. On the other hand, utilisation of hybrid nanomaterials in creating hybrid nanofluids also demonstrated that

such emerging combinations of nanoparticles is able to acquire a remarkable thermal conductivity enhancement, surpassing mono nanofluids and even the conventional base fluids. In general, hybridisation of nanomaterials not only enhances the thermal conductivity but it also offers high dispersion stability. It is well noted that thermal conductivity improvement comes with the increase of temperature and high particle loading. Since hybrid nanomaterials are still considered as new and under the developing phase, extensive research must be carried out in order to bring them to a commercial scale or to be employed in real life applications. Therefore, the synthesis routes, characterization and the practical applications of hybrid nanomaterials must be understood rigorously. It should be noted that the current progress made on hybrid nanomaterials is very limited especially on the theoretical models in evaluating the performance of hybrid nanomaterials. This will create a gap between experimental works performed by various researchers even though the same hybrid nanomaterials were used. In this review paper, we have focused on recent trends and advances made on hybrid nanomaterials in the field of electrochemical energy storage and heat transfer applications. We also comprehensively summarized numerous synthesis routes adapted by various researchers to produce hybrid nanomaterials and their findings on hybrid structures were well discussed. Although there are a lot of synthesis routes currently available to fabricate hybrid nanomaterials, an efficient and highly scalable synthesis technique still needs to be considered in order to produce high quality hybrid nanomaterials at a low cost.

## 6. Current Challenges and New Opportunities

Hybrid nanomaterials seem to provide a significant contribution in improving the overall performances of advanced heat transfer devices and also able to provide an outstanding performance of electrodes for energy storage devices. However, hybrid nanomaterials are facing some challenges that may hinder it from the extensive applications. Below, we highlighted several challenges faced by hybrid nanomaterials and provide new opportunities that may be useful for future research:

- Firstly, the use of different synthesis routes with different parameters by different researchers have eventually led to uncertain results due to lack of agreement with the results achieved. This will therefore create a gap between the results obtained from one research to another even though the same materials were being used. Therefore, there exists an urgent need to develop a theoretical model to predict the behaviour of the nanocomposites, which can serve as a reference or guidance for the experimental work.
- The fabrication cost for hybrid nanomaterials is usually high. For the hybrid nanomaterials to be implemented commercially, it requires a low-cost fabrication technique with high-quality products for large-scale production. To date, there is only a little emphasis made for low-cost fabrication techniques, however, there are some literatures that have introduced facile methods for the synthesis of hybrid nanomaterials such as using one-step hydrothermal strategy, *in situ* solvent method and solvothermal method. Therefore, the key for a wide application of hybrid nanomaterials is to find the alternative fabrication method, however, there is still a need for exploration on the kinds of emerging hybrid nanomaterials that are useful for particular purposes.
- Next, it is important to merge and integrate suitable nanomaterials together as the right combination of hybrid nanomaterials will give rise to the synergistic effect. It is understood that an unfavorable combination of nanomaterials will lead to the poor thermal performance, resulting in the low efficiency of the systems. However, there is no proper guidance available for the suitable combination of nanomaterials, highlighting that hybrid nanomaterials are the new kinds of nanomaterial and their performance and suitability evaluation are in the phase of development.
- Furthermore, there is no optimum mixing ratio of nanoparticles for the high performance of hybrid nanomaterials developed, causing the implementation of this emerging hybrid nanomaterials as a big challenge. However, since hybrid nanomaterials give us the flexibility

to tailor their physicochemical properties, it is important to study and analyze the optimum mixing ratio of nanoparticles in nanocomposites on a case-by-case basis.

- In addition, even though employing hybrid nanomaterials as heat transfer fluids gives a significant improvement to the overall efficiency of the devices due to the improved heat transfer capability, the stability of the dispersion still remains a huge challenge. The difficulty of hybrid nanofluids to sustain the suspension for a long time will affect its performance. It is well understood that stability is one of the important factors in hybrid nanofluids and it is the key to the high thermal performance which enhances the heat transfer capability. Therefore, it is important to evaluate the stability performance of hybrid nanofluids and explore any new possibility to improve the suspension stability.
- Viscosity also has been one of the major issues related to hybrid nanofluids. It has always been reported that thermal conductivity enhancement increases with the increase of particle concentration. This will lead to high viscosity. As we know, high viscosity will create high surface tension which may cause high penalties in pressure drops and requires a high pumping power ,which results in high operating costs. Hence, it is important to assess viscosity measurement and their effect towards the system operation. This could be done using simulation models and analysis.

## 7. ACKNOWLEDGEMENTS

"Authors would like to acknowledge the financial support provided by the Sunway University, Malaysia internal Grant scheme through the project No. # GRTIN-RSF-SHMS-CBP-03-2020".

## 8. REFERENCES

[1] A. Borode, N. Ahmed, and P. Olubambi, "A review of solar collectors using carbon-based nanofluids," *J. Clean. Prod.*, vol. 241, p. 118311, 2019, doi: 10.1016/j.jclepro.2019.118311.

[2] IEA, "Global Energy Review 2020," *Iea*, 2020, [Online]. Available: https://www.iea.org/reports/global-energy-review-2020.

[3] International Energy Agency (IEA), "Market Report Series Renewables 2O18 Analysis and Forecast to 2023," *Int. Energy Agency*, p. 211, 2018, [Online]. Available: https://www.iea.org/reports/renewables-2018.

[4] P. Raj and S. Subudhi, “A review of studies using nanofluids in flat-plate and direct absorption solar collectors,” *Renew. Sustain. Energy Rev.*, vol. 84, no. August 2017, pp. 54–74, 2018, doi: 10.1016/j.rser.2017.10.012.
[5] C. Yu *et al.*, “High Temperature Energy Storage (HiTES) with Pebble Heater Technology and Gas Turbine,” *Intech*, p. 13, 2012, doi: 10.1016/j.colsurfa.2011.12.014.
[6] Y. Kameya and K. Hanamura, “Enhancement of solar radiation absorption using nanoparticle suspension,” *Sol. Energy*, vol. 85, no. 2, pp. 299–307, 2011, doi: 10.1016/j.solener.2010.11.021.
[7] A. Lenert, E. Wang, and Y. Nam, “Heat Transfer Fluids,” *Annu. Rev. Heat Transf. ,* vol. 15, no. January, pp. 93–129, 2012, doi: 10.1615/AnnualRevHeatTransfer.2012004122.
[8] H. Wang, X. Liang, J. Wang, S. Jiao, and D. Xue, “Multifunctional inorganic nanomaterials for energy applications,” *Nanoscale*, vol. 12, no. 1, pp. 14–42, 2020, doi: 10.1039/c9nr07008g.
[9] Y. Q. Wu *et al.*, “SnS2 nanoparticle-integrated graphene nanosheets as high-performance and cycle-stable anodes for lithium and sodium storage,” *J. Alloys Compd.*, vol. 822, p. 153686, 2020, doi: 10.1016/j.jallcom.2020.153686.
[10] X. Zhan, C. Si, J. Zhou, and Z. Sun, “MXene and MXene-based composites: Synthesis, properties and environment-related applications,” *Nanoscale Horizons*, vol. 5, no. 2, pp. 235–258, 2020, doi: 10.1039/c9nh00571d.
[11] Z. Zhou, J. Gong, Y. Guo, and L. Mu, “Multifunctional Hybrid Nanomaterials for Energy Storage,” *J. Nanomater.*, vol. 2019, pp. 1–3, 2019, doi: 10.1155/2019/3013594.
[12] D. Kumar and V. A. Amirtham, “A review on preparation , characterization , properties and applications of nano fl uids,” vol. 60, pp. 21–40, 2016.
[13] D. Meroni and S. Ardizzone, “Preparation and application of hybrid nanomaterials,” *Nanomaterials*, vol. 8, no. 11, pp. 2–5, 2018, doi: 10.3390/nano8110891.
[14] R. Hayami *et al.*, “Preparation and properties of organic-inorganic hybrid materials using titanium phosphonate cluster,” *Polym. J.*, vol. 49, no. 9, pp. 665–669, 2017, doi: 10.1038/pj.2017.34.
[15] V. Selvaraj and H. Krishnan, “Synthesis of graphene encased alumina and its application as nanofluid for cooling of heat-generating electronic devices,” *Powder Technol.*, vol. 363, pp. 665–675, 2020, doi: 10.1016/j.powtec.2020.01.050.
[16] M. F. Zawrah, R. M. Khattab, L. G. Girgis, H. El Daidamony, and R. E. Abdel Aziz, “ Stability and electrical conductivity of water-base Al 2 O 3 nanofluids for different applications ,” *HBRC J.*, vol. 12, no. 3, pp. 227–234, 2016, doi: 10.1016/j.hbrcj.2014.12.001.
[17] Y. Tong, T. Boldoo, J. Ham, and H. Cho, “Improvement of photo-thermal energy conversion performance of MWCNT/Fe3O4 hybrid nanofluid compared to Fe3O4 nanofluid,” *Energy*, vol. 196, p. 117086, 2020, doi: 10.1016/j.energy.2020.117086.
[18] H. Li, Y. Hou, F. Wang, M. R. Lohe, X. Zhuang, and L. Niu, “Flexible All-Solid-State Supercapacitors with High Volumetric Capacitances Boosted by Solution Processable MXene and Electrochemically Exfoliated Graphene,” pp. 2–7, 2016, doi: 10.1002/aenm.201601847.
[19] G. Bharath *et al.*, “Synthesis of hierarchical Mn3O4 nanowires on reduced graphene oxide nanoarchitecture as effective pseudocapacitive electrodes for capacitive desalination application,” *Electrochim. Acta*, vol. 337, p. 135668, 2020, doi: 10.1016/j.electacta.2020.135668.
[20] L. Yang, W. Ji, M. Mao, and J. nan Huang, “An updated review on the properties, fabrication and application of hybrid-nanofluids along with their environmental effects,” *J. Clean. Prod.*, vol. 257, p. 120408, 2020, doi: 10.1016/j.jclepro.2020.120408.
[21] M. Gupta, V. Singh, S. Kumar, S. Kumar, N. Dilbaghi, and Z. Said, “Up to date review on the synthesis and thermophysical properties of hybrid nanofluids,” *J. Clean. Prod.*, vol. 190, pp. 169–192, 2018, doi: 10.1016/j.jclepro.2018.04.146.

[22] P. Thangadurai, S. Joicy, R. Beura, J. Santhosh Kumar, and K. Chitrarasu, *Emerging Nanomaterials in Energy and Environmental Science: An Overview*. 2019.
[23] S. K. Tiwari, V. Kumar, A. Huczko, R. Oraon, A. De Adhikari, and G. C. Nayak, "Magical Allotropes of Carbon: Prospects and Applications," *Crit. Rev. Solid State Mater. Sci.*, vol. 41, no. 4, pp. 257–317, 2016, doi: 10.1080/10408436.2015.1127206.
[24] J. Pitroda, "A Critical Review on Carbon Nanotubes," *Int. J. Constr. Res. Civ. Eng.*, vol. 2, no. 5, pp. 36–42, 2016, doi: 10.20431/2454-8693.0205007.
[25] N. Saifuddin, A. Z. Raziah, and A. R. Junizah, "Carbon nanotubes: A review on structure and their interaction with proteins," *J. Chem.*, vol. 2013, 2013, doi: 10.1155/2013/676815.
[26] T. Han, A. Nag, S. Chandra Mukhopadhyay, and Y. Xu, "Carbon nanotubes and its gas-sensing applications: A review," *Sensors Actuators, A Phys.*, vol. 291, pp. 107–143, 2019, doi: 10.1016/j.sna.2019.03.053.
[27] H. P. Cong, J. F. Chen, and S. H. Yu, "Graphene-based macroscopic assemblies and architectures: An emerging material system," *Chem. Soc. Rev.*, vol. 43, no. 21, pp. 7295–7325, 2014, doi: 10.1039/c4cs00181h.
[28] Q. Zheng and J.-K. Kim, *Graphene for Transparent Conductors*. 2015.
[29] Z. Zhen and H. Zhu, *Structure and Properties of Graphene*. Elsevier Inc., 2018.
[30] S. K. Tiwari, S. Sahoo, N. Wang, and A. Huczko, "Graphene research and their outputs: Status and prospect," *J. Sci. Adv. Mater. Devices*, vol. 5, no. 1, pp. 10–29, 2020, doi: 10.1016/j.jsamd.2020.01.006.
[31] K. S. Kim *et al.*, "Large-scale pattern growth of graphene films for stretchable transparent electrodes," *Nature*, vol. 457, no. 7230, pp. 706–710, 2009, doi: 10.1038/nature07719.
[32] X. Li and L. Zhi, "Graphene hybridization for energy storage applications," *Chem. Soc. Rev.*, vol. 47, no. 9, pp. 3189–3216, 2018, doi: 10.1039/c7cs00871f.
[33] R. R. Nair *et al.*, "Fine structure constant defines visual transparency of graphene," *Science (80-. ).*, vol. 320, no. 5881, p. 1308, 2008, doi: 10.1126/science.1156965.
[34] M. Tahriri *et al.*, "Graphene and its derivatives: Opportunities and challenges in dentistry," *Mater. Sci. Eng. C*, vol. 102, no. April, pp. 171–185, 2019, doi: 10.1016/j.msec.2019.04.051.
[35] S. J. Rowley-Neale, E. P. Randviir, A. S. Abo Dena, and C. E. Banks, "An overview of recent applications of reduced graphene oxide as a basis of electroanalytical sensing platforms," *Appl. Mater. Today*, vol. 10, pp. 218–226, 2018, doi: 10.1016/j.apmt.2017.11.010.
[36] J. Yang *et al.*, "Studies on directly grown few layer graphene processed using tape-peeling method," *Carbon N. Y.*, vol. 158, no. xxxx, pp. 749–755, 2020, doi: 10.1016/j.carbon.2019.11.049.
[37] W. Wu *et al.*, "Fast chemical exfoliation of graphite to few-layer graphene with high quality and large size via a two-step microwave-assisted process," *Chem. Eng. J.*, vol. 381, no. August 2019, 2020, doi: 10.1016/j.cej.2019.122592.
[38] S. Thamer, B. H. Al-Tamimi, and S. B. H. Farid, "Preparation of graphene nano-sheets from graphite flakes via milling-ultrasonication promoted process," *Mater. Today Proc.*, vol. 20, no. xxxx, pp. 579–582, 2020, doi: 10.1016/j.matpr.2019.09.192.
[39] H. Zhang, F. Ding, H. Li, F. Qu, H. Meng, and H. Gu, "Controlled synthesis of monolayer graphene with a high quality by pyrolysis of silicon carbide," *Mater. Lett.*, vol. 244, pp. 171–174, 2019, doi: 10.1016/j.matlet.2019.02.038.
[40] H. K. Hong *et al.*, "Synthesis of high-quality monolayer graphene by low-power plasma," *Curr. Appl. Phys.*, vol. 19, no. 1, pp. 44–49, 2019, doi: 10.1016/j.cap.2018.11.003.
[41] D. Dai *et al.*, "Thermal CVD growth of graphene on copper particles targeting tungsten-copper composites with superior wear and arc ablation resistance properties," *Diam. Relat. Mater.*, vol. 104, no. December 2019, p. 107765, 2020, doi: 10.1016/j.diamond.2020.107765.
[42] M. Naguib *et al.*, "Two-dimensional nanocrystals produced by exfoliation of Ti 3AlC 2," *Adv. Mater.*, vol. 23, no. 37, pp. 4248–4253, 2011, doi: 10.1002/adma.201102306.

[43] M. Naguib *et al.*, “Two-dimensional transition metal carbides,” *ACS Nano*, vol. 6, no. 2, pp. 1322–1331, 2012, doi: 10.1021/nn204153h.
[44] Q. Yang *et al.*, “MXene/graphene hybrid fibers for high performance flexible supercapacitors,” *J. Mater. Chem. A*, vol. 5, no. 42, pp. 22113–22119, 2017, doi: 10.1039/c7ta07999k.
[45] Y. Liu, J. Yu, D. Guo, Z. Li, and Y. Su, “Ti3C2Tx MXene/graphene nanocomposites: Synthesis and application in electrochemical energy storage,” *J. Alloys Compd.*, vol. 815, p. 152403, 2020, doi: 10.1016/j.jallcom.2019.152403.
[46] X. Wang *et al.*, “Pseudocapacitance of MXene nanosheets for high-power sodium-ion hybrid capacitors,” *Nat. Commun.*, vol. 6, pp. 1–6, 2015, doi: 10.1038/ncomms7544.
[47] K. Hantanasirisakul and Y. Gogotsi, “Electronic and Optical Properties of 2D Transition Metal Carbides and Nitrides (MXenes),” *Adv. Mater.*, vol. 30, no. 52, pp. 1–30, 2018, doi: 10.1002/adma.201804779.
[48] J. Pang *et al.*, “Applications of 2D MXenes in energy conversion and storage systems,” *Chem. Soc. Rev.*, vol. 48, no. 1, pp. 72–133, 2019, doi: 10.1039/c8cs00324f.
[49] N. Aslfattahi, L. Samylingam, A. S. Abdelrazik, A. Arifutzzaman, and R. Saidur, “MXene based new class of silicone oil nanofluids for the performance improvement of concentrated photovoltaic thermal collector,” *Sol. Energy Mater. Sol. Cells*, vol. 211, no. April, p. 110526, 2020, doi: 10.1016/j.solmat.2020.110526.
[50] N. R. Hemanth and B. Kandasubramanian, “Recent advances in 2D MXenes for enhanced cation intercalation in energy harvesting Applications: A review,” *Chem. Eng. J.*, p. 123678, 2019, doi: 10.1016/j.cej.2019.123678.
[51] S. Venkateshalu and A. N. Grace, “MXenes—A new class of 2D layered materials: Synthesis, properties, applications as supercapacitor electrode and beyond,” *Appl. Mater. Today*, vol. 18, p. 100509, 2020, doi: 10.1016/j.apmt.2019.100509.
[52] J. Mei, G. A. Ayoko, C. Hu, J. M. Bell, and Z. Sun, “Two-dimensional fluorine-free mesoporous Mo2C MXene via UV-induced selective etching of Mo2Ga2C for energy storage,” *Sustain. Mater. Technol.*, vol. 25, p. e00156, 2020, doi: 10.1016/j.susmat.2020.e00156.
[53] M. Alhabeb *et al.*, “Selective Etching of Silicon from Ti3SiC2 (MAX) To Obtain 2D Titanium Carbide (MXene),” *Angew. Chemie - Int. Ed.*, vol. 57, no. 19, pp. 5444–5448, 2018, doi: 10.1002/anie.201802232.
[54] T. Li *et al.*, “Fluorine-Free Synthesis of High-Purity Ti3C2Tx (T=OH, O) via Alkali Treatment,” *Angew. Chemie - Int. Ed.*, vol. 57, no. 21, pp. 6115–6119, 2018, doi: 10.1002/anie.201800887.
[55] A. Feng *et al.*, “Fabrication and thermal stability of NH4HF2-etched Ti3C2 MXene,” *Ceram. Int.*, vol. 43, no. 8, pp. 6322–6328, 2017, doi: 10.1016/j.ceramint.2017.02.039.
[56] T. Zhang *et al.*, “Synthesis of two-dimensional Ti3C2TxMXene using HCl+LiF etchant: Enhanced exfoliation and delamination,” *J. Alloys Compd.*, vol. 695, pp. 818–826, 2017, doi: 10.1016/j.jallcom.2016.10.127.
[57] W. Sun *et al.*, “Electrochemical etching of Ti2AlC to Ti2CT:X (MXene) in low-concentration hydrochloric acid solution,” *J. Mater. Chem. A*, vol. 5, no. 41, pp. 21663–21668, 2017, doi: 10.1039/c7ta05574a.
[58] P. Urbankowski *et al.*, “Synthesis of two-dimensional titanium nitride Ti4N3 (MXene),” *Nanoscale*, vol. 8, no. 22, pp. 11385–11391, 2016, doi: 10.1039/c6nr02253g.
[59] C. (John) Zhang *et al.*, “Two-Dimensional Transition Metal Carbides and Nitrides (MXenes): Synthesis, Properties, and Electrochemical Energy Storage Applications,” *Energy Environ. Mater.*, pp. 1–27, 2019, doi: 10.1002/eem2.12058.
[60] R. M. Ronchi, J. T. Arantes, and S. F. Santos, “Synthesis, structure, properties and applications of MXenes: Current status and perspectives,” *Ceram. Int.*, vol. 45, no. 15, pp.

18167–18188, 2019, doi: 10.1016/j.ceramint.2019.06.114.
[61] L. Verger, V. Natu, M. Carey, and M. W. Barsoum, “MXenes: An Introduction of Their Synthesis, Select Properties, and Applications,” *Trends Chem.*, vol. 1, no. 7, pp. 656–669, 2019, doi: 10.1016/j.trechm.2019.04.006.
[62] A. Ali, A. Belaidi, S. Ali, M. I. Helal, and K. A. Mahmoud, “Transparent and conductive Ti3C2Tx (MXene) thin film fabrication by electrohydrodynamic atomization technique,” *J. Mater. Sci. Mater. Electron.*, vol. 27, no. 5, pp. 5440–5445, 2016, doi: 10.1007/s10854-016-4447-z.
[63] Y. L. and M. Ballauff, *Hybrid Nanomaterials*. United States: Wiley, 2011.
[64] Y. Wu and T. van Ree, *Introduction: Energy technologies and their role in our life*. Elsevier Inc., 2018.
[65] V. Bhalla, V. Khullar, and H. Tyagi, “Experimental investigation of photo-thermal analysis of blended nanoparticles (Al2O3/Co3O4) for direct absorption solar thermal collector,” *Renew. Energy*, vol. 123, no. February, pp. 616–626, 2018, doi: 10.1016/j.renene.2018.01.042.
[66] I. Chopkar, S. Sudarshan, P. K. Das, and I. Manna, “Effect of particle size on thermal conductivity of nanofluid,” *Metall. Mater. Trans. A Phys. Metall. Mater. Sci.*, vol. 39, no. 7, pp. 1535–1542, 2008, doi: 10.1007/s11661-007-9444-7.
[67] F. Kong *et al.*, “Further surface modification by carbon coating for in-situ growth of Fe3O4 nanoparticles on MXene Ti3C2 multilayers for advanced Li-ion storage,” *Electrochim. Acta*, vol. 289, pp. 228–237, 2018, doi: 10.1016/j.electacta.2018.09.007.
[68] P. Van Trinh, N. N. Anh, N. T. Hong, P. N. Hong, P. N. Minh, and B. H. Thang, “Experimental study on the thermal conductivity of ethylene glycol-based nanofluid containing Gr-CNT hybrid material,” *J. Mol. Liq.*, vol. 269, pp. 344–353, 2018, doi: 10.1016/j.molliq.2018.08.071.
[69] C. Zhao, Q. Wang, H. Zhang, S. Passerini, and X. Qian, “Two-Dimensional Titanium Carbide/RGO Composite for High-Performance Supercapacitors,” *ACS Appl. Mater. Interfaces*, vol. 8, no. 24, pp. 15661–15667, 2016, doi: 10.1021/acsami.6b04767.
[70] J.-F. Berret *et al.*, “Electrostatic Self-assembly : A New Route Towards Nanostructures,” p. 5, 2005, [Online]. Available: http://arxiv.org/abs/cond-mat/0501083.
[71] X. Jin *et al.*, “Superior role of MXene nanosheet as hybridization matrix over graphene in enhancing interfacial electronic coupling and functionalities of metal oxide,” *Nano Energy*, vol. 53, pp. 841–848, 2018, doi: 10.1016/j.nanoen.2018.09.055.
[72] Z. Wang *et al.*, “Facile fabrication of flexible rGO/MXene hybrid fiber-like electrode with high volumetric capacitance,” *J. Power Sources*, vol. 448, no. August, p. 227398, 2020, doi: 10.1016/j.jpowsour.2019.227398.
[73] X. W. Liu, F. Y. Wang, F. Zhen, and J. R. Huang, “In situ growth of Au nanoparticles on the surfaces of Cu2O nanocubes for chemical sensors with enhanced performance,” *RSC Adv.*, vol. 2, no. 20, pp. 7647–7651, 2012, doi: 10.1039/c2ra20789c.
[74] L. S. Sundar, M. K. Singh, and A. C. M. Sousa, “Turbulent heat transfer and friction factor of nanodiamond-nickel hybrid nanofluids flow in a tube: An experimental study,” *Int. J. Heat Mass Transf.*, vol. 117, pp. 223–234, 2018, doi: 10.1016/j.ijheatmasstransfer.2017.09.109.
[75] X. Li, J. Zhu, L. Wang, W. Wu, and Y. Fang, “In–situ growth of carbon nanotubes on two–dimensional titanium carbide for enhanced electrochemical prformance,” *Electrochim. Acta*, vol. 258, pp. 291–301, 2017, doi: 10.1016/j.electacta.2017.11.004.
[76] A. M. Pourrahimi, D. Liu, V. Ström, M. S. Hedenqvist, R. T. Olsson, and U. W. Gedde, “Heat treatment of ZnO nanoparticles: new methods to achieve high-purity nanoparticles for high-voltage applications,” *J. Mater. Chem. A*, vol. 3, no. 33, pp. 17190–17200, 2015, doi: 10.1039/c5ta03120f.
[77] I. Sengupta, S. Chakraborty, M. Talukdar, S. K. Pal, and S. Chakraborty, “Thermal reduction of graphene oxide: How temperature influences purity,” *J. Mater. Res.*, vol. 33, no. 23, pp.

4113–4122, 2018, doi: 10.1557/jmr.2018.338.
[78] C. Shen *et al.*, “Novel Li4Ti5O12/Ti3C2Tx nanocomposite as a high rate anode material for lithium ion batteries,” *J. Alloys Compd.*, vol. 735, pp. 530–535, 2018, doi: 10.1016/j.jallcom.2017.11.164.
[79] J. Tu *et al.*, “Facile synthesis of TiN nanocrystals/graphene hybrid to chemically suppress the shuttle effect for lithium-sulfur batteries,” *J. Alloys Compd.*, vol. 822, p. 153751, 2020, doi: 10.1016/j.jallcom.2020.153751.
[80] H. Shi *et al.*, “Synthesis of TiN nanostructures by Mg-assisted nitriding TiO2 in N2 for lithium ion storage,” *Chem. Eng. J.*, vol. 336, no. August 2017, pp. 12–19, 2018, doi: 10.1016/j.cej.2017.11.036.
[81] N. K. Chaudhari, H. Jin, B. Kim, D. San Baek, S. H. Joo, and K. Lee, “MXene: An emerging two-dimensional material for future energy conversion and storage applications,” *J. Mater. Chem. A*, vol. 5, no. 47, pp. 24564–24579, 2017, doi: 10.1039/c7ta09094c.
[82] M. Boota *et al.*, “Interaction of Polar and Nonpolar Polyfluorenes with Layers of Two-Dimensional Titanium Carbide (MXene): Intercalation and Pseudocapacitance,” *Chem. Mater.*, vol. 29, no. 7, pp. 2731–2738, 2017, doi: 10.1021/acs.chemmater.6b03933.
[83] M. Sethi, H. Bantawal, U. S. Shenoy, and D. K. Bhat, “Eco-friendly synthesis of porous graphene and its utilization as high performance supercapacitor electrode material,” *J. Alloys Compd.*, vol. 799, pp. 256–266, 2019, doi: 10.1016/j.jallcom.2019.05.302.
[84] A. Yu, V. Chabot, and J. Zhang, *Electrochemical Supercapacitors For Energy Storage and Delivery*. 2013.
[85] I. Piñeiro-Prado, D. Salinas-Torres, R. Ruiz-Rosas, E. Morallón, and D. Cazorla-Amorós, “Design of activated carbon/activated carbon asymmetric capacitors,” *Front. Mater.*, vol. 3, no. March, pp. 1–12, 2016, doi: 10.3389/fmats.2016.00016.
[86] M. Inagaki, F. Kang, M. Toyoda, and H. Konno, “Carbon Materials for Electrochemical Capacitors,” *Adv. Mater. Sci. Eng. Carbon*, vol. 2, pp. 237–265, 2014, doi: 10.1016/b978-0-12-407789-8.00011-9.
[87] M. Sevilla, R. Mokaya, and A. B. Fuertes, “Ultrahigh surface area polypyrrole-based carbons with superior performance for hydrogen storage,” *Energy Environ. Sci.*, vol. 4, no. 8, pp. 2930–2936, 2011, doi: 10.1039/c1ee01608c.
[88] X. Peng, L. Peng, C. Wu, and Y. Xie, “Two dimensional nanomaterials for flexible supercapacitors,” *Chem. Soc. Rev.*, vol. 43, no. 10, pp. 3303–3323, 2014, doi: 10.1039/c3cs60407a.
[89] H. Hwang, C. H. Kim, J. H. Wee, J. H. Han, and C. M. Yang, “High-density graphene/single-walled carbon nanohorn composite supercapacitor electrode with high volumetric capacitance,” *Appl. Surf. Sci.*, vol. 489, no. May, pp. 708–716, 2019, doi: 10.1016/j.apsusc.2019.05.332.
[90] Y. Zheng, Y. Tian, S. Sarwar, J. Luo, and X. Zhang, “Carbon nanotubes decorated NiSe2 nanosheets for high-performance supercapacitors,” *J. Power Sources*, vol. 452, no. August 2019, p. 227793, 2020, doi: 10.1016/j.jpowsour.2020.227793.
[91] A. Chang, C. Zhang, Y. Yu, Y. Yu, and B. Zhang, “Plasma-Assisted Synthesis of NiSe 2 Ultrathin Porous Nanosheets with Selenium Vacancies for Supercapacitor,” *ACS Appl. Mater. Interfaces*, vol. 10, no. 49, pp. 41861–41865, 2018, doi: 10.1021/acsami.8b16072.
[92] H. Jiang *et al.*, “A novel MnO2/Ti3C2Tx MXene nanocomposite as high performance electrode materials for flexible supercapacitors,” *Electrochim. Acta*, vol. 290, pp. 695–703, 2018, doi: 10.1016/j.electacta.2018.08.096.
[93] J. B. Goodenough and K. S. Park, “The Li-ion rechargeable battery: A perspective,” *J. Am. Chem. Soc.*, vol. 135, no. 4, pp. 1167–1176, 2013, doi: 10.1021/ja3091438.
[94] H. Yang *et al.*, “Hierarchical porous mnco2o4 yolk-shell microspheres from mofs as secondary nanomaterials for high power lithium ion batteries,” *Dalt. Trans.*, vol. 48, no. 25,

pp. 9205–9213, 2019, doi: 10.1039/c9dt00613c.
[95] H. Xu, Z. Sun, and J. Chen, *Graphene-based anode materials for lithium-ion batteries*. INC, 2020.
[96] C. Jiang, E. Hosono, and H. Zhou, "Nanomaterials for lithium ion batteries," *Nano Today*, vol. 1, no. 4, pp. 28–33, 2006, doi: 10.1016/S1748-0132(06)70114-1.
[97] Y. Fang *et al.*, "MXene-derived TiO2/reduced graphene oxide composite with an enhanced capacitive capacity for Li-ion and K-ion batteries," *J. Mater. Chem. A*, vol. 7, no. 10, pp. 5363–5372, 2019, doi: 10.1039/c8ta12069b.
[98] H. Luo *et al.*, "Highly conductive graphene-modified TiO2 hierarchical film electrode for flexible Li-ion battery anode," *Electrochim. Acta*, vol. 313, pp. 10–19, 2019, doi: 10.1016/j.electacta.2019.05.018.
[99] I. Dincer and Y. Bicer, *System integration for multigeneration*. 2020.
[100] L. Mongibello, M. Capezzuto, and G. Graditi, "Technical and cost analyses of two different heat storage systems for residential micro-CHP plants," *Appl. Therm. Eng.*, vol. 71, no. 2, pp. 636–642, 2014, doi: 10.1016/j.applthermaleng.2013.10.026.
[101] S. Song *et al.*, "Polyethylene glycol/halloysite@Ag nanocomposite PCM for thermal energy storage: Simultaneously high latent heat and enhanced thermal conductivity," *Sol. Energy Mater. Sol. Cells*, vol. 193, no. December 2018, pp. 237–245, 2019, doi: 10.1016/j.solmat.2019.01.023.
[102] D. S. Ezhumalai, G. Sriharan, and S. Harikrishnan, "Improved Thermal Energy Storage Behavior of CuO/Palmitic acid Composite as Phase Change Material," *Mater. Today Proc.*, vol. 5, no. 6, pp. 14618–14627, 2018, doi: 10.1016/j.matpr.2018.03.053.
[103] G. Q. Qi *et al.*, "Enhanced comprehensive performance of polyethylene glycol based phase change material with hybrid graphene nanomaterials for thermal energy storage," *Carbon N. Y.*, vol. 88, pp. 196–205, 2015, doi: 10.1016/j.carbon.2015.03.009.
[104] Y. Zhou, C. Li, H. Wu, and S. Guo, "Construction of hybrid graphene oxide/graphene nanoplates shell in paraffin microencapsulated phase change materials to improve thermal conductivity for thermal energy storage," *Colloids Surfaces A Physicochem. Eng. Asp.*, vol. 597, no. February, p. 124780, 2020, doi: 10.1016/j.colsurfa.2020.124780.
[105] H. K. Sharma, S. K. Verma, P. K. Singh, S. Kumar, M. Kant Paswan, and P. Singhal, "Performance analysis of paraffin wax as PCM by using hybrid zinc-cobalt-iron oxide nano-fluid on latent heat energy storage system," *Mater. Today Proc.*, vol. 26, no. xxxx, pp. 1461–1464, 2020, doi: 10.1016/j.matpr.2020.02.300.
[106] Z. Liu, Z. Chen, and F. Yu, "Enhanced thermal conductivity of microencapsulated phase change materials based on graphene oxide and carbon nanotube hybrid filler," *Sol. Energy Mater. Sol. Cells*, vol. 192, no. December 2018, pp. 72–80, 2019, doi: 10.1016/j.solmat.2018.12.014.
[107] S. Akilu, A. T. Baheta, S. Chowdhury, E. Padmanabhan, and K. V. Sharma, "Thermophysical profile of SiC–CuO/C nanocomposite in base liquid ethylene glycol," *Powder Technol.*, vol. 354, pp. 540–551, 2019, doi: 10.1016/j.powtec.2019.04.061.
[108] M. H. Esfe, S. Esfandeh, M. K. Amiri, and M. Afrand, "A novel applicable experimental study on the thermal behavior of SWCNTs(60%)-MgO(40%)/EG hybrid nanofluid by focusing on the thermal conductivity," *Powder Technol.*, vol. 342, pp. 998–1007, 2019, doi: 10.1016/j.powtec.2018.10.008.
[109] A. Kakavandi and M. Akbari, "Experimental investigation of thermal conductivity of nanofluids containing of hybrid nanoparticles suspended in binary base fluids and propose a new correlation," *Int. J. Heat Mass Transf.*, vol. 124, pp. 742–751, 2018, doi: 10.1016/j.ijheatmasstransfer.2018.03.103.
[110] H. W. Xian, N. A. C. Sidik, and R. Saidur, "Impact of different surfactants and ultrasonication time on the stability and thermophysical properties of hybrid nanofluids," *Int. Commun. Heat*

*Mass Transf.*, vol. 110, 2020, doi: 10.1016/j.icheatmasstransfer.2019.104389.
[111] A. Alshare, W. Al-Kouz, and W. Khan, "Cu-Al2O3 water hybrid nanofluid transport in a periodic structure," *Processes*, vol. 8, no. 3, 2020, doi: 10.3390/pr8030285.
[112] Z. Said, M. A. Abdelkareem, H. Rezk, A. M. Nassef, and H. Z. Atwany, *Stability, thermophysical and electrical properties of synthesized carbon nanofiber and reduced-graphene oxide-based nanofluids and their hybrid along with fuzzy modeling approach*, vol. 364. Elsevier B.V, 2020.
[113] E. C. Okonkwo, I. Wole-Osho, D. Kavaz, and M. Abid, "Comparison of experimental and theoretical methods of obtaining the thermal properties of alumina/iron mono and hybrid nanofluids," *J. Mol. Liq.*, vol. 292, p. 111377, 2019, doi: 10.1016/j.molliq.2019.111377.
[114] S. M. Mousavi, F. Esmaeilzadeh, and X. P. Wang, "A detailed investigation on the thermo-physical and rheological behavior of MgO/TiO 2 aqueous dual hybrid nanofluid," *J. Mol. Liq.*, vol. 282, pp. 323–339, 2019, doi: 10.1016/j.molliq.2019.02.100.
[115] A. Asadi, M. Asadi, A. Rezaniakolaei, L. A. Rosendahl, M. Afrand, and S. Wongwises, "Heat transfer efficiency of Al2O3-MWCNT/thermal oil hybrid nanofluid as a cooling fluid in thermal and energy management applications: An experimental and theoretical investigation," *Int. J. Heat Mass Transf.*, vol. 117, pp. 474–486, 2018, doi: 10.1016/j.ijheatmasstransfer.2017.10.036.
[116] S. Akilu, A. T. Baheta, and K. V. Sharma, "Experimental measurements of thermal conductivity and viscosity of ethylene glycol-based hybrid nanofluid with TiO2-CuO/C inclusions," *J. Mol. Liq.*, vol. 246, pp. 396–405, 2017, doi: 10.1016/j.molliq.2017.09.017.
[117] S. Kannaiyan, C. Boobalan, A. Umasankaran, A. Ravirajan, S. Sathyan, and T. Thomas, "Comparison of experimental and calculated thermophysical properties of alumina/cupric oxide hybrid nanofluids," *J. Mol. Liq.*, vol. 244, pp. 469–477, 2017, doi: 10.1016/j.molliq.2017.09.035.
[118] M. S. Kumar, V. Vasu, and A. V. Gopal, "Thermal conductivity and rheological studies for Cu–Zn hybrid nanofluids with various basefluids," *J. Taiwan Inst. Chem. Eng.*, vol. 66, pp. 321–327, 2016, doi: 10.1016/j.jtice.2016.05.033.
[119] S. Aberoumand and A. Jafarimoghaddam, "Tungsten (III) oxide (WO3) – Silver/transformer oil hybrid nanofluid: Preparation, stability, thermal conductivity and dielectric strength," *Alexandria Eng. J.*, vol. 57, no. 1, pp. 169–174, 2018, doi: 10.1016/j.aej.2016.11.003.
[120] M. Tahmasebi Sulgani and A. Karimipour, "Improve the thermal conductivity of 10w40-engine oil at various temperature by addition of Al 2 O 3 /Fe 2 O 3 nanoparticles," *J. Mol. Liq.*, vol. 283, pp. 660–666, 2019, doi: 10.1016/j.molliq.2019.03.140.
[121] S. H. Qing, W. Rashmi, M. Khalid, T. C. S. M. Gupta, M. Nabipoor, and M. T. Hajibeigy, "Thermal conductivity and electrical properties of Hybrid SiO2-graphene naphthenic mineral oil nanofluid as potential transformer oil," *Mater. Res. Express*, vol. 4, no. 1, 2017, doi: 10.1088/2053-1591/aa550e.
[122] M. Karami, "Experimental investigation of first and second laws in a direct absorption solar collector using hybrid Fe 3 O 4 /SiO 2 nanofluid," *J. Therm. Anal. Calorim.*, vol. 136, no. 2, pp. 661–671, 2019, doi: 10.1007/s10973-018-7624-x.
[123] A. Ahmed, H. Baig, S. Sundaram, and T. K. Mallick, "Use of Nanofluids in Solar PV/Thermal Systems," *Int. J. Photoenergy*, vol. 2019, pp. 1–17, 2019, doi: 10.1155/2019/8039129.
[124] T. R. Shah and H. M. Ali, "Applications of hybrid nanofluids in solar energy, practical limitations and challenges: A critical review," *Sol. Energy*, vol. 183, no. February, pp. 173–203, 2019, doi: 10.1016/j.solener.2019.03.012.
[125] J. Zeng and Y. Xuan, "Enhanced solar thermal conversion and thermal conduction of MWCNT-SiO2/Ag binary nanofluids," *Appl. Energy*, vol. 212, no. December 2017, pp. 809–819, 2018, doi: 10.1016/j.apenergy.2017.12.083.
[126] J. Fang and Y. Xuan, "Investigation of optical absorption and photothermal conversion

characteristics of binary CuO/ZnO nanofluids," *RSC Adv.*, vol. 7, no. 88, pp. 56023–56033, 2017, doi: 10.1039/c7ra12022b.
[127] M. Chen, Y. He, J. Huang, and J. Zhu, "Synthesis and solar photo-thermal conversion of Au, Ag, and Au-Ag blended plasmonic nanoparticles," *Energy Convers. Manag.*, vol. 127, pp. 293–300, 2016, doi: 10.1016/j.enconman.2016.09.015.
[128] X. Wang, Y. He, M. Chen, and Y. Hu, "ZnO-Au composite hierarchical particles dispersed oil-based nanofluids for direct absorption solar collectors," *Sol. Energy Mater. Sol. Cells*, vol. 179, no. August 2017, pp. 185–193, 2018, doi: 10.1016/j.solmat.2017.11.012.
[129] E. Farajzadeh, S. Movahed, and R. Hosseini, "Experimental and numerical investigations on the effect of Al2O3/TiO2-H2O nanofluids on thermal efficiency of the flat plate solar collector," *Renew. Energy*, vol. 118, pp. 122–130, 2018, doi: 10.1016/j.renene.2017.10.102.
[130] D. Wang *et al.*, "Enhanced photothermal conversion properties of magnetic nanofluids through rotating magnetic field for direct absorption solar collector," *J. Colloid Interface Sci.*, vol. 557, pp. 266–275, 2019, doi: 10.1016/j.jcis.2019.09.022.
[131] A. Younis, M. Onsa, Y. Alhorr, and E. Elsarrag, "The Influence of Al2O3- ZnO-H2O Nanofluid on the Thermodynamic Performance of Photovoltaic- Thermal Hybrid Solar Collector System," *Innov. Energy Res.*, vol. 07, no. 01, pp. 1–8, 2018, doi: 10.4172/2576-1463.1000187.
[132] A. H. A. Al-Waeli *et al.*, "Evaluation of the nanofluid and nano-PCM based photovoltaic thermal (PVT) system: An experimental study," *Energy Convers. Manag.*, vol. 151, no. September, pp. 693–708, 2017, doi: 10.1016/j.enconman.2017.09.032.
[133] F. Crisostomo, N. Hjerrild, S. Mesgari, Q. Li, and R. A. Taylor, "A hybrid PV/T collector using spectrally selective absorbing nanofluids," *Appl. Energy*, vol. 193, pp. 1–14, 2017, doi: 10.1016/j.apenergy.2017.02.028.
[134] R. Nasrin, S. Parvin, and M. A. Alim, "Heat transfer and collector efficiency through a direct absorption solar collector with radiative heat flux effect," *Numer. Heat Transf. Part A Appl.*, vol. 68, no. 8, pp. 887–907, 2015, doi: 10.1080/10407782.2015.1023122.
[135] M. Du, G. H. Tang, and T. M. Wang, "Exergy analysis of a hybrid PV/T system based on plasmonic nanofluids and silica aerogel glazing," *Sol. Energy*, vol. 183, no. November 2018, pp. 501–511, 2019, doi: 10.1016/j.solener.2019.03.057.
[136] M. Hissouf, M. Feddaoui, M. Najim, and A. Charef, "Numerical study of a covered Photovoltaic-Thermal Collector (PVT) enhancement using nanofluids," *Sol. Energy*, vol. 199, no. August 2019, pp. 115–127, 2020, doi: 10.1016/j.solener.2020.01.083.
[137] A. S. Abdelrazik, K. H. Tan, N. Aslfattahi, A. Arifutzzaman, R. Saidur, and F. A. Al-Sulaiman, "Optical, stability and energy performance of water-based MXene nanofluids in hybrid PV/thermal solar systems," *Sol. Energy*, vol. 204, no. December 2019, pp. 32–47, 2020, doi: 10.1016/j.solener.2020.04.063.
[138] X. Han, X. Chen, Y. Sun, and J. Qu, "Performance improvement of a PV/T system utilizing Ag/CoSO4-propylene glycol nanofluid optical filter," *Energy*, vol. 192, p. 116611, 2020, doi: 10.1016/j.energy.2019.116611.
[139] S. S. Khaleduzzaman *et al.*, "Energy and exergy analysis of alumina-water nanofluid for an electronic liquid cooling system," *Int. Commun. Heat Mass Transf.*, vol. 57, pp. 118–127, 2014, doi: 10.1016/j.icheatmasstransfer.2014.07.015.
[140] R. Saidur, K. Y. Leong, and H. A. Mohammed, "A review on applications and challenges of nanofluids," *Renew. Sustain. Energy Rev.*, vol. 15, no. 3, pp. 1646–1668, 2011, doi: 10.1016/j.rser.2010.11.035.
[141] S. M. Sohel Murshed and C. A. Nieto de Castro, "A critical review of traditional and emerging techniques and fluids for electronics cooling," *Renew. Sustain. Energy Rev.*, vol. 78, no. February, pp. 821–833, 2017, doi: 10.1016/j.rser.2017.04.112.
[142] B. Agostini, M. Fabbri, J. E. Park, L. Wojtan, J. R. Thome, and B. Michel, "State of the art of

high heat flux cooling technologies," *Heat Transf. Eng.*, vol. 28, no. 4, pp. 258–281, 2007, doi: 10.1080/01457630601117799.
[143] M. Bahiraei and S. Heshmatian, "Efficacy of a novel liquid block working with a nanofluid containing graphene nanoplatelets decorated with silver nanoparticles compared with conventional CPU coolers," *Appl. Therm. Eng.*, vol. 127, pp. 1233–1245, 2017, doi: 10.1016/j.applthermaleng.2017.08.136.
[144] S. D. Barewar, S. Tawri, and S. S. Chougule, "Experimental investigation of thermal conductivity and its ANN modeling for glycol-based Ag/ZnO hybrid nanofluids with low concentration," *J. Therm. Anal. Calorim.*, vol. 139, no. 3, pp. 1779–1790, 2020, doi: 10.1007/s10973-019-08618-6.
[145] R. K. Bumataria, N. K. Chavda, and H. Panchal, "Current research aspects in mono and hybrid nanofluid based heat pipe technologies," *Heliyon*, vol. 5, no. 5, p. e01627, 2019, doi: 10.1016/j.heliyon.2019.e01627.
[146] R. Ramachandran, K. Ganesan, M. R. Rajkumar, L. G. Asirvatham, and S. Wongwises, "Comparative study of the effect of hybrid nanoparticle on the thermal performance of cylindrical screen mesh heat pipe," *Int. Commun. Heat Mass Transf.*, vol. 76, pp. 294–300, 2016, doi: 10.1016/j.icheatmasstransfer.2016.05.030.
[147] K. Swapnil, P. Dhananjay, Z. Gaurav, R. Anand, and D. P. Kamble, "Heat Transfer Enhancement of Circular Heat Pipe with Al2O3 BN / Water Hybrid Nanofluid," vol. 4, no. 4, pp. 138–143, 2016.
[148] R. N. Ramachandran, K. Ganesan, and L. G. Asirvatham, "The role of hybrid nanofluids in improving the thermal characteristics of screen mesh cylindrical heat pipes," *Therm. Sci.*, vol. 20, no. 6, pp. 2027–2035, 2016, doi: 10.2298/TSCI150710006R.
[149] S. Anitha, T. Thomas, V. Parthiban, and M. Pichumani, "What dominates heat transfer performance of hybrid nanofluid in single pass shell and tube heat exchanger?," *Adv. Powder Technol.*, vol. 30, no. 12, pp. 3107–3117, 2019, doi: 10.1016/j.apt.2019.09.018.
[150] N. Ahammed, L. G. Asirvatham, and S. Wongwises, "Entropy generation analysis of graphene–alumina hybrid nanofluid in multiport minichannel heat exchanger coupled with thermoelectric cooler," *Int. J. Heat Mass Transf.*, vol. 103, pp. 1084–1097, 2016, doi: 10.1016/j.ijheatmasstransfer.2016.07.070.
[151] M. H. Ahmadi, M. Ghazvini, M. Sadeghzadeh, M. Alhuyi Nazari, and M. Ghalandari, "Utilization of hybrid nanofluids in solar energy applications: A review," *Nano-Structures and Nano-Objects*, vol. 20, p. 100386, 2019, doi: 10.1016/j.nanoso.2019.100386.
[152] M. H. Aghabozorg, A. Rashidi, and S. Mohammadi, "Experimental investigation of heat transfer enhancement of Fe2O3-CNT/water magnetic nanofluids under laminar, transient and turbulent flow inside a horizontal shell and tube heat exchanger," *Exp. Therm. Fluid Sci.*, vol. 72, pp. 182–189, 2016, doi: 10.1016/j.expthermflusci.2015.11.011.
[153] A. Bhattad, J. Sarkar, and P. Ghosh, "Experimentation on effect of particle ratio on hydrothermal performance of plate heat exchanger using hybrid nanofluid," *Appl. Therm. Eng.*, vol. 162, no. April, p. 114309, 2019, doi: 10.1016/j.applthermaleng.2019.114309.
[154] S. A. Kaska, R. A. Khalefa, and A. M. Hussein, "Hybrid nanofluid to enhance heat transfer under turbulent flow in a flat tube," *Case Stud. Therm. Eng.*, vol. 13, no. March, p. 100398, 2019, doi: 10.1016/j.csite.2019.100398.
[155] H. R. Allahyar, F. Hormozi, and B. ZareNezhad, "Experimental investigation on the thermal performance of a coiled heat exchanger using a new hybrid nanofluid," *Exp. Therm. Fluid Sci.*, vol. 76, pp. 324–329, 2016, doi: 10.1016/j.expthermflusci.2016.03.027.